In compliance with the
Canadian Privacy Legislation
some supporting forms
may have been removed from
this dissertation.

While these forms may be included
in the document page count,
their removal does not represent
any loss of content from the dissertation.

SPONTANEOUS AND CATALYZED HYDROGEN SHIFTS IN RADICAL CATIONS HAVING A PHOSPHORYL OR CARBONYL GROUP :

A TANDEM MASS SPECTROMETRY AND CBS-QB3 COMPUTATIONAL STUDY

By

LISA NATASHA HEYDORN, B.Sc.

A Thesis

Submitted to the School of Graduate Studies

in Partial Fulfillment of the Requirements

for the Degree

Doctor of Philosophy

McMaster University

SPONTANEOUS AND CATALYZED HYDROGEN SHIFTS IN RADICAL CATIONS HAVING A PHOSPHORYL OR CARBONYL GROUP:

A TANDEM MASS SPECTROMETRY AND CBS-QB3 COMPUTATIONAL STUDY

For me

DOCTOR OF PHILOSOPHY (2003)
(Chemistry)

McMaster University
Hamilton, Ontario

TITLE : SPONTANEOUS AND CATALYZED HYDROGEN SHIFTS IN RADICAL CATIONS HAVING A PHOSPHORYL OR CARBONYL GROUP

AUTHOR : Lisa Natasha Heydorn, B.Sc. (McMaster University)

SUPERVISOR : Professor Johan K. Terlouw

NUMBER OF PAGES : xvii, 233

Abstract

Intermolecular and intramolecular hydrogen shifts represent a key component of a vast number of chemical reactions. This is particularly true for radical cations, whose high reactivity makes them prone to isomerization and dissociation reactions. In the context of the experimental work in this thesis, hydrogen transfers involved in both the intra- and inter-molecular isomerization of radical cations containing a phosporyl (P=O) or carbonyl (C=O) functionality have been studied.

The radical cations studied were generated in the rarefied gas-phase of the mass spectrometer by common ionization methods. Their structure and reactivity was studied by a variety of tandem mass spectrometry based techniques : metastable ion (MI) and collision-induced dissociation (CID) spectrometry, neutralization-reionization mass spectrometry (NRMS), collision induced dissociative ionization (CIDI) spectrometry and a number of hybrid techniques, including CID/CID, NR/CID and CIDI/CID. The use of deuterium, 18-oxygen and 13-carbon labelled isotopologues and quantum chemical calculations at the CBS-QB3 level of theory formed an essential component in the interpretation of the results.

A single hydrogen shift can lead to the isomerization of a keto radical cation into its thermodynamically more favourable enol isomer. However, if the isomerization of a solitary ion into its more stable counterpart involves a 1,2- or 1,3-H shift, it is often prohibited by a high energy barrier. Thus, the "keto" ion $(CH_3O)_2P(H)=O^{\bullet+}$, ionized dimethyl phosphonate ($\mathbf{1}^{\bullet+}$), does not readily isomerize into its "enol" tautomer $(CH_3O)_2P\text{-}OH^{\bullet+}$, ionized dimethyl phosphite ($\mathbf{1b}^{\bullet+}$). Instead, $\mathbf{1}^{\bullet+}$ readily isomerizes via a 1,4-H shift to the very stable distonic ion $CH_2O\text{-}(CH_3O)P(H)OH^{\bullet+}$ ($\mathbf{1a}^{\bullet+}$) and related ion-dipole complexes, which serve as precursors for the low energy loss of $CH_2=O$. In fact, in the μs timeframe ions $\mathbf{1}^{\bullet+}$ have completely isomerized into distonic ions $\mathbf{1a}^{\bullet+}$ which do not significantly communicate with their more stable enol counterpart. In contrast, an ion-molecule reaction of $\mathbf{1}^{\bullet+}$ with a benzonitrile molecule readily leads to a complete

enolization. This is by virtue of a benzonitrile-catalyzed lowering of the high 1,3-H shift barrier separating the isomers $\mathbf{1a}^{\bullet+}$ and $\mathbf{1b}^{\bullet+}$.

In the same vein, a facile tautomerization of the cyclic ethylene phosphonate "keto" ion $[\text{-}OCH_2CH_2O\text{-}]P(H)=O^{\bullet+}$ ($\mathbf{2a}^{\bullet+}$) into its more stable "enol" isomer, ethylene phosphite $[\text{-}OCH_2CH_2O\text{-}]P\text{-}OH^{\bullet+}$ ($\mathbf{2b}^{\bullet+}$), is prevented by a substantial 1,2-H shift barrier, 14 kcal/mol relative to $\mathbf{2a}^{\bullet+}$. In line with this conclusion, the collision-induced dissociation (CID) and neutralization-reionization (NR) spectra of the two isomers are characteristically different. Unlike the corresponding acyclic tautomers $\mathbf{1}^{\bullet+}$ and $\mathbf{1b}^{\bullet+}$, where the phosphonate isomer rapidly loses its structure identity by a facile distonicization, the barrier for this reaction in $\mathbf{2a}^{\bullet+}$ is prohibitively high and the cyclic distonic 1,2-H shift isomer $[\text{-}OCH_2CH_2O(H)\text{-}]P=O^{\bullet+}$, $\mathbf{2c}^{\bullet+}$, is not directly accessible. Thus, non-dissociating "keto" ions $\mathbf{2a}^{\bullet+}$ retain their structure identity in the μs timeframe. Here too, the interaction of **2a** with a benzonitrile molecule in a chemical ionization type experiment readily yields the more stable "enol" type ion $\mathbf{2b}^{\bullet+}$. Experiments with benzonitrile-d_5 show that this reaction does not involve true proton-transport catalysis but rather a quid-pro-quo mechanism, analogous to that proposed for the benzonitrile-assisted enolization of acetamide.

Hydrogen shifts are often induced when electronegative atoms such as oxygen are present in the radical cation. This trend is evident in the relatively small $CH_3O\text{-}P=O^{\bullet+}$ ion, which has more than fifteen stable isomers, not including rotational or conformational isomers. This ion has a fairly low heat of formation but it is not as stable as its distonic H-shift isomer $CH_2O\text{-}P\text{-}OH^{\bullet+}$, or its "enol" isomer $CH_2=P(OH)=O^{\bullet+}$, which represents the global minimum on the $CH_3O_2P^{\bullet+}$ potential energy-surface. Several $CH_3O_2P^{\bullet+}$ isomers were characterized experimentally and found to display a remarkable low energy decarbonylation reaction that requires three consecutive H-shifts. A detailed computational study revealed that the complex mechanism for this reaction involves the ion-dipole complex $[O=C(H)\text{-}H\bullet\bullet\bullet POH]^{\bullet+}$ and the hydrogen bridged radical cation, $[CH_2O\text{-}H\bullet\bullet\bullet O=P]^{\bullet+}$ as key intermediates.

Characterization of the various $CH_3O_2P^{\bullet+}$ isomers also proved to be important in the context of differentiating the isobaric ions $CH_3O_2P^{\bullet+}$ and CH_5NOP^+. Both m/z 78 ions are generated in equal abundance via dissociative electron ionization of acephate. The $CH_3O_2P^{\bullet+}$ component was found to consist of $CH_3O\text{-}P{=}O^{\bullet+}$ and $CH_2O\text{-}P\text{-}OH^{\bullet+}$, whereas the N-containing component was identified as $CH_3O\text{-}P\text{-}NH_2^+$. Therefore, the recovery signal at m/z 78 in the previously reported neutralization-reionization spectrum of acephate does not demonstrate that $CH_3O\text{-}P{=}O^{\bullet+}$ has a stable neutral counterpart. Collision-induced dissociative ionization experiments on the reaction $C_6H_5\text{-}P(=O)OCH_3^+ \rightarrow C_6H_5^+ + CH_3O\text{-}P{=}O$ leave little doubt that $CH_3O\text{-}P{=}O$ is a stable molecule in the dilute gas-phase.

The $CH_3O_2P^{\bullet+}$ isomer $CH_3\text{-}P(=O)_2^{\bullet+}$ is only marginally stable but its neutral counterpart is predicted by theory to lie in a deep potential well. The stability of this elusive neutral was probed by a collision induced dissociative ionization (CIDI) experiment on the reaction $(C_6H_5CH_2O)_2P(=O)CH_3^{\bullet+} \rightarrow (C_7H_7O)(C_6H_5CHO)P(OH)CH_3^{\bullet+} \rightarrow (C_6H_5CHO)P(=O)(OH)CH_3^+ + C_7H_7^{\bullet} \rightarrow C_6H_5CH\text{-}OH^+ + CH_3\text{-}P(=O)_2$ and a CIDI/CID experiment confirmed its structure identity.

An enol radical cation is as a rule more stable than its keto isomer but this appears not to be true for the acetanilide ion. Its enol, $C_6H_5NH(OH){=}CH_2^{\bullet+}$, was calculated to be higher in energy than the keto tautomer. The enol ion was found to eliminate HNCO at low internal energy and not ketene as reported previously. This HNCO loss occurs via an intriguing skeletal rearrangement, whose mechanism was explored using isotopic labelling and computational chemistry. As the ionized enol is *less* stable than its keto counterpart, it is not surprising that molecule-assisted enolization reactions of ionized acetanilide cannot be realized. However, the reverse process, i.e. a molecule-assisted ketonization of the enol ion, does not take place either but this may be due to the formation of unreactive encounter complexes.

When a radical cation dissociates by loss of a radical, the reaction often involves a simple bond cleavage but hidden hydrogen shifts may also occur. Theory and experiment agree that the prominent loss of $CH_3^{\bullet}$ from ionized sorbic acid,

$CH_3CH=CHCH=CHCOOH^{\bullet+}$, is not a direct bond cleavage nor a hidden H-rearrangement. Instead, this dissociation is proposed to be a displacement reaction in which a very stable cyclic product ion, protonated 2*H*-pyran-2-one, is generated.

Hydrogen shifts also feature prominently in the dissociation chemistry of even-electron ions. The low energy oxonium ions $CH_3CH=CH\text{-}C^+(H)OCH_3$, $CH_2=CH\text{-}C^+(CH_3)\text{-}OCH_3$, $CH_2=C(CH_3)\text{-}C^+(H)OCH_3$ and $CH_2=CH\text{-}CH(CH_3)\text{-}OCH_2^+$ all abundantly lose CH_2O. The chemistries of these $C_5H_9O^+$ isomers are closely related but they are not identical and the distinctions become clearer when labelled analogues are examined. Elimination of CH_2O from the three $C_4H_6OCH_3^+$ ions is proposed to involve a largely irreversible 1,5-H shift, from the OCH_3 group to the hydrocarbon chain, followed by a dipole-assisted 1,3-H shift to give energy-rich ion-neutral complexes of 1- or 2-methallyl cations and neutral CH_2O, which dissociate. For the $CH_2=CH\text{-}CH(CH_3)OCH_2^+$ ion, the CH_2O loss is associated with a very small kinetic energy release, suggesting that it generates the most stable $C_4H_7^+$ ion, 1-methallyl cation, at the thermochemical threshold. The enthalpies of formation for the key ions in this study were obtained from CBS-QB3 calculations and thermochemical estimates.

Preface

The larger part of this thesis describes the results obtained by the author during four years of experimental and computational research in gas phase ion chemistry. This field is ideally suited to the investigation by both experimental and theoretical methodologies. Indeed, the common set of conditions involved in mass spectrometric experiments and computational chemistry, i.e. the study of isolated particles, makes the two approaches complementary. Such investigations necessitate the collaboration of both experimental and theoretical chemists. Collaborative contributions from, Prof. Richard D. Bowen (Chapter 7 and 9) and Prof. Chava Lifshitz (Chapter 2) are greatly appreciated. Furthermore, two individuals deserve special mention in the context of collaboration : Dr. Peter C. Burgers (Chapters 3, 4 and 6) and Prof. Paul J.A. Ruttink (Chapters 3, 4 and 6). Their insights, suggestions, computational contributions, and critical evaluations have significantly shaped the way that the results have been presented.

The permission of the Elsevier Science and Oldenbourg Wissenschaftsverlag to reproduce the data and text, which have previously been published, is also appreciated.

List of Publications

1. L.N. Heydorn, Y. Ling, G. de Oliveira, J.M.L. Martin, Ch. Lifshitz and J.K. Terlouw, Zeitschrift für Physikalische Chemie **215** (2001) 141-182.
Tautomerization and dissociation of dimethyl phosphonate ions $(CH_3O)_2P(H)=O^{\bullet+}$ *: theory and experiment in concert* (Jürgen Troe issue)

2. R.D. Bowen, L.N. Heydorn and J.K. Terlouw, Int. J. Mass Spectrom. **209** (2001) 153-169.
The chemistry of some low energy $C_5H_9O^+$ *oxonium ions*

3. R.D. Bowen, L.N. Heydorn and J.K. Terlouw, Int. J. Mass Spectrom. **217** (2002) 109-118.
Reactions of low-energy pentenyl methyl ether radical cations $C_2H_5CH=CHCH_2OCH_3^{\bullet+}$, $CH_2=CHCH(C_2H_5)OCH_3^{\bullet+}$ *and* $CH_2=C(C_2H_5)CH_2OCH_3^{\bullet+}$

4. L.N. Heydorn, P.C. Burgers, P.J.A. Ruttink and J.K. Terlouw, Int. J. Mass Spectrom. (2002) in press.
Tautomerization and dissociation of ethylene phosphonate ions $[-OCH_2CH_2O-]P(H)=O^{\bullet+}$ *: an experiment and CBS-QB3 computational study*

5. L.N. Heydorn, C.Y. Wong, R. Srinivas and J.K. Terlouw, Int. J. Mass Spectrom. **225** (2003) 11-23.
The isobaric ions $CH_3O\text{-}P=O^{\bullet+}$ *and* $CH_3O\text{-}P\text{-}NH_2^+$ *and their neutral counterparts: a tandem mass spectrometry and CBS-QB3 computational study*

6. L.N. Heydorn, P.C. Burgers, P.J.A. Ruttink and J.K. Terlouw, Chem. Phys. Lett. **368** (2003) 584-588.
Generation of the elusive methyl dioxophosphorane molecule, $CH_3P(=O)_2$*, by delayed dissociation of selected precursors*

7. L.N. Heydorn, P.C. Burgers, P.J.A. Ruttink and J.K. Terlouw, Int. J. Mass Spectrom. (2002) submitted.
The low energy decarbonylation of the $CH_3O\text{-}P=O^{\bullet+}$ *family of ions : an experimental and CBS-QB3 computational study*

Acknowledgements

This section is dedicated to recognizing those people who have helped me through my journey as a graduate student here at McMaster. Let me begin by saying how deeply indebted I am to my supervisor, Dr Terlouw. He is an excellent teacher, a dedicated researcher and a strict taskmaster, and thus was able to ensure that I was led down the correct path. His vast knowledge of chemistry and mass spectrometry laid a strong foundation upon which I could build my knowledge.

A heartfelt thank you goes to my supervisory committee, comprising Professors Brian McCarry and Paul Berti, for their strong support and guidance. Their insightful conversations have truly been helpful. I must also thank Dr Berti for the use (or perhaps abuse) of his SGI computer (BB2).

I am also grateful to Dr Peter Burgers and Professor Paul Ruttink for their knowledgeable input and generous hospitality when I visited them abroad. Thank you for welcoming me into your homes.

I would like to acknowledge the Department of Chemistry and Micromass for the Sherman Award and the Micromass-Canada Graduate Student Scholarship.

I would like to show my appreciation to my friends and lab mates (past and present) for their support through the good and the bad, particularly the Chemistry geeks Sue, Cathy and Bernie, also my friends from home Annette, Margaret, Melissa, Murph and Wayne, and my Hamilton friends Horatiu and Lisa.

Most importantly I am very grateful to my family, my parents Bernard and Vivienne and my brothers Sean and Graham, without them I would not be where I am today. Dad, I do believe my corvette is long overdue – red would be nice. Sean and Graham, thank you for the financial support. Finally, I would like to thank my role model, my mother, for always listening.

Table of Contents

List of Figures

List of Abreviations

AE	=	appearance energy
B	=	magnetic sector
B3LYP	=	(Becke 3 term, Lee Yang, Parr) hybrid Hartree-Fock/density functional theory
CA	=	collisional-activation
CCSD(T)	=	coupled cluster singles, doubles and triples
CE	=	charge exchange
CI	=	chemical ionization
CID	=	collision-induced dissociation
CIDI	=	collision-induced dissociative ionization
CS	=	charge-stripping
DFT	=	density functional theory
DMP	=	dimethyl phosphonate
E_{el}	=	energy of the ionizing electrons
E_i	=	internal energy
$E_i^{\neq}$	=	the non-fixed energy of the activated complex
E_{ESA}	=	potential on the electric sector plates
E_o	=	activation energy
E_o^r	=	the reverse activation energy
$\Delta E_{0.5}$	=	width of a metastable peak at half-height in ESA volts
EI	=	electron impact
EP	=	ethylene phosphonate
ESA	=	electrostatic analyzer
eV	=	electron Volt (1 eV = 23.06 kcal/mol)
ffr	=	field-free region
ΔH_f	=	enthalpy of formation
HF	=	Hartree-Fock
IE	=	ionization energy
k	=	rate constant
KE	=	kinetic energy
KER	=	kinetic energy release
m	=	mass
m*	=	metastable ion
MI	=	metastable ion
MIKES	=	mass-selected ion kinetic energy spectrum
MP	=	Møller-Plesset (perturbation theory)
MS	=	mass spectrometry
MS/MS	=	tandem mass spectrometry
m/z	=	mass to charge ratio

NDMA	=	N,N-dimethyl aniline
NRMS	=	neutralization-reionization mass spectrometry
PA	=	proton affinity
PTC	=	proton-transport catalysis
QET	=	Quasi-Equilibrium Theory
QpQ	=	quid-pro-quo
r	=	radius
RRKM	=	Rice, Rampsburger, Kassel and Marcus
s	=	degrees of freedom
SCF	=	self-consistent field
T	=	total kinetic energy released
$T_{0.5}$	=	kinetic energy release value from the peak width at half-height
$T^{\neq}$	=	kinetic energy released as a result of the non-fixed energy of the activated complex
T^{r}	=	kinetic energy released as a result of the reverse activation energy
TMP	=	trimethyl phosphate
TPEPICO	=	threshold photoelectron photoion coincidence
TS	=	transition state
ν	=	frequency factor
v	=	velocity
V	=	accelerating voltage
V_{ESA}	=	the electric sector voltage used to transmit the ions of a given KE
z	=	charge
ZAB-R	=	BEE three-sector mass spectrometer
ZPVE	=	zero-point vibrational energy

Chapter 1

Introduction

1.1 Scope of the thesis

The studies described in this thesis are based on mass spectrometric experiments in conjunction with computational chemistry. These tools were used to examine the chemistry of small organic ions in the gas-phase by exploring their structure and reactivity. Most of the ions studied are radical cations, that is, species generated by the removal of an electron from a gaseous organic molecule in the high-vacuum of the mass spectrometer. The reactivity of such an ionized species is much higher than that of its neutral counterpart. This is true both under high-vacuum conditions where only intramolecular interactions may occur and at higher pressures where intermolecular interactions dominate. Intramolecular interactions may cause a solitary radical cation to isomerize into more stable isomers whose neutral counterparts are "unbottleable" species. These species are of unconventional structure and include distonic ions, ion-dipole complexes and hydrogen-bridged radical cations. It is these intriguing species that play a key role in the chemistry of the various radical cations that feature in this thesis.

Where isomerization of a solitary radical cation into a more stable counterpart is prohibited by a high energy barrier, the reaction may be realized via catalysis by a single "solvent" molecule at elevated pressures (c. 10^{-5} Torr). Such molecule-assisted isomerization reactions form the theme of Chapters 2 and 3, which deal with the phosphonate-phosphite tautomerization in organophosphorus compounds and of Chapter 7, which discusses the keto-enol tautomerization in acetanilide.

The role of the catalyst in a molecule-assisted isomerization reaction can only be probed if the unimolecular chemistry of the ionic components is thoroughly understood. Therefore, Chapters 2 and 3 also deal with the complex unimolecular chemistry of the tautomers of the organophosphorus ions $(CH_3O)_2P(H)=O^{\bullet+}$, ionized dimethyl

phosphonate, and [-OCH_2CH_2O-]P(H)=$O^{\bullet+}$, ionized ethylene phosphonate. In the context of these studies it was observed that several low energy $CH_3PO_2^{\bullet+}$ ions readily decarbonylate. The mechanism of this remarkable reaction, which involves a triple H-transfer, was studied in detail by theory and experiment, and the results are presented in Chapter 4. In this system of isomeric ions, hydrogen-bridged radical cations again play a key role in the interconversion of the various ions prior to their decomposition.

In Chapters 5 and 6 the technique of neutralization-reionization mass spectrometry was used to probe the structure and stability of the neutral counterpart of some of these $CH_3PO_2^{\bullet+}$ ions. This work led to the identification of the elusive CH_3O-P=O and CH_3PO_2 molecules as stable species in the rarefied gas-phase. These species are thought to be important transient molecules in the combustion chemistry of organophosphorus pesticides and nerve gases.

In Chapter 8 it is shown that the loss of a radical from a radical cation does not necessarily involve dissociation by simple bond cleavage. It is shown that the prominent $CH_3^{\bullet}$ loss from the sorbic acid radical cation, CH_3-CH=CH-CH=CH-$COOH^{\bullet+}$, involves an interesting cyclization process leading to a very stable product ion.

Finally, in Chapter 9 an even-electron ion system is discussed. The dissociation chemistry of a set of $C_5H_9O^+$ oxonium ions was studied. Here too, ion-dipole complexes play a key role in the observed dissociation reactions.

In the next section, 1.2, some background information for the uninitiated reader is presented on the mass spectrometric and computational techniques that form the basis of this thesis. This is followed by Section 1.3, which first describes the various reaction mechanisms that may operate in the catalysis of the ion's isomerization by the neutral molecule in an ion-molecule encounter complex. To illustrate how such catalysis experiments are performed in a magnetic-sector mass spectrometer, a brief description of the acetophenone keto-enol system is presented.

The findings in Chapters 2-6 and 8 have been published in scientific Journals. Several of these studies involved collaborative research projects. It is the synergy of my work and the complementary experimental, theoretical and intellectual input of the collaborators that made it possible realize the work described in this thesis. In this

context, I performed most of the experimental work, using the state-of-the-art instrumentation available in our research group. Access to various McMaster (super)computers also allowed me to obtain a great many of the computational results reported.

1.2 How the chemistry of radical cations was studied

In this thesis two main tools were used to study the chemistry of radical cations : mass spectrometry and computational chemistry. The first part of this section describes the various types of experiments one may perform with the ZAB-R magnetic sector mass spectrometer. The second part describes the computational chemistry and the type of calculations used in this thesis.

The compound of interest is introduced, either directly or via a leak valve, into the mass spectrometer such that a vapour pressure of ca 10^{-7} torr is maintained in the ion source. Ionization occurs within 10^{-16} s [1] by the ejection of an electron from the gaseous sample molecule with a fast moving electron (50-100 eV) generated from a tungsten filament outside of the source. This method of ionization results in the formation of radical cations and is known as electron impact ionization (EI), a very common technique of ionization [2]. Only a small fraction (2 in 10^6 molecules) of the sample vapour is ionized and the internal energy of the incipient ions, i.e. the energy imparted above what is required for ionization, varies considerably. As a result, some ions fragment, others undergo rearrangement, while those ions whose internal energy content lies below the dissociation of lowest energy requirement, do not react at all.

The excess internal energy of the solitary molecular ions is rapidly distributed among their various vibrational modes long before dissociation occurs, as the dissociation processes are relatively slow – the fastest dissociation is a direct bond cleavage ($t \sim 10^{-13}$ s). This follows from both RRK [3] and QET theory [1,4], which postulate a simplified relationship that relates the rate constant k to the internal energy, E_i, and the activation energy, E_o :

$$k = \nu [(E_i - E_o)/ E_i]^{s-1} \qquad \text{Eq. 3}$$

where ν = frequency factor and s = degrees of freedom. The frequency factor is related to the "looseness of the activated complex" or the transition state [4]. Each reaction is defined by its rate constant. Whether or not it is observed is determined by the amount of internal energy a given ion has.

Organic radical cations are deficient by one electron and may be described as odd-electron ions [2,5]. This electron deficiency contributes to the enhanced reactivity of the ionized species. In contrast, even-electron ions or cations [5], which may be formed via protonation in a chemical ionization (CI) experiment [2,6], are not electron deficient and do not dissociate extensively. Where an odd-electron ion may dissociate by eliminating a molecule or a radical, an even-electron ion typically loses a molecule, often via a rearrangement reaction.

A rearrangement reaction in an odd-electron ion can only effectively compete with a simple bond cleavage if its energy requirement is considerably lower. This is because rearrangement reactions are associated with a smaller rate constant. A direct bond cleavage reaction only requires enough time for the energy to accumulate in the dissociating bond, which may not take more than 10^{-13} - 10^{-14} s, the time needed for one vibration. In contrast, more bonds must be activated in the reacting configuration for a rearrangement reaction : such a process has stricter steric requirements. Given that the two reactions have the same energy requirement, the probability that the rearrangement reaction will occur is much lower. This is expressed by the so-called frequency factor, ν, which may lie between 10^{10} - 10^{12} s^{-1} depending on the type of rearrangement [1,5].

The incipient molecular ions have a fairly broad energy distribution and may undergo a wide range of dissociations. However, for a dissociation to take place in the source it must have a rate constant, k, of $\geq 10^6$ s^{-1}. This is because the ions only reside in the source for ca 1 μs before a positively charged repeller electrode pushes them out. Next, the ions are accelerated towards the entrance slit of the first field free region (1ffr) under the influence of a strong electric field. As a result, all singly charged positive ions generated in the ion source acquire the same translational energy, irrespective of their mass. Typical values lie between 6 and 10 keV, depending on the accelerating voltage used. The fast moving ions are then analyzed by the magnet of our magnetic sector

instrument of reverse geometry, see Fig. 1.1. The mass analysis is described by Eq. 1, where B = magnetic field strength, r = radius of the ion's path in the magnet and V = accelerating voltage [1,5].

$$m/z = \frac{B^2r^2}{2V} \qquad \text{Eq.1}$$

By varying the magnetic field strength B, the various ions are separated according to their m/z values and the EI mass spectrum is obtained. Alternatively, since the instrument is a tandem mass spectrometer with multiple analyzers, ions of a given mass can be selected by the magnet and be further studied by performing a variety of experiments in the second or third field free region (ffr).

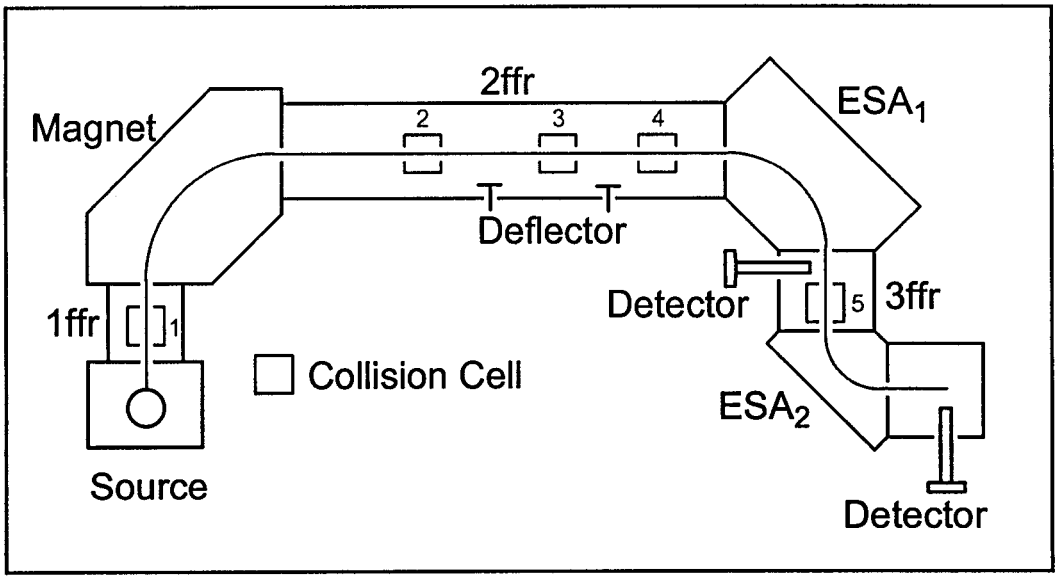

Fig.1.1. The VG ZAB-R mass spectrometer of reversed Nier-Johnson geometry used in this study [1]. This instrument has three analyzers : a magnet and two electrostatic analyzers (ESA). There are 5 collision cells, two deflectors and two detectors. There are 5 sets of movable slits, which can be partially closed to increase the resolution or to run a MIKE spectrum (see Section 1.2.1 on metastable ions).

1.2.1. Tandem mass spectrometry

Tandem mass spectrometry [7], also known as MS/MS, involves the use of one or more additional analyzers. The first analyzer of our instrument, the magnet, is used to mass select a given precursor ion $AB^{\bullet+}$ having a fixed translational energy in the keV range. When such an ion $AB^{\bullet+}$ enters the 2ffr and dissociates into $A^+ + B^{\bullet}$, either spontaneously or by collisional activation, the resulting product ion A^+ carries the fraction m_A/m_{AB} of the translational energy of $AB^{\bullet+}$.

The second analyzer in our instrument, see Fig. 1.1, serves as a translational energy analyzer. It is an electrostatic analyzer (ESA), which can be used to derive the mass of the product ion on the basis of its translational energy. The transmission of an ion of translational energy eV through the sector is governed by :

$$r_e = \frac{2V}{E_{ESA}} \qquad \text{Eq. 2}$$

where r_e is the radius of the circular path of ions transmitted through the sector, and E_{ESA} represents the potential of the sector plates [1]. The mass m of the ion does not appear in this equation so that ions of all masses will follow the same radius through the sector provided only that they have the same translational energy. On the other hand, only ions with a predetermined translational energy, eV, will describe the radius r_e and be transmitted. The radial electric field of the sector behaves analogously to a prism in producing energy dispersion in the ion beam. Therefore, the sector acts as an energy filter if a slit is placed behind it and by scanning E_{ESA} the precursor ion of energy eV can be selectively transmitted followed by its product ions of decreasing mass and translational energy. In this way an MS/MS spectrum is obtained. A more revealing name is a MIKE spectrum : a Mass Analyzed Ion Kinetic Energy spectrum.

It will be shown that there are several variations of the MS/MS technique, each one probing a certain feature of the mass-selected ion under examination. The simplest, yet often most revealing of these experiments is a metastable ion spectrum.

Metastable ion mass spectra

Most of the fragment ions generated by EI ionization result from dissociation reactions that take place in the ion source where the ions reside for ca 1 μs. A range of rate constants, k, which varies from 10^6 to 10^{14} s^{-1}, characterizes these dissociation reactions. Once the ions have been accelerated, it takes ca 10 μs for them to reach the detector. During this time an ion may spontaneously dissociate and if it does so it is called a metastable ion. Therefore, metastable ions dissociate outside of the source as ions of high translational energy. If the dissociation takes place in a field free region preceding an electrostatic analyzer, fragment ions F^+ will be detected in the MIKE spectrum as a signal at a fraction (m_F/m_P) of the ESA voltage needed to transmit the precursor ion $P^{\bullet+}$.

As the reactions of metastable ions are characterized by smaller rate constants, $10^4 < k < 10^6$ s^{-1}, they often result from a rearrangement. Indeed, a metastable ion spectrum typically contains few peaks and these often represent low energy rearrangement reactions, rather than direct bond cleavage processes.

In addition, the shapes of the peaks in an MI spectrum may provide valuable information about the amount of kinetic energy released upon dissociation, i.e. they indicate how "explosive" a given spontaneous dissociation reaction is [1,8]. As shown in Fig. 1.2, the released kinetic energy, T, results from two factors : the non-fixed energy of the activated complex, $E_i^{\neq}$, and the reverse activation energy, E_o^r. Some portion of $E_i^{\neq}$ will appear as kinetic energy $T^{\neq}$ and some portion of E_o^r will appear as kinetic energy T^r. The partitioning coefficients are difficult to predict and only the total energy release $T = T^{\neq} + T^r$ is experimentally accessible.

The relatively small rate constants of dissociating metastable ions lie within a narrow window as illustrated by the energy band of $E_i^{\neq}$ in Fig. 1.2. Upon dissociation, this excess internal energy may be distributed over the vibrational modes of the ionic and neutral products, but part of it may be released as translational energy.

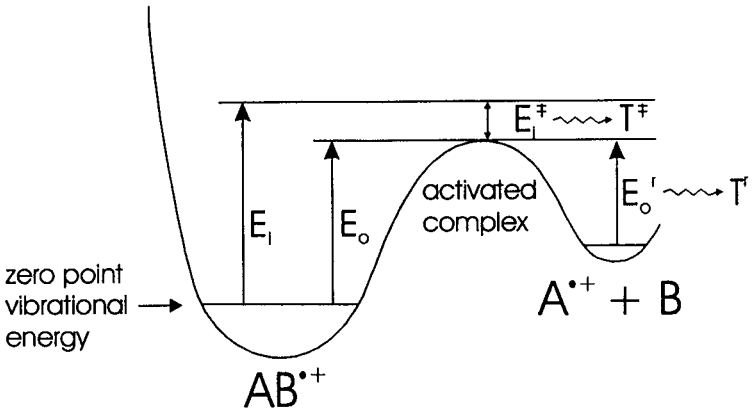

Fig. 1.2. Energy diagram for an endothermic reaction, where E_o is the activation energy and E_i is the internal energy of the reactant $AB^{\bullet+}$.

The reverse activation energy, E_o^r, is the difference between the enthalpy of formation of the dissociation products and the energy of the activated complex, the transition state. For most direct bond cleavage reactions and rearrangements involving ion-dipole complexes, E_o^r is negligibly small and typical T values (which are derived from $T^{\neq}$) for these reactions lie between 0.1 – 20 meV. However, E_o^r may be significant for certain rearrangement reactions, particularly when the formation of a double bond is involved [9]. Such processes are characterized by much higher T values typically between 50 – 2000 meV. Dissociations associated with a small energy release yield metastable peaks of a Gaussian shape, a large kinetic energy release may display a flat-topped or even a dish-shaped metastable peak because of ion-optical discrimination effects.

In either case, the kinetic energy, T, released in a given dissociation of a metastable ion m_1^+ into $m_2^+ + m_3$ manifests itself in the MI spectrum by a broadening of the peak for m_2^+ relative to that of the main beam of non-dissociating ions m_1^+. The T value is normally obtained by measuring the width of the metastable peak m_2^+ at half-height in ESA volts, $\Delta E_{0.5}$, by using the relationship :

$$T_{0.5}\,(eV) = \frac{(m_1)^2 V}{16(m_2)(m_3)} \cdot \frac{(\Delta E_{0.5})^2}{V_{ESA}^2} \qquad \text{Eq. 4}$$

where V = the accelerating voltage and V_{ESA} = the electric sector voltage used to transmit the main beam of ions m_1^+. The average kinetic energy release, <T>, can also be derived from the peak broadening and, when necessary, the ΔE values used are corrected for the contribution of the intrinsic beam width of the precursor ion.

The magnitude of the kinetic energy release provides important information about the reverse activation energy barrier, the type of reacting configuration and whether or not two isomeric species dissociate via the same mechanism [8a]. Thus, obtaining a metastable ion spectrum is a simple, informative experiment which often provides crucial information if the mechanism of an ionic dissociation is examined. The MI spectrum is less useful if one wants to probe the structure (atom connectivity) of the non-reacting ions.

Collision-induced dissociation mass spectra

A collision-induced dissociation (CID) spectrum represents the most common MS/MS experiment. The spectrum is obtained in the same manner as the metastable ion spectrum [10] but now the keV beam of mass-selected ions passes through a 1 cm x 1 cm cell with narrow entrance and exit slits in the 2ffr. The cell, c_4 in Fig. 1.1, is pressurized with an inert gas like He or O_2, referred to as the collision gas. Differential pumping ensures that only within the cell a relatively high collision gas pressure, ca 10^{-5} torr, is maintained.

The experimental set up is such that we are primarily monitoring the ionic dissociation products of a single glancing collision of the high energy ion with the stationary collision gas. Such an interaction between the ion and the electrons of the collision gas leads to electronic excitation of the ion rather than transfer of momentum between the ion and the nuclei of the collision gas. Note that the collision gas cannot chemically react with the ion. CID spectra obtained with He, O_2 and other collision gases like Ar and N_2 are normally closely similar in appearance. However, the use of O_2 sometimes yields CID spectra which show a unique peak of minor intensity but of great structure diagnostic value [11].

The collision gas acts to impart internal energy into the ion of interest to promote its dissociation. As in electron impact ionization, the collisional activation process yields ions with a fairly broad range of internal energies. As a result a CID spectrum displays a range of dissociation reactions. Some of these may be energy demanding direct bond cleavage reactions which may be used to elucidate the structure of the ion. However, CID spectra are more often used as mere fingerprint spectra to characterize the ion, particularly in quadrupole type experiments, see below.

The intensity of a CID fragment ion depends on the energy requirement for the dissociation reaction in question relative to that of competing processes. Thus, one may deduce the structure of an ion on the basis of the collision induced dissociations that it displays and the thermochemistry of these reactions. The appropriate heats of formation may not be available, especially for the ionic components, and, if a rearrangement is involved, a reverse energy barrier must also be accounted for. Here computational chemistry plays an increasingly important role, see Section 1.2.2.

As the number of collisions is limited to one, the mean free path of the precursor ions in the cell is still quite high and so the degree of fragmentation observed is only modest, less than 1%. On the other hand, high energy CID spectra are of more structure diagnostic value than the CID spectra obtained in the quadrupole collision cell of a triple quadrupole mass spectrometer. In CID mass spectrometry with quadrupoles, nowadays a very common technique, we are dealing with mass selected (first quadrupole) precursor ions of low translational energy (only a few eV) that undergo multiple collisions in the second rf-only quadrupole resulting in only a few dissociations. The precursor ion beam remains focused during the collision processes because the rf-only field steers any collisionally scattered ions back to the path of the main beam [12].

If the high energy ions in a magnetic sector instrument are decelerated to a few eV before they enter the collision gas chamber, it is possible to observe structure diagnostic associative ion-molecule reactions [13]. The experimental set up for such an experiment is not routinely available : it is a special feature of a magnetic sector/ quadrupole hybrid instrument [14].

Neutralization-reionization mass spectra

Neutralization-reionization (NR) mass spectrometry is an MS/MS technique eminently suited to explore the structure and reactivity of "unbottleable" neutral species [15].

To obtain a NR spectrum the collision chambers c_2 and c_4 in the 2ffr of the instrument, see Fig. 1.1, are both pressurized. The first chamber is pressurized to 10^{-4} torr with a gas that promotes collisional neutralization by charge exchange but is less prone to cause collision-induced dissociation. Good neutralization gases are organic vapours of low ionization energy like N,N-dimethyl aniline (NDMA) and CH_3SSCH_3 but other target gases including Hg vapour, Xe and NO are also suitable [16,17].

The neutralization gas will neutralize a small portion of the incoming beam of mass selected ions (a vertical process). All unreacted precursor ions as well ionic dissociation products are deflected by the charged deflector electrode and so only fast moving neutrals enter chamber c_4, see Fig. 1.3. Here, they are reionized by collision with O_2 (or He) and part of the reionized species will dissociate. The resulting ions are then analyzed by ESA_1 and detected by the first detector to obtain the neutralization-reionization mass spectrum. The neutralization-reionization efficiency is much lower, by a factor of 1000, than the CID efficiency and thus NR spectra are obtained at a much higher detector gain than CID spectra.

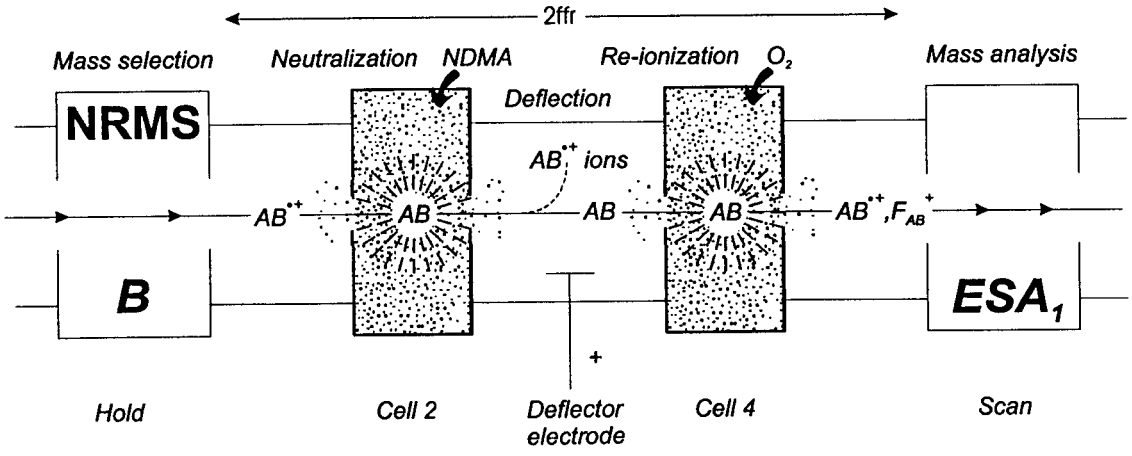

Fig. 1.3. The 2ffr of the instrument set up for a neutralization-reionization experiment, where B is the magnet and ESA_1 is the first electrostatic analyzer.

A NR spectrum is useful to ascertain whether or not a given ion has a stable neutral counterpart or whether it simply dissociates upon neutralization. If the mass-selected ion $AB^{\bullet+}$ remains intact in the reaction sequence $AB^{\bullet+}$ –[neutralization]→ AB – [reionization]→ $AB^{\bullet+}$, the NR spectrum will display a peak at the m/z value of $AB^{\bullet+}$, a "survivor" ion peak. A CID spectrum of the "survivor" ion makes it possible to determine if the incipient neutral species has rearranged into a more stable isomer prior to reionization. Provided the "survivor" ion intensity is sufficiently high, such a NR/CID spectrum may be obtained in the 3ffr, by mass selecting $AB^{\bullet+}$ with ESA_1, pressurizing c_5 with O_2 and scanning ESA_2. The "survivor" CID spectrum of $AB^{\bullet+}$ is then compared with the CID spectrum of source-generated ions $AB^{\bullet+}$, preferably a spectrum obtained in the 3ffr. If the two spectra are virtually the same, this provides good evidence that the neutral counterpart of $AB^{\bullet+}$ is stable and has retained its structure identity. If the spectra are different, the interpretation is not so straightforward. One possibility is that the species AB has isomerized into a more stable neutral isomer BA. This can easily be verified if a reference CID spectrum of $BA^{\bullet+}$ can be obtained. Alternatively, the mass-selected beam of source-generated ions may be isomerically or isobarically impure. This scenario is further discussed in Chapter 5.

Collision-induced dissociative ionization spectra

A collision-induced dissociative ionization (CIDI) experiment is used to identify the neutral lost from a spontaneous dissociation [18]. The ions of interest, $AB^{\bullet+}$, are mass-selected by the magnet and enter the 2ffr where a small fraction spontaneously dissociates, $AB^{\bullet+} \rightarrow A^{+} + B$, in front of the positively charged deflector electrode, see Fig. 1.4. Note that cell c_2 is not pressurized in this experiment, as spontaneous dissociations are normally probed in a CIDI experiment. As the beam of fast moving ions and neutrals reaches the deflector electrode, all ions are deflected away. However, the neutrals with a translational energy (m_B/m_{AB})eV continue to travel down the flight tube. Upon entering collision cell c_4 these neutrals are collisionally ionized, usually with oxygen. The efficiency of this process is not high but the ion yield increases when the

translational energy of the neutral is raised. The ionized neutrals and their charged dissociation products are then analyzed by scanning ESA_1, to yield the CIDI spectrum. The structure of the ionized neutral $B^{\bullet+}$ may be further probed on the basis of its CID spectrum. This spectrum is obtained by selectively transmitting $B^{\bullet+}$ with ESA_1, pressurizing c_5 in the 3ffr with O_2, and analyzing the resulting fragment ions with ESA_2.

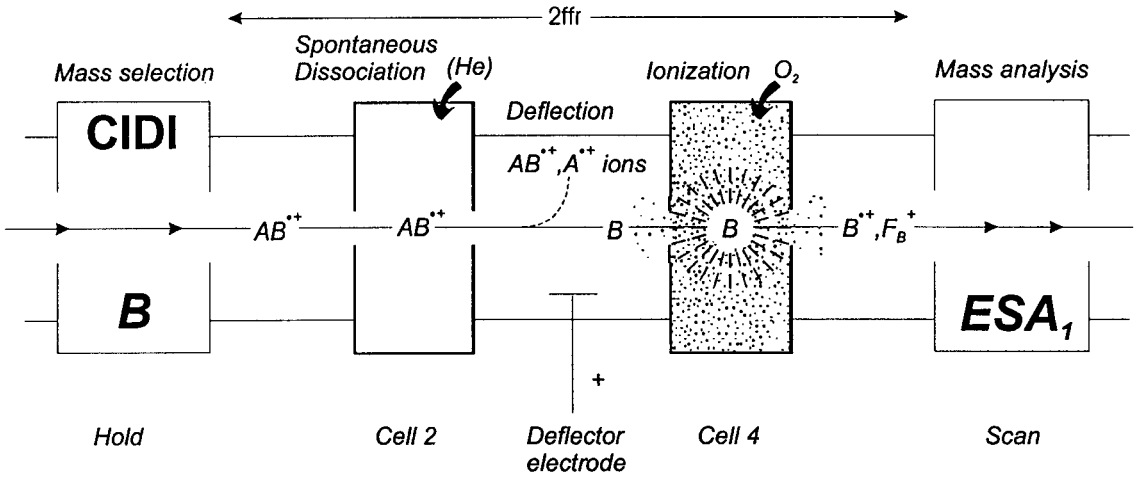

Fig. 1.4. The 2ffr of the instrument set up for a collision-induced dissociative ionization experiment, where B is the magnet and ESA_1 is the first electrostatic analyzer.

Although conceptually simple, CIDI spectra and particularly CIDI/CID spectra are not easy to obtain because the signal strength is usually very low. The signal strength in CIDI/CID spectra can be improved by pressurizing cell c_2 with He : to increase the neutral yield by CID, and by putting a voltage of 2-3 kV on cell c_4 : to increase the fairly low translational energy of the ionized neutral.

1.2.2. Computational chemistry

This thesis deals with the dissociation chemistry of relatively small organic species. Nevertheless, there is a paucity of pertinent thermochemical data, particularly for the organophosphorus ionic and neutral systems studied. Energetic information is indispensable in the study of reaction mechanisms and ion structures and this is why computational chemistry plays a key role in modern gas-phase ion chemistry.

Over the past decade spectacular progress has been made in the field of computational chemistry. An *ab initio* calculation of the energy of a given ion or neutral performed at a certain level of theory with the appropriate basis set results in a fairly crude energy value. From this type of computation only the relative energy of a set of ionic or neutral isomers may be confidently obtained. However, with the recent development of complete model chemistries [19,20], absolute enthalpies of formation can also be calculated. This provides a much better link between the computational results and the energetic information derived from experiment. The accuracy of these enthalpy calculations is high, ± 1 kcal/mol [21], while for small species the computation time on a PC using the Gaussian 98 program [22] is quite reasonable - on the order of a day or two for the ions of Chapter 4. This makes it possible to construct an energy diagram for a given system based on calculations and use that as a guide for the interpretation of the experimental observations. The larger systems described in Chapters 7 and 9 cannot be dealt with on a PC but with the advent of a new generation of super computers, the potential to analyze these larger systems of molecules and ions has become feasible.

In this thesis the CBS-QB3 model chemistry was used [19], where CBS-Q stands for Complete Basis Set extrapolation with Quadratic configuration interaction for geometry optimization and B3 indicates that a B3LYP calculation is used instead for geometry optimization and the frequency calculation. This model chemistry is a composite method comprised of four calculations performed at different levels of theory.

The first calculation involves the geometry optimization of the molecular species under examination. It uses the input geometry and optimizes it to a stationary

point, which corresponds to either a minimum (no imaginary frequencies) or a transition state (one imaginary frequency). The choice of the input geometry is quite important particularly in transition state calculations. This is because the potential energy surface (PES) of a system of ions is usually quite complex. The PES may contain a great many minima, which correspond to stable isomers and conformers residing in energy wells of varying depth. The geometry optimization is performed at the B3LYP/CBSB7 level of theory [23]. This type of calculation is based on density-functional theory (DFT), which uses the total electron density to calculate the energy [24]. Following the geometry optimization, the B3LYP/CBSB7 energy is calculated but not further used. Next this geometry is used for a B3LYP/CBSB7 frequency calculation [25], which gives the 3N-6 vibrational frequencies for the optimized structure of a non linear species (where N = the number of atoms in the species). For a transition state structure, there will be 3N-7 normal frequencies given and one imaginary (negative) frequency, which corresponds to the transition state vibration, i.e. the movement to go from reactant to product. The frequency calculation also provides the zero-point vibrational energy (ZPVE).

The remaining three computational components focus on an *ab initio* calculation of the energy of the optimized structure. A calculation at the MP2 level of theory forms the basis. Two more calculations are performed at higher levels of theory : CCSD(T) and MP4(SDQ) calculations, which are used to estimate the higher-order electron correlation needed to extrapolate the MP2 energy to a more accurate value. The higher level calculations use smaller basis sets than the MP2 calculation.

A basis set mathematically describes the shape of an atom's orbitals and so is a function of each orbital's shape or symmetry [24]. Molecular orbitals are derived from basis functions and angular functions. In the description of an orbital, only the space that is covered by the basis set will be calculated. Therefore, the larger the basis set, the larger the space covered, and so the more accurately the molecular orbital can be calculated. The CBS model chemistry is based on the assumption that the largest error in the *ab initio* calculations comes from the truncation of the basis set and on the assumption that extrapolation at the MP2 level is sufficient, so it extrapolates to the complete basis set limit [26].

As the basic HF calculation averages the electron-electron interaction – this is known as the self-consistent field approximation – it will not provide an accurate total energy for the species [24]. A better energy value may be obtained by adding a correction factor derived from electron correlation methods. This is done by performing Møller-Plesset (MP) type calculations, where MP2 represents a second order perturbation (for singly and doubly excited determinants) and MP4(SDQ) denotes a fourth order perturbation which corrects the HF energy for singly, doubly and quadruply excited determinants, but not triply excited determinants [24b]. In addition, coupled cluster (CC) calculations are used to calculate the electron correlation to an infinite order for a given determinant. The CCSD(T) calculation considers singly and doubly excited determinants to the infinite order and non-iterative triply excited determinants.

The final step of a CBS-QB3 calculation takes the MP2 HF energy for the largest basis set and corrects this value using the CCSD(T) and MP4(SDQ) values for smaller basis sets to yield the desired total energy after the basis set extrapolation, E(CBS-QB3). This total energy refers to the total energy of the ionic or neutral species at zero degrees Kelvin (0K). The 298K enthalpy of formation for the calculated species is obtained by :

$$\Delta H_{f,298} = E(\text{CBS-QB3}) - E_{at} - ZPVE + E_{th} + \Delta H_{f,0}(\text{exp}) - \Delta H_{298}(\text{exp})$$

where E_{at} is the sum of the atomization energies for each atom in the species, ZPVE is the zero point vibrational energy (obtained from the frequency calculation and multiplied by a correction factor of 0.99), E_{th} is the thermal energy correction (obtained from the frequency calculation), $\Delta H_{f,0}(\text{exp})$ is the sum of the experimental $\Delta H_{f,0}$ for each atom in the species and $\Delta H_{298}(\text{exp})$ is the sum of the experimental ΔH_{298} for each atom in the species. The $\Delta H_{f,0}(\text{exp})$ and $\Delta H_{298}(\text{exp})$ values for first and second row elements are given in Ref. 20b.

1.3 Catalyzing the isomerization of a radical cation

A neutral ketone is invariably more stable than its enol counterpart but the removal of an electron by EI ionization leads to a reversal of stability : an ionized enol is thermodynamically more favourable than its keto tautomer. Keto-enol tautomerization is an important aspect of the chemistry of neutral and ionic species containing a carbonyl group [27]. In solution, tautomerization reactions of neutral species take place readily via intermolecular interactions. In the dilute gas-phase, a facile tautomerization does not normally occur : the reaction can only be realized intramolecularly but the barrier for the associated 1,3-H shift is often prohibitively high.

This scenario also pertains to the solitary radical cations generated in an EI experiment. It is not restricted to keto-enol tautomerizations : it applies equally well to the conversion of a radical cation into a more stable distonic isomer via an energetically demanding 1,2-H shift. A distonic ion is a radical cation in which the charge and the radical are located on separate atoms [28]. The name was first coined by Radom et al. [28a] in 1984 to describe the α-distonic ion $^{\bullet}CH_2O^{+}H_2$, an isomer of the methanol radical cation $CH_3OH^{\bullet+}$. This distonic ion is 7 kcal/mol more stable than its isomer of conventional structure [29]. Nevertheless, the isomerization $CH_3OH^{\bullet+} \rightarrow {}^{\bullet}CH_2O^{+}H_2$ is not observed as a unimolecular reaction because the barrier for the intramolecular 1,2-H shift is too high (26 kcal/mol).

To surmount such barriers, one must venture into the field of catalysis. This entails the involvement of a second species, a catalyst, to facilitate the formation of the more stable isomer [30]. The catalyzed isomerization of radical cations in the gas-phase may take place via three mechanisms [31] : proton-transport catalysis in which a neutral molecule acting as a base catalyzes the isomerization [32], a quid-pro-quo mechanism where the catalyst acts as an acid [33] and a "spectator" mechanism in which the catalyst is not directly involved at the site of isomerization [31, 32ac]. The term self-catalysis is used when the neutral counterpart of the substrate ion functions as the catalyst [34]. The mechanism of these reactions will be described briefly in Section 1.3.1. The catalyst must be in close proximity to the substrate and in our gas-phase experiments this is accomplished by forming an encounter complex. How these

encounter complexes are formed and studied in our experimental setup will be discussed in Section 1.3.2.

When the neutral catalyst molecule N approaches the radical cation $M^{\bullet+}$, a stable ion-neutral complex $[M^{\bullet+}\cdots N]$ may be formed. Such a species is characterized by a fairly long electrostatic bond. The stability it enjoys may be considerable if the catalyst has a significant dipole moment. For an ion-dipole complex $[M^{\bullet+}\cdots N]$, the stabilization energy (SE) is given by SE (kcal/mol) = $69\mu\cos\theta/r^2$. In this equation μ (in Debye) is the dipole moment of the catalyst, r (in Å) is the distance between the positive charge and the middle of the dipole vector and θ (in degrees) is the angle between the dipole vector and r [35]. Maximum stabilization is achieved when the dipole vector points directly at the charge. A typical value is 25 kcal/mol (using μ = 1.5 D and r =2 Å) and thus an ion-dipole bond may be energetically on a par with a weak covalent bond.

The long electrostatic bond of the ion-dipole complex allows the catalyst molecule and the ion to adopt a great many configurations by rotation. Some of these may easily lead to the formation of hydrogen-bridged radical cations (HBRCs).

Representing the radical cation $M^{\bullet+}$ as a protonated radical $RH^{\bullet+}$, the HBRCs generated from the ion-dipole complex $[M^{\bullet+}\cdots N]$ are best described as hydrogen-bridged ion-neutral complexes of the type $[R\text{-}H^{\bullet+}\cdots N]$ or $[R^{\bullet}\cdots H\text{-}N^{+}]$, with the bridging H closer to the partner of higher proton affinity. These species typically have a linear R-H-N bridge while most of the stabilization energy is still provided by ion-dipole attractions.

In this context it should be noted that often more than one type of HBRC can be formed. For example, if $M^{\bullet+}$ is $CH_3OH^{\bullet+}$ and N is H_2O the ion-dipole complex $[CH_3OH^{\bullet+}\cdots OH_2]$ could rearrange into an O-H-O bridged ion $[CH_3O\text{-}H\cdots OH_2]^{\bullet+}$ or a C-H-O bridged ion $[HO\text{-}C(H_2)\text{-}H\cdots OH_2]^{\bullet+}$. The C-H-O bridged ion has a much smaller stabilization energy than its O-H-O bridged isomer. Nevertheless, it serves as the key intermediate in the isomerization of $CH_3OH^{\bullet+}$ by proton-transport catalysis, yielding the HBRC $[CH_2O(H)\text{-}H\cdots OH_2]^{\bullet+}$ as the final product. The O-H-O bridged isomer may only play a role in catalysis via the spectator mechanism.

The stabilization energy of HBRCs is very difficult to determine by experiment : a few reliable values are available, but these are confined to O-H-O bridged species. The

SE of O-H-O bridged species can also be confidently estimated by using the empirical relationship SE = 30.4 - 0.30|ΔPA|, where ΔPA is the difference in proton affinity of $R^{\bullet}$ and N [36]. This relationship comes from detailed experimental studies of the SE of the corresponding proton-bound dimers, even electron ions whose energetics is easily accessible via high-pressure mass spectrometry. No such relationship is available for the SE of C-H-O bridged species but fortunately the model chemistries, including CBS-QB3, make it possible to calculate the SE of HBRCs with a high degree of accuracy.

Two more points deserve comment :

(i) If the neutralization energy of $M^{\bullet+}$ equals or exceeds the ionization energy (IE) of the catalyst N, a charge transfer reaction may take place in the ion-dipole complex $[M^{\bullet+}\cdots N]$, yielding ion-neutral complexes of the type $[M\cdots N^{\bullet+}]$. This reaction is undesirable if one wants to probe the isomerization of $M^{\bullet+}$ via a true proton-transport catalysis mechanism. The ionized catalyst molecule may still promote the isomerization of $M^{\bullet+}$ via a variant of the quid-pro-quo mechanism.

(ii) Although only one catalyst molecule is involved in the isomerization reaction, a relatively high concentration of catalyst molecules is often used in our experimental setup. This implies that not only the proton affinity, dipole moment and ionization energy of a potential catalyst are to be considered but also its tendency to undergo self-protonation via the reaction $N^{\bullet+} + N \rightarrow NH^{+} + [N - H]^{\bullet}$. This condition limits the choice of the catalyst to molecules for which this reaction is endothermic.

The conversion of the initially formed ion-dipole complexes into HBRCs enables a H-transfer to take place between the radical cation and the catalyst. The associated mechanisms mentioned above, which involve these encounter complexes are discussed in the next Section.

1.3.1. Mechanisms of catalysis

Proton-transport catalysis

The term proton-transport catalysis (PTC) was first introduced by Böhme [31a] in 1992 in a review article. Following this review, a number of elegant experimental and theoretical studies [30-32] have reported reactions by which a gaseous conventional radical $[H\text{-}X\text{-}Y]^{\bullet+}$ isomerizes into its more stable distonic isomer $[X\text{-}Y\text{-}H]^{\bullet+}$ via interaction with a single catalyst molecule, N. In general, the catalysis reaction described in Eq. 5 has been proposed to take place when the proton affinity (PA) of the catalyst N lies between the PA of the deprotonated radical cation $[X\text{-}Y]^{\bullet}$ at X and Y [30, 31].

$$[H\text{-}X\text{-}Y]^{\bullet+} + N \rightarrow [N\text{••}H^{+}\text{••}X\text{-}Y^{\bullet}] \rightarrow [N\text{••}H^{+}\text{••}Y\text{-}X^{\bullet}] \rightarrow N + [X\text{-}Y\text{-}H]^{\bullet+} \qquad \text{Eq. 5}$$

In this mechanism, the catalyst acts as a base and the two H-shifts involve the transfer of a proton and not a hydrogen radical in the participating HBRCs. It is the stabilization energy of the complexes that makes the isomerization less energy demanding. The catalyst should have the correct PA and IE, and preferably also a large dipole moment to increase the stabilization energy. The water catalyzed isomerization of $CH_3OH^{\bullet+}$ into $CH_2OH_2^{\bullet+}$ [31a] and the enolization of the acetone radical cation with benzonitrile [32e] are two systems in which this mechanism is operative. "Self-proton-transport catalysis" has been documented for the enolization of the acetaldehyde [31b] and acetone radical cations [34].

Quid-pro-quo mechanism

In the quid-pro-quo (QpQ) reaction [31b,33] the catalyst N contains one or more H atoms. The catalyst, represented as A**H**, acts as an acid in this mechanism by first donating the hydrogen radical $\mathbf{H}^{\bullet}$ to the substrate radical cation $HXY^{\bullet+}$. The resulting $HXY\mathbf{H}^{+}$ ion then gives back a different $H^{\bullet}$ to the catalyst to generate $XY\mathbf{H}^{\bullet+}$ ions. The catalyst retains its structure, albeit it now contains one of the substrate's hydrogen atoms :

$$HXY^{\bullet+} + \mathbf{H}A \rightarrow [HXY^{\bullet+}\text{•••}\mathbf{H}\text{-}A] \rightarrow [HXY\text{-}\mathbf{H}^{+}\text{•••}A^{\bullet}] \rightarrow [A^{\bullet}\text{•••}HXY\mathbf{H}^{+}] \rightarrow XY\mathbf{H}^{\bullet+} + HA \qquad \text{Eq. 6}$$

In a variant of the QpQ mechanism, the substrate ion in the encounter complex is first neutralized by charge exchange with the catalyst so that the first hydrogen transfer is that of a proton, H^+. The second hydrogen transfer involves a different atom which is back-donated as a radical, $H^\bullet$:

$$HXY^{\bullet+} + HA \rightarrow [HXY\cdots H\text{-}A^{\bullet+}] \rightarrow [HXY\text{-}H^+\cdots A^\bullet] \rightarrow [A^\bullet\cdots HXYH^+] \rightarrow XYH^{\bullet+} + HA \qquad \text{Eq. 7}$$

This option requires that the IE of the catalyst be lower than the neutralization energy of the substrate ion.

A deuterium labelling experiment can be used to differentiate between a QpQ mechanism and true proton-transport catalysis. Using *either* a fully deuterated substrate *or* a fully deuterated catalyst, the QpQ mechanism will lead to a H/D exchange between the substrate and the catalyst and thus give rise to a 1 Da mass shift of the isomerized product ion.

The catalyst in the QpQ mechanism acts as an acid and not as a base as in the PTC mechanism. Therefore, the criterion for a successful catalyzed isomerization is not the proton-affinity but the bond dissociation energy (BDE). In the QpQ reaction the H-A and H-X bonds are broken, whereas the H-Y bond remains intact. Burgers and Ruttink, in a detailed computational study on the catalyzed tautomerization of ionized acetaldehyde [31b], have proposed that the catalysis will be successful if the BDE [H-$XYH^{\bullet+}$] < BDE [H-A] < BDE [$HXY\text{-}H^{\bullet+}$]. This criterion ensures that the hydrogen abstraction from the catalyst is an irreversible process.

The enolization of the acetamide radical cation with benzonitrile is an example of a well-documented QpQ reaction [33b]. This reaction is also responsible for the tautomerization of the ethylene phosphonate radical cation studied in Chapter 3.

Spectator mechanism

In this mechanism, the catalyst forms a stable complex with the radical cation via ion-dipole interactions and/or hydrogen bridging, but it does not abstract or donate a proton or a hydrogen radical :

$$[H\text{-}X\text{-}Y]^{\bullet+} + N \rightarrow [N\bullet\bullet YX\text{-}H^{\bullet+}] \rightarrow [N\bullet\bullet Y(H)\text{-}X^{\bullet+}] \rightarrow N + [H\text{-}Y\text{-}X]^{\bullet+} \qquad \text{Eq. 8}$$

A catalyst with a large dipole moment may stabilize the [N••YX-H$^{\bullet+}$] complex to such an extent that the transition state (TS) for the ion's isomerization in the complex lies at or below the energy level for HXY$^{\bullet+}$ + N at large separation. Note that this does not necessarily mean that the H-shift barrier has become lower than that of the unassisted isomerization. In fact, in the spectator mechanism describing the water assisted isomerization of $CH_3OH^{\bullet+}$, the ion-dipole complex [$CH_3OH^{\bullet+}$•••OH_2] rearranges into the O-H-O bridged ion [CH_3O-H•••OH_2]$^{\bullet+}$ whose isomerization into [CH_2O(H)-H•••OH_2]$^{\bullet+}$ requires slightly more energy than the unassisted distonicization. On the other hand, the overall reaction as described in Eq. 8 starting from $CH_3OH^{\bullet+}$ + H_2O is slightly exothermic [31a].

So far, only computational information on the feasibility of this mechanism is available. For the $CH_3OH^{\bullet+}$ + H_2O system the reaction is in principle possible but it cannot compete with proton-transport catalysis, which is energetically much more attractive. This is also true for the enolization of acetaldehyde ions [31b] and probably for all keto-enol tautomerizations.

1.3.2. Studying molecule-assisted isomerization reactions in the ZAB-R mass spectrometer

This section gives a brief account of the research methodology used to study catalysis in ion-molecule encounter-complexes with a magnetic deflection type mass spectrometer. We will use unpublished observations on the catalyzed tautomerization of the acetophenone radical cation, $C_6H_5C(=O)CH_3^{\bullet+}$, **1**$^{\bullet+}$, as an example. The unimolecular chemistry of **1**$^{\bullet+}$ and that of its enol $C_6H_5C(OH)=CH_2^{\bullet+}$, **2**$^{\bullet+}$, has been documented [37]. The catalyzed tautomerization has also been reported [38], but using Fourier Transform-Ion Cyclotron Resonance (FT-ICR) as the methodology.

The enol is not available as a neutral molecule but its ionic counterpart can be conveniently generated by dissociative ionization of the commercially available butyrophenone, $C_6H_5C(=O)CH_2CH_2CH_3$, via a McLafferty rearrangement :

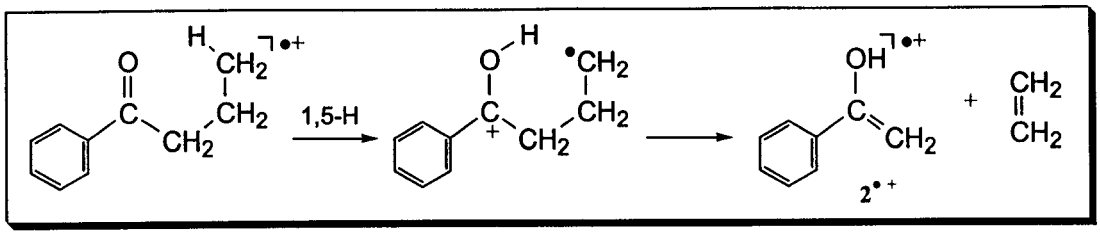

Scheme 1.1

The energy diagram of Scheme 1.2, which is based solely on experimental observations [37-39], summarizes the available information on the tautomerization of solitary ions $\mathbf{1}^{\bullet+}$.

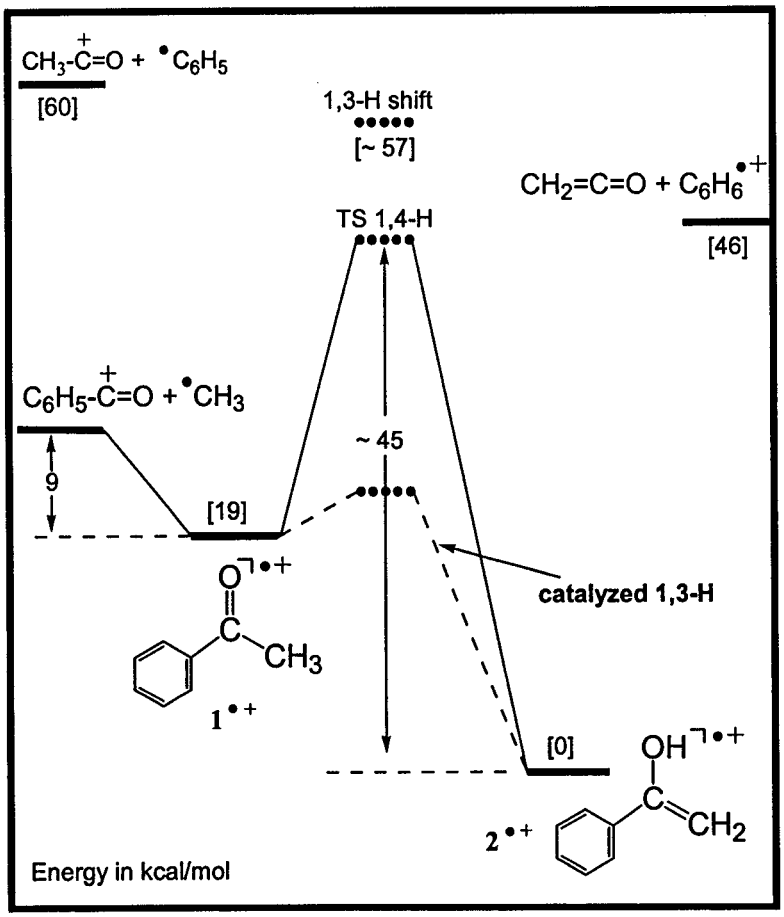

Scheme 1.2

It is seen that the enol ion $\mathbf{2}^{\bullet+}$ is considerably more stable than its keto tautomer. However, the keto ion $\mathbf{1}^{\bullet+}$ does not enolize : the enolization barrier is much higher in energy than direct dissociation by loss of $CH_3^{\bullet}$, the only reaction observed in the MI

spectrum of $\mathbf{1}^{\bullet+}$. We further note that tautomerization via a 1,3-H shift is more energy demanding than isomerization via two consecutive 1,4-H shifts :

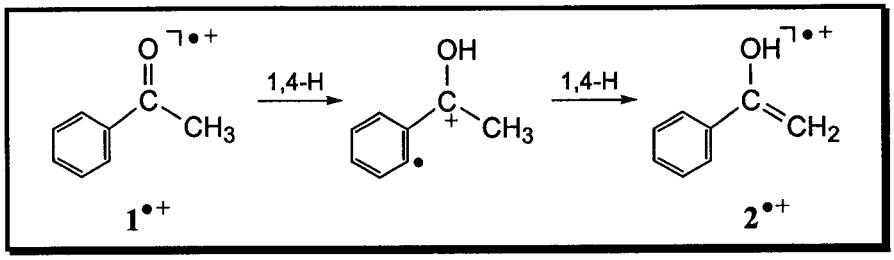

$\mathbf{1}^{\bullet+}$ $\mathbf{2}^{\bullet+}$

Scheme 1.3

This follows from an analysis of the MI spectrum of $\mathbf{2}^{\bullet+}$ and selected deuterium labelled isotopologues. Metastable ions $\mathbf{2}^{\bullet+}$ lose both CH_2=C=O and $CH_3^{\bullet}$. The latter reaction involves the reverse of the route depicted in Scheme 1.3 to yield highly excited keto ions that immediately dissociate. The MI spectra are therefore less suited for the characterization of the two tautomers than their CID spectra. The CID spectra are presented in Fig. 1.5 as items (a) and (b). It is seen that the spectrum of the keto ion, $\mathbf{1}^{\bullet+}$, is dominated by loss of $CH_3^{\bullet}$, whereas that of the enol ion, $\mathbf{2}^{\bullet+}$, is characterized by structure diagnostic peaks at m/z 42, H_2C=C=$O^{\bullet+}$, m/z 78, $C_6H_6^{\bullet+}$ and m/z 102, $C_8H_6^{\bullet+}$. These peaks are cleanly shifted to m/z 44, m/z 84 and m/z 108, respectively in the CID spectrum of the fully deuterated isotopologue.

The energy diagram of Scheme 1.2 further dictates that a catalyzed enolization of $\mathbf{1}^{\bullet+}$ can only be achieved if the catalyst lowers the isomerization barrier to less than 9 kcal/mol relative to the keto ion.

As mentioned above, a successful catalytic enolization of $\mathbf{1}^{\bullet+}$ has been reported by the Audier group using an FT-ICR instrument [38]. In their experiments acetone was used as the catalyst. Using the deuterium labelled isotopologue $C_6D_5C(=O)CH_3^{\bullet+}$ as the substrate keto ion, it could be shown that its acetone-catalyzed enolization takes place via a 1,3-H transfer : $C_6D_5C(=O)CH_3^{\bullet+} \rightarrow C_6D_5C(OH)=CH_2^{\bullet+}$. The resulting enol ion was characterized by ion-molecule reactions.

If the molecule assisted isomerization of $\mathbf{1}^{\bullet+}$ involves proton-transport catalysis, the PTC criterion, see the previous section, stipulates that the PA of the catalyst lie between that of **C** and **O** in the $C_6H_5C(=O)CH_2^{\bullet}$ radical. Accurate numbers are not available but an estimate yields 190 – 210 kcal/mol. Acetone has a PA of 197 kcal/mol [40] and thus it satisfies the PTC criterion. We cannot use acetone in our experimental setup because it readily undergoes self-protonation under conditions of chemical ionization. However, benzonitrile and acetophenone itself (PA = 194 and 206 kcal/mol respectively [40]) are viable alternatives as seen in the next section.

1.3.3 Catalysis of acetophenone ions in encounter complexes

To study the catalyzed enolization of acetophenone ions $\mathbf{1}^{\bullet+}$ in our instrument, radical cations of the type [$\mathbf{1}^{\bullet+}$•••catalyst] were generated as stable species in a chemical ionization (CI) experiment. This was accomplished by introducing a 10 : 1 mixture of catalyst (benzonitrile) and substrate (acetophenone) into the ion source to give a measured pressure of ca 10^{-4} torr. The relatively high source pressure allows the energy rich encounter complexes to lose part of their internal energy by unreactive collisions. In this manner (meta)stable complexes are formed which, upon acceleration and mass analysis, enter the 2ffr where their dissociation characteristics can be probed. The encounter complexes were not stabilized in the FT-ICR experiments described above.

The mass spectrum of this CI type experiment displays an intense peak at m/z 223, the m/z value of [$\mathbf{1}^{\bullet+}$•••BN] but there is also a sizable peak at m/z 240 corresponding with the dimer radical cation [$\mathbf{1}^{\bullet+}$•••**1**] in which the neutral substrate may act as the catalyst. A subsequent MI or CID experiment in the 2ffr shows that both ions abundantly generate m/z 120 ions*. These ions will be either enol ions $\mathbf{2}^{\bullet+}$ or keto ions $\mathbf{1}^{\bullet+}$, depending on whether or not the catalysis was successful.

*Benzonitrile has a higher IE, 9.62 eV [39], than either **1** (9.29 eV) [39] or **2** (8.01 eV) [41]. Hence, BN will be the neutral lost from metastable ions [**1**/$\mathbf{2}^{\bullet+}$•••BN]. On the other hand, **2** has a lower IE than **1**, thus **1** should be the neutral lost metastably from the [**1**/$\mathbf{2}^{\bullet+}$•••**1**] dimer ions should enolization occur.

The structure of these m/z 120 ions was examined by a CID experiment in the 3ffr, see items (c) and (d) in Fig. 1.5. A comparison of these spectra with the reference spectra for $\mathbf{1}^{\bullet+}$ and $\mathbf{2}^{\bullet+}$ in Fig. 1.5, leaves little doubt that benzonitrile does not promote the enolization, whereas acetophenone does.

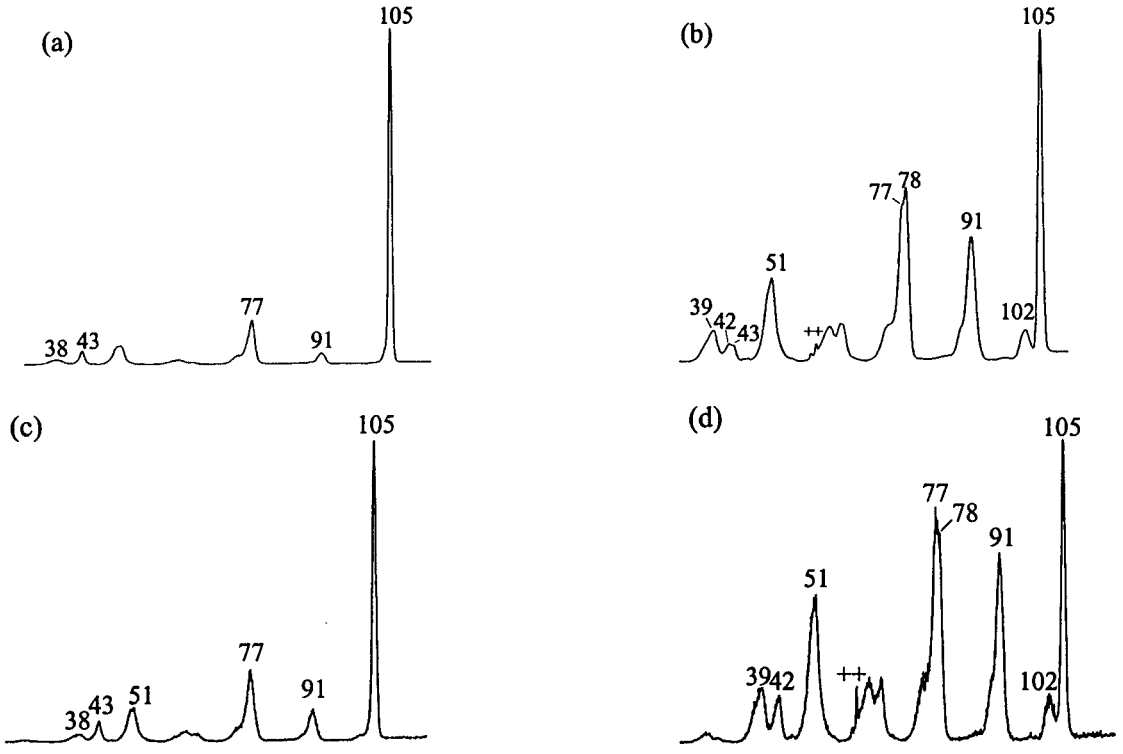

Fig. 1.5. CID spectra of ion $\mathbf{1}^{\bullet+}$, item (a) and its enol $\mathbf{2}^{\bullet+}$, item (b) ; items (c) and (d) represent the CID spectra of m/z 120 ions generated from metastable ions [$\mathbf{1/2}^{\bullet+}$•••BN] and [$\mathbf{1/2}^{\bullet+}$•••**1**] respectively.

Thus benzonitrile does not catalyze the enolization of the acetophenone radical cation. On the other hand, the self-catalysis is clearly successful and experiments with the deuterium labelled isotopologues $C_6D_5C(=O)CH_3$ and $C_6D_5C(OH)=CH_2$ can now be used to probe the mechanism. Metastable dimer ions [$\mathbf{1}(d_5)^{\bullet+}$•••$\mathbf{1}(d_5)$] generate m/z 125 ions exclusively and their CID spectrum is presented in Fig. 1.6, item (a). This spectrum is virtually identical with that of the reference ion $C_6D_5C(OH)=CH_2^{\bullet+}$, $\mathbf{2}^{\bullet+}(d_5)$, compare

with item (b) of Fig. 1.6. The reference ion $\mathbf{2}^{\bullet+}(d_5)$ was generated by dissociative electron impact ionization of the butyrophenone isotopologue $C_6D_5C(=O)CH_2CH_2CH_3^{\bullet+}$, which cleanly loses C_2H_4, via a McLafferty rearrangement.

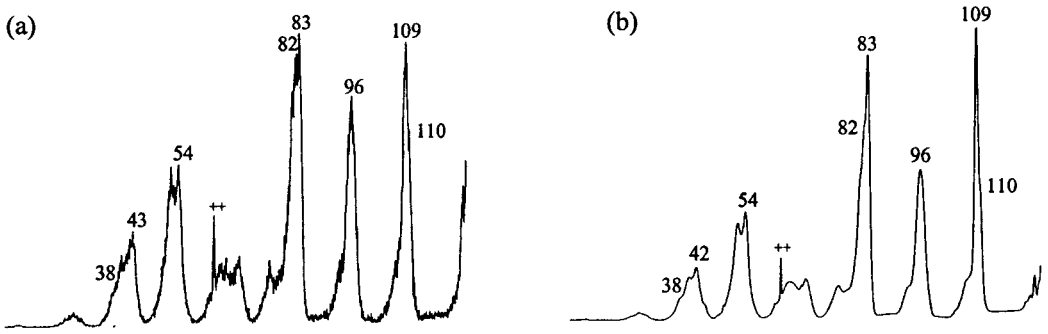

Figure 1.6. CID spectra of m/z 125 ions (a) generated from $[AP(d_5)/AP(d_5)]^{\bullet+}$ (b) of $\mathbf{2}^{\bullet+}(d_5)$ generated from d_5-butyrophenone ions

In summary, in ion-molecule reactions between acetophenone ions and neutrals, dimer radical cations $[\mathbf{1}^{\bullet+}\bullet\bullet\mathbf{1}]$ are generated in which the ion undergoes a molecule-assisted enolization yielding $[\mathbf{2}^{\bullet+}\bullet\bullet\mathbf{1}]$. From the deuterium labelling experiments it follows that the enolization takes place via a 1,3-H shift, as in the case of Audier's FT-ICR experiments with acetone. Both reactions may take place via the PTC mechanism : this could be substantiated by further labelling experiments. Benzonitrile has a similar PA to acetone but, surprisingly, it does not promote enolization in our experiments.

References

[1] R.G. Cooks, J.H. Beynon, R.M. Caprioli, G.R. Lester, *Metastable Ions*, Elsevier, Amsterdam (1973).

[2] A.E. Ashcroft, *Ionization Methods in Organic Mass Spectrometry*, The Royal Society of Chemistry, Cambridge (1997).

[3] (a) W. Frost, *J. Chim. Phys. Phys.-Chim. Biolog.* **87** (1990) 715; (b) W. Frost, *Chem. Rev.* **71** (1971) 339; (c) T. Baer, P.M. Mayer, *J. Am. Soc. Mass Spectrom.* **8** (1997) 103.

[4] K. Levsen, *Progress in Mass Spectrometry : Fundamental Aspects of Organic Mass Spectrometry*, Vol. 4, H. Budzikiewicz, Ed., Verlag Chemie, Weinheim (1978).

[5] F.W. McLafferty, F. Tureček, *Interpretation of Mass Spectra*, 4th ed., University Science Books, California (1993).

[6] (a) A.G. Harrison, *Chemical Ionization Mass Spectrometry*, 2nd ed., CRC Press, Florida (1992); (b) J. Chapman, *Practical Organic Mass Spectrometry : A Guide for Chemical and Biochemical Analysis*, Wiley, New York (1993).

[7] (a) K.L. Busch, G.L. Glish, S.A. McLuckey, *Mass Spectrometry/Mass Spectrometry: Techniques and Applications of Tandem Mass Spectrometr*, VCH Publishers Inc., New York (1988); (b) F.W. McLafferty, Ed., *Tandem Mass Spectrometry*, John Wiley and Sons, New York (1983).

[8] (a) J.L. Holmes, J.K. Terlouw, *Org. Mass Spectrom.* **15** (1980) 383; (b) J. Laskin, Ch. Lifshitz, *J. Mass Spectrom.* **36** (2001) 459.

[9] (a) W. Bertrand, G. Bouchoux, *Rapid Commun. Mass Spectrom.* **12** (1998) 1697; (b) J.K. Terlouw, J. Wezenberg, P.C. Burgers and J.L. Holmes, *Chem. Commun.* (1983) 1121.

[10] (a) R.G. Cooks, *J. Mass Spectrom.* **30** (1995) 1215; (b) B. Stevens, *Collisional Activation in Gases*, Pergamon Press, Oxford (1967).

[11] R. Flammang, V. Henrotte, P. Gerbaux, M.T. Nguyen, *Eur. Mass Spectrom.* **6** (2000) 3.

[12] K.R. Jennings, *Int. J. Mass Spectrom.* **200** (2000) 479.

[13] (a) P. Gerbaux, M. Barbieux-Flammang, J.K. Terlouw, R. Flammang, *Int. J. Mass Spectrom.* **206** (2001) 91; (b) M.A. Trikoupis, P. Gerbaux, D.J. Lavorato, R. Flammang, J.K. Terlouw, *Int. J. Mass Spectrom.* **217** (2002) 1.

[14] (a) R.H. Bateman, J. Brown, M. Lefevere, R. Flammang, Y. van Haverbeke, *Int. J. Mass Spectrom. Ion Processes* **115** (1992) 205; (b) R. Flammang, Y. van Haverbeke, C. Braybrook, J. Brown, *Rapid Commun. Mass Spectrom.* **9** (1995) 795.

[15] For selected reviews see : (a) G. Schalley, G. Hornung, D. Schröder, H. Schwarz, *Chem. Soc. Rev.* **27** (1998) 91; (b) N. Goldberg, H. Schwarz, *Acc. Chem. Res.* **27** (1994) 34.

[16] C.E.C.A. Hop, J.L. Holmes, *Org. Mass Spectrom.* **26** (1991) 476.

[17] (a) F. Tueček, M. Gu, C.E.C.A. Hop, *J. Phys. Chem.* **99** (1995) 2278; (b) S. Vivekananda, R. Srinivas, *Int. J. Mass Spectrom. Ion Proc.* **171** (1997) 79.

[18] (a) J.K. Terlouw, H. Schwarz, *Angew. Chem. Int. Ed. Engl.* **26** (1987) 805; (b) M.A. Trikoupis, J.K. Terlouw, P.C. Burgers, M. Peres, Ch. Lifshitz, *J. Am. Soc. Mass Spectrom.* **10** (1999) 869.

[19] (a) J.A. Montgomery Jr, M.J. Frisch, J.W. Ochterski, G.A. Petersson, J. Chem. Phys. **110** (1999) 2822; (b) ibid. **112** (2000) 6532.

[20] (a) L.A. Curtis, K. Raghavachari, G.W. Trucks, J.A. Pople, J. Chem. Phys. **94** (1991) 7221; (b) A. Nicolaides, A. Rauk, M.N. Glukhovtsev, L. Radom, *J. Phys. Chem.* **100** (1996) 17460.

[21] (a) G.A. Petersson, D.K. Malick, W.G. Wilson, J.W. Ochterski, J.A. Montgomery Jr, M.J. Frisch, *J. Chem. Phys.* **109** (1998) 10570; (b) L.A. Curtiss, K. Raghavachari, P.C. Redfern, B.B Stefanov, *J. Chem. Phys.* **108** (1998) 692; (c) L.A. Curtiss, K. Raghavachari, P.C. Redfern, J.A. Pople, *J. Chem. Phys.* **106** (1997) 1063.

[22] M.J. Frisch et al., Gaussian 98, Revision A.9, Gaussian, Inc.: Pittsburgh, PA, 1998.

[23] (a) A.D. Becke, *J. Chem. Phys.* **98** (1993) 5648; (b) C. Lee, W. Yang, and R. G. Parr, *Phys. Rev. B* **37** (1988) 785; (c) R. Krishnan, J. S. Binkley, R. Seeger and J. A. Pople, *J. Chem. Phys.* 72 (1980) 650.

[24] (a) D.C. Young, *Computational Chemistry : A practical guide for applying techniques to real-world problems*, Wiley Interscience, New York (2001); (b) F. Jensen, *Introduction to Computational Chemistry*, John Wiley and Sons Ltd., Chichester (1999).

[25] J.B. Foresman, M.J. Frisch, *Exploring Chemistry with Electronic Structure Methods*, 2nd ed., Gaussian, Inc., Pittsburgh (1996).

[26] J.A. Montgomery Jr, J.W. Ochterski, G.A. Petersson, *J. Chem. Phys.* **101** (1994) 5900.

[27] B. Capon, B.-Z. Guo, F.C. Kwok, A. K. Siddhanta, Z. Zucco, *Acc. Chem. Res.* **21** (1988) 135.

[28] (a) L. Radom, W.J. Bouma, R.H. Nobes, B.F. Yates, *Pure Appl. Chem.* **56** (1984) 1831; (b) S. Hammerum, *Mass Spectrom. Rev.* **7** (1988) 123; (c) K.M. Stirk, L.K.M. Kiminkinen, H.I. Kenttämaa, *Chem. Rev.* 92 (1992) 1649; (d) H.I. Kenttämaa, *Org. Mass Spectrom.* **29** (1994) 1.

[29] (a) W.J. Bouma, J.K. MacLeod, L. Radom, *J. Am. Chem. Soc.* **104** (1982) 2930; (b) J.L. Holmes, F.P. Lossing, J.K. Terlouw, P.C. Burgers, *J. Am. Chem. Soc.* **104** (1982) 2931; (c) B.F. Yates, W.J. Bouma, L. Radom, *J. Am. Chem. Soc.* **109** (1987) 2250; (d) J.W. Gauld, L. Radom, *J. Phys. Chem.* **98** (1994) 777.

[30] For an early review see : D.K. Böhme, Int. J. Mass Spectrom.Ion Proc. **115** (1992) 95.

[31] (a) J.W. Gauld and L. Radom, J. Am. Chem. Soc. **119** (1997) 9831; (b) M. Haranczyk, P.C. Burgers, P.J.A. Ruttink, *Int. J. Mass Spectrom.* **220** (2002) 53.

[32] For selected references see: (a) J.W. Gauld, H-E. Audier, J. Fossey and L. Radom, J. Am. Chem. Soc. **118** (1996) 6299; (b) A.J. Chalk and L. Radom, J. Am. Chem. Soc. **119** (1997) 7573; (c) A.J. Chalk and L. Radom, J. Am. Chem. Soc. **121** (1999) 1574; (d) M. A. Trikoupis, D. J. Lavarato, J. K. Terlouw, P. J. A. Ruttink and P. C. Burgers, European Mass Spectrom. **5** (1999) 431; (e) M.A. Trikoupis, J.K. Terlouw, P.C. Burgers, *J. Am. Chem. Soc.* **120** (1998) 12131.

[33] (a) L.N. Heydorn, P.C. Burgers, P.J.A. Ruttink, J.K. Terlouw, *Int. J. Mass Spectrom.*, in press; (b) M.A. Trikoupis, P.C. Burgers, P.J.A. Ruttink, J.K. Terlouw, *Int. J. Mass Spectrom.* **210/211** (2001) 489.

[34] M.A. Trikoupis, P.C. Burgers, P.J.A. Ruttink, J.K. Terlouw, *Int. J. Mass Spectrom.* **217** (2002) 97.

[35] P.C. Burgers, J.K. Terlouw, *Encyclopedia of Spectroscopy and Spectrometry*, J.C. Lindon, G.E. Tranter, J.L. Holmes (Eds.), Academic Press, London (2000) 990 – 1000.

[36] M. Meot-Ner (Mautner), *J. Am. Chem. Soc.* **106** (1984) 1257.

[37] (a) J.H. Beynon, R.M. Caprioli and T.W. Shannon, Org. Mass Spectrom. **5** (1971) 967; (b) K.B. Tomer, C. Djerassi, Org. Mass Spectrom. **6** (1972) 1285.

[38] J. Chamot-Rooke, G. van der Rest, P. Mourgues, H.E. Audier, *Int. J. Mass Spectrom.* **195/196** (2000) 385.

[39] S.G. Lias, J.E. Bartmess, J.F. Liebman, J.L. Holmes, R.D. Levin and W.G. Mallard, *Gas Phase Ion and Neutral Thermochemistry*, American Chemical Society & The American Institute of Physics for the National Bureau of Standards, New York (1988).
[40] E. P. Hunter and S. G. Lias, *J. Phys. Chem. Ref. Data* **27** (1998) 413.
[41] F. Tueček, Tetrahedron Lett. **27** (1986) 4219.

Chapter 2

Tautomerization and Dissociation of Dimethyl Phosphonate Ions $(CH_3O)_2P(H)=O^{\bullet+}$: Theory and Experiment in Concert

The unimolecular gas phase chemistry of the title ion, $(CH_3O)_2P(H)=O^{\bullet+}$, ($\mathbf{1}^{\bullet+}$) and its tautomer dimethyl phosphite, $(CH_3O)_2P\text{-}OH^{\bullet+}$, ($\mathbf{2}^{\bullet+}$) was investigated using mass spectrometry based experiments in conjunction with computational quantum chemistry. A facile tautomerization of the "keto" ion $\mathbf{1}^{\bullet+}$ into its "enol" isomer $\mathbf{2}^{\bullet+}$ is prevented by a high 1,2-H shift barrier. Instead, $\mathbf{1}^{\bullet+}$ readily isomerizes via a 1,4-H shift to the very stable distonic ion $CH_2O\text{-}(CH_3O)P(H)OH^{\bullet+}$ ($\mathbf{1a}^{\bullet+}$) and related ion-dipole complexes which serve as precursors for the low energy loss of CH_2=O. Loss of CH_2=O is also the major dissociation of the enol ion $\mathbf{2}^{\bullet+}$, which is more stable than $\mathbf{1}^{\bullet+}$ by 31 kcal/mol. The reaction involves a 1,3-H shift leading to $\mathbf{1a}^{\bullet+}$ and, at a marginally higher energy, a competing 1,4-H shift leading to the ion-dipole complex $CH_2O\text{-}P(OH)\text{-}O(H)CH_3^{\bullet+}$ ($\mathbf{1b}^{\bullet+}$). The resulting product ions, viz $(CH_3O)P(H)OH^{\bullet+}$ and $P(OH)\text{-}O(H)CH_3^{\bullet+}$, are separated by a high 1,2-H shift barrier (44 kcal/mol). However, the CH_2O moiety in $\mathbf{1a}^{\bullet+}$ and $\mathbf{1b}^{\bullet+}$ is calculated to reduce this barrier significantly by a mechanism coined as proton-transport catalysis.

The identity of the ions was probed by tandem mass spectrometry methods. These include MI (metastable ion) or CID (collision induced dissociation) spectra, consecutive MI/CID and CID/CID spectra, NRMS (neutralization-reionization mass spectra), NR/CID and CIDI (collision induced dissociative ionization) spectra, time-resolved CID spectra and deuterium labelling. The energetics of the CH_2=O loss from $\mathbf{1}^{\bullet+}$ and $\mathbf{2}^{\bullet+}$ was derived from ionization and appearance energies determined by VUV photoionization. The experimental results agree quite well with the computational findings. Heats of formation, isomerization barriers and dissociation energies of the various ionic and neutral species were obtained by the wavefunction-based CBS-QB3 method. Essentially identical energy profiles on the $C_2H_7O_3P^{\bullet+}$ surface were obtained with the computationally less demanding novel MPW1K empirical DFT method in conjunction with the aug-cc-pVTZ basis set.

Theory and experiment yield a consistent potential energy profile that describes the isomerization and low energy dissociation chemistry of ions $\mathbf{1}^{\bullet+}$ and $\mathbf{2}^{\bullet+}$ (Scheme 2.4). In the μs timeframe ions $\mathbf{1}^{\bullet+}$ have completely isomerized into distonic ions $\mathbf{1a}^{\bullet+}$ which do not significantly communicate with their more stable enol counterparts. However, ion-molecule reactions of $\mathbf{1}^{\bullet+}$ with benzonitrile lead to a complete enolization. This is by virtue of a dipole-assisted lowering of the 1,3-H shift barrier separating $\mathbf{1a}^{\bullet+}$ and $\mathbf{2}^{\bullet+}$.

The work described here has been published previously in an article under the same title: L.N. Heydorn, Y. Ling, G. de Oliveira, J.M.L. Martin, Ch. Lifshitz and J.K. Terlouw, Zeitschrift für Physikalische Chemie **215** (2001) 141-182.

2.1. Introduction

Gas-phase phosphorus ion chemistry is intimately related to solution phosphorus chemistry [1] and the need for its study derives from the intrinsic and practical importance of phosphorus compounds [2, 3] and from the significant role of mass spectrometry in their characterization as pesticides, drugs, and toxic agents [4].

One class of compounds that has attracted a great deal of interest [5] are organophosphorus esters which are widely used as pesticides. The conventional electron impact mass spectra of alkyl and aryl phosphates and phosphites were already studied when the technique was still in its infancy [6] and (crude) energetic information from ionization and appearance energy measurements using non mono-energetic electrons was also obtained [7]. Renewed interest in the gas-phase ion chemistry of these esters started in the mid-eighties when tandem mass spectrometry (MS/MS) [8] using both high and low-energy collision induced dissociation (CID) experiments [9] on magnetic deflection, quadrupole, FT-ICR and ion trap mass spectrometers became available to probe the structure of stable and isomerizing ions [10]. One important highlight of the seminal studies of the Purdue groups of Cooks and Kenttämaa [11] is that the long-lived radical cations of simple organophosphates isomerize spontaneously to more stable distonic ions [11b, 12]. The computational finding that a localized radical center is present at the *oxo* oxygen atom of the initially generated molecular ion may provide a chemical rationalization for this behavior [13].

A case in point is the behavior of trimethyl phosphate (TMP) which upon electron impact rearranges into the distonic ion depicted in Scheme 2.1 and whose lowest energy dissociation route, loss of CH_2=O, yields the m/z 110 radical cation of dimethyl phosphite, $\mathbf{2}^{\bullet+}$. This ion represents the "enol" counterpart of the "keto" ion $\mathbf{1}^{\bullet+}$, ionized dimethyl phosphonate (DMP). The latter ion can be conveniently generated by electron impact ionization of commercially available dimethyl phosphonate, which unfortunately is still sold under the misleading name of dimethyl phosphite [14].

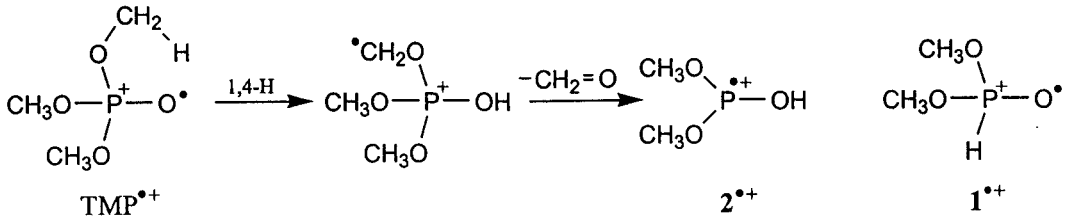

Scheme 2.1

Keto-to-enol isomerization reactions in simple organic radical cations and their neutral counterparts are of fundamental importance and have therefore been studied in great detail by both theory and experiment [15]. In line with this, the tautomerization of DMP has also received considerable attention [11a]. For the neutral counterparts experimental evidence has been presented [16] that the keto form **1** (dimethyl phosphonate) is more stable than the enol form **2** (dimethyl phosphite), by 6.5 kcal/mol. A more recent computational study [17] confirms that the keto form is more stable than the enol form and predicts that the barrier for isomerization is quite high, 62 kcal/mol. Upon one electron oxidation a reversal of stability takes effect analogous to the simple keto-enol system "acetone/ enol of acetone" [18]. By combining experimental results from diverse sources Cooks and Kenttämaa [11a] estimated that the ionized enol, $\mathbf{2}^{\bullet+}$, is more stable than the keto form, by 28 kcal/mol, and that the enolization of the keto ion involves a barrier of 16 – 32 kcal/mol. From the results of single collision experiments, it was further concluded that : "the less stable phosphonate structure, $\mathbf{1}^{\bullet+}$, dissociates almost exclusively via isomerization to the stable phosphite "enol" structure when gently activated, CH_2=O and $CH_3^{\bullet}$ loss; otherwise it fragments directly from structure $\mathbf{1}^{\bullet+}$." In subsequent studies [11b,d] the conclusion is maintained that, in the absence of multiple activating collisions, DMP ions retain their structural integrity on the μs timeframe. From CID experiments in a FT-ICR instrument it was further concluded that at a lifetime of ≥ 1s, DMP ions undergo at least a partial isomerization into the phosphite structure $\mathbf{2}^{\bullet+}$.

Despite this interest in the enolization of ionized dimethyl phosphonate, little or no attention has been paid to the mechanism of the reaction. One possibility, which seems to be implicitly assumed in the existing literature, is that the reaction involves a 1,2-H shift. For the parent acids, i.e. the system phosphorus acid, $HPO(OH)_2$, vs.

trihydroxyphosphine, $P(OH)_3$, this is the only option. A combined computational and experimental study [13] has reported that the lowest energy enol isomer is 11 kcal/mol less stable than $HPO(OH)_2$ but is separated by a barrier of 54 kcal/mol. Conversely, the enol ion is 32.5 kcal/mol more stable than its keto counterpart. Unfortunately the 1,2-H shift barrier for enolization has not been reported. However, the experiments show that the two isomeric ions do retain their structure integrity and thus a sizable isomerization barrier must be involved.

In this context it is of interest to note that in simple ionized ketones like acetone, a large barrier for the 1,3-H shift (37 kcal/mol) prevents isomerization into their more stable enol counterpart [18]. On the other hand, in ionized methyl acetate [19] two less energy demanding (~12 kcal/mol) and therefore more rapid 1,4-H shifts lead to interconversion of ionized keto and enol forms via a distonic ion: $[keto]^{\bullet+} \rightarrow [distonic]^{\bullet+} \rightarrow [enol]^{\bullet+}$, see Scheme 2.2.

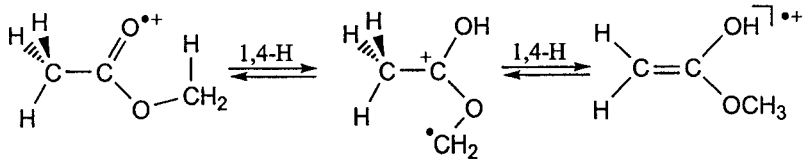

Scheme 2.2

Given the finding referred to above, that the molecular ions of organophosphorus esters are prone to isomerize into more stable distonic ions, it seems likely that such species also play a key role in the keto-enol tautomerization of the DMP system and the common dissociation reaction of lowest energy requirement, loss of CH_2=O. Scheme 2.3 depicts the a priori reasonable possibilities that derive from this concept:

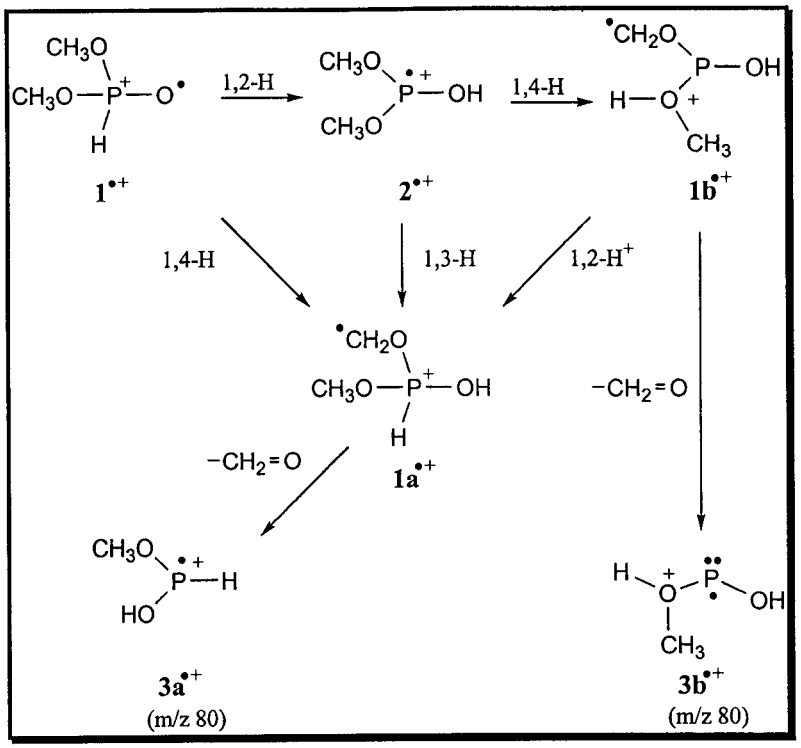

Scheme 2.3

From this Scheme it becomes apparent that the loss of CH_2=O from ions initially generated as $\mathbf{1}^{\bullet+}$ (i.e. by direct ionization of **1**) does not necessarily involve enolization into $\mathbf{2}^{\bullet+}$ as proposed in the literature, see above. Neither must the loss of CH_2=O from $\mathbf{2}^{\bullet+}$ involve $\mathbf{1a}^{\bullet+}$: the enol ions could be envisaged to lose CH_2=O via a 1,4-H shift, yielding m/z 80 product ions, $\mathbf{3b}^{\bullet+}$, having a structure that is different from those generated from the keto ion, $\mathbf{3a}^{\bullet+}$.

It was anticipated that analysis of the m/z 80 product ion structures would shed light on this question. Indeed the tandem mass spectrometry based methodology used in the study (see Section 2.2.2) was successfully used to probe this aspect of the problem. Another significant preliminary observation, which militates against the simple picture that ions $\mathbf{1}^{\bullet+}$ enolize prior to the loss of CH_2=O, is the kinetic energy release [20] associated with this reaction: low energy (metastable) DMP ions yield a $T_{0.5}$ value of 17 meV which is not larger but slightly smaller than that measured for metastable enol ions $\mathbf{2}^{\bullet+}$ derived from TMP, $T_{0.5}$ =21 meV.

Although observations from tandem mass spectrometry based experiments – and also ion-molecule studies using techniques like FT-ICR [11c] – may provide important clues regarding the mechanistic possibilities outlined in Scheme 2.3, energetic information both from experiment and theory is clearly required to arrive at a coherent description of such a system. The available experimentally derived energetic information is incomplete and based on crude experiments and thus we have measured the energetics of both DMP and TMP – the precursor molecule for the enol ion $\mathbf{2}^{\bullet+}$ - using the more reliable technique of single photon VUV photoionization mass spectrometry (PIMS) [21] (see Section 2.2.1). Such experiments may establish the stability of the keto and enol ions and also the energy requirement for CH_2=O loss therefrom, but they do not provide much information on the stabilities of the intermediate distonic ions or on the height of the various barriers for (inter)conversion. Computational chemistry ideally provides this information but until the advent of the very recently published CBS-QB3 hybrid empirical correction/pair extrapolation method [22] (see Section 2.2.3), it would have been very difficult to obtain reliable energetic information on a system of this size and complexity. It is this computational procedure which forms the key element in our three-pronged approach to evaluate the mechanistic pathways associated with the tautomerization of DMP as outlined in Scheme 2.3.

In the first part of this paper we will provide evidence that the DMP ion has a very low barrier towards isomerization into its much more stable distonic counterpart $\mathbf{1a}^{\bullet+}$. As a consequence, the stable and metastable DMP ions sampled for further analysis in the μs timeframe have (very largely) lost their structure integrity and adopted the structure of the distonic ion $\mathbf{1a}^{\bullet+}$ and ion-dipole complexes of the type $\mathbf{3a}^{\bullet+}/CH_2$=O, **ID-**$\mathbf{3a}^{\bullet+}$, derived therefrom. These ions serve as the unique precursor for the CH_2=O loss yielding exclusively product ions of structure $\mathbf{3a}^{\bullet+}$, see Scheme 2.3.

The barrier for enolization of $\mathbf{1}^{\bullet+}$ into $\mathbf{2}^{\bullet+}$ via the kinetically favored 1,2-H shift lies above the threshold for CH_2=O loss and thus this reaction does not take place in low energy ions $\mathbf{1}^{\bullet+}$. On the other hand, experiments with the deuterium labeled DMP isotopologue $(CH_3O)_2P(D)=O^{\bullet+}$ indicate that this rearrangement does occur en route to

some of the fast dissociation reactions of the high energy fraction of DMP molecular ions generated by 70 eV electron ionization and also in the collision induced dissociative ionization (CIDI) of DMP molecules with keV translational energies generated from the decomposition of the proton bound dimer $[DMP{\bullet\bullet\bullet}H{\bullet\bullet\bullet}DMP]^+$.

It will be further shown that the enol ions $\mathbf{2}^{\bullet+}$ reside in a very deep potential well separated by interconversion barriers towards the distonic ions $\mathbf{1a}^{\bullet+}$ and $\mathbf{1b}^{\bullet+}$ which lie close to the threshold for loss of CH_2=O, their dissociation of lowest energy requirement. Metastable enol ions exclusively dissociate via the route $\mathbf{2}^{\bullet+} \rightarrow \mathbf{1a}^{\bullet+} \rightarrow \mathbf{3a}^{\bullet+} + CH_2$=O but, when the stable ions are collisionally activated, the route $\mathbf{2}^{\bullet+} \rightarrow \mathbf{1b}^{\bullet+} \rightarrow \mathbf{3b}^{\bullet+} +$ CH_2=O also becomes accessible. The D-labeled distonic ion $CH_2O(CH_3O)P(D)–(OH)^{\bullet+}$ $(\mathbf{1a}\text{-D})^{\bullet+}$ and the enol ion $(CH_3O)_2P–OD^{\bullet+}$, $\mathbf{2}\text{-OD}^{\bullet+}$, both show a highly specific loss of CH_2=O (80 and 100% respectively) and thus the enol ion and the distonic ion do not readily interconvert.

In this Section we will also present the results of Neutralization-Reionization experiments (NRMS) [23] on ions $\mathbf{1/1a}^{\bullet+}$ and $\mathbf{2}^{\bullet+}$ as well as the product ions $\mathbf{3a}^{\bullet+}$ and $\mathbf{3b}^{\bullet+}$. These experiments, it will be shown, not only provide complementary information regarding the structure assignment of the ions but they also answer the question whether the elusive dimethyl phosphite neutral **2** isomerizes into its more stable counterpart **1**, DMP.

In the second part of the paper we will focus on the behavior of distonic ion $\mathbf{1b}^{\bullet+}$ whose CH_2=O loss may explain the co-generation of m/z 80 ions of structure $\mathbf{3b}^{\bullet+}$ from the enol ion $\mathbf{2}^{\bullet+}$. Ion $\mathbf{1b}^{\bullet+}$ cannot isomerize into the more stable distonic isomer $\mathbf{1a}^{\bullet+}$ because the barrier for the associated 1,2-H shift is prohibitively high. However, it will be shown, ion $\mathbf{1b}^{\bullet+}$ can adopt the configuration of a stable ion-dipole complex of the type $\mathbf{3b}^{\bullet+}/CH_2$=O, $\mathbf{ID\text{-}3b}^{\bullet+}$. This raises the intriguing question whether the CH_2=O dipole in this complex may promote the isomerization of the ionic component $\mathbf{3b}^{\bullet+}$ into its more stable isomer $\mathbf{3a}^{\bullet+}$, via a mechanism which has been coined as intramolecular proton-transport catalysis [24]. Computational evidence will be presented that indeed the barrier for the isomerization of $\mathbf{3b}^{\bullet+}/CH_2$=O into $\mathbf{3a}^{\bullet+}/CH_2$=O is much lower than that for

the 1,2-H shift in the unsolvated ions (13 vs. 44 kcal/mol). Nevertheless, the barrier remains too high to allow a facile interconversion of the distonic ions $\mathbf{1b}^{\bullet+}$ and $\mathbf{1a}^{\bullet+}$.

Proton-transport catalysis in ion-molecule encounter complexes, that is the phenomenon that the neutral promotes the tautomerization of the ionic component of the complex, has recently received a great deal of attention both from theory and experiment [25]. One interesting example is the benzonitrile-assisted enolization of ionized acetone [18]. As mentioned above, enolization of the acetone radical cation into its more stable isomer CH_2=C(OH)$CH_3^{\bullet+}$ does not occur unassisted because the associated 1,3-H shift imposes a high barrier. However, benzonitrile has a proton affinity which is higher than that of the CH_2 and equal to that of the O in the CH_2=C($O^{\bullet}$)CH_3 radical and it successfully catalyzes the enolization. In the third part of this study we will discuss preliminary experimental observations that indicate that benzonitrile also promotes enolization in the dimethyl phosphonate system. However, it is, we propose, the 1,3-H shift barrier for the conversion of the distonic ion $\mathbf{1a}^{\bullet+}$ into the enol ion which is lowered by the BN molecule rather than that BN catalyzes the direct enolization of DMP ions $\mathbf{1}^{\bullet+}$ via the 1,2-H shift.

2.2. Experimental and theoretical preliminaries

2.2.1. Photoionization mass spectrometry

Photoionization mass spectrometry was performed at the Hebrew University on a home-built instrument, which has the hydrogen many-line Hinteregger discharge and helium Hopfield continuum spectra as light sources. The VUV light is dispersed by a 1-m near-normal incidence monochromator. The photoionization efficiency (PIE) scans are obtained by mass analyzing the ions with a quadrupole mass filter and collecting the ion signal as a function of the photon energy. The instrument and method have been extensively reviewed [26, 27]. The results of the IE and AE experiments on DMP and TMP samples (obtained from Aldrich and used without further purification) are collected in Table 2.1, while Fig. 2.1 displays some representative PIE scans.

Table 2.1. Energetic information for the ionized dimethyl phosphonate system derived from Ionization (IE) and Appearance (AE) energy measurements on trimethyl phosphate (TMP) and dimethyl phosphonate (DMP) using VUV Photoionization.

Precursor molecule	IE/AE (eV) this work	IE/AE (eV) literature [ref]		Neutral(s) Lost	m/z	ΔH°_f (298 K) kcal/mol	Ion Structure
TMP	9.95 ± 0.05	9.99	[33]		140	-26	$(CH_3O)_3P{=}O^{\bullet+}$
		10.7 ± 0.1	[7a]				
DMP	10.5 ± 0.05	10.5	[7c]		110	54	$(CH_3O)_2P(H){=}O^{\bullet+}$ **1**$^{\bullet+}$
		10.53	[34]				
TMP	10.7 ± 0.05	11.6 ± 0.1	[7a]	$CH_2{=}O$	110	18	$(CH_3O)_2P(OH)^{\bullet+}$ **2**$^{\bullet+}$
DMP	11.8 ± 0.2	12.7	[7c]	$H^{\bullet}$	109	32	$(CH_3O)_2P{=}O^{+}$
DMP	11.3 ± 0.1	11.9	[7c]	$CH_3^{\bullet}$	95	38	$CH_3O\text{-}P(OH){=}O^{+}$
DMP	10.8 ± 0.1	11.2	[7c]	$CH_2{=}O$	80	88	$CH_3O\text{-}P(H)OH^{\bullet+}$ **3a**$^{\bullet+}$
TMP	12.75 ± 0.05	12.9 ± 0.1	[7a]	2 $CH_2{=}O$	80	92	$CH_3O\text{-}P(H)OH^{\bullet+}$ **3a**$^{\bullet+}$
DMP	12.0 ± 0.2	13.5	[7c]	$CH_2{=}O + H^{\bullet}$	79	64	$CH_3O\text{-}P\text{-}OH^{+}$
				$CH_3O^{\bullet}$	79	(85)	
TMP	14.2 ± 0.1	14.9 ± 0.2	[7a]	2 $CH_2{=}O + H^{\bullet}$	79	73	$CH_3O\text{-}P\text{-}OH^{+}$
				$CH_3O^{\bullet} + CH_2{=}O$	79	(94)	

Table 2.1 also lists ΔH_f (298 K) values for the principal ions of the system studied. These values were calculated by simply using the observed onset energy and 298 K heats of formation of relevant neutral species (see Introduction to [28]) rather than using a more sophisticated treatment [29]. One reason for this approach is the uncertainty in the heats of formation of the parent molecules DMP and TMP. Surprisingly, there are no experimental values [30-32] for either compound and we have thus adopted the CBS-QB3 derived values listed in Table 2.2b, which we expect to be reliable within ± 2 kcal/mol, see below.

The Table shows that there is good agreement between the present IE values and literature results from photoelectron spectroscopy, for TMP [33] and DMP [34], respectively. Electron impact values for the IE of the two precursor molecules and AEs for fragment ions thereof [7a,c] are as usual equal within experimental error or higher than the present PI values and the latter are considered to be more reliable.

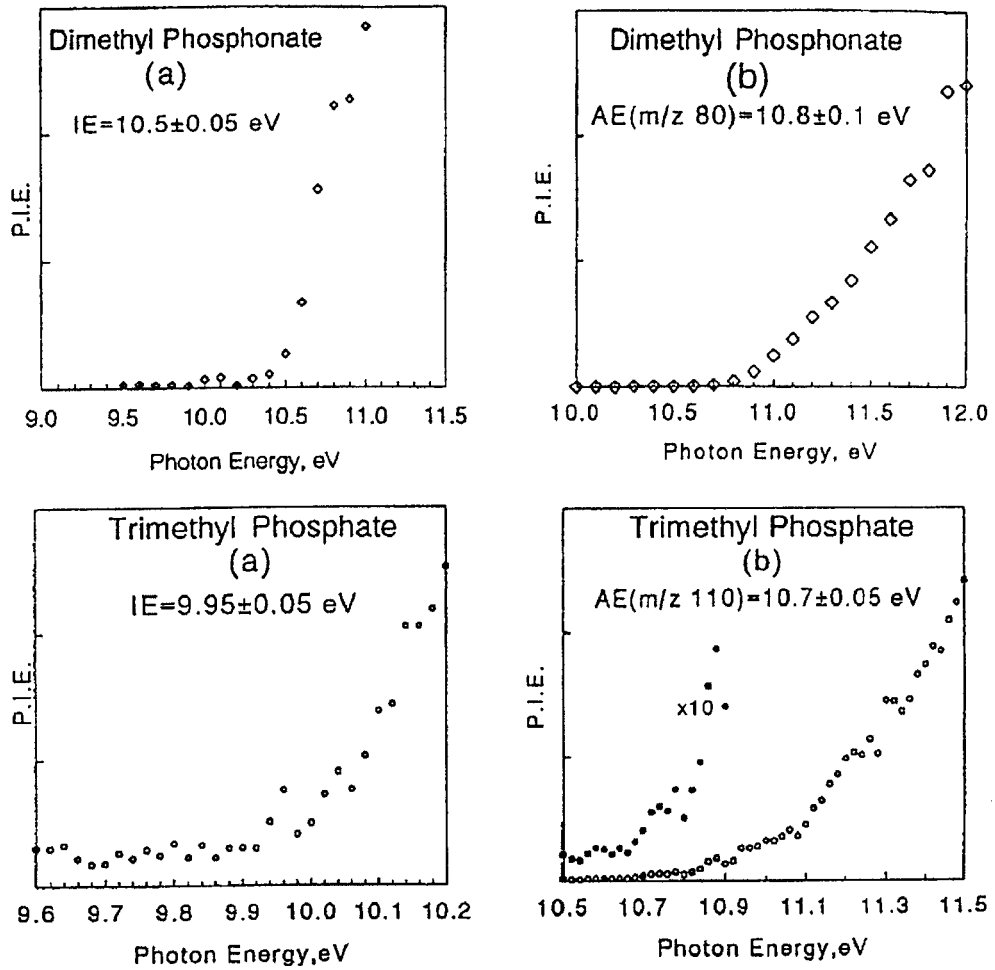

Fig. 2.1. Photoionization efficiency (PIE) curves (in arbitrary units) for dimethyl phosphonate (DMP) and trimethyl phosphate (TMP): (a) molecular ions and (b) fragment ions due to formaldehyde elimination. Ionization of DMP leads to the keto ion $\mathbf{1}^{\bullet+}$ at a mass to charge ratio, m/z 110; elimination of formaldehyde from TMP leads to an ion at m/z 110 that is the enol tautomer $\mathbf{2}^{\bullet+}$ (Scheme 2.1). IE-ionization energy; AE-appearance energy.

2.2.2. Tandem mass spectrometry

Most of the tandem mass spectrometry based experiments were performed with the McMaster University ZAB-R mass spectrometer [35], a three-sector BE_1E_2 (B = magnetic sector, E = electric sector) type instrument whose design is based on the geometry of the VG Analytical ZAB-2F. The instrument is equipped with four collision gas chambers of which the two located in the second field free region (2ffr, in front of E_1) were used for the neutralization-reionization (NR) experiments.

The DMP and TMP samples as well as the 1,2-diaminoethane and benzonitrile used in the ion-molecule experiments were of research grade (Aldrich) and introduced into the ion source (kept at 100 °C) via an all-glass heated inlet system equipped with a leak valve or a direct insertion-type probe having a glass bore and reservoir. The DMP isotopologue $(CH_3O)_2P(D)=O^{\bullet+}$, **1**-D $^{\bullet+}$ was synthesized by the reaction of PCl_3 with CH_3OD in refluxing CCl_4 and displayed an isotopic purity of 90% in the mass spectrometric experiments [36]. The spectrum Fig. 2.2b has been corrected for the contribution of the unlabelled component.

Ions generated in the source by either electron ionization (EI) or ion-molecule reactions under conditions of chemical ionization (CI), were accelerated to 8 or 10 keV prior to recording their spontaneous or collision induced dissociations in the second or the third field free regions as MI (metastable ion) or CID (collision induced dissociation) spectra respectively. The structure of a given product ion in a 2ffr MI or CID spectrum was probed by selectively transmitting the ion by E_1 to a collision chamber in the 3ffr pressurized with O_2 or He and mass-analyzing its ionic dissociation products by scanning E_2. The resulting MS/MS type spectra are denoted as MI/CID and CID/CID spectra respectively. All the (high energy) collision experiments were performed at a main beam transmittance (~ 70%) such that the probability for multiple collisions is negligible [10].

For neutralization–reionization mass spectra (NRMS) [23] 8 or 10 keV ions, $m^{\bullet+}$ are selectively transmitted by B to the 2ffr where, in the first collision chamber, charge-exchange neutralization occurs with *N,N*-dimethyl aniline (NDMA) : $m^{\bullet+}$ [10 keV] + NDMA $\rightarrow$ m [10 keV] + $NDMA^{\bullet+}$. The unreacted ions are deflected away and the remaining fast neutrals are reionized with O_2 in the second collision cell. Scanning E_1 yields the spectrum of the reionized neutrals $m^{\bullet+}$, the "survivor" ions, and their (structure characteristic) charged dissociation products. For CID/NR "survivor" spectra the "survivor" ions resulting from the NR experiment are selectively transmitted by E_1 to the collision chamber in the 3ffr where they undergo collisions with O_2. The ionic dissociation products are mass analyzed by scanning E_2.

CIDI (collision induced dissociative ionization) spectra [37] refer to collisional ionization followed by (partial) dissociation of neutral species N generated from the dissociation of mass selected metastable ions m_1^+ in the 2ffr: m_1^+ [10 keV] $\rightarrow$ m_2^+ [m_2/m_1 • 10 keV] + N [N/m_1 • 10 keV]. Such spectra are obtained with the instrumental setup for NRMS but without using the collision gas chamber for neutralization. Mass selected proton bound dimer ions $[DMP\bullet\bullet\bullet H\bullet\bullet\bullet B]^+$ were used to obtain the CIDI spectrum of DMP. Provided the proton affinity (PA) of B is higher than that of DMP, BH^+ ions and DMP neutrals will dominate the MI spectrum of the mixed proton bound dimer ions. We have chosen $NH_2CH_2CH_2NH_2$ as the base: its PA (227 kcal/mol) [38] is higher than that of DMP (206 kcal/mol) [39] while its relatively low mass improves the resolution of the CIDI spectrum which is strongly dependent on the translational energy of the neutrals. The CIDI spectrum of the D labeled DMP isotopologue $(CH_3O)_2P(D)=O^{\bullet+}$, **1**-$D^{\bullet+}$ or DMP-D, could not be obtained in this way because extensive D/H exchange reactions with the diamine precede the formation of the mixed proton bound dimer ions. However, a satisfactory spectrum could be obtained from a CI self-protonation experiment with DMP-D. This yielded a cluster of proton bound dimer ions at m/z 222, 223 and 224 (intensity ratio 1 : 6 : 6) of which the m/z 223 $(DMP\text{-}D)_2H^+$ and m/z 224 $(DMP\text{-}D)_2D^+$ ions, whose MI spectra display a single peak at m/z 112 and m/z 113 respectively, were used as precursors for the formation of high translational energy DMP-D neutrals.

The methoxy groups in TMP can easily be exchanged with CD_3OD to yield mixtures of the D-labeled isotopologues $(CD_3O)_n(CH_3O)_{3-n}P=O$ (n = 0-3) which would prima facie serve as ideal precursors to generate specifically D labeled enol ions, including $(CH_3O)_2P\text{–}OD^{\bullet+}$, **2**-$OD^{\bullet+}$ generated by loss of $CD_2=O$ from $(CD_3O)(CH_3O)_2P=O^{\bullet+}$. Unfortunately, extensive H/D exchange reactions (to the statistical limit for the metastable molecular ions) appear to precede the formaldehyde loss from labeled TMP molecular ions and this severely compromises the analysis. Nevertheless, the desired ions **2**-$OD^{\bullet+}$ could cleanly be generated to study their 3ffr MI and CID spectra by the 2ffr collision induced methoxy loss from ions $(CH_3O)_3P\text{-}OD^+$

generated by the deuteronation of TMP with C_2D_5I under conditions of chemical ionization.

All spectra obtained on the ZAB-R instrument were recorded using a small PC-based data system developed by Mommers Technologies Inc. (Ottawa).

In the above experiments, the mass selected ions sampled for further analysis have lifetimes in the μs timeframe. To study DMP's isomerization behavior at longer lifetimes (up to the ms timeframe), some time-resolved CID spectra were obtained using the home-built ion trap-ion source of the Hebrew University ZAB-2F instrument [40].

2.2.3. Computational chemistry

Most ab initio and density functional theory calculations were carried out using Gaussian 98 revision A.3 [41] running on the SGI Origin 2000 minisupercomputer of the Faculty of Chemistry at the Weizmann Institute of Science. Analytical second derivatives were employed in all optimizations, and the correct identity of transition states verified (where not trivially evident) by means of Intrinsic Reaction Coordinate (IRC) calculations [42] using the Gonzales-Schlegel [43] algorithm implemented in Gaussian 98.

Initial geometries for minima and transition states were determined using the B3LYP (Becke 3-parameter exchange [44] and Lee-Yang-Parr correlation [45] functionals) density functional method in combination with the fairly small 6-31G** and 6-31+G** basis sets. These geometries were then refined at the B3LYP level with the standard Pople 6-311G(d,p) basis set [46] on hydrogen and first-row atoms, and the McLean-Chandler [47] basis set, augmented with two d polarization functions, on second-row atoms; this basis set is denoted 6-311G(2d,d,p). Zero-point vibrational energies and RRHO (rigid rotor-harmonic oscillator) thermal corrections were obtained from the geometries and harmonic frequencies obtained at that level of theory.

Charge distributions using the APT (Atomic Polarizability Tensor) method of Cioslowski [48] were obtained as a by-product of the frequency calculations.

Energetics were evaluated at these reference geometries using the recently published CBS-QB3 hybrid empirical correction/pair extrapolation method [22] as

implemented in Gaussian 98 revision A.3. For a number of the larger species involved, the calculations were run in parallel over four CPUs. This method, which is a hybrid empirical correction/pair correlation energy extrapolation scheme, should on average be reliable to about 1-2 kcal/mol for total atomization energies.

The CBS-QB3 method of Petersson and coworkers has been described in detail in [22]. It involves a combination of CCSD(T) (coupled cluster with all single and double substitutions and quasiperturbative connected triple excitations [49], an electron correlation method generally close to the exact basis set correlation energy [50]) calculations in fairly small basis sets with perturbation theory calculations in larger basis sets; in addition, pair correlation energies obtained from the latter are extrapolated to the infinite basis limit using a procedure detailed in [51], and in addition some empirical corrections detailed in [22] are applied. For the 148 molecular atomization energies and 63 ionization energies and electron affinities in the extended G2 test set [52], mean absolute deviation from experiment of the CBS-QB3 values from experiment was 0.87 kcal/mol [22].

Reliability for relative energies within an isomer series should normally be higher than for total atomization energies. Since none of the transition states considered here exhibit excessive nondynamical correlation effects (i.e. the Hartree-Fock determinant is a good zero-order description in all cases), we would normally consider CBS-QB3 acceptable for those as well. The B3LYP density functional method, while a considerable improvement over "pure DFT" exchange-correlation functionals, is anything but a panacea for calculations of reaction barrier heights [53], and it is not inconceivable that its inadequacies may translate in (much smaller) errors in the CBS-QB3 energies due to inadequacies in the reference geometry. Consequently, we affix ±4 kcal/mol as a conservative estimate for the uncertainty in computed barrier heights.

The results of the calculations are summarized in Table 2.2a for the ions and Table 2.2b for the neutrals. Fig. 2.2 presents a selection of the optimized geometries: Cartesian coordinates of all stationary points obtained in the present work can be obtained as electronic supplementary material [54].

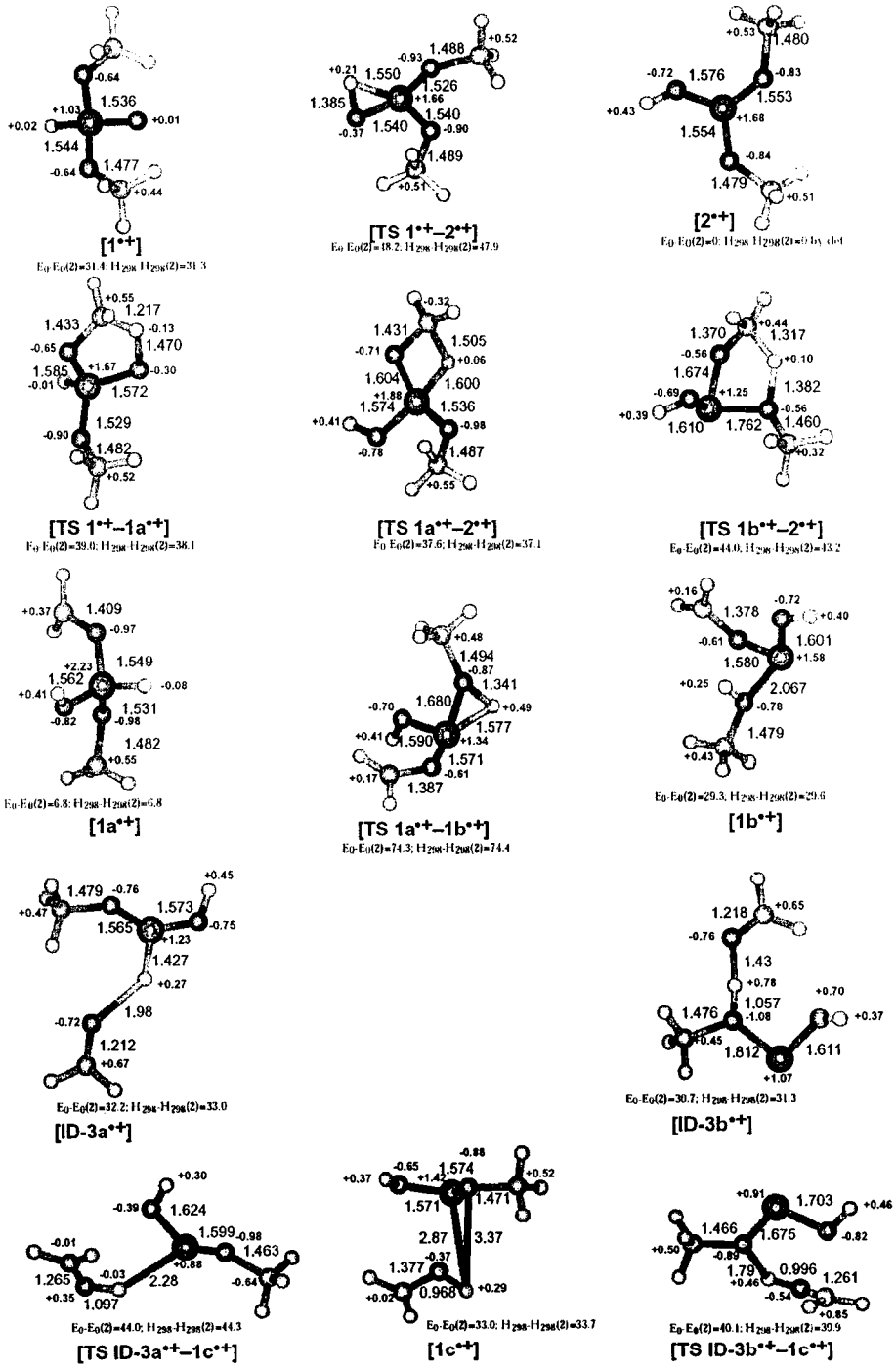

Fig. 2.2a. Stationary points on the $C_2H_7O_3P^{\bullet+}$ potential surface. Energetics (kcal/mol) are at the CBS-QB3 level; selected geometric parameters and APT charges (in blue) at the B3LYP/6-311G(2d,d,p) level are also given.

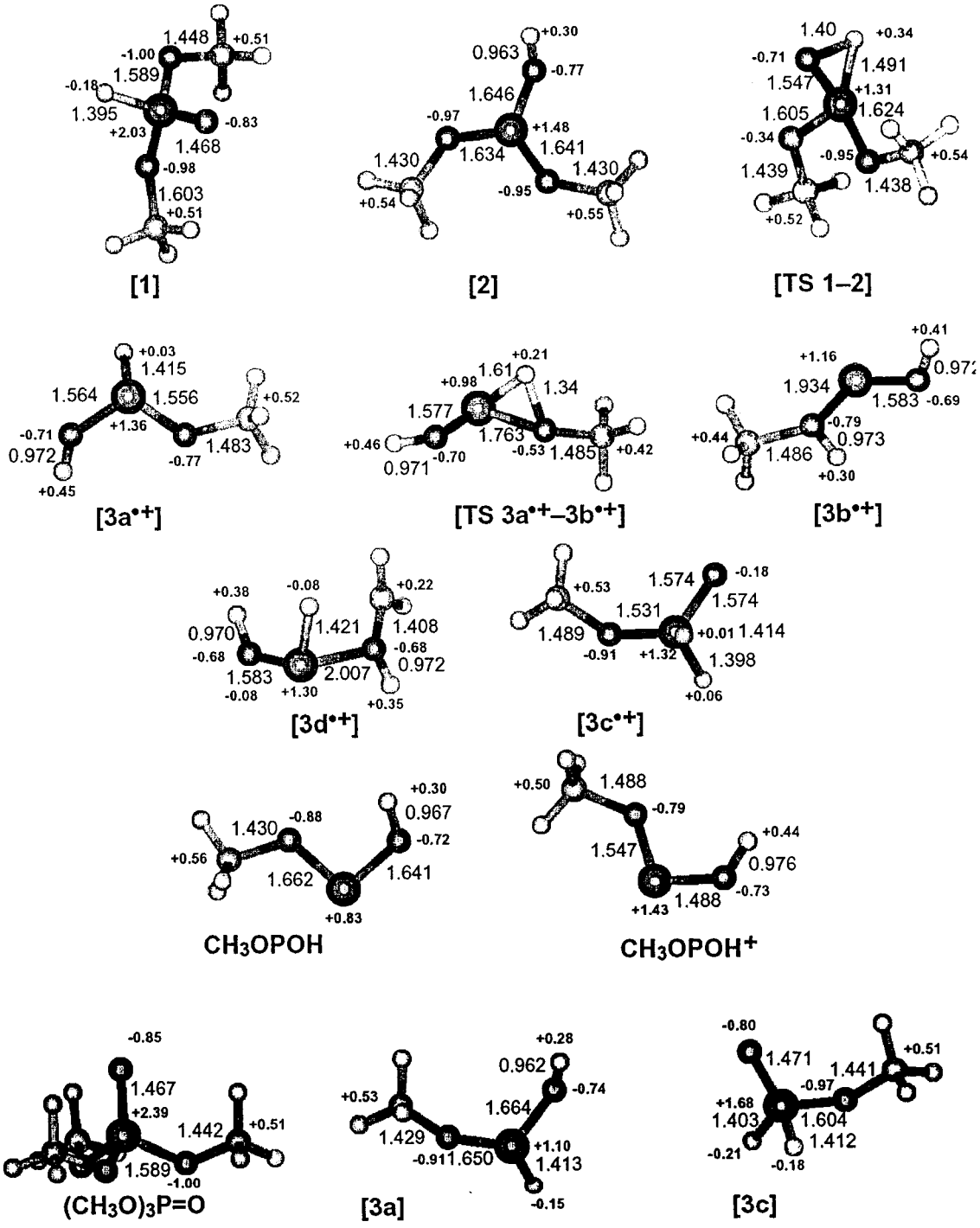

Fig. 2.2b. See caption to Fig. 2.2a.

In an attempt to validate the CBS-QB3 method for the present problem — in particular for the heats of formation of the neutral species — total atomization energies (TAEs) of some selected smaller species were also obtained using the very recent W1 (Weizmann-1) method of Martin and de Oliveira [55, 56]. While much more demanding computationally than CBS-QB3, this particular method calculated total atomization energies of its "training set" of molecules with a mean absolute error of less than 0.4 kcal/mol. In addition, it is entirely free of empirically derived parameters and hence not biased towards a particular type of molecule. The various steps involved in the W1 calculations (see [55] for details) were carried out using MOLPRO [57] on the SGI Origin 2000. From the results of the present validation calculations (Table 2.2c) for H_3PO and CH_2SO (as well as from previous benchmark studies on SO_3 [56], SiF_4 [58], and on related molecules in the W1 training set [55] such as SO_2), it would appear that CBS-QB3 indeed does produce energetics reliable to the target accuracy for compounds of the type of interest (i.e. involving a second-row atom bound to a highly electronegative element), and that it appears to outperform the comparably expensive G3 method [59] in this respect.

Even for the systems studied here, the computational cost of CBS-QB3 is fairly extravagant, and its application to larger systems still would be problematic using the computational resources available to us. Therefore we explored some alternatives, specifically two new DFT exchange-correlation functionals which have been claimed to be more reliable for reaction barrier heights than B3LYP. The first is the modified Perdew-Wang [60] exchange-correlation functional (mPW1PW91) recently proposed by Adamo and Barone [61]. The second is a very recent empirical modification of the latter by Truhlar and coworkers [62], denoted mPW1K (where the "K" stands for "kinetics").

In these calculations, we employed the 6-311G(2d,d,p) basis set defined above, the same basis augmented with one set of diffuse (low-exponent) s and p functions on each nonhydrogen atom, denoted 6-311+G(2d,d,p) (exponents were taken from [63]), the simple 6-31+G** basis set used in the original parametrization of mPW1K, and the augmented correlation-consistent polarized valence triple zeta (aug-cc-pVTZ) basis set

of Dunning and coworkers [64, 65]. In our experience [66], the latter is very close to the one-particle basis set limit for density functional calculations. Reference geometries were those obtained at the B3LYP/6-311G(2d,d,p) level in all cases.

Table 2.2d lists deviations for a number of combinations of basis set and exchange-correlation functional from the bottom-of-the-well CBS-QB3 relative energies of 15 stationary points on the $C_2H_7O_3P^{\bullet+}$ potential surface. Comparing the results with the 6-311G(2d,d,p) basis set, it is immediately seen that the performance of B3LYP leaves a lot to be desired: mean absolute deviation (MAD) is 6.4 kcal/mol, with several individual errors in the 12 kcal/mol range. We note such large errors not only for some barrier heights, but also for the relative stability of some of the proton transfer complexes. It was noted previously [67], that BHLYP (Becke half-and-half-LYP, in which the exchange part of the functional is taken to be a simple 50:50 hybrid of Hartree-Fock and Becke1988 exchange) appears to perform better for reaction barrier heights; and in fact, MAD for our 15 relative energies is 4.6 kcal/mol at the BHLYP/6-311G(2d,d,p) level, with improvements seen chiefly (but not exclusively) for the transition states. The mPW1PW91 functional (which was adjusted for better reproduction of long-range interactions) is likewise an improvement of B3LYP, with an MAD at the mPW1PW91/6-311G(2d,d,p) of 4.8 kcal/mol. Maximum errors are reduced to 8-9 kcal/mol at most for both BHLYP and mPW1PW91. With the new mPW1K functional, which combines a close to 50:50 hybrid of the exchange with the desirable features of the mPW1PW91 functional, MAD drops to 3.0 kcal/mol, with individual errors of at most 5-6 kcal/mol.

Let us now consider basis set dependence for the mPW1K results. Using the small 6-31+G** basis set that was originally employed for parametrizing mPW1K, MAD in relative energetics deteriorates to 4.3 kcal/mol; clearly this basis set is simply too limited. Adding diffuse functions to the 6-311G(2d,d,p) basis set does not improve agreement with experiment: it probably would have had this been an anionic rather than a cationic surface. Using the aug-cc-pVTZ basis set, however, MAD drops to 1.1 kcal/mol, the largest deviations being +2.6 kcal/mol for the direct keto-enol transition state, and -2.0 kcal/mol for distonic ion $\mathbf{1b}^{\bullet+}$. In fact, we obtain essentially identical

energetics (at a fraction of the CPU time) using the (unaugmented) cc-pVTZ basis set: this again probably would not have been the case on an anionic (or possibly a neutral) surface.

It was noted previously [68, 69] that addition of high-exponent *d* and *f* functions (so-called "inner polarization functions") to the basis set on second-row atoms is essential for accurate energetics and properties of second-row compounds where the second-row element is bound to a highly electronegative element like O or F. We have therefore also computed relative energetics at the mPW1K level with the cc-pVTZ+1 basis set [69], where the "+1" stands for the addition of a single high-exponent *d* function. While this does considerably affect the relative energetics of the system (and it cannot be ruled out that the mPW1K/cc-pVTZ+1 values are in fact closer to Nature than the mPW1K/cc-pVTZ values — verification would require calculations at still higher levels than CBS-QB3), this does not appear to fundamentally affect the mechanistic conclusions (see next Section).

We can draw a methodological and a chemical conclusion from all of the above. In terms of methodology, it appears that mPW1K in combination with a basis set of at least cc-pVTZ or cc-pVTZ+1 quality is a relatively inexpensive (and definitely more favorably scaling!) alternative to the costly CBS-QB3 calculations for applications of this type; this is an important conclusion for future studies on similar surfaces in larger systems. In terms of chemistry, we find that the best wavefunction-based ("conventional ab initio") and density functional methods that we can afford to apply to this system predict essentially the same energetics, which buttresses our computed potential energy profile, which will be discussed below in conjunction with the experiments.

We also note in passing that the smaller aug-cc-pVDZ basis set is clearly inadequate for the purpose, and in fact performs *worse* than even the simple 6-31+G** basis set. Probably, the underlying cc-pVDZ basis set is so far from convergence for the relative energies on this surface (total energies at the MPW1K/aug-cc-pVDZ level are on average 58 millihartree above those at the MPW1K/6-311G(2d,d,p) level for the present systems) that the addition of a large number of diffuse functions causes severe

basis set superposition errors which do not cancel between the (sometimes very different) tautomers and transition states.

Table 2.2a. Heats of formation, isomerization barriers and dissociation energies of the dimethyl phosphonate ion, $1^{\bullet+}$, and its tautomers derived from CBS-QB3 calculations.

		E_{total} (0 K)	ZPVE*	H298-H0	spin-orbit	TAE0	$\Delta H°_f$ (0 K)	$\Delta H°_f$ (298 K)
		Hartree	kcal/mol	kcal/mol	kcal/mol	kcal/mol	kcal/mol	kcal/mol
$(CH_3O)_2P(H)=O^{\bullet+}$	Keto $\mathbf{1}^{\bullet+}$	-646.28252	60.98	6.11	-0.84	898.3	55.4	50.1
$(CH_3O)_2POH^{\bullet+}$	Enol $\mathbf{2}^{\bullet+}$	-646.33261	61.97	6.25	-0.84	929.8	24.0	18.8
Dist $\mathbf{1a}^{\bullet+}$		-646.32176	59.93	6.20	-0.84	923.0	30.8	25.6
Dist $\mathbf{1b}^{\bullet+}$		-646.28587	59.92	6.56	-0.84	900.4	53.3	48.5
TS $\mathbf{1}^{\bullet+} \rightarrow \mathbf{1a}^{\bullet+}$		-646.27042	57.92	5.34	-0.84	890.8	63.0	56.9
TS $\mathbf{2}^{\bullet+} \rightarrow \mathbf{1a}^{\bullet+}$		-646.27263	58.57	5.69	-0.84	892.1	61.6	55.9
TS $\mathbf{1}^{\bullet+} \rightarrow \mathbf{2}^{\bullet+}$		-646.25588	58.91	5.98	-0.84	881.6	72.2	66.7
TS $\mathbf{2}^{\bullet+} \rightarrow \mathbf{1b}^{\bullet+}$		-646.26256	57.92	5.44	-0.84	885.8	68.0	62.0
TS $\mathbf{1a}^{\bullet+} \rightarrow \mathbf{1b}^{\bullet+}$		-646.21428	55.90	6.42	-0.84	855.5	98.3	93.3
$CH_3O\text{-}P(H)OH^{\bullet+}$	$\mathbf{3a}^{\bullet+}$ (m/z 80)	-531.91714	40.58	4.47	-0.53	526.7	94.9	91.0
$CH_3O(H)\text{-}POH^{\bullet+}$	$\mathbf{3b}^{\bullet+}$ (m/z 80)	-531.90428	41.82	4.70	-0.53	518.6	102.9	99.3
TS $\mathbf{3a}^{\bullet+} \rightarrow \mathbf{3b}^{\bullet+}$		-531.84692	37.93	4.43	-0.53	482.6	138.9	135.0
$CH_3O(H)P(H)=O^{\bullet+}$	$\mathbf{3c}^{\bullet+}$ (m/z 80)	-531.86527	39.44	4.28	-0.53	494.2	127.4	123.3
$CH_2O(H)\text{-}P(H)OH^{\bullet+}$	$\mathbf{3d}^{\bullet+}$ (m/z 80)	-531.85962	39.12	4.75	-0.53	490.6	130.9	127.4
$CH_3\text{-}P(OH)_2^{\bullet+}$	$\mathbf{3e}^{\bullet+}$ (m/z 80)	-531.95992	40.79	4.45	-0.53	553.6	68.2	64.0
$(CH_3O)_2P(H)OH^+$	(m/z 111)	-646.98726	69.09	6.18	-0.84	1026.9	-21.3	-28.1
$(CH_3O)_2P=O^+$	(m/z 109)	-645.74518	56.11	5.78	-0.84	874.8	27.5	23.4
$CH_3O\text{-}P(OH)=O^+$	(m/z 95)	-606.51995	38.59	4.59	-0.75	598.7	30.5	26.4
$CH_2O\text{-}P(OH)_2^+$	(m/z 95)	-606.52645	36.80	4.90	-0.75	602.7	26.4	22.6
$CH_3O\text{-}P\text{-}OCH_3^+$	(m/z 93)	-570.58168	53.02	5.24	-0.62	764.7	78.7	74.0
$CH_3O\text{-}P\text{-}OH^+$	(m/z 79)	-531.36680	35.56	4.02	-0.53	495.0	75.1	71.5
$HO\text{-}P\text{-}OH^+$	(m/z 65)	-492.14113	17.93	2.93	-0.45	218.6	78.3	75.8
$HO\text{-}P(H)=O^+$	(m/z 65)	-492.09318	16.67	2.96	-0.45	188.5	108.4	105.9
$H\text{-}P\text{-}OH^+$	(m/z 49)	-416.91532	14.05	2.48	-0.22	69.4	168.5	166.6
$H\text{-}P(H)=O^+$	(m/z 49)	-416.88529	12.51	2.51	-0.22	50.5	187.5	185.5
$P\text{-}OH^{\bullet+}$	(m/z 48)	-416.29431	7.70	2.44	-0.22	-6.7	192.9	192.0
$P=O^+$	(m/z 47)	-415.72469	2.06	2.08	-0.22	50.1	185.1	184.8
$CH_3O\text{-}P(H)OH^{\bullet+}/CH_2=O$	$\mathbf{ID\text{-}3a}^{\bullet+}$	-646.28137	58.57	7.09	-0.84	897.6	56.3	51.8
$CH_3O(H)\text{-}POH^{\bullet+}/CH_2=O$	$\mathbf{ID\text{-}3b}^{\bullet+}$	-646.28376	59.51	6.89	-0.84	899.1	54.7	50.1
$CH_3O\text{-}P\text{-}OH^+/CH_2OH^{\bullet}$	$\mathbf{1c}^{\bullet+}$	-646.28003	59.47	6.95	-0.84	896.8	57.0	52.5
TS $\mathbf{ID\text{-}3a}^{\bullet+} \rightarrow \mathbf{1c}^{\bullet+}$		-646.26243	59.38	6.52	-0.84	885.7	68.0	63.1
TS $\mathbf{ID\text{-}3b}^{\bullet+} \rightarrow \mathbf{1c}^{\bullet+}$		-646.26867	61.38	6.04	-0.84	889.7	64.1	58.7
TS $\mathbf{ID\text{-}3b}^{\bullet+} \rightarrow \mathbf{1b}^{\bullet+}$ **		-646.26196	59.24	7.03	-0.84	885.4	68.5	63.6

* scaled by 0.99

**This TS has not been rigorously defined.

Table 2.2b. Auxiliary energetic information for the dimethyl phosphonate system derived from CBS-QB3 calculations.

	E_{total} (0 K) Hartree	ZPVE* kcal/mol	H298-H0 kcal/mol	spin-orbit kcal/mol	TAE0 kcal/mol	$\Delta H°_f$(0 K) kcal/mol	$\Delta H°_f$(298 K) Kcal/mol
$(CH_3O)_3P=O$ (TMP)	-761.06930	83.05	7.46	-1.15	1534.4	-248.4	-255.5
$(CH_3O)_2P(H)=O$ Keto **1**	-646.66086	62.16	5.72	-0.84	1135.8	-182.0	-187.7
$(CH_3O)_2P(OH)$ Enol **2**	-646.63741	61.69	6.11	-0.84	1121.0	-167.2	-172.6
TS **1** $\rightarrow$ **2**	-646.55976	58.59	5.93	-0.84	1072.3	-118.3	-124.4
$^{\bullet}CH_2O(CH_3O)P(OH)$	-645.98468	52.87	6.06	-0.84	1025.1	-122.7	-126.6
CH_3O-P(H)OH **3a**	-532.23329	41.26	4.19	-0.53	725.1	-103.4	-107.8
$CH_3O(H)P(H)=O$ **3c**	-532.24977	40.94	3.97	-0.53	735.4	-113.9	-118.2
CH_3O-P-OH$^{\bullet}$	-531.61398	34.40	4.46	-0.53	650.6	-80.5	-83.7
$H_3P=O$	-417.84347	19.15	2.50	-0.22	338.1	-48.8	-51.5
$CH_2=O$	-114.34410	16.46	2.39	-0.31	358.3	-26.1	-26.8
$CH_3O^{\bullet}$	-114.87434	22.55	2.48	-0.31	377.4	6.5	4.7
$CH_3^{\bullet}$	-39.744804	18.36	2.52	-0.09	288.6	36.4	35.6
$OH^{\bullet}$	-75.649693	5.24	2.07	-0.02	101.8	8.8	8.8

*scaled by 0.99

Table 2.2c. Validation of CBS-QB3 against W1' theory for total atomization energies of H_3PO and CH_2SO. All values in kcal/mol.

	CH_2SO	H_3PO
SCF limit	271.39	239.60
CCSD valence correlation limit	136.25	111.14
valence (T) correlation limit	14.59	6.67
inner-shell correlation	1.68	0.19
scalar relativistic	-0.75	-1.17
atomic spin-orbit	-0.87	-0.22
TAE_e(W1')	422.30	356.20
ZPVE (B3LYP/cc-pVTZ+1)	17.94	19.00
TAE_0(W1')	404.36	337.19
$\Delta H^0_{f,0}$	-6.42	-47.86
TAE_0(CBS-QB3) w.spin-orbit	404.25	338.13
TAE_0(G3)	401.75	333.13
TAE_0(G3B3)	401.83	333.66

Table 2.2d. Deviations (kcal/mol) from the CBS-QB3 (bottom-of-the-well) relative energetics on the $C_2H_7O_3P^{\bullet+}$ potential surface with a variety of density functional methods. Enol-**2**$^{\bullet+}$ has been taken as the reference.

	B3LYP 6-311G (2d,d,p)	mPW1PW91 6-311G (2d,d,p)	BHLYP 6-311G (2d,d,p)	MPW1K/ 6-311G (2d,d,p)	MPW1K/ 6-31+G**	MPW1K/ 6-311+G (2d,d,p)	MPW1K/ Aug-cc-pVDZ	MPW1K/ cc-pVTZ	MPW1K/ Aug-cc-pVTZ	MPW1K/ cc-pVTZ+1
Keto **1**$^{\bullet+}$	-3.73	-2.80	-5.67	-3.62	-1.02	-2.77	1.39	-1.04	-0.71	-2.80
Dist **1a**$^{\bullet+}$	2.72	1.13	-2.29	-1.78	0.97	-1.20	2.55	-0.21	-0.11	-1.89
Dist **1b**$^{\bullet+}$	-7.90	-6.23	-6.11	-4.87	-7.05	-5.39	-11.32	-1.96	-1.99	1.04
Enol **2**$^{\bullet+}$	0.00	0.00	0.00	0.00	0.00	0.00	0.00	0.00	0.00	0.00
1c$^{\bullet+}$	-9.27	-6.68	-6.29	-4.56	-6.03	-5.11	-10.22	-1.41	-1.44	1.47
TS **1**$^{\bullet+}$ → **1a**$^{\bullet+}$	-3.02	-3.90	-1.00	-2.57	-0.28	-1.83	-1.12	-1.58	-1.44	-2.85
TS **1**$^{\bullet+}$ → **2**$^{\bullet+}$	-0.54	-1.08	3.37	1.34	4.92	1.82	5.02	2.63	2.63	0.72
TS **ID-3b**$^{\bullet+}$ → **1b**$^{\bullet+}$	-12.53	-7.72	-8.73	-4.90	-8.52	-6.67	-15.66	0.14	-0.03	5.03
TS **ID-3a**$^{\bullet+}$ → **1c**$^{\bullet+}$	-12.95	-8.83	-5.78	-4.20	-7.03	-5.56	-13.03	-1.65	-1.93	1.96
TS **1a**$^{\bullet+}$→**1b**$^{\bullet+}$	-3.87	-4.22	2.62	-0.33	-1.40	-0.72	-4.41	-0.38	-0.39	0.63
TS **ID-3b**$^{\bullet+}$ → **1c**$^{\bullet+}$	-11.16	-8.30	-8.45	-6.26	-10.20	-6.94	-15.78	-1.09	-1.05	3.65
ID-3a$^{\bullet+}$	-8.62	-4.92	-5.05	-2.52	-2.17	-2.88	-6.20	1.44	1.50	3.53
ID-3b$^{\bullet+}$	-12.09	-8.20	-8.84	-5.82	-9.83	-6.76	-16.42	-1.68	-1.62	3.09
TS **2**$^{\bullet+}$ → **1a**$^{\bullet+}$	1.00	-2.03	2.99	-1.06	0.74	-0.91	-2.02	-1.00	-1.01	-1.62
TS **2**$^{\bullet+}$ →**1b**$^{\bullet+}$	-6.03	-5.58	1.51	-1.04	-4.63	-1.41	-11.19	-0.43	-0.50	2.68
Mean absolute deviation	**6.36**	**4.78**	**4.58**	**2.99**	**4.32**	**3.33**	**7.76**	**1.11**	**1.09**	**2.20**
Mean signed deviation	-5.87	-4.62	-3.18	-2.81	-3.44	-3.09	-6.56	-0.55	-0.54	+0.98

2.3. Results and Discussion : The isomerization and dissociation behavior of the DMP ion $(CH_3O)_2P(H)=O^{\bullet+}$ ($\mathbf{1}^{\bullet+}$) and its enol counterpart $(CH_3O)_2P\text{-}OH^{\bullet+}$ ($\mathbf{2}^{\bullet+}$)

2.3.1. Computational results

In our analysis of the experimental and theoretical results we will use the energy diagram of Scheme 2.4 as our starting point. This diagram summarizes the CBS-QB3 (298 K) computational results on the various isomerization routes for ions $\mathbf{1}^{\bullet+}$ and $\mathbf{2}^{\bullet+}$ and their low energy dissociation by loss of $CH_2=O$ as depicted in Scheme 2.3. That this dissociation generates product ions of structure $\mathbf{3a/b}^{\bullet+}$ and not any of the isomeric structures $\mathbf{3c/d/e}^{\bullet+}$ listed in Table 2.2a, will be discussed in Section 2.3.4. The energetic information presented in the diagram uses the enol ion $\mathbf{2}^{\bullet+}$ as the zero reference point and is based on the computational results compiled in the top Section of Table 2.2a.

Scheme 2.4 shows that the enol ion $\mathbf{2}^{\bullet+}$ is the most stable species: it lies 31 kcal/mol lower in energy than its keto counterpart $\mathbf{1}^{\bullet+}$, which has about the same stability as the distonic ion $\mathbf{1b}^{\bullet+}$ and its ion-dipole counterpart $\mathbf{ID\text{-}3b}^{\bullet+}$. The other distonic ion, $\mathbf{1a}^{\bullet+}$, is much more stable and lies only 7 kcal/mol above the enol ion. Inspection of the optimized geometries in Fig. 2.2 supports the notation of the ions $\mathbf{1}^{\bullet+}$, $\mathbf{1a}^{\bullet+}$ and $\mathbf{2}^{\bullet+}$ in Scheme 2.3, but not that of the distonic ion $\mathbf{1b}^{\bullet+}$. This ion has a fairly long P-O(H)CH_3 bond (2.067 Å) and moreover from the calculated charge distribution it follows that the -O(H)CH_3 moiety has a net zero charge. The ion is therefore better represented by the structure in Scheme 2.4, that is as a $^{\bullet}CH_2O\text{-}P^{+}\text{-}OH$ distonic ion in which the positively charged P atom interacts with the oxygen lone pair electrons of the methanol dipole molecule. In this context we also note that, whereas the optimized geometry of $\mathbf{ID\text{-}3a}^{\bullet+}$ represents a simple ion-dipole complex, $\mathbf{ID\text{-}3b}^{\bullet+}$ is better described as a hydrogen-bridged radical cation (HBRC) [24] where both the ion-dipole interaction and the H-bridge contribute to a high stabilization energy (22 kcal/mol vs. 12 kcal/mol for $\mathbf{ID\text{-}3a}^{\bullet+}$). In the ion-dipole interaction between $CH_2=O$ and $\mathbf{3a}^{\bullet+}$ local minima other than $\mathbf{ID\text{-}3a}^{\bullet+}$, including the HBRC $[CH_3O\text{-}P(H)\text{-}O\cdots H\cdots O=CH_2]^{\bullet+}$, may well exist but these have not been further investigated.

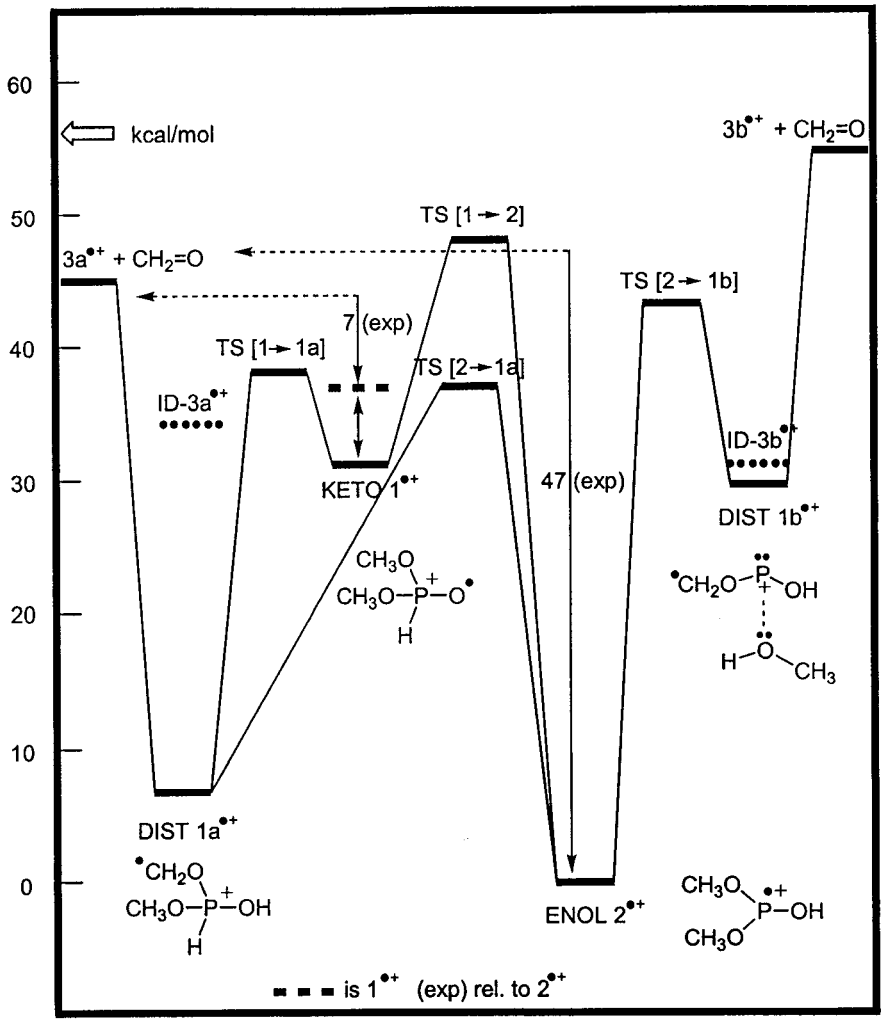

Scheme 2.4

The Scheme further indicates that the enol ion $\mathbf{2}^{\bullet+}$ is separated by high H-shift barriers from its distonic isomers $\mathbf{1a}^{\bullet+}$ and $\mathbf{1b}^{\bullet+}$. Nevertheless, TS [$\mathbf{2}^{\bullet+} \rightarrow \mathbf{1a}^{\bullet+}$] still lies below the dissociation threshold for the direct bond cleavage $\mathbf{1a}^{\bullet+} \rightarrow \mathbf{3a}^{\bullet+}$ + CH_2=O and thus theory predicts that metastable enol ions will dissociate via the route $\mathbf{2}^{\bullet+} \rightarrow \mathbf{1a}^{\bullet+} \rightarrow \mathbf{3a}^{\bullet+}$ + CH_2=O. The alternative pathway $\mathbf{2}^{\bullet+} \rightarrow \mathbf{1b}^{\bullet+} \rightarrow \mathbf{3b}^{\bullet+}$ + CH_2=O is characterized by a somewhat higher TS and an energetically less favorable product ion and could participate in the collision induced CH_2=O loss from the enol ion.

The 1,2-H shift barrier associated with the tautomerization $\mathbf{2}^{\bullet+} \rightarrow \mathbf{1}^{\bullet+}$ lies above the dissociation threshold for loss of CH_2=O and thus metastable ions $\mathbf{2}^{\bullet+}$ should **not**

"ketonize" via this route. Neither are low energy keto ions $\mathbf{1}^{\bullet+}$ expected to "enolize" via a 1,2-H shift, as suggested in the literature, see Introduction. Rather, the scenario emerging from the computations is that keto ions $\mathbf{1}^{\bullet+}$ are only marginally stable towards isomerization into $\mathbf{1a}^{\bullet+}$ via the 1,4-H shift represented by the low-lying TS [$\mathbf{1}^{\bullet+} \rightarrow \mathbf{1a}^{\bullet+}$]. Consequently, most of the stable and all of the metastable keto ions $\mathbf{1}^{\bullet+}$ generated by electron ionization of DMP, reach the deep potential well of ion $\mathbf{1a}^{\bullet+}$ during their μs lifetime. According to the diagram the resulting solitary distonic ions $\mathbf{1a}^{\bullet+}$ are sufficiently energy rich to access the even deeper potential well of the enol since TS [$\mathbf{1a}^{\bullet+} \rightarrow \mathbf{2}^{\bullet+}$] lies at about the same energy as TS [$\mathbf{1}^{\bullet+} \rightarrow \mathbf{1a}^{\bullet+}$]. However, the incipient energy rich ions $\mathbf{1a}^{\bullet+}$ may also adopt one of the many ion-dipole configurations akin to the stable minimum represented by **ID-3a**$^{\bullet+}$ and this should make their enolization less likely.

2.3.2. The isomerization and dissociation chemistry of the enol ion $2^{\bullet+}$

We will begin our analysis of the experimental and theoretical results by examining the energetics and the (spontaneous and collision induced) dissociation characteristics of the enol ion $\mathbf{2}^{\bullet+}$. As indicated in Scheme 2.1 (see Introduction), these ions can be generated by the loss of CH_2=O from the TMP molecular ion. Indeed, the 70 eV mass spectrum of TMP, see Fig. 2.3a, displays prominent m/z 110 ions of putative structure $\mathbf{2}^{\bullet+}$. The MI spectrum of the m/z 140 molecular ions (not shown) displays only one signal, a narrow Gaussian shaped peak at m/z 110. Thus loss of CH_2=O represents the reaction of lowest energy requirement and does not appear to be associated with a significant reverse activation energy. The measured AE for this reaction, see Table 2.1, should therefore reflect the threshold generation of the m/z 110 enol ions $\mathbf{2}^{\bullet+}$. From Table 2.1 it follows that the experimentally derived $\Delta H_f[\mathbf{2}^{\bullet+}]$ is 18 kcal/mol. Agreement with the CBS-QB3 derived value listed in Table 2.2a, 18.8 kcal/mol, is excellent and confirms the correctness of the ion structure assignment.

To examine the enol ion's dissociation and isomerization characteristics, MI and CID spectra were obtained of the m/z 110 source generated ions from TMP. The MI

spectrum (not shown) features a narrow Gaussian shaped peak at m/z 80 (100%, $T_{0.5}$ = 21 meV). A minor and broad Gaussian peak (4%, $T_{0.5}$ = 60 meV) is also present, at m/z 95, signifying that the loss of CH_2=O is the reaction of lowest energy requirement with loss of $CH_3^\bullet$ only marginally competing. From the AE of the [$\mathbf{2}^{\bullet+}$ – CH_2=O] product ion at m/z 80, 12.75 ± 0.05 eV, see Table 2.1, an apparent ΔH_f [m/z 80] = 92 kcal/mol is derived. This value is entirely compatible with the threshold generation of product ions of structure $\mathbf{3a}^{\bullet+}$ whose calculated ΔH_f is 91 kcal/mol, see Table 2.2a and Scheme 2.4, where the "47 (exp)" reflects the difference between AE (m/z 110, $\mathbf{2}^{\bullet+}$) and AE (m/z 80, $\mathbf{3a}^{\bullet+}$). Confirmatory evidence that the **metastable** enol ions exclusively generate product ions of structure $\mathbf{3a}^{\bullet+}$ will be presented in Section 2.3.4 where the CID characteristics of m/z 80 ions from TMP and DMP are discussed.

CID spectra of the enol ion are presented in Fig. 2.3b/c : Fig. 2.3b displays the CID chemistry of source generated ions, while Fig. 2.3c deals with the CID of enol ions of much lower internal energy content generated from the dissociation of metastable TMP molecular ions. Both spectra display the same primary reactions *viz.* a prominent loss of $CH_3^\bullet$ (m/z 95) and $CH_3O^\bullet$ (m/z 79) and a weak loss of $H^\bullet$ (m/z 109) and $OH^\bullet$ (m/z 93). Ions at lower m/z values, including m/z 47 (PO^+) obviously result from multistep reactions. The rearrangement ion at m/z 80 that dominates the MI spectrum is the second most intense peak in the CID of the source generated ions but its intensity becomes drastically lower in the CID of the low energy enol ions. This indicates that the enol ion's rearrangement into either of the distonic ions $\mathbf{1a}^{\bullet+}$ and $\mathbf{1b}^{\bullet+}$ that could serve as a precursor for the CH_2=O loss, see Scheme 2.3, involves a significant energy barrier, as predicted by theory. The dissociation characteristics of the enol isotopologue $(CH_3O)_2$P-$OD^{\bullet+}$, **2**-$OD^{\bullet+}$, show that this indeed is the case. Metastable ions **2**-$OD^{\bullet+}$ show very little interconversion with the distonic ion $\mathbf{1a}^{\bullet+}$ as witnessed by the high H-atom specificity in the formaldehyde loss (> 90 %). In the same vein, the CID spectrum of the ion, see Fig. 2.3d, displays isotopically clean losses of $^\bullet CH_3$ (m/z 96), $^\bullet OD$ (m/z 93), CH_2=O (m/z 81) and $CH_3O^\bullet$ (m/z 80).

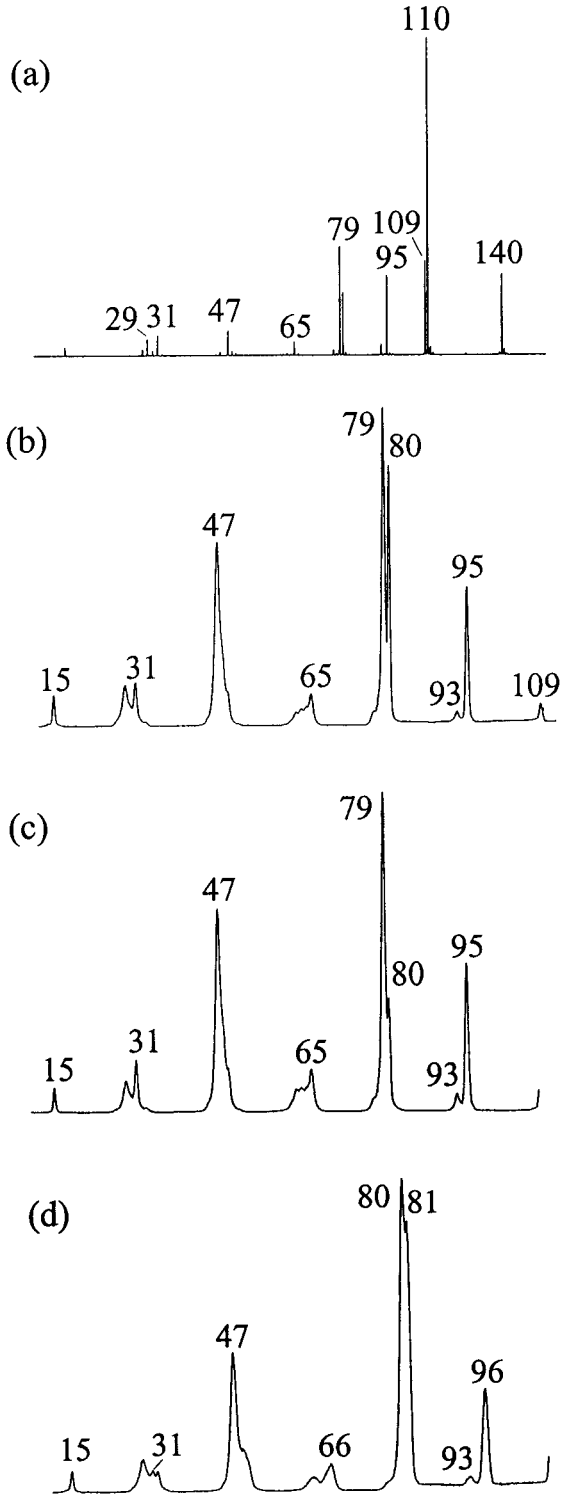

Fig. 2.3. TMP mass spectra and CID spectra for enol ions $\mathbf{2}^{\bullet+}$ derived from TMP. **(a)** 70 eV electron impact (EI) mass spectrum of TMP; **(b)** CID spectrum of source generated m/z 110 ions; **(c)** MI/CID spectrum of metastably generated m/z 110 ions; **(d)** MI/CID spectrum of **2**-$OD^{\bullet+}$ (m/z 111) ions.

The above labeling experiment suggests that the primary fragment ions at m/z 109, 95,93 and 79 in the CID spectra of the enol may well originate from direct bond cleavage (dbc) reactions. In support of this, essentially constant m/z 79/95 and 95/93 peak intensity ratios were observed in a series of time-resolved CID experiments, see Section 2.2.2. These ions could therefore potentially be of structure diagnostic value in the interpretation of the CID spectra of the isomeric ions. The four ions: $(CH_3O)_2P{=}O^+$ (m/z 109), $CH_3O\text{-}P(OH){=}O^+$ (m/z 95), $CH_3O\text{-}P\text{-}OCH_3^+$ (m/z 93) and $CH_3O\text{-}P\text{-}OH^+$ (m/z 79) yield CID spectra which are compatible with the proposed structures [70].

Their calculated ΔH_f values are given in the middle Section of Table 2.2a which also lists the ΔH_f values for the isomeric pairs of $HO\text{-}P\text{-}OH^+$ and $HO\text{-}P(H){=}O^+$ ions at m/z 65 and $H\text{-}P\text{-}OH^+$ and $H\text{-}P(H){=}O^+$ at m/z 49. It is seen that the two-coordinated ions $HO\text{-}P\text{-}OH^+$ and $H\text{-}P\text{-}OH^+$ are considerably lower in energy (by ~ 30 kcal/mol) than their four-coordinated counterparts. By analogy, we infer that the m/z 79 product ion $CH_3O\text{-}P\text{-}OH^+$ is much more stable than its isomer $CH_3O\text{-}P(H){=}O^+$. Thus, collisionally excited ions $(\mathbf{2}^{\bullet+})^*$ will lose $CH_3O^\bullet$ via the proposed dbc. However, the same loss from collisionally excited keto ions $(\mathbf{1}^{\bullet+})^*$ may well involve the post-collisional isomerization $(\mathbf{1}^{\bullet+})^* \rightarrow 1,2\text{-H} \rightarrow (\mathbf{2}^{\bullet+})^* \rightarrow CH_3O\text{-}P\text{-}OH^+ + CH_3O^\bullet$ which theory predicts to be more favorable than the dbc $(\mathbf{1}^{\bullet+})^* \rightarrow CH_3O\text{-}P(H){=}O^+ + CH_3O^\bullet$.

From the calculated ΔH_f values of the above four product ions (Table 2.2a) and the associated neutral species lost (Table 2.2b), we derive the following values (kcal/mol) for the minimum energy requirement of the four dbc dissociations of $(\mathbf{2}^{\bullet+})^*$: m/z 109 + $H^\bullet$ (57); m/z 95 + $CH_3^\bullet$ (43); m/z 93 + $OH^\bullet$ (64) and m/z 79 + $CH_3O^\bullet$ (57). On the basis of these results one would expect m/z 95 (loss of $CH_3^\bullet$) to dominate the CID spectrum of $(\mathbf{2}^{\bullet+})^*$ with losses of $H^\bullet$ and $CH_3O^\bullet$ yielding sizable peaks of comparable intensity at m/z 109 and 79 respectively. This, see Fig. 2.3 b/c, is clearly not the case! The solution to this problem becomes apparent when we consider the rearrangement reaction $\mathbf{2}^{\bullet+} \rightarrow \mathbf{3a}^{\bullet+} + CH_2{=}O$. As shown above, this clearly is the reaction of lowest energy requirement but its established activation energy, 47 kcal/mol (see Scheme 2.4), is *higher* than that calculated for the dbc loss of $CH_3^\bullet$, 42 kcal/mol. This does not imply

that the calculated value is in error but rather that the dbc loss of $CH_3^\bullet$ from $\mathbf{2}^{\bullet+}$ is associated with a significant reverse activation energy [71]. This phenomenon is well documented for the dbc reactions $CH_3\text{-}C^{\bullet+}\text{-}O\text{-}H \rightarrow CH_3\text{-}C^{\bullet+}{=}O + H^\bullet$ and $HO\text{-}C^{\bullet+}\text{-}O\text{-}CH_3 \rightarrow HO\text{-}C^{\bullet+}{=}O + CH_3^\bullet$ [72]. Both processes have a significant reverse activation energy, which finds its origin in the electron reorganization involved in the C-O single to double bond conversion en route to the dissociation. The loss of $CH_3^\bullet$ from $\mathbf{2}^{\bullet+}$ and by the same token also that of $H^\bullet$, features a similar single to double bond conversion : $CH_3O(HO)P^{\bullet+}\text{-}O\text{-}CH_3 \rightarrow CH_3O(HO)\text{-}P^{+}{=}O + CH_3^\bullet$ and $(CH_3O)_2P^{\bullet+}\text{-}O\text{-}H \rightarrow (CH_3O)_2P^{+}{=}O + H^\bullet$. We propose that both reactions have significant reverse activation energies, probably in the upper 10 kcal/mol range, and that this provides a satisfactory rationale for the interpretation of the CID spectrum of the enol ions.

2.3.3. The isomerization and dissociation chemistry of the keto ion $1^{\bullet+}$

We now turn to the spectra of Fig. 2.4 to discuss the behavior of DMP ions $\mathbf{1}^{\bullet+}$. Fig. 2.4a displays the high mass region of the 70 eV EI spectra of DMP (left side) and its isotopologue $(CH_3O)_2P(D){=}O$, **1**-D (right side). Loss of formaldehyde dominates both spectra as exemplified by the peaks at m/z 80 and 81 respectively. When the energy of the ionizing electrons is lowered to (nominally) 14 eV, **1**-D displays a mass spectrum (not shown) with fragment ion peaks at m/z 81 and 80 only, in a ratio of 20 : 1. This shows that (i) loss of $CH_2{=}O$ is the process of lowest energy requirement and (ii) that this loss is highly H-atom specific. In line with this observation the MI spectrum of **1**-$D^{\bullet+}$ is dominated by intense peaks at m/z 81 (loss of $CH_2{=}O$) and m/z 80 (loss of $CHD{=}O$) still in a high intensity ratio, 7.5 : 1, with $T_{0.5}$ values of 15 and 20 meV respectively. Further, the CID spectra of the m/z 80 ions generated from DMP ions in the ion source, metastable DMP ions and **metastable** enol ions are closely similar and compatible with the formation of ions $\mathbf{3a}^{\bullet+}$, see Section 2.3.4.

These observations strongly support the scenario depicted in the energy diagram Scheme 2.4 and the discussion in Section 2.3.1, where it was anticipated that keto ions $\mathbf{1}^{\bullet+}$ undergo a fast isomerization in the μs time scale into distonic ions $\mathbf{1a}^{\bullet+}$ which show

little tendency to further isomerize into their more stable enol counterpart. The somewhat higher KER for the loss of CHD=O from $\mathbf{1}^{\bullet+}$-D signifies that interconversion with the enol becomes only feasible with the high energy fraction of the metastable ions and again this is compatible with the location of the TS's for "distonicization" and "enolization".

In agreement with the above proposal, the CID spectra of $\mathbf{1}^{\bullet+}$ and $\mathbf{1}^{\bullet+}$-D, see Fig. 2.4c, are found to be dominated by formaldehyde loss. We further note that m/z 109 ions are barely detectable in these spectra whereas they figure prominently in the 70 eV EI and also the CIDI spectra of **1**/**1**-D, see Fig. 2.4a/b. Considering that these ions most likely result from P–H/D direct bond cleavage in the intact DMP molecular ions, we infer that the non-dissociating DMP ions with lifetimes of a few μs sampled by CID have lost their structure identity.

Two more points deserve comment *viz.* the loss of $OH^{\bullet}$ and that of $CH_3^{\bullet}$ in the EI, CIDI and CID spectra of **1**/**1**-D. Although the distonic ion $\mathbf{1a}^{\bullet+}$ contains an OH group that could conceivably be lost upon collisional activation, the CID spectrum of Fig. 2.4c clearly shows that this reaction is insignificant. On the other hand, m/z 93 ions are found in the EI, and even more prominently, in the CIDI spectrum of DMP that does **not** contain an OH moiety. In the corresponding spectra of the **1**-D isotopologue m/z 93 is not shifted and thus $OD^{\bullet}$ is specifically lost. These observations in conjunction with Scheme 2.4 suggest that high-energy keto ions lose $OH^{\bullet}$ via a fast 1,2-H shift into vibrationally excited enol ions $(\mathbf{2}^{\bullet+})^*$ which, see Fig. 2.3, do indeed lose $OH^{\bullet}$. The fact that this loss is so prominent in the CIDI spectrum may be due to the high internal energy (as exemplified by the weak molecular ion) imparted by the collisional ionization process and possibly dissociation from an electronically excited state of $\mathbf{2}^{\bullet+}$. The latter point is corroborated by the observation that when in the CIDI experiment O_2 is replaced by He, which is more prone to electronic excitation [73], no molecular and m/z 80 rearrangement ions are detected while the m/z 93 ion becomes even more prominent (ratio m/z 109 : 95 : 93 : 79 = 14 : 2 : 6 : 100).

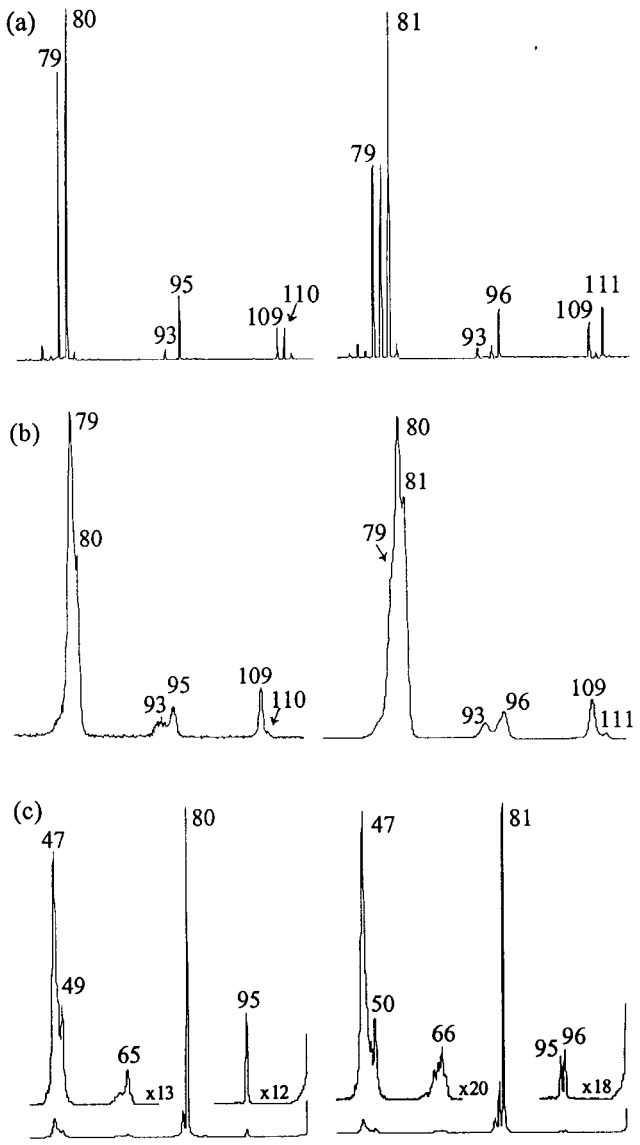

Fig. 2.4. (a) 70 eV EI mass spectra and **(b)** CIDI spectra for DMP, $\mathbf{1}^{\bullet+}$ (left side) and its isotopologue $(CH_3O)_2P(D)=O$, **1-D** (right side), and **(c)** CID spectra for $\mathbf{1}^{\bullet+}$ (left side) and **1-D**$^{\bullet+}$ (right side).

Considering the structure of the product ion, the loss of $CH_3^{\bullet}$ observed in the EI and CIDI spectra of DMP is unlikely the result of a direct bond cleavage, but rather also involves isomerization into excited ions $\mathbf{2}^{\bullet+}$: $(\mathbf{1}^{\bullet+})^* \rightarrow$ 1,2-H $\rightarrow (\mathbf{2}^{\bullet+})^* \rightarrow$ $CH_3O{-}P(OH){=}O^+$ (m/z 95) + $CH_3^{\bullet}$. Indeed, the CID spectrum of the m/z 95 ions in the EI spectrum of DMP is indistinguishable from that of the m/z 95 ions generated from TMP (see Section 2.3.2.) while the CID spectrum of the m/z 96 ions in the EI spectrum

of **1**-D shows a largely specific loss of CH_2=O compatible with the CH_3O–P(OD)=O^+ structure. However, the loss of methyl is not quite H-atom specific and both DMP-D ions subjected to EI and CIDI also show a minor loss of $CH_2D^\bullet$ (possibly to about the same extent but this is difficult to decide because of the poor resolution in the CIDI spectrum). This loss, we propose on the basis of Scheme 2.4, originates from the competing isomerization (**1**-$D^{\bullet+}$)*→(**1a**-$D^{\bullet+}$)*→((CH_3O)(CH_2DO)P–$OH^{\bullet+}$) (**2**-$CD^{\bullet+}$)*. Note that this proposal implies that the observed equivalence in the methyl loss in the CID spectrum of **1**-$D^{\bullet+}$ is **not** due to interconversion with the enol ions but rather to a **post-collisional** isomerization **1a**$^{\bullet+}$→(**2**$^{\bullet+}$)*→ products. Such a mechanism probably also accounts for the $CH_3O^\bullet$ loss leading to the m/z 79 ions observed in the CID spectrum of DMP.

The m/z 79 ions in its EI spectrum on the other hand defy such an analysis since, apart from the direct route $110^{\bullet+}\rightarrow79^+$, they are (as demonstrated by MI and CID observations) also formed by the pathways $110^{\bullet+}\rightarrow109^+\rightarrow79^+$ and $110^{\bullet+}\rightarrow80^{\bullet+}\rightarrow79^+$. For this reason the AE derived ΔH_f (79^+) values in Table 2.1 remain somewhat ambiguous.

From the key PI data on DMP presented in Table 2.1, *viz.* IE (DMP) = 10.5 eV and AE (m/z 80) = 10.8 eV, it follows that the loss of CH_2=O from the molecular ion requires only 7 kcal/mol, denoted as "7(exp)" in Scheme 2.4. The AE of the m/z 80 product ion yields an apparent ΔH_f [**1**$^{\bullet+}$-CH_2=O] = 88 kcal/mol, which is 3 kcal/mol lower than the calculated value for ion **3a**$^{\bullet+}$ whose structure as depicted in Fig. 2.2 represents the lowest energy conformer at our level of theory. Nevertheless, considering the uncertainties associated with the experimental and computational observations, theory and experiment are still in satisfactory agreement in the description of the dissociation chemistry of the DMP molecular ion. Another small discrepancy between theory and experiment concerns the ΔH_f of the keto ion : the "experimental" value, denoted by the dashed level in Scheme 2.4, and derived from ΔH_f (**1**$^{\bullet+}$)(exp) = ΔH_f (**1**)(CBS-QB3) + IE (**1**) lies 4 kcal/mol higher in energy than the level derived from the computation on the ion, ΔH_f (**1**$^{\bullet+}$)(CBS-QB3). One reason for this discrepancy could be

that the ΔH_f (**1**)(CBS-QB3) value is too high. However, this is unlikely because adopting a higher value for neutral DMP would lead to a greater discrepancy in the derived heat of formation of the product ion $\mathbf{3a}^{\bullet+}$. Moreover, the calculated value for DMP shows a beautiful consistency when its PA is calculated from the expression : PA (DMP) = ΔH_f (**1**)(CBS-QB3) + ΔH_f (H^+) – ΔH_f (**1**+H^+)(CBS-QB3). Using the value presented in Table 2.2a for ΔH_f (**1**+H^+) [m/z 111, $(CH_3O)_2P(H)OH^+$] we derive PA (298) = 206.2 kcal/mol which compares very well with the experimental value, 206.4 kcal/mol [39]. More likely is the hypothesis that the IE (exp) = 10.5 eV, does not quite represent the adiabatic value : from ΔH_f ($\mathbf{1}^{\bullet+}$)(CBS-QB3) and ΔH_f (**1**)(CBS-QB3) we derive IE_{ad} (theory) = 10.3 eV, some 4 kcal/mol lower than the experimental value. In support of this suggestion, we note that the optimized geometries of neutral and ionized DMP are considerably different. If this interpretation is correct, then all EI generated (meta)stable DMP ions will have energies at or above the dashed level in Scheme 2.4, i.e. so close to TS [$\mathbf{1}^{\bullet+} \rightarrow \mathbf{1a}^{\bullet+}$] that they will virtually all have "distonicized" during their μs lifetime, as corroborated by the above CID experiment.

2.3.4. The structure of the [$1^{\bullet+}$-CH_2=O] and [$2^{\bullet+}$-CH_2=O] product ions $3a^{\bullet+}$ and $3b^{\bullet+}$

To underpin the foregoing analysis of the DMP system, we will now briefly discuss the experimental evidence that led to the assignment of the m/z 80 product ion structure(s) generated by the loss of CH_2=O from the precursor ions $\mathbf{1}^{\bullet+}$ and $\mathbf{2}^{\bullet+}$. The CID spectra of the source generated m/z 80 ions from the two tautomers are displayed in Fig. 2.5a and 2.5b respectively. The two spectra share a common intense $H^{\bullet}$ loss but differ in the intensity of another primary loss *viz.* that of $CH_3^{\bullet}$, which is much more pronounced in the spectrum derived from the enol ion : relative to the common m/z 47 (PO^+) peak we find a ratio with m/z 65 of 1.0 whereas for the keto ion the ratio becomes 4.1. This observation led us initially to believe that DMP and the enol ions from TMP produced different product ions upon loss of CH_2=O. We therefore considered a number of *a*

priori reasonable product ion structures which, in addition to $\mathbf{3a}^{\bullet+}$ and $\mathbf{3b}^{\bullet+}$ included the keto analogue of $\mathbf{3a}^{\bullet+}$, $CH_3O(H)P(H)=O^{\bullet+}$, $\mathbf{3c}^{\bullet+}$, the ylide ion $CH_2O(H)-P(H)-OH^{\bullet+}$, $\mathbf{3d}^{\bullet+}$, and $CH_3-P(OH)_2^{\bullet+}$, $\mathbf{3e}^{\bullet+}$, and calculated their ionic heats of formation, see Table 2.2a. By combining this information with the available energetics, it became readily apparent that isomers $\mathbf{3c}^{\bullet+}$ and $\mathbf{3d}^{\bullet+}$ lie far too high in energy to be considered. This left us with $\mathbf{3a}^{\bullet+}$ and $\mathbf{3b}^{\bullet+}$ and the very stable isomer $\mathbf{3e}^{\bullet+}$. The latter ion was envisaged to be generated from the dissociative ionization of diethyl methane phosphonate, $(C_2H_5O)_2P(CH_3)=O$, (by the consecutive loss of $CH_3CH=O$ and C_2H_4) and its CID spectrum was obtained. Although dominated by an intense $CH_3^{\bullet}$ loss, the spectrum of $\mathbf{3e}^{\bullet+}$ (not shown) also contains tell-tale peaks at m/z 45 and 44 (CH_2P/CHP type species) which are barely detectable in the spectra of Fig. 2.5a/b and thus rule out its participation.

The next crucial piece of experimental evidence pertaining to the structure assignment was the observation that whereas the CID mass spectrum of the **source** generated ions from the enol is different, the spectrum of the **metastable** enol ions appeared to be virtually identical with that of both the source and metastably generated m/z 80 ions derived from DMP. Two more experimental observations support that these ions have the proposed structure $\mathbf{3a}^{\bullet+}$. First, the m/z 81 ions of putative structure $CH_3O-P(D)-OH^{\bullet+}$ derived from $\mathbf{1}\text{-}D^{\bullet+}$ show a specific loss of $D^{\bullet}$ in their CID spectrum, while this is the only reaction observed in their MI spectrum. This is indeed to be expected for the dissociation of ions $\mathbf{3a}^{\bullet+}$: from the tabulated ΔH_f values it follows that loss of $H^{\bullet}$ yielding $CH_3-O-POH^+$ ($\Sigma\Delta H_f$ products = 123 kcal/mol) is energetically far more favorable than either loss of $CH_3^{\bullet}$ into $HO-P(H)=O^+$ ($\Sigma\Delta H_f$ products = 158 kcal/mol) or loss of $CH_3O^{\bullet}$ into $H-P-OH^+$ ($\Sigma\Delta H_f$ products = 171 kcal/mol).

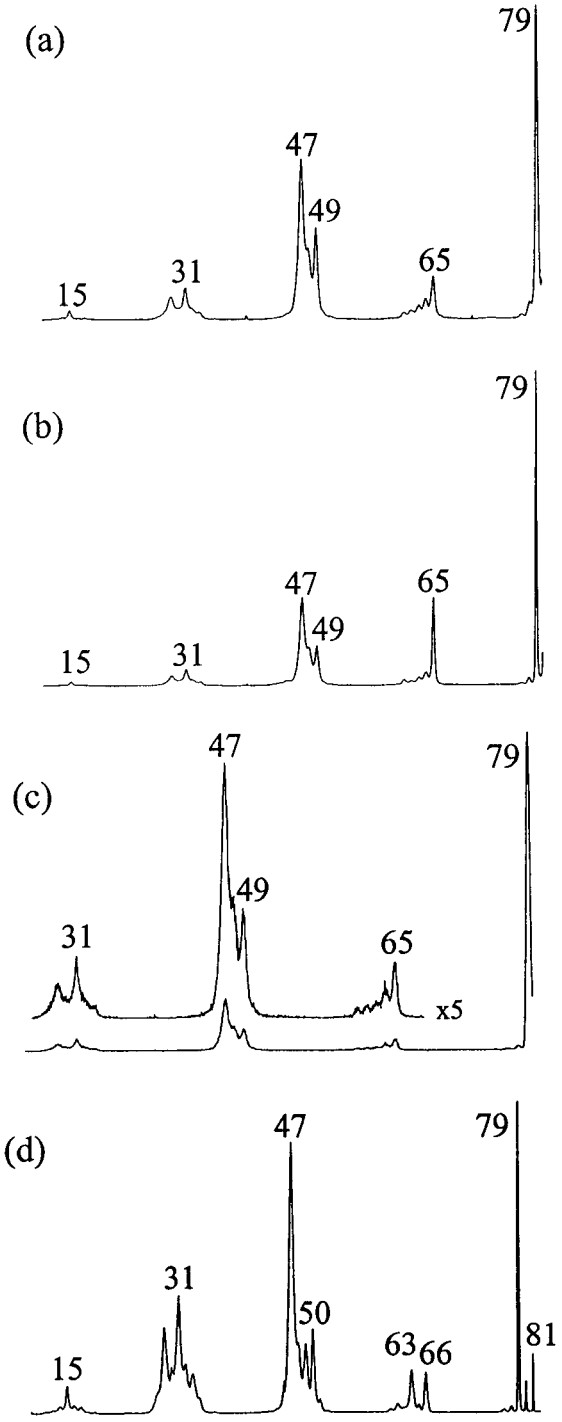

Fig. 2.5. CID and NR spectra of m/z 80 ions and their isotopologues: **(a)** CID spectrum of source generated m/z 80 ions from DMP, **1**; **(b)** CID spectrum of source generated m/z 80 ions from TMP; **(c)** CID/NR spectrum of m/z 80 "survivor" ions following neutralization and reionization of m/z 80 ions derived from **1**; **(d)** NRMS of m/z 81 derived from **1-D**.

What then does the spectrum of Fig. 2.5b, i.e. that of the source generated m/z 80 ions from TMP, signify? Scheme 2.4 predicts that loss of CH_2=O via two mechanisms yielding a mixture of product ions **3a**$^{\bullet+}$ and **3b**$^{\bullet+}$ is an inherent property of high-energy enol ions **2**$^{\bullet+}$. In this context we note that the solitary ions **3a**$^{\bullet+}$ and **3b**$^{\bullet+}$ do not readily interconvert because the calculated barrier for the associated 1,2-H shift is quite high, 44 kcal/mol, Table 2.2a.

That the CID spectrum of Fig. 2.5b indeed represents a mixture of non-interconverting ions **3a**$^{\bullet+}$ and **3b**$^{\bullet+}$ comes from the following two observations: (i) the corresponding MI spectrum contains two narrow peaks associated with losses of H$^{\bullet}$ and $CH_3^{\bullet}$. The loss of H$^{\bullet}$ is readily assigned to dissociation from **3a**$^{\bullet+}$ (see above) whereas that of $CH_3^{\bullet}$ is to be expected for metastable ions **3b**$^{\bullet+}$. For these ions, loss of $CH_3^{\bullet}$ yielding HO–P–OH$^+$ ($\Sigma\Delta H_f$ products = 111 kcal/mol) is clearly energetically much more favorable than loss of H$^{\bullet}$ yielding CH_3O–P–OH$^+$ ($\Sigma\Delta H_f$ products = 123 kcal/mol) and thus only loss of $CH_3^{\bullet}$ should be present in the MI spectrum of isomerically pure ions **3b**$^{\bullet+}$; (ii) whereas the CID spectra of m/z 80 ions generated from metastable enol ions clearly have the structure of **3a**$^{\bullet+}$, CID experiments on the m/z 80 ions featuring in the CID spectra of Fig. 2.3b and 2.3c yield spectra with increased m/z 47 : m/z 65 ratios (2.4 and 1.5 respectively) showing that upon collisional excitation indeed mixtures of **3a**$^{\bullet+}$ and **3b**$^{\bullet+}$ are generated.

To further confirm the isomeric purity of the **3a**$^{\bullet+}$ ions generated from DMP we have also obtained NR spectra of the m/z 80 ions from **1**$^{\bullet+}$ and the m/z 81 CH_3O–P(D)–OH$^{\bullet+}$ ions derived from **1-D**$^{\bullet+}$. The latter spectrum is shown as item d in Fig. 2.5 and displays a "survivor" signal of reasonable intensity. The corresponding "survivor" ions in the spectrum of the unlabelled ion were mass selected and subjected to a CID experiment yielding the CID "survivor" spectrum of Fig. 2.5c. This spectrum displays a m/z 47/65 ratio (4.8) which is very close to that of the CID spectrum of Fig. 2.5a, thus showing that we are indeed dealing with isomerically pure ions **3a**$^{\bullet+}$. That the m/z 79 ions are more prominent in the CID "survivor" spectrum is in keeping with the general observation that ions generated by the NR sequence often have a higher internal

energy (and thus contain a larger fraction of metastable ions) than those sampled in the CID experiment.

Finally, we note that loss of $D^{\bullet}$ rather than $H^{\bullet}$ characterizes the NR spectrum of the $\mathbf{3a}^{\bullet+}$ isotopologue $CH_3O–P(D)–OH^{\bullet+}$. This provides compelling evidence that the incipient neutral enol species $CH_3O–P(D)–OH$ do not isomerize into their more stable neutral keto counterpart $CH_3O(H)P(D)=O$. (The neutral keto isomer, **3c** in Table 2.2b, is more stable than it's enol **3a** by 10 kcal/mol). If this were so, the equivalently bonded H and D atoms would be lost to about the same extent in the dissociation of the reionized species. This is clearly not the case : the neutral enol retains its structure integrity and, in line with the discussion in the next Section for the neutral counterpart of enol $\mathbf{2}^{\bullet+}$, this is because the "keto" and "enol" type neutral species are separated by a high 1,2-H shift barrier.

2.3.5. Neutralization-reionization experiments on ions $1^{\bullet+}$ and $2^{\bullet+}$: does the neutral enol 2 isomerize into its more stable DMP counterpart ?

We will interpret the neutralization reionization mass spectra of $\mathbf{1}^{\bullet+}$ and $\mathbf{2}^{\bullet+}$ presented in Fig. 2.6 using the energy diagram of Scheme 2.5 as our guide. The top part of this diagram is based on Scheme 2.4 and summarizes the relationship between the ions, whereas the bottom part deals with our computational results for the corresponding neutrals and the barrier for their interconversion by a 1,2-H shift. This energy barrier is quite high, 63 kcal/mol relative to **1**, which is more stable than its enol counterpart by 15 kcal/mol (Table 2.2b) [74]. From the enthalpy difference between $\mathbf{2}^{\bullet+}$ and **2** (Table 2.2a/b) an adiabatic ionization energy, IE_{ad} (**2**), is derived of 8.3 eV, which compares reasonably well with the available experimental value, 8.4 eV, [33] for the related compound $(CH_3O)_3P$, trimethyl phosphite.

The neutralization and collisional ionization events in a NR experiment with ions of keV translational energy are essentially vertical processes [23]. We have therefore estimated the vertical neutralization energy of $\mathbf{2}^{\bullet+}$ (~ 7.5 eV) as well as the vertical IE of the neutral (~ 9.5 eV), see the labelled arrows in Scheme 2.5. These

estimates are derived from energy calculations (at the B3LYP/6-311G (2d,d,p) level of theory) on the neutral having the optimized geometry of the ion and vice versa.

On the basis of the simple picture of the NR process shown in Scheme 2.5 (which ignores the dissociation chemistry of the excited neutrals), we anticipate that neutralization of (low energy) ions $\mathbf{2}^{\bullet+}$ yields excited neutrals **2** at the dashed energy level in the neutral enol well. Since this level lies well below the TS for ketonization, it is unlikely that the neutralization will lead to a significant degree of ketonization. Collisional ionization of the neutrals is expected to yield excited ions, at or above the dashed level in the well of ion $\mathbf{2}^{\bullet+}$, but not to such an extent that a complete dissociation takes place. In other words, we anticipate that the NR spectrum of $\mathbf{2}^{\bullet+}$ shows a "survivor" ion and no evidence for the ketonization of the neutral. This is indeed borne out by the NR spectrum presented in Fig. 2.6a : a survivor ion at m/z 110 is clearly present, while the intensity distribution of the primary fragment ions at m/z 95, 93, 80 and 79, is clearly compatible with that of enol ions, compare Fig. 2.3b/c. Moreover, the m/z 109 peak is barely detectable and considering that this is a tell-tale peak in the collisional ionization of DMP neutrals, see Fig. 2.4b, it follows that ketonization of the incipient neutral enol in the NR of $\mathbf{2}^{\bullet+}$ has **not** occurred.

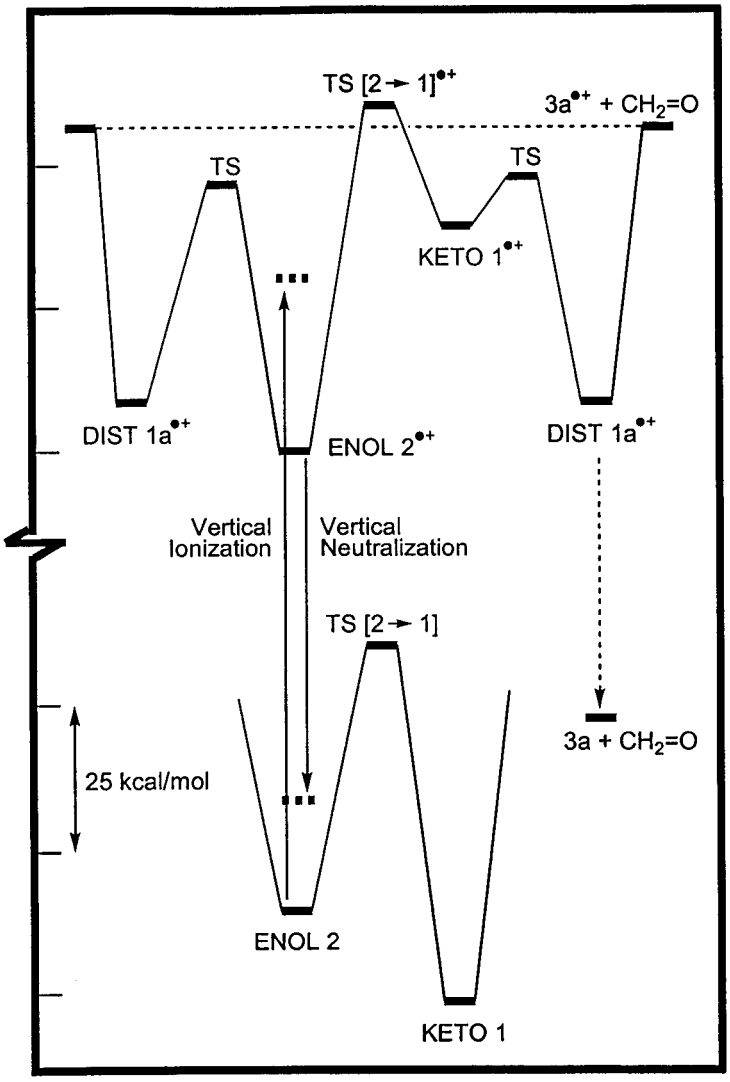

Scheme 2. 5

The CID spectrum of the m/z 110 "survivor" ions in Fig. 2.6a was also obtained and is presented in Fig. 2.6b. This spectrum indicates that most of the survivor enol ions have an internal energy close to the dissociation threshold for loss of CH_2=O as witnessed by the intense m/z 80 signal. Unlike the CID spectra of $\mathbf{1}^{\bullet+}$/ $\mathbf{1a}^{\bullet+}$ and $\mathbf{2}^{\bullet+}$ (see Fig. 2.4c and 2.3b/c) this spectrum shows a much more pronounced loss of $CH_3^{\bullet}$ (m/z 95) vs. that of $CH_3O^{\bullet}$ (m/z 79). We tentatively propose that this is because the "survivor" enol ions gain sufficient internal energy in the collisional ionization process to access the potential well of $\mathbf{1b}^{\bullet+}$: these distonic ions are expected to lose CH_2=O and $CH_3^{\bullet}$ but not $CH_3O^{\bullet}$. Moreover, the $^{+}CH_2$-O-P(OH)$_2$ ion generated by loss of $CH_3^{\bullet}$ from

1b$^{\bullet+}$ is ~ 4 kcal/mol more stable than CH_3O-P(OH)=O$^+$ produced from **2**$^{\bullet+}$, see Table 2.2a.

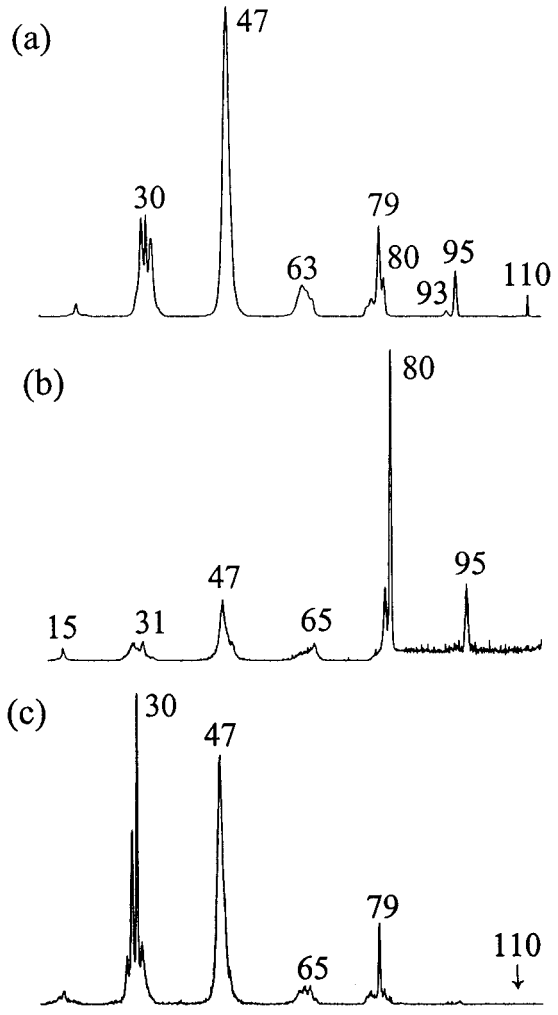

Fig. 2.6. NR and CID spectra of m/z 110 ions: **(a)** NRMS of ion **2**$^{\bullet+}$ derived from TMP; **(b)** CID/NR spectrum of m/z 110 "survivor" ion from **2**$^{\bullet+}$; **(c)** NRMS of ions **1**$^{\bullet+}$/**1a**$^{\bullet+}$ derived from DMP.

The NR spectrum of **1**$^{\bullet+}$ is presented in Fig. 2.6c. The base peak at m/z 30 largely results from CIDI of the CH_2=O neutrals that are abundantly generated in the dissociation of metastable ions. More importantly, the spectrum does not show a "survivor" signal at m/z 110 and no peak at m/z 109 either. This reinforces our proposal that ions **1**$^{\bullet+}$ with lifetimes in the μs timeframe have all "distonicized". Neutralization of

$\mathbf{1a}^{\bullet+}$ is not expected to yield a stable neutral counterpart but rather, see Scheme 2.5, its (excited) dissociation products CH_3O-P(H)-OH (**3a**) + CH_2=O. Considering the NR spectrum of **3a**, see Fig. 2.5d, which shows prominent peaks at m/z 79 and 47 and only a survivor ion of moderate intensity, we conclude that the NR spectrum of Fig. 2.6c is indeed compatible with that of the distonic ion $\mathbf{1a}^{\bullet+}$.

2.4. Dipole molecule assisted lowering of barriers for H-shifts

2.4.1. Does proton transport catalysis play a role in the isomerization reactions of ions $1a^{\bullet+}$ and $1b^{\bullet+}$?

Proton transport catalysis has been coined as a generic term to describe the experimental and theoretical findings [25a] that a high H-shift barrier between a pair of solitary isomeric ions $[H\text{-}X\text{-}Y]^{\bullet+}$ and $[X\text{-}Y\text{-}H]^{\bullet+}$ can become drastically lower when these ions can interact with a single "solvent" molecule B in an ion-(dipole) molecule complex.

One prominent example concerns X=CH_2 and Y=OH, that is the α-distonic $[CH_2OH_2]^{\bullet+}$ ion. This ion is more stable than its isomer $[CH_3OH]^{\bullet+}$ and the solitary ions do not interconvert because of a high 1,2-H shift barrier. A single water molecule (B), however, catalyzes this shift and promotes a smooth transformation of $[CH_3OH]^{\bullet+}$ into $[CH_2OH_2]^{\bullet+}$ [25b].

In more general terms the "catalysis" has been proposed [25c] to be most efficient when the proton affinity (PA) of the base B, lies between the PA of [X-Y] at X and Y, according to :

$$[H\text{-}X\text{-}Y]^{\bullet+} + B \rightarrow [B\bullet\bullet\bullet H^{+}\bullet\bullet\bullet(X\text{-}Y)^{\bullet}] \rightarrow [B\bullet\bullet\bullet H^{+}\bullet\bullet\bullet(Y\text{-}X)^{\bullet}] \rightarrow B + [X\text{-}Y\text{-}H]^{\bullet+} \qquad \text{[Eqn. 1]}$$

Such catalysis is not restricted to bimolecular reactions but also takes place in dissociative rearrangement reactions where ion-dipole complexes and/or H-bridged radical cations (HBRC) intervene [24]. It could therefore also play a role in the dissociation chemistry of the DMP system as described in Scheme 2.4, where the ions $\mathbf{ID\text{-}3a}^{\bullet+}$ and $\mathbf{ID\text{-}3b}^{\bullet+}$ represent complexes of a CH_2=O molecule with the 1,2-H shift isomers $\mathbf{3a}^{\bullet+}$ and $\mathbf{3b}^{\bullet+}$. As was established in Section 2.3.4 and is depicted in the upper part of Scheme 2.6, the two solitary ions do not interconvert. However, interaction with

the CH_2=O molecule in the complexes could lower the 1,2-H shift barrier to such an extent that the interconversion **ID-3b**$^{\bullet+}$/**ID-3a**$^{\bullet+}$ and thereby also that of their distonic "partner" ions **1b**$^{\bullet+}$/**1a**$^{\bullet+}$ becomes feasible. Not surprisingly, the direct communication between the two distonic ions via a 1,2-H shift, see TS **1a**$^{\bullet+}$→**1b**$^{\bullet+}$ in Table 2.2a, has a prohibitively high barrier.

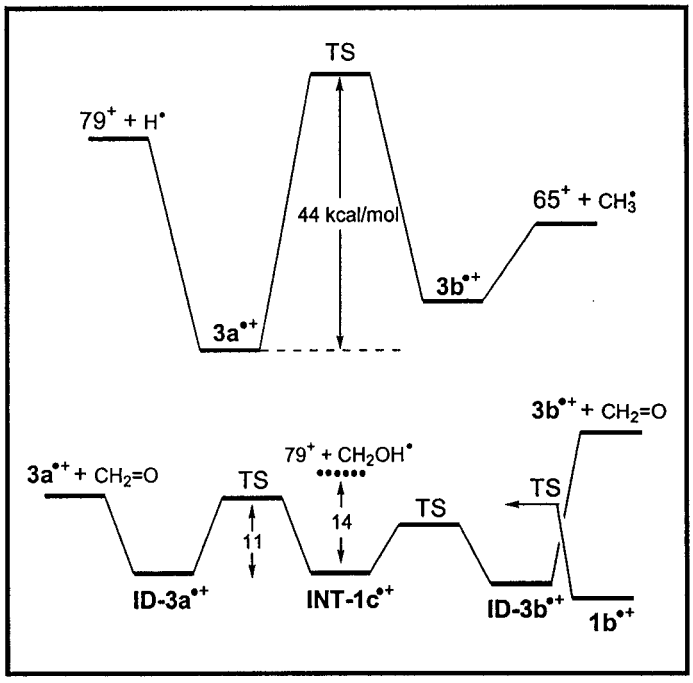

Scheme 2.6

The results of our computational findings on this question are depicted in the bottom part of Scheme 2.6. The actual energies for the various species and their connecting transition states are given in Table 2.2a (bottom part) while the associated optimized geometries are presented in Fig. 2.2. It is seen from Scheme 2.6 that the high 1,2-H shift barrier between solitary ions **3a**$^{\bullet+}$ and **3b**$^{\bullet+}$ is indeed significantly lowered in the complexes with CH_2=O, from 44 kcal/mol to 11 kcal/mol! However, the remaining barrier lies so close to the dissociation threshold **3a**$^{\bullet+}$ + CH_2=O that, whereas the dissociative isomerization route **1b**$^{\bullet+}$→**ID-3b**$^{\bullet+}$→**ID-3a**$^{\bullet+}$→**3a**$^{\bullet+}$ + CH_2=O should be feasible, a facile interconversion between **1b**$^{\bullet+}$ and **1a**$^{\bullet+}$ clearly is not. This pathway therefore has no immediate bearing on the analysis of the experimental results presented in Section 2.3.

Two further points deserve comment. First, from the enthalpies listed in Table 2.2 for the radical CH_3-**O**-P-$OH^{\bullet}$ and the ions CH_3-**O**-P(H)-$OH^{\bullet+}$, **3a**$^{\bullet+}$, and CH_3-**O**(H)-P-$OH^{\bullet+}$, **3b**$^{\bullet+}$, we derive PA values for protonation at [P] and [**O**] in the radical of 191 and 183 kcal/mol respectively. These values are higher than PA of CH_2=O, 170 kcal/mol [28] and thus, according to the criterion mentioned above, formaldehyde is not the "ideal" base for the catalysis. The other point concerns the structure of the stable intermediate, INT-**1c**$^{\bullet+}$, involved in the transformation **ID-3b**$^{\bullet+}$ →**ID-3a**$^{\bullet+}$. This ion, see Fig. 2.2, consists of a CH_3O-P-OH moiety connected, by a fairly long CH_2-O(H)•••P bond of 2.87 Å, with the CH_2OH moiety. The geometry of the CH_3O-P-OH moiety is closely similar to that calculated for the solitary **ion** (m/z 79) while the calculated charge distribution for INT-**1c**$^{\bullet+}$ shows that it carries 90 % of the positive charge, which is largely located on the P atom. Thus INT-**1c**$^{\bullet+}$ is best represented as a CH_3O-P^+-OH ion in which the positively charged P atom interacts with the oxygen lone pair electrons of the $^{\bullet}CH_2OH$ dipole radical. As indicated in Scheme 2.6, the intermediate enjoys a stabilization energy of 14 kcal/mol relative to its dissociation products 79^+ + $^{\bullet}CH_2OH$ which, considering that μ ($^{\bullet}CH_2OH$) = ~ 1.5 D, may be largely ascribed to an ion-dipole interaction.

One final point bears addressing, namely the formation of INT-**1c**$^{\bullet+}$ from the HBRC **ID-3b**$^{\bullet+}$. In this ion the bridging H carries a large fractional charge (0.78) suggesting that a **proton** is being transferred rather than a $H^{\bullet}$ radical and indeed the charge distribution and the geometrical parameters of TS **ID-3b**$^{\bullet+}$→INT-**1c**$^{\bullet+}$ seem to support this. However, while the CH_2OH moiety roughly carries a (+1) charge in **ID-3b**$^{\bullet+}$, its net change in INT-**1c**$^{\bullet+}$ is close to zero. This suggests that an avoided crossing takes place along the path from **ID-3b**$^{\bullet+}$ to INT-**1c**$^{\bullet+}$: considering the fact that at the CBS-QB3 level, the $H_2COH^{\bullet}$ + CH_3OPOH^+ limit lies 17.0 kcal/mol below the H_2COH^+ + $CH_3OPOH^{\bullet}$ limit, this should not come as a surprise. It does suggest that both structure and energetics of TS **ID-3b**$^{\bullet+}$→INT-**1c**$^{\bullet+}$ are not rigorously defined: nevertheless, this is unlikely to materially affect any conclusions being made here.

2.4.2. Ion-molecule reactions with benzonitrile lead to a complete enolization of DMP

From the discussion in Section 2.3, it has become clear that in the μs timeframe DMP ions $\mathbf{1}^{\bullet+}$ have completely "distonicized" into $\mathbf{1a}^{\bullet+}$ but do not significantly communicate with their more stable enol counterparts $\mathbf{2}^{\bullet+}$. We note that this conclusion is consistent with the quote from [11d] mentioned in the introduction that at a lifetime of ≥ 1s, DMP ions undergo at least a partial isomerization into the phosphite structure $\mathbf{2}^{\bullet+}$. Time-resolved CID [40] experiments that we have carried out on ions $\mathbf{1}^{\bullet+}$ and $\mathbf{2}^{\bullet+}$ have indicated that structure specific peak intensity ratios such as 95/93 remain different for the two ions on a time scale of several hundred microseconds. This would indicate that enolization does not take place unimolecularly on the millisecond time scale. However, if the high 1,3-H shift barrier responsible for this phenomenon, TS [**2**→**1a**] in Scheme 2.4, could be lowered by the interaction of $\mathbf{1a}^{\bullet+}$ with a suitable base in an ion-molecule reaction the enolization could be accomplished.

From the calculated enthalpies listed in Table 2.2 for the radical $^{\bullet}CH_2O$-P(OH)(OCH_3) and the ions $^{\bullet}CH_2O$-P^{+}(H)(OH)(OCH_3), $\mathbf{1a}^{\bullet+}$ and CH_3O-P(OH)(OCH_3)$^{\bullet+}$, $\mathbf{2}^{\bullet+}$, we derive PA values for protonation at [P] and [C] in the radical of 214 and 221 kcal/mol respectively. Thus the ideal base should have a PA in this range. Benzonitrile (BN) has a somewhat lower PA (194 kcal/mol). Since it has other desirable properties including a high dipole moment (μ = 4.2 D) and little tendency to self-protonation, it was chosen as the base.

When BN and DMP were introduced into the chemical ionization source of the instrument in a 10 : 1 ratio at a pressure of 4 x 10^{-5} Torr, the mass spectrum of Fig. 2.7a was obtained. Apart from the expected intense BN derived ions at m/z 103 ($BN^{\bullet+}$), 104 (BNH^{+}), 179 ($BN+C_6H_5^{+}$), 206 ($[BN]_2^{\bullet+}$) and 207 ($[BN]_2H^{\bullet+}$), there are also peaks of sizable intensity for DMP containing ions : m/z 214 (BN-H-DMP^{+}), m/z 221 ($[DMP]_2H^{+}$) and the ion of interest at m/z 213, ["DMP"•••C_6H_5CN]$^{\bullet+}$. Next, the MI and CID spectra of the m/z 213 complex ion were obtained and both spectra appeared to be dominated by a peak at m/z 110. This already indicates that the DMP component in the complex has not retained its structure identity. This is because IE (DMP) (10.5 eV) is larger than

IE (BN) (9.8 eV) and thus, had the DMP structure been retained, the MI spectrum should have been dominated by $BN^{\bullet+}$ ions at m/z 103, which is not the case. The CID mass spectra of these m/z 110 ions as recorded in MI/CID or CID/CID experiments were closely similar. A representative spectrum is shown in Fig. 2.7b and comparison with the spectra of Fig. 2.3b/c and Fig. 2.4c leaves little doubt that the "DMP" ions in the complex have the enol structure $\mathbf{2}^{\bullet+}$. The same is true for the weak m/z 110 ions that are found in the mass spectrum of Fig. 2.7a. Thus we conclude that BN effectively catalyzes the enolization of DMP ions. The mechanism most likely involves a BN promoted lowering of the 1,3-H shift barrier in DMP's distonic ion $\mathbf{1a}^{\bullet+}$. The alternative, that the base BN would lower the 1,2-H shift barrier in DMP molecular ions is less likely because in encounter complexes between $DMP^{\bullet+}$ and BN the positive charge will be transferred to the benzonitrile moiety.

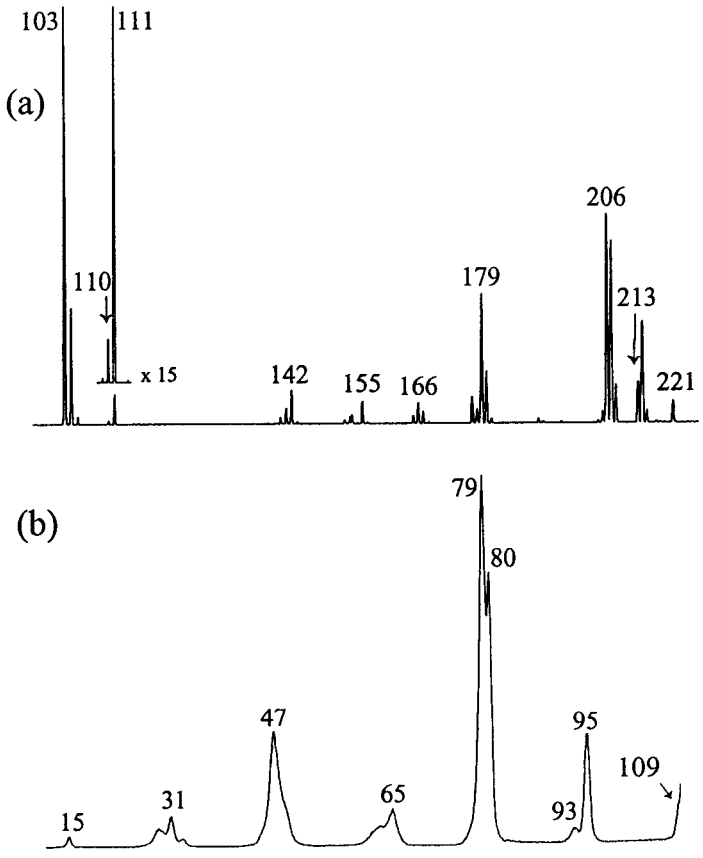

Fig. 2.7. Benzonitrile (BN) chemical ionization of DMP: (a) Mass spectrum at a pressure of 4 x 10^{-5} Torr and a BN:DMP = 10:1 ratio; (b) A CID/CID spectrum - CID of m/z 110 ions generated by CID from m/z 213 ions.

References

[1] D. E. C. Corbridge, *Phosphorus: an outline of its chemistry, biochemistry, and uses*, 5th ed., Elsevier, New York, 1995.

[2] J. Emsley and D. Hall, *The Chemistry of Phosphorus*, Harper and Row Ltd., London, 1976.

[3] M. Eto, Organophosphorus Pesticides: Organic and Biological Chemistry, CRC Press, Cleveland, Ohio (1974).

[4] Selected reviews: (a) R. A. J. O'Hair, in: *The Chemistry of Organophosphorus Compounds*, *Vol. 4*, ed. F. R. Hartley, John Wiley and Sons Ltd., 1996, Chapter 8. (b) R. G. Gillis and J. L. Occolowitz, in: *Mass Spectrometry of Phosphorus Compounds* in *Analytical Chemistry of Phosphorus Compounds*, ed. M. Halmann, Wiley-Interscience, New York, 1972, Chapter 8. (c) J. R. Chapman, *Organophosphorus Chem.* 1983, **14**, 278. (d) J. Granoth, *Top. Phosphorus Chem.* **8** (1976) 41.

[5] (a) S.Gevrey, A. Luna, M-H.Taphanel, J. Tortajada and J-P.Morizur, *Int. J. Mass Spectrom.* **195/196** (2000) 545. (b) J-F. Gal, M. Herreros, P. C. Maria, L. Operti, C. Pettigiani, R. Rabezanna and G. A. Vaglio, *J. Mass Spectrom.* **34** (1999) 1296. (c) B. L. M. van Baar, A. G. Hulst and E. R. J. Wils, *J. Mass Spectrom.* **32** (1998) 1104.

[6] (a) J. L. Occolowitz and G. L. White, *Anal. Chem.* **35** (1963)1179. (b) J. G. Pritchard, *Org. Mass Spectrom.* **3** (1970) 163.

[7] (a) E. Santoro, *Org. Mass Spectrom.* **7** (1973) 589. (b) D. A. Bafus, E. J. Gallegos and R. W. Kiser, *J. Phys. Chem.* **70** (1966) 2614 and ASTIA, AD 84063, NBS No 6A219 (1955) quoted therein. (c) J. Fischler and M. Halman, *J. Chem. Soc.* 1964, 31.

[8] (a) *Tandem Mass Spectrometry*, ed. F. W. McLafferty, Wiley, New York, 1983. (b) K. Levsen and H. Schwarz, *Mass Spectrom. Rev.* **2** (1983) 77.

[9] K. L. Busch, G. L. Glish and S. A. McLuckey, *Mass Spectrometry/Mass Spectrometry*, VCH, New York, 1988.

[10] J. L. Holmes, *Org. Mass Spectrom.* **20** (1985) 169.

[11] (a) H. I. Kenttämaa and R. G. Cooks, *J. Am. Chem. Soc.* **107** (1985) 1881. (b) J. S. Brodbelt, H. I. Kenttämaa and R. G. Cooks, *Org. Mass Spectrom.* **23** (1988) 6. (c) L. Zeller, J. Farrell Jr., P. Vainiotalo and H. I. Kenttämaa, *J. Am. Chem. Soc.* **114** (1992) 1205. (d) K. M. Stirk, P. Lin, T. D. Ranatunga, L. C. Zeller, J. T. Farrell Jr. and H. I. Kenttämaa, *Int. J. Mass Spectrom. Ion Proc.* **130**, (1994) 187.

[12] (a) J. R. Holtzclaw, J. R. Wyatt and J. E. Campana, *Org. Mass Spectrom.* **20** (1985) 90. (b) J.R. Holtzclaw and J. R.Wyatt, *Org. Mass Spectrom.* **23** (1988) 261.

[13] F. Tureček, M. Gu and C. E. C. A. Hop, *J. Phys. Chem.* **99** (1995) 2278.

[14] G. O. Doak and L. D. Freedman, *Chem. Rev.* **61** (1961) 31.

[15] *The Chemistry of Enols*, ed. Z. Rappoport, Wiley, New York, 1990.

[16] W. J. Pietro and W. J. Hehre, *J. Am. Chem. Soc.* **104** (1982) 3594.

[17] E. M. Georgiev, J. Kaneti, K. Troev and D. M. Roundhill, *J. Am. Chem. Soc.* **115**, (1993) 10964.

[18] M. A. Trikoupis, J. K. Terlouw and P. C. Burgers, *J. Am. Chem. Soc.* **120** (1998) 12131 and references therein.

[19] (a) N. Heinrich, J. Schmidt, H. Schwarz and Y. Apeloig, *J. Am. Chem. Soc.* **109** (1987) 1317. (b) D. Suh, J. T. Francis, J. K. Terlouw, P. C. Burgers, and R. D. Bowen, *Eur. Mass. Spectrom.* **1** (1995) 545.

[20] J. L. Holmes and J. K. Terlouw, *Org. Mass Spectrom.* **15** (1980) 383.

[21] J. Berkowitz, *Photoabsorption, Photoionization and Photoelectron Spectroscopy*, Academic Press, New York, 1979.

[22] (a) J. A. Montgomery Jr, M. J. Frisch, J. W. Ochterski, and G. A. Petersson, *J. Chem. Phys.* **110** (1999) 2822. (b) ibid. **112** (2000) 6532.

[23] For a recent review see: G. Schalley, G. Hornung, D. Schröder and H. Schwarz, *Chem. Soc. Rev.* **27** (1998) 91.

[24] (a) P. J. A. Ruttink, P. C. Burgers, L. M. Fell and J. K. Terlouw, *J. Phys. Chem. A* **102** (1998) 2976. (b) L. M. Fell, P. J. A. Ruttink, P. C. Burgers, M. A. Trikoupis and J. K. Terlouw, *Int. J. Mass Spectrom.* **195/196** (2000) 85. (c) for a brief review see: J. K. Terlouw, in *Proceedings of the 8th ISMAS Symposium*, ed. S. K. Aggarwal, Hyderabad, India, 1999, Chapter 31.

[25] For selected references see: (a) D. K. Böhme, *Int. J. Mass Spectrom. Ion Proc.* **115** (1992) 95. (b) J. W. Gauld, H-E. Audier, J. Fossey and L. Radom, *J. Am. Chem. Soc.* **118** (1996) 6299. (c) J. W. Gauld and L. Radom, *J. Am. Chem. Soc.* **119** (1997) 9831. (d) A. J. Chalk and L. Radom, *J. Am. Chem. Soc.* **119** (1997) 7573. (e) A. J. Chalk and L. Radom, *J. Am. Chem. Soc.* **121** (1999) 1574. (f) J. Chamot-Rooke, G. van der Rest, P. Mourgues, and H-E. Audier, *Int. J. Mass Spectrom.* **195/196** (2000) 385. (g) M. A. Trikoupis, D. J. Lavarato, J. K. Terlouw, P. J. A. Ruttink and P. C. Burgers, *European Mass Spectrom.* **5** (1999) 431.

[26] C. Lifshitz, *Int. J. Mass Spectrom. Ion Processes* **106** (1991) 159.

[27] Y. Ling and C. Lifshitz, *J. Phys. Chem. A* **102** (1998) 708.

[28] S. G. Lias, J. E. Bartmess, J. F. Liebman, J. L. Holmes, R. D. Levin, W. G. Mallard, *J. Phys. Chem. Ref. Data* **17** (1988) Suppl. 1; see also NIST Chemistry WebBook, http://webbook.nist.gov/chemistry/

[29] J. C. Traeger and B. M. Kompe, in: *Energetics of Organic Free Radicals*, ed. J. A. Martinho Simoes, A. Greenberg and J. F. Liebman, Blackie Academic & Professional, New York , 1996, Chapter 3.

[30] For TMP [7b] uses –239.4 kcal/mol from an unverifiable source while the tabulation [28] quotes –265 kcal/mol as an unspecified estimate. The Pedley compilation[31] contains very few PO compounds but from its listed ΔH_f values for $(C_2H_5O)_3P{=}O$ is –283.6 ± 1.4 ; $(CH_3O)_3P$ is –168.6 ± 17.6 and $(C_2H_5O)_3P$ is –194.4 ± 1.3 kcal/mol, we estimate ΔH_f (298K) $(CH_3O)_3P{=}O$ is –257 kcal/mol, supporting the CBS-QB3 value of –255.5 kcal/mol (Table 2.2b). For DMP where no such estimate can be made and whose CBS-QB3 value is –187.7 kcal/mol, the situation is even more problematic: the value reported in [32], -198.1 kcal/mol, is clearly in error because the Benson additivity term for O(H)P=O used in the calculation is nonexistent whereas for the estimate given in [28], -200 kcal/mol no justification is available (J. F. Liebman, personal communication, February 1999).

[31] J. B. Pedley, R. D. Naylor and S. P. Kirby, *Thermochemical Data of Organic Compounds*, 2nd ed., Chapman and Hall, London, 1986.

[32] R. M. McDonald, A. K. Chowdhury, W. Y. Gung and K. D. Witt, in: *Nucleophilic Reactivity in Anionic Ion-Molecule Reactions in Nucleophilicity*, ed. J. M. Harris and S. P. McManus, American Chemical Society, Washington, 1987.

[33] S. Chattorpadhyay, G. L. Findley, S. P. McGlynn, *J. Electron Spectrosc. Rel. Phenom.* **24** (1981) 27.

[34] V. V. Zverev and Y. Y. Villem, *J. Struct. Chem.* (USSR) **21** (1980) 22.

[35] H. F. van Garderen, P. J. A. Ruttink, P. C. Burgers, G. A. McGibbon and J. K. Terlouw, *Int. J. Mass Spectrom. Ion Proc.* **121** (1992) 159.

[36] C. Glidewell and P. J. Pogorzelec, *J. Chem. Ed.* **57** (1980) 740.

[37] M. A. Trikoupis, J. K. Terlouw, P. C. Burgers, M. Peres and C. Lifshitz, *J. Am. Soc. Mass Spectrom.* **10** (1999) 869 and references cited therein.

[38] E. P. Hunter and S. G. Lias, *J. Phys. Chem. Ref. Data* **27** (1998) 413.
[39] [16] reports that the gas-phase proton affinity of DMP is 2.4 kcal/mol greater than that of standard ammonia. Using PA (NH_3) = 204.0 kcal/mol ([38]) the absolute PA of DMP is assigned a value of 206.4 kcal/mol. This value is supported by the gas-phase basicity measurements reported in [5b]. The incorrect PA value (214 kcal/mol) reported in [38] may be due to a transcription error.
[40] C. Lifshitz, E. Nadav, M. Peres, T. Peres, J. Laskin, B. Karsenty and M. Shaked, 1994, *Int. J. Mass Spectrom. Ion Proc.* **133** (1994) L11.
[41] M. J. Frisch, G. W. Trucks, H. B. Schlegel, G. E. Scuseria, M. A. Robb, J. R. Cheeseman, V. G. Zakrzewski, J. A. Montgomery, R. E. Stratmann, J. C. Burant, S. Dapprich, J. M. Millam, A. D. Daniels, K. N. Kudin, M. C. Strain, O. Farkas, J. Tomasi, V. Barone, M. Cossi, R. Cammi, B. Mennucci, C. Pomelli, C. Adamo, S. Clifford, J. Ochterski, G. A. Petersson, P. Y. Ayala, Q. Cui, K. Morokuma, D. K. Malick, A. D. Rabuck, K. Raghavachari, J. B. Foresman, J. Cioslowski, J. V. Ortiz, B. B. Stefanov, G. Liu, A. Liashenko, P. Piskorz, I. Komaromi, R. Gomperts, R. L. Martin, D. J. Fox, T. Keith, M. A. Al-Laham, C. Y. Peng, A. Nanayakkara, C. Gonzalez, M. Challacombe, P. M. W. Gill, B. G. Johnson, W. Chen, M. W. Wong, J. L. Andres, M. Head-Gordon, E. S. Replogle, and J. A. Pople, *Gaussian 98, Revision A.3*, Gaussian, Inc., Pittsburgh, PA, 1998.
[42] K. Fukui, *Acc. Chem. Res.* **14** (1981) 363.
[43] C. Gonzalez and H. B. Schlegel, *J. Phys. Chem.* **94** (1990) 5523.
[44] A. D. Becke, *J. Chem. Phys.* **98** (1993) 5648.
[45] C. Lee, W. Yang, and R. G. Parr, *Phys. Rev. B* **37** (1988) 785.
[46] R. Krishnan, J. S. Binkley, R. Seeger and J. A. Pople, *J. Chem. Phys.* **72** (1980) 650.
[47] A. D. McLean, G. S. Chandler, *J. Chem. Phys.* **72** (1980) 5639.
[48] J. Cioslowski, *J. Am. Chem. Soc.* **111** (1989) 8333.
[49] K. Raghavachari, G. W. Trucks, J. A. Pople, and M. Head-Gordon, *Chem. Phys. Lett.* **157** (1989) 479.
[50] T. J. Lee and G. E. Scuseria, in: *Quantum mechanical electronic structure calculations with chemical accuracy*, ed. S. R. Langhoff (Kluwer Academic Publishers, Dordrecht, The Netherlands, 1995).
[51] G. A. Petersson and M. A. Al-Laham, *J. Chem. Phys.* **94** (1991) 6081; M. R. Nyden and G. A. Petersson, *J. Chem. Phys.* **75** (1981) 1843; G. A. Petersson, A. K. Yee, and A. Bennett, *J. Chem. Phys.* **83** (1985) 5105.
[52] L. A. Curtis, K. Raghavachari, P. C. Redfern, and J. A. Pople, *J. Chem. Phys.* **106** (1997) 1063.
[53] J. Baker, M. Muir, and J. Andzelm, *J. Chem. Phys.* **102** (1995) 2063; J. Andzelm and P. R. Taylor, *Chem. Phys. Lett.* **237** (1995) 53.
[54] http://theochem.weizmann.ac.il/web/papers/phosphonates.html
[55] J. M. L. Martin and G. de Oliveira, *J. Chem. Phys.* **111** (1999) 1843; specifically, the recently proposed W1' variant [56] was used, which exhibits greatly improved performance for second-row molecules at no additional cost.
[56] J. M. L. Martin, *Chem. Phys. Lett.* **310** (1999) 271.
[57] MOLPRO is a package of ab initio programs written by H.-J. Werner, P. J. Knowles, with contributions from J. Almlöf, R. D. Amos, A. Berning, D. L. Cooper, M. J. O. Deegan, A. J. Dobbyn, F. Eckert, S. T. Elbert, C.Hampel, R. Lindh, A. W. Lloyd, W. Meyer, A. Nicklass, K. A. Peterson, R. M. Pitzer, A. J. Stone, P. R. Taylor, M. E. Mura, P. Pulay, M. Schütz, H. Stoll and T. Thorsteinsson.
[58] J. M. L. Martin and P. R. Taylor, *J. Phys. Chem. A* **103** (1999) 4427.

[59] L. A. Curtiss, K. Raghavachari, P. C. Redfern, V. Rassolov, and J. A. Pople, *J. Chem. Phys.* **109** (1998) 7764; for the G3B3 variation, see A. G. Baboul, L. A. Curtiss, P. C. Redfern, and K. Raghavachari, *J. Chem. Phys.* **110** (1999) 7650.

[60] J. P. Perdew, J. A. Chevary, S. H. Vosko, K. A. Jackson, M. R. Pederson, D. J. Singh, C. Fiolhais, *Phys. Rev. B* **46** (1992) 6671 and references therein.

[61] C. Adamo and V. Barone, *J. Chem. Phys.* **108** (1998) 664.

[62] B. M. Lynch, P. L. Fast, M. Harris, and D. G. Truhlar, *J. Phys. Chem. A* **104** (2000) 4811.

[63] T. Clark, J. Chandrasekhar, G. W. Spitznagel, and P. v R. Schleyer, *J. Comp. Chem.* **4** (1983) 294.

[64] T. H. Dunning Jr., *J. Chem. Phys.* **90** (1989) 1007.

[65] R. A. Kendall, T. H. Dunning Jr. and R. J. Harrison, *J. Chem. Phys.* **96** (1992) 6796.

[66] J. M. L. Martin, "Some observations and case studies on basis set convergence in density functional theory", in *Density Functional Theory: a bridge between Chemistry and Physics*, P. Geerlings, F. De Proft, and W. Langenaeker (eds.), VUB Press, Brussels (2000).

[67] T. N. Truong, and W. Duncan, *J. Chem. Phys.* **101** (1994) 7408; Q. Zhang, R. Bell, and T. N. Truong, *J. Phys. Chem.* **99** (1995) 592; J. L. Durant, *Chem. Phys. Lett.* **256** (1996) 595.

[68] C. W. Bauschlicher Jr. and H. Partridge, *Chem. Phys. Lett.* **240** (1995) 533; J. M. L. Martin, *J. Chem. Phys.* **108**, 2791 (1998).

[69] J. M. L. Martin and O. Uzan, *Chem. Phys. Lett.* **282** (1998) 19.

[70] The CID spectra of the m/z 109, 95 and 93 ions are dominated by the loss of CH_2=O whereas loss of CH_3OH yields the base peak at m/z 47 in the spectrum of the m/z 79 ions.

[71] The relatively high kinetic energy release for this loss supports the proposal that the reaction has a reverse activation energy [20].

[72] (a) W. Bertrand and G. Bouchoux, *Rapid Commun. Mass Spectrom.* **12** (1998) 1697. (b) J. K. Terlouw, J. Wezenberg, P. C. Burgers and J. L. Holmes, *Chem. Commun.* (1983) 1121.

[73] R. G. Cooks, J. H. Beynon, R. M. Caprioli and G. R. Lester, *Metastable Ions*, Elsevier Scientific Publishing Company, Amsterdam, 1973, Chapter 4, page 153 ff.

[74] The experiments described in [16] and mentioned in the Introduction lead to a keto-enol difference of only 6.5 kcal/mol. We do not have a clear explanation for this large discrepancy between theory and experiment but intend to address this problem in future work.

Chapter 3

Tautomerization and dissociation of ethylene phosphonate ions [-OCH_2CH_2O-]P(H)=$O^{\bullet+}$: an experimental and CBS-QB3 computational study

The unimolecular gas phase chemistry of the cyclic title ion, [-OCH_2CH_2O-]P(H)=$O^{\bullet+}$, **1a**$^{\bullet+}$, and its tautomer ethylene phosphite, [-OCH_2CH_2O-]P-$OH^{\bullet+}$, **1b**$^{\bullet+}$, was investigated using mass spectrometry based experiments in conjunction with isotopic labelling and computational quantum chemistry, at the CBS-QB3 level of theory. A facile tautomerization of the "keto" ion **1a**$^{\bullet+}$ into its more stable (by 34 kcal/mol) "enol" isomer **1b**$^{\bullet+}$ is prevented by a substantial 1,2-H shift barrier (14 kcal/mol relative to **1a**$^{\bullet+}$). In line with this, the collision-induced dissociation (CID) and neutralization-reionization (NR) spectra of the two isomers are characteristically different. Unlike the corresponding acyclic dimethyl phosphonate/phosphite tautomers, $(CH_3O)_2P(H)=O^{\bullet+}$ / $(CH_3O)_2P$-$OH^{\bullet+}$, where the phosphonate isomer rapidly loses its structure identity by a facile distonicization into CH_2O-$(CH_3O)P(H)OH^{\bullet+}$, the barrier for this reaction in **1a**$^{\bullet+}$ is prohibitively high and the cyclic distonic 1,2-H shift isomer [-$OCH_2CH_2O(H)$-]P=$O^{\bullet+}$, **1c**$^{\bullet+}$, is not directly accessible.

The 1,2-H shift barrier separating **1a**$^{\bullet+}$ and **1b**$^{\bullet+}$ is calculated to lie close to the thermochemical threshold for the formation of $C_2H_4^{\bullet+}$ + HO-$P(=O)_2$. This reaction dominates the closely similar metastable ion (MI) spectra of these tautomers. At these elevated energies, the "enol" ion **1b**$^{\bullet+}$ can undergo ring-opening by CH_2-O or CH_2-CH_2 cleavage, yielding ion-dipole complexes of the type $[C_2H_4]^{\bullet+}$/HO-$P(=O)_2$, **1e**$^{\bullet+}$, and H-bridged radical cations CH_2=O•••[H-O-P-OCH_2]$^{\bullet+}$, **1f**$^{\bullet+}$, respectively. Moreover, communication of **1b**$^{\bullet+}$ with the distonic ion **1c**$^{\bullet+}$ now also becomes feasible. These computational findings account for the similarity of the MI spectra and provide a rationale for the observation that in the losses of CO, HCO$^{\bullet}$ and $C_2H_3O^{\bullet}$ from metastable ions [-OCH_2CH_2O-]P(H)=$^{18}O^{\bullet+}$ and [-OCH_2CH_2O-]P-$^{18}OH^{\bullet+}$, the ^{18}O-atom loses its positional identity.

Theory and experiment yield a consistent potential energy profile for the cyclic phosphonate/phosphite system showing that non-dissociating ions **1a**$^{\bullet+}$ retain their structure identity in the μs time-frame. However, the interaction of **1a** with a benzonitrile (BN) molecule in a chemical ionization type experiment readily yields the more stable "enol" type ion **1b**$^{\bullet+}$. Experiments with benzonitrile-d_5 support the proposal that this interaction does not involve the lowering of the 1,2-H shift barrier between the tautomers, via a proton-transport catalysis type mechanism. Rather, a "quid-pro-quo" mechanism is operative, analogous to that proposed for the benzonitrile-assisted enolization of acetamide (*Int. J. Mass Spectrom.* 210/211 (2001) 489).

The work described here has been accepted for publication in an article under the same title: L.N. Heydorn, P.C. Burgers, P.J.A. Ruttink and J.K. Terlouw, Int. J. Mass Spectrom. (Gaseous Ion Thermochemistry and Solvation Issue)

3.1. Introduction

Gas-phase phosphorus ion chemistry is intimately related to solution phosphorus chemistry [1] and an incentive for its study derives from the intrinsic and practical importance of phosphorus compounds [2, 3] and from the significant role of mass spectrometry in their characterization as pesticides, drugs, and toxic agents [4].

One class of compounds that has attracted a great deal of interest [5] are organophosphorus esters which are widely used as pesticides. The conventional electron impact mass spectra of alkyl and aryl phosphates and phosphites were already studied when organic mass spectrometry was still in its infancy [6]. Renewed interest in the gas-phase ion chemistry of these esters started in the mid-eighties when tandem mass spectrometry (MS/MS) [7] using both high and low-energy collision induced dissociation (CID) experiments [8] on magnetic deflection, quadrupole, Fourier transform ion cyclotron resonance (FT-ICR) and ion trap mass spectrometers became available to probe the structure of stable and isomerizing ions [9]. One important highlight of the seminal studies of the Purdue groups of Cooks and Kenttämaa [10] is that the long-lived radical cations of simple organophosphates isomerize spontaneously to more stable distonic ions (ions with formally separate radical and charge sites) [10b, 11]. The computational finding that a localized radical center is present at the *oxo* oxygen atom of the initially generated molecular ion may provide a chemical rationalization for this behaviour [12].

A case in point is the behaviour of trimethyl phosphate (TMP) which upon electron impact rearranges into the distonic ion depicted in the Scheme below and whose lowest energy dissociation route, loss of CH_2=O, yields the radical cation of dimethyl phosphite, $\mathbf{a_2}^{\bullet+}$.

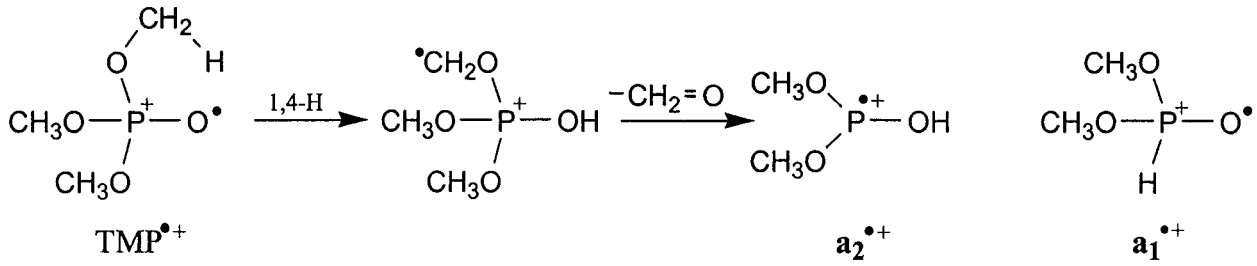

Ion $\mathbf{a_2}^{\bullet+}$ represents the "enol" tautomer of the "keto" ion $\mathbf{a_1}^{\bullet+}$, ionized dimethyl phosphonate (DMP). Its neutral counterpart, $\mathbf{a_2}$, is less stable than the phosphonate, $\mathbf{a_1}$, by 15 kcal/mol and in the condensed phase the phosphite intermolecularly rearranges into the phosphonate. However, upon ionization the stability order reverses and $\mathbf{a_2}^{\bullet+}$ is more stable than $\mathbf{a_1}^{\bullet+}$, by 31 kcal/mol [13]. Tautomerization in simple organic radical cations and their neutral counterparts is of fundamental importance and has therefore been studied in great detail, particularly for keto-to-enol isomerization reactions [14]. In this context, proton transport catalysis in ion-molecule encounter complexes, that is the phenomenon that the neutral promotes the tautomerization of the ionic component of the complex, has recently received a great deal of attention both from theory and experiment [15]. One interesting example is the benzonitrile-assisted enolization of ionized acetone [16]. Enolization of the acetone radical cation into its more stable isomer CH_2=C(OH)$CH_3^{\bullet+}$ does not occur unassisted because the associated 1,3-H shift imposes a high barrier. However, benzonitrile has a proton affinity which is higher than that of the CH_2 and equal to that of the O in the $CH_2C(O)CH_3^{\bullet}$ radical and it successfully catalyzes the enolization. Benzonitrile also catalyzes the enolization of acetamide, but here a different mechanism is operative [17].

In line with the above, both the spontaneous and the benzonitrile-assisted tautomerization of DMP has recently been studied in considerable detail by a variety of experimental methods and computational chemistry at the CBS-QB3 level of theory [13], see below.

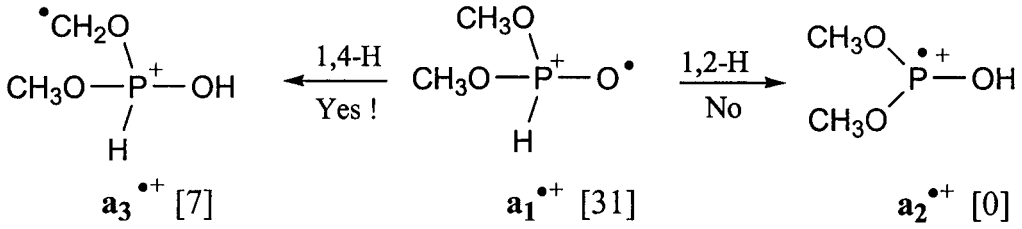

$\mathbf{a_3}^{\bullet+}$ [7] $\mathbf{a_1}^{\bullet+}$ [31] $\mathbf{a_2}^{\bullet+}$ [0]

It was concluded that in the microsecond time-frame DMP ions $\mathbf{a_1}^{\bullet+}$ have completely isomerized into the very stable distonic ions $\mathbf{a_3}^{\bullet+}$ by way of a 1,4-H shift. Experiments clearly show that further isomerization of $\mathbf{a_3}^{\bullet+}$ into the even more stable enol ions $\mathbf{a_2}^{\bullet+}$ via a 1,3-H shift does not take effect. However, this latter reaction can be induced to occur by interaction of $\mathbf{a_1}^{\bullet+}$ with a suitable base molecule such as benzonitrile in a chemical ionization type experiment. Thus benzonitrile effectively catalyzes the enolization of DMP ions, not directly via the 1,2-H shift, but via the more circuitous but less energy demanding route $\mathbf{a_1}^{\bullet+} \rightarrow \mathbf{a_3}^{\bullet+} \rightarrow \mathbf{a_2}^{\bullet+}$.

The successful lowering of very large 1,2-H shifts by way of catalysis by a base molecule presents a particularly challenging case [15g]. For example, the very large barrier (~60 kcal/mol) for the 1,2-H shift which separates the pyridine radical cation from its α-ylide isomer can be lowered to a mere 9 kcal/mol by interaction with a judiciously chosen base [15g]. The 1,2-H shift in DMP ions, which has a calculated barrier of 17 kcal/mol, would constitute an even more challenging case in phosphorous containing ions, but as discussed above, an alternative, more economical route is available.

To study direct "keto-to-enol" transformations in phosphorous containing ions, a system should be chosen which cannot undergo facile alternative rearrangements (i.e. 1,3- and 1,4-H shifts) and so we decided to investigate the "keto" and "enol" ions of ethylene phosphonate, i.e. $\mathbf{1a}^{\bullet+}$ and $\mathbf{1b}^{\bullet+}$, see below. In this model system formation of a distonic ion (i.e. $\mathbf{1c}^{\bullet+}$) is still possible, but only via an undoubtedly energy demanding 1,2-H shift. Thus in this model system, we should be able to study enolization, both unimolecularly and molecule-assisted.

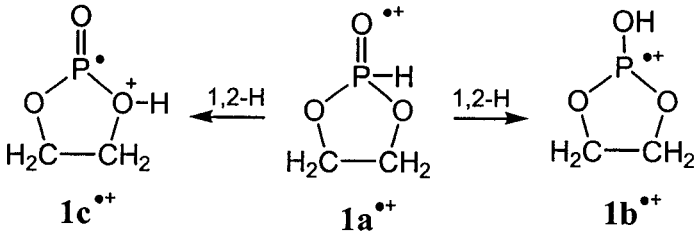

3.2. Experimental and theoretical methods

Sample preparation procedures

Ethylene phosphonate (1,3,2-dioxaphospholane, 2-oxide), **1a**, is the parent compound of the class of cyclic phosphonic acid esters which are called cyclic phosphorous acid esters or cyclic hydrogen phosphites in the older literature [18]. The lower members of this class are highly viscous materials with high boiling points, which are very prone to hydrolysis and difficult to purify. These compounds can be obtained by (i) the reaction of PCl_3 with a given diol, (ii) transesterification of an alkyl phosphonate with 1,2- or 1,3-diols or (iii) hydrolysis, under carefully controlled conditions, of cyclic chlorophosphites [18]. However, with ethylene glycol as the substrate, the first synthetic route leads, as we have been able to confirm, to highly viscous polymeric products while in the transesterification procedure only the cyclic diethylene diphosphite could be isolated [18a]. Hydrolysis of ethylene chlorophosphite (2-chloro-1,3,2-dioxaphospholane), **I**, with a stoichiometric quantity of water in an inert organic solvent [18c] appeared to be a more profitable route :

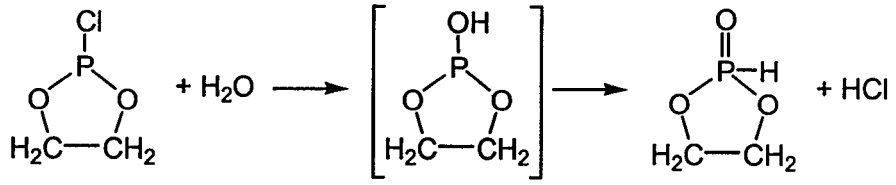

We have adapted this synthesis to the milligram scale and further modified it by performing the reaction in the presence of an acid-binding agent, pyridine or picoline.

Optimal results were obtained by using stoichiometric quantities of all three components, and working under vacuum at low temperatures. In a typical experiment, 200 μL of ethylene chlorophosphite (Aldrich) was transferred to a small glass bulb and frozen (using liquid N_2). Next, the H_2O/pyridine mixture was added and quickly frozen on top of the still frozen chlorophosphite layer. The bulb was then immediately evacuated using a rotary pump and while pumping continuously the two layers were allowed to gradually come to room temperature over a period of 1.5 h, using dry ice as the cooling agent. In this manner a clear viscous liquid is obtained in which a white precipitate of the pyridine or picoline hydrochloride is suspended. The hydrochloride could be removed by prolonged pumping (~ 7 h) at c 50°C with a diffusion pump. The resulting ethylene phosphonate is a clear, colourless, viscous oil, which gave the clean mass spectrum of Fig. 3.2a. A 1:1 mixture of the phosphonate with its ^{18}O-labelled isotopologue, **1a** (^{18}O) [-OCH_2CH_2O-]P(H)=^{18}O was obtained from 50% ^{18}O-enriched water (Ventron GMBH, Karlsruhe). The isotopologue **1a** (P-D), [-OCH_2CH_2O-]P(D)=O, was prepared in the same way using D_2O.

Ethyl ethylene phosphite, **II**, is a high boiling liquid, stable to distillation and to storage in the absence of moisture and air [18b]. Samples of the unlabelled compound as well as the ^{18}O- and D-labelled isotopologues [-OCH_2CH_2O-]P-$^{18}OC_2H_5$ and [-OCH_2CH_2O-]P-OC_2D_5 were prepared by essentially the same procedure as described above for **1a**, replacing water by a slight excess of (the appropriately labelled) ethanol. No attempts were made to remove the precipitated hydrochloride from the sample as it did not interfere with the experiments.

Methyl ethylene phosphate, **III**, is a well characterized liquid at room temperature whose rapid hydrolysis has been studied in considerable detail [19]. Samples of the unlabelled compound as well as ^{13}C- and D-labelled isotopologues [-OCH_2CH_2O-]P(=O)O*CH_3 and [-OCH_2CH_2O-]P(=O)OCD_3 were prepared by the methanolysis of 2-chloro-1,3,2-dioxaphospholane-2-oxide (Aldrich) with stoichiometric quantities of the (appropriately labelled) alcohol and picoline, using the procedure described above. Here too, no attempts were made to remove the suspended picoline hydrochloride from the sample.

The benzonitrile and benzonitrile-d_5 samples used in the ion-molecule experiments were of research grade and obtained from Aldrich and C/D/N Isotopes Inc. respectively.

Tandem mass spectrometry

The tandem mass spectrometry based experiments were performed with the McMaster University ZAB-R mass spectrometer, a three-sector BE_1E_2 (B = magnetic sector, E = electric sector) type instrument [20]. The instrument is equipped with four collision gas chambers of which the two located in the second field free region (2ffr, in front of E_1) were used for the neutralization-reionization (NR) experiments [21].

The compounds were introduced into the ion source (kept at 100°C) via a wide-bore all-quartz direct insertion probe connected via an o-ring with a small glass bulb that contains the sample. Ions generated in the source by either electron ionization (EI) or ion-molecule reactions under conditions of chemical ionization (CI), were accelerated to 8 or 10 keV prior to recording their spontaneous or collision induced dissociations in the second or the third field free regions as MI (metastable ion) or CID (collision induced dissociation) spectra respectively. The structure of a given product ion in a 2ffr MI or CID spectrum was probed by selectively transmitting the ion by E_1 to a collision chamber in the 3ffr pressurized with O_2 and mass-analyzing its ionic dissociation products by scanning E_2. The resulting MS/MS/MS type spectra are denoted as MI/CID and CID/CID spectra respectively. All the (high energy) collision experiments were performed at a main beam transmittance (~70%) such that the probability for multiple collisions is negligible.

For neutralization–reionization mass spectra (NRMS) [21] 8 or 10 keV ions, $m^{\bullet+}$ are selectively transmitted by B to the 2ffr where, in the first collision chamber, charge-exchange neutralization occurs with *N,N*-dimethyl aniline (NDMA) : $m^{\bullet+}$ [8 or 10 keV] + NDMA $\rightarrow$ m [8 or 10 keV] + $NDMA^{\bullet+}$. The unreacted ions are deflected away and the remaining fast neutrals are reionized with O_2 in the second collision cell. Scanning E_1 yields the spectrum of the reionized neutrals $m^{\bullet+}$, the "survivor" ions, and their (structure characteristic) charged dissociation products.

All spectra were recorded using a small PC-based data system developed by Mommers Technologies Inc. (Ottawa).

Computational procedures

The calculations were performed using Gaussian 98 revision A.9 [22] and GAMESS-UK [23]. The standard CBS-QB3 model chemistry [24] was used to probe structures and energies of the key isomeric ions, connecting transition states and dissociation products associated with the ethylene phosphonate/ phosphite $C_2H_5O_3P^{\bullet+}$ potential energy surface. The energetic results are presented in Table 3.1a (equilibrium and transition state energies), Table 3.1b (dissociation limits) and Scheme 3.3 while detailed geometries of selected species are displayed in Fig. 3.1 (the complete set of geometries is available upon request). Frequency calculations gave the correct number of negative eigenvalues for all minima and transition states and the spin contamination was within the acceptable range. The connections of the transition states have been checked by geometry optimizations and frequency calculations.

From a recent validation study [13], it appears that the CBS-QB3 method accurately reproduces the heats of formation of species comprised of a second row element (S or P) bonded to a highly electronegative element. While the computational cost for the present system is fairly high, the CBS-QB3 model chemistry does seem to outperform the comparably expensive G3 method.

Table 3.1a. CBS-QB3 derived energies for the main isomerization reactions of the ethylene phosphonate ion, $\mathbf{1a}^{\bullet+}$.

		E_{total}* [B3LYP/CBSB7] Hartree	$E_{total\ (0\ K)}$ [CBS-QB3] Hartree	$E_{rel\ (298\ K)}$ [CBS-QB3] kcal/mol
$CH_2{=}CH_2^{\bullet+}$ + $HOP(=O)_2$	m/z 28	-645.93450	-645.06053	0
$[\text{-}OCH_2CH_2O\text{-}]P(H){=}O^{\bullet+}$	$\mathbf{1a}^{\bullet+}$	-645.95227	-645.08210	-15.0
$[\text{-}OCH_2CH_2O\text{-}]POH^{\bullet+}$	$\mathbf{1b}^{\bullet+}$	-645.99849	-645.13727	-49.0
$[\text{-}OCH_2CH_2O(H)\text{-}]P{=}O^{\bullet+}$	$\mathbf{1c}^{\bullet+}$	-645.96969	-645.09858	-25.0
$HOCH_2CH_2O\text{-}P{=}O^{\bullet+}$	$\mathbf{1d}^{\bullet+}$	-645.95824	-645.07099	-7.5
$[CH_2\text{-}CH_2\text{-}O\text{-}P(=O)OH]^{\bullet+}$	$\mathbf{1e}^{\bullet+}(\alpha)$	-645.97067	-645.09780	-23.5
$[CH_2\text{-}CH_2\text{-}O\text{-}P(=O)OH]^{\bullet+}$	$\mathbf{1e}^{\bullet+}(\beta)$	-645.96927	-645.09516	-21.5
$[CH_2O\text{-}P\text{-}OH]^{\bullet+}\bullet\bullet\bullet O{=}CH_2$	$\mathbf{1f}^{\bullet+}$	-645.97574	-645.08440	-17.5
$CH_3\text{-}O\text{-}P(=O)OCH_2^{\bullet+}$	$\mathbf{1g}^{\bullet+}$	-645.96195	-645.08494	-15.0
TS $\mathbf{1a}^{\bullet+} \rightarrow \mathbf{1b}^{\bullet+}$		-645.92174	-645.05956	-0.5
TS $\mathbf{1a}^{\bullet+} \rightarrow \mathbf{1c}^{\bullet+}$		-645.90047	-645.03147	17.0
TS $\mathbf{1c}^{\bullet+} \rightarrow \mathbf{1b}^{\bullet+}$		-645.92366	-645.05914	-1.0
TS $\mathbf{1d}^{\bullet+} \rightarrow \mathbf{1c}^{\bullet+}$		-645.94200	-645.05672	1.4
TS $\mathbf{1b}^{\bullet+} \rightarrow \mathbf{1e}^{\bullet+}(\alpha)$		-645.94821	-645.06988	-6.5
TS $\mathbf{1e}^{\bullet+}(\beta) \rightarrow \mathbf{1e}^{\bullet+}(\alpha)$		-645.96665	-645.09202	-20.0
TS $\mathbf{1e}^{\bullet+}(\beta) \rightarrow \mathbf{1c}^{\bullet+}$		-645.93931	-645.05951	-0.5
TS $\mathbf{1b}^{\bullet+} \rightarrow \mathbf{1f}^{\bullet+}$		-645.95269	-645.07262	-8.0

* The B3LYP energies include ZPVE contributions, scaled by 0.99.

Table 3.1b. Auxiliary energetic information for the ethylene phosphonate system derived from CBS-QB3 calculations

		E_{total} [0 K] Hartree	$\Delta H°_f$[0 K] kcal/mol	$\Delta H°_f$[298 K] kcal/mol
[-OCH_2CH_2O-]P(H)=$O^{\bullet+}$	**1a**$^{\bullet+}$	-645.08210	77.3	71.7
[-OCH_2CH_2O-]P(H)=O	**1a**	-645.47424	-168.7	-174.5
[-OCH_2CH_2O-]$POH^{\bullet+}$	**1b**$^{\bullet+}$	-645.13727	42.7	37.6
[-OCH_2CH_2O-]POH	**1b**	-645.46323	-161.8	-167.3
[-OCH_2CH_2O-]P(H)OH^+	[**1a**+H]$^+$	-645.79180	-2.7	-9.2
[-OCH_2CH_2O-]P=$O^{\bullet}$	[**1a**-H]$^{\bullet}$	-644.83006	-129.8	-134.6
[-OCH_2CH_2O-]$POCH_2CH_3^{\bullet+}$	**II**$^{\bullet+}$	-723.58963	35.6	27.5
[-OCH_2CH_2O-]P^+	m/z 91	-569.39617	91.3	87.0
$OH^{\bullet}$		-75.64970	8.8	8.8
$(HO)_2P{=}O^+$	m/z 81	-567.29844	30.1	27.1
$CH_2{=}CH^{\bullet}$		-77.74299	72.7	71.7
HO-$P(=O)_2^{\bullet+}$	m/z 80	-566.58274	114.0	112.1
[-O-O-]P-$OH^{\bullet+}$	m/z80	-566.52164	152.3	150.6
$CH_2{=}CH_2$		-78.41263	15.3	13.2
CH_3O-P(H)$OH^{\bullet+}$	m/z 80	-531.91692	94.4	90.3
CO		-113.18197	-27.7	-26.9
CH_3O-P-OH^+	m/z 79	-531.36681	74.4	70.7
CH_3O(H)-P=O^+	m/z 79	-531.33760	92.7	89.4
$HCO^{\bullet}$		-113.70496	9.4	9.5
CH_2O-P-$OH^{\bullet+}$	m/z 78	-530.70506	124.3	121.5
$CH_2{=}O$		-114.34411	-26.4	-27.3
HO-P-OH^+	m/z 65	-429.14302	76.4	74.0
$CH_2{=}CHO^{\bullet}$		-152.93279	4.8	3.0
$CH_2{=}CHOH^{\bullet+}$	m/z 44	-153.22518	186.6	183.9
HO-P=O		-491.85809	-110.0	-111.6
H-$P(=O)_2$		-491.84042	-98.9	-100.6
$CH_2{=}CH_2^{\bullet+}$	m/z 28	-78.02908	258.5	256.5
HO-$P(=O)_2$		-567.03144	-167.6	-169.9
[-O-O-]P-OH		-566.90217	-86.5	-88.5
[-O-O-]P(H)=O		-566.90065	-85.5	-87.9

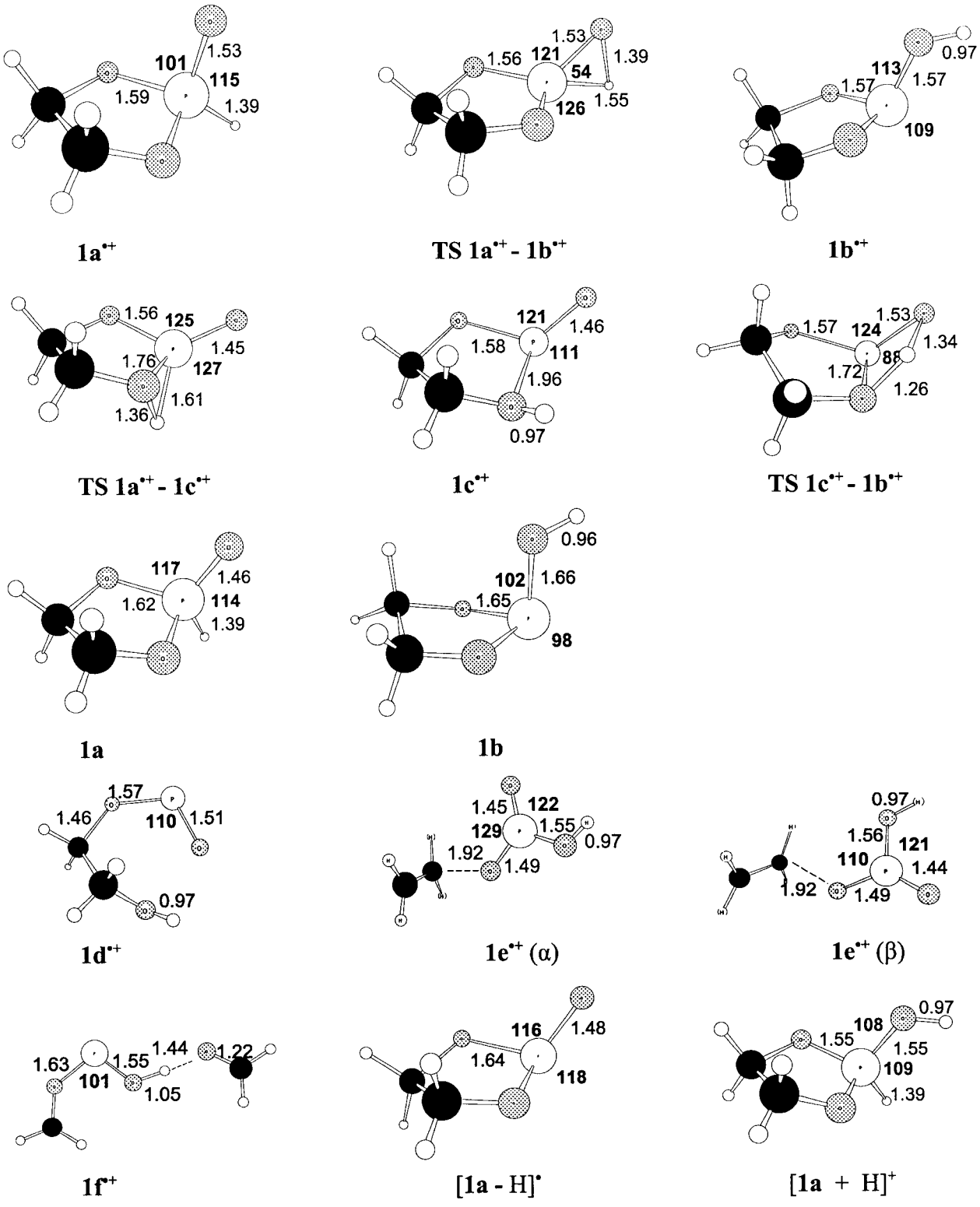

Fig. 3.1. Optimized geometries of selected ions and neutrals of the ethylene phosphonate system. The bond lengths (Å) and angles are presented in normal and bold font, respectively.

3.3. Results and discussion

3.3.1. Formation and identification of the "keto and "enol" ions 1a$^{\bullet+}$ and 1b$^{\bullet+}$

Ions **1a**$^{\bullet+}$ were obtained by electron ionization of ethylene phosphonate and the resulting 70 eV EI mass spectrum is presented in Fig. 3.2a. This spectrum displays a moderately intense molecular ion and principal fragment ions at m/z 78 (loss of CH_2O) and m/z 28 ($C_2H_4^{\bullet+}$, loss of HPO_3). These two reactions also dominate the CID spectrum of the molecular ion, which is shown in Fig. 3.3. As will be discussed elsewhere [25], the m/z 78 ions do not have the CH_2O-P(H)=O$^{\bullet+}$ connectivity expected from CH_2O elimination from the unrearranged molecular ion, **1a**$^{\bullet+}$. Instead, prior to loss of CH_2O, energy-rich ions **1a**$^{\bullet+}$ undergo a fast 1,2-H shift into the "enol" tautomer **1b**$^{\bullet+}$ to yield the more stable CH_2O-P-OH$^{\bullet+}$ isomer (by 18.5 kcal/mol [25]). Similarly, the formation of $C_2H_4^{\bullet+}$ may also be preceded by the tautomerization **1a**$^{\bullet+}$ → **1b**$^{\bullet+}$ (or alternatively **1a**$^{\bullet+}$ → **1c**$^{\bullet+}$) leading to the loss of an energetically much more favourable neutral, i.e. HO-P(=O)$_2$, metaphosphoric acid. The IE of C_2H_4 (10.51 eV [26]) is considerably lower than that of metaphosphoric acid (12.2 eV, Table 3.1b, this work), thus explaining why the complementary process to HO-P(=O)$_2^{\bullet+}$ (m/z 80) + C_2H_4 does not occur.

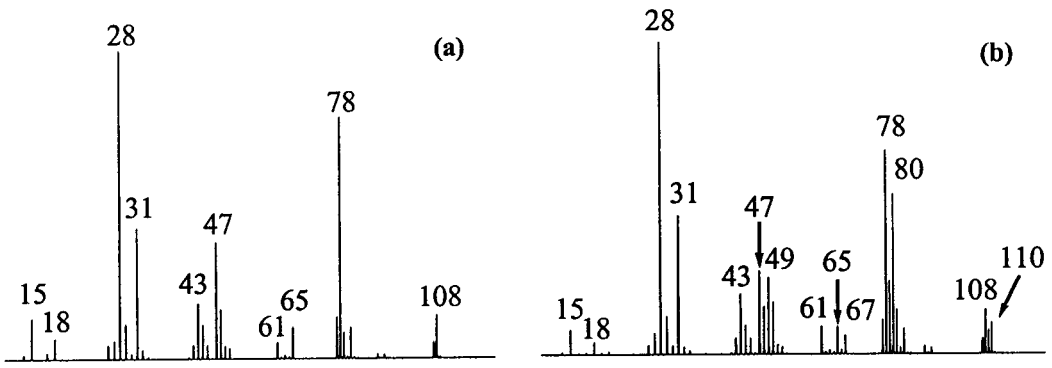

Fig. 3.2a. EI mass spectra of **(a)** ethylene phosphonate, **1a** and **(b)** a 1:1 mixture with its P=O^{18} isotopomer **1a** (^{18}O)

The formation of m/z 28 $C_2H_4^{\bullet+}$ ions also dominates the MI spectrum of the molecular ion, see Fig. 3.2b, but loss of CH_2O is now absent. Instead, peaks are observed at m/z 79 and 80 which correspond to the losses of HCO$^{\bullet}$ and CO, respectively. The product ions generated in these reactions are CH_3O-P-OH$^+$ and CH_3O-P(H)-OH$^{\bullet+}$,

respectively (from a comparison of their CID spectra with the reference spectra of Ref. 13). Both processes represent slow rearrangement reactions which do not feature in either the CID spectrum or the EI mass spectrum. This is also true for the prominent loss of HOPO which yields ions of m/z 44 whose structure was established as CH_2=CH-$OH^{\bullet+}$. The MI spectrum of the ^{18}O-labelled isotopologue, **1a**$^{\bullet+}$ (^{18}O), [-OCH_2CH_2O-]P(H)=^{18}O, inset Fig. 3.2b, reveals that, notably in the loss of $HCO^{\bullet}$ and the concomitant decarbonylation, all oxygen atoms have become equivalent, indicating that these slow dissociations are accompanied by extensive skeletal rearrangements via ring-opened structures. On the other hand, in the stable ions sampled by the CID experiment, the labelled O-atom retains its structural integrity : ions **1a**$^{\bullet+}$ (^{18}O) specifically lose CH_2O, see Fig. 3.3.

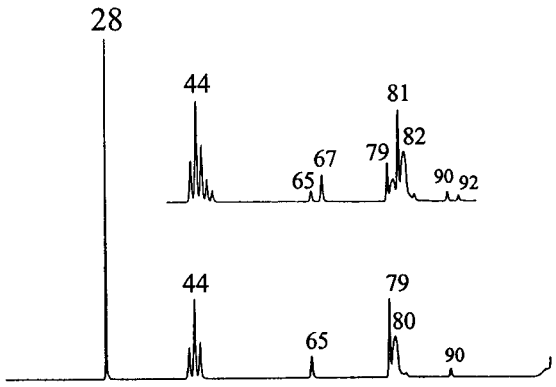

Fig. 3.2b. MI spectrum (2ffr, 8 keV) of the m/z 108 molecular ion of ethylene phosphonate, **1a**. The inset shows the partial spectrum of the m/z 110 ions of the P=O^{18} isotopomer **1a** (^{18}O)

The kinetic energy release (KER) [27] values associated with most of the reactions displayed in the MI spectrum of Fig. 3.2b are unexceptional. However, the m/z 28 peak is characteristically narrow and the KER derived from its width at half-height, $T_{0.5}$, is < 0.5 meV. Such small KER values often indicate that the rearrangement/dissociations reactions proceed via ion-dipole complexes. In contrast, the peak at m/z 80 is broad and associated with a large energy release, $T_{0.5}$ = 240 meV, indicating that the decarbonylation reaction is associated with a considerable reverse activation energy.

The ethylene phosphite tautomer $\mathbf{1b}^{\bullet+}$ was generated via the following three routes :

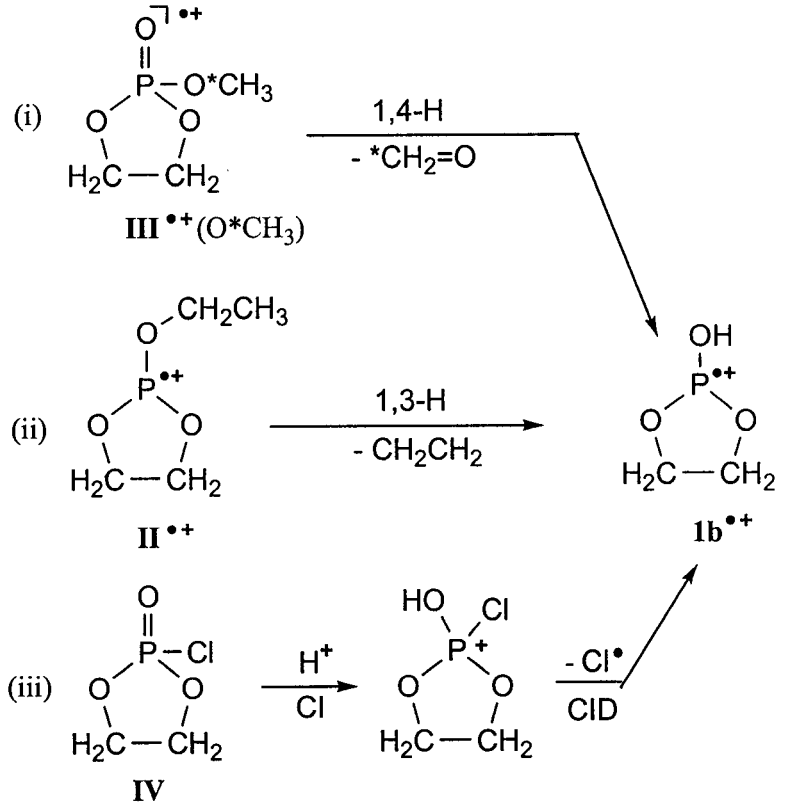

Scheme 3.1

As mentioned in the Introduction, ionized dimethyl phosphonate (DMP) readily isomerizes via a 1,4-H shift into its distonic counterpart CH_2O-$(CH_3O)P(H)OH^{\bullet+}$. This distonic ion serves as the immediate precursor for the abundant loss of CH_2=O that characterizes the EI spectrum of DMP. By analogy, it may be expected that the m/z 108 ions generated by loss of CH_2=O from ionized III – which form the base peak in its EI mass spectrum – are generated in the same way, producing the desired "enol" ion $\mathbf{1b}^{\bullet+}$, see route (i) of Scheme 3.1.

However, formaldehyde loss from $III^{\bullet+}$ could also involve elimination of the -CH_2-O- moiety of the ring, to yield distonic ions of structure CH_2-O-P(=O)$OCH_3^{\bullet+}$ (ion $\mathbf{1g}^{\bullet+}$ of Table 3.1a) instead. Examination of the spectra of labelled isotopologues revealed that the latter reaction does take place, albeit to a small extent : in their EI mass spectra III ($O^{13}CH_3$) and III (OCD_3) display losses of $^{13}CH_2O/CH_2O$ and CD_2O/CH_2O in a

ratio of 10:1. We have therefore used these labelled isotopologues for the generation of ions of putative structure $\mathbf{1b}^{\bullet+}$ and $\mathbf{1b}^{\bullet+}$ (OD). In this context we note that the MI spectrum of m/z 108 ions CH_2-O-P(=O)$OCH_3^{\bullet+}$ ($\mathbf{1g}^{\bullet+}$) is dominated by loss of HCO$^{\bullet}$ yielding product ions of structure CH_3O-P-OH^+ (from a comparison of the CID spectrum with a reference CID spectrum obtained in the work of Ref. 13). The HCO$^{\bullet}$ loss is highly specific : the isotopologues CH_2-O-P(=O)O$^{13}CH_3^{\bullet+}$ and CH_2-O-P(=O)$OCD_3^{\bullet+}$ exclusively lose HCO$^{\bullet}$.

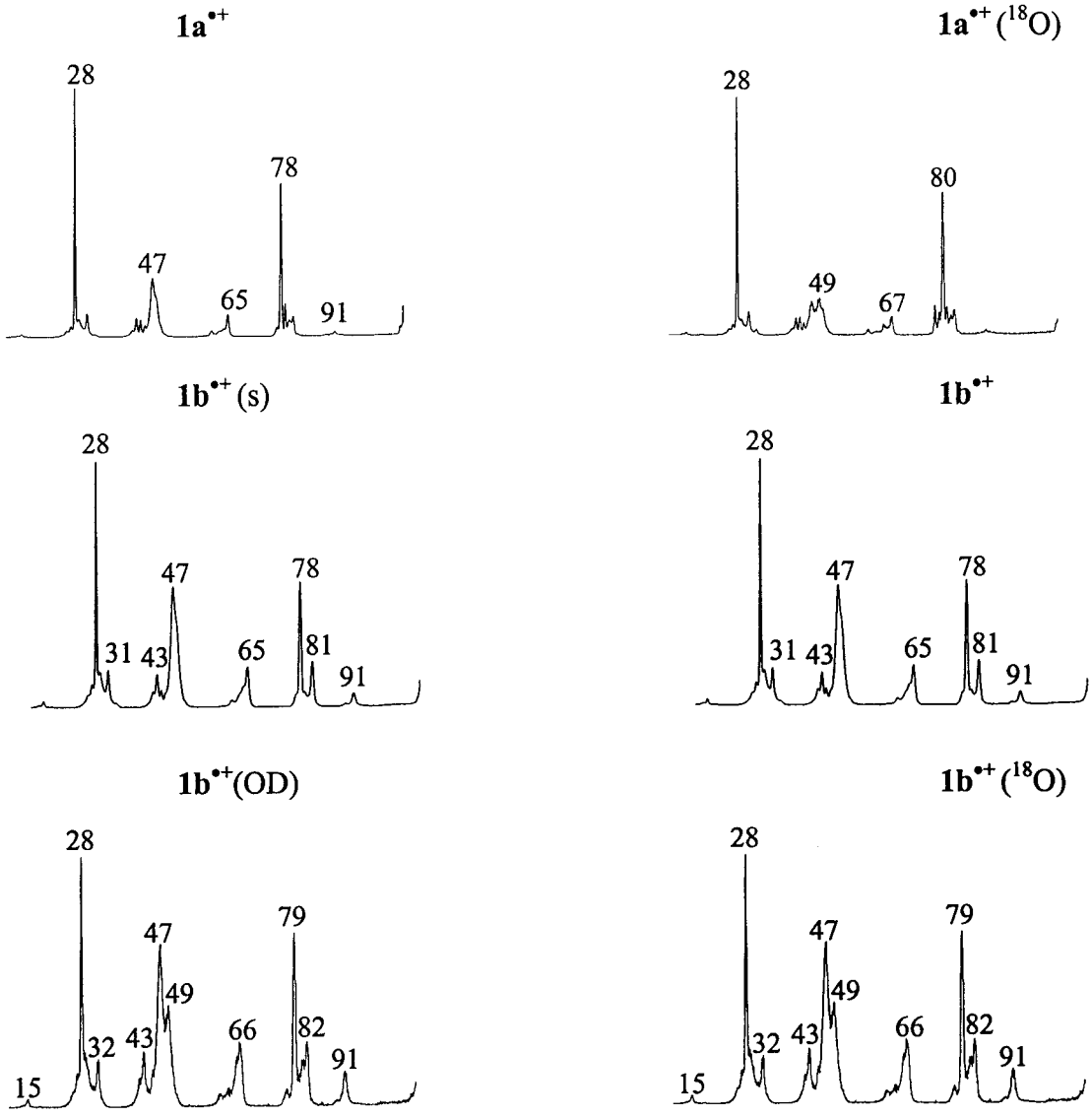

Fig. 3.3. CID mass spectra (3ffr) of ethylene phosphonate ions $\mathbf{1a}^{\bullet+}$ and ethylene phosphite ions $\mathbf{1b}^{\bullet+}$ and selected labelled isotopologues. Ions $\mathbf{1b}^{\bullet+}$ (s) are source generated ions; all other enol type ions were "cold" ions generated by CID of the metastable precursor ions.

The MI spectrum of source generated ions $\mathbf{1b}^{\bullet+}$ from III ($O^{13}CH_3$) was obtained and the spectrum (not shown) appeared to be identical with that presented in Fig. 3.2b for ions $\mathbf{1a}^{\bullet+}$ generated from ethylene phosphonate. Similarly, the MI spectra of the m/z 109 ions $\mathbf{1b}^{\bullet+}$ (OD) generated from III (OCD_3) and $\mathbf{1a}^{\bullet+}$ (P-D) from P-D labelled ethylene phosphonate were found to be identical.

In contrast, the CID spectrum of $\mathbf{1b}^{\bullet+}$, see Fig. 3.3, is clearly and characteristically different from that of $\mathbf{1a}^{\bullet+}$. Upon collisional activation, ions $\mathbf{1b}^{\bullet+}$ uniquely lose $C_2H_3^{\bullet}$ and $OH^{\bullet}$, yielding m/z 81 $(HO)_2P{=}O^+$ ions and (cyclic) m/z 91 ions, respectively; the calculations indicate, see Table 3.1b and also Scheme 3.3, that these two dissociations have about the same minimum energy requirement.

The observation that the MI spectra of $\mathbf{1a}^{\bullet+}$ and $\mathbf{1b}^{\bullet+}$ are identical raises the possibility that the CID spectrum of source generated ions $\mathbf{1b}^{\bullet+}$ actually represents a mixture of ions $\mathbf{1b}^{\bullet+}$ and $\mathbf{1a}^{\bullet+}$ (and perhaps also of other isomers). To probe this possibility, we set out to generate ions $\mathbf{1b}^{\bullet+}$ at lower internal energies, where formation of the higher energy species $\mathbf{1a}^{\bullet+}$ cannot compete. One way to achieve this is to generate ions $\mathbf{1b}^{\bullet+}$ from *metastable* precursor ions. Unfortunately, compound III cannot be used for this purpose as the loss of $CH_2{=}O$ is an insignificant reaction of metastable ions $\mathbf{III}^{\bullet+}$. Rather these precursor ions dissociate almost exclusively, via a remarkable skeletal rearrangement, by loss of $C_3H_3^{\bullet}$ to yield m/z 99 H_4PO_4 ions, most likely protonated phosphoric acid.

Loss of C_2H_4 from ionized ethyl ethylene phosphite, $\mathbf{II}^{\bullet+}$, depicted as route (ii) in Scheme 3.1, proved to be a better choice for the generation of ions $\mathbf{1b}^{\bullet+}$ of low internal energy. The MI spectrum (and also the CID spectrum) of $\mathbf{II}^{\bullet+}$ is dominated by two competing processes, *viz.* loss of $C_2H_3^{\bullet}$ and C_2H_4 yielding peaks at m/z 109 and m/z 108 with an intensity ratio of 1.5. The loss of $C_2H_3^{\bullet}$ involves a double H-transfer and yields protonated ethylene phosphonate, $[\mathbf{1a} + H]^+$. A plausible mechanism for this reaction loss involves a 1,4-H shift to yield an intermediate ion that develops into an ion-dipole complex $[\mathbf{1a}\ /C_2H_4^{\bullet+}]$ from which $[\mathbf{1a} + H]^+$ is formed by a proton transfer, Scheme 3.2.

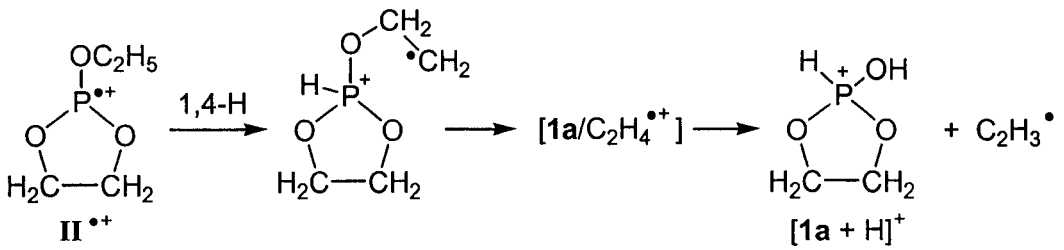

Scheme 3.2

The minimum (thermochemical) energy requirement for the above reaction is 35 kcal/mol (from ΔH_f $II^{\bullet+}$ = 28 kcal/mol [Table 3.1b], ΔH_f [**1a** + H]$^+$ = -9 kcal/mol [Table 3.1b] and ΔH_f $C_2H_3^\bullet$ = 72 kcal/mol [28]). In contrast, generation of $\mathbf{1a}^{\bullet+}$ by loss of C_2H_4 from either of the intermediate ions in the Scheme above has a minimum energy requirement of 57 kcal/mol (from ΔH_f $\mathbf{1a}^{\bullet+}$ = 72 kcal/mol [Table 3.1b] and ΔH_f C_2H_4 = 12.5 kcal/mol [26]), 22 kcal/mol higher than that calculated for the $C_2H_3^\bullet$ loss. Moreover, since IE(C_2H_4), 10.5 eV [26], is lower than that of **1a**, 10.7 eV [this work, Table 3.1b], dissociation into $C_2H_4^{\bullet+}$ + **1a** rather than C_2H_4 + $\mathbf{1a}^{\bullet+}$ is expected and this process is not observed. Thus, the competing loss of C_2H_4 observed in the MI spectrum of $II^{\bullet+}$ does not yield "keto" ions $\mathbf{1a}^{\bullet+}$.

Another possibility, namely that the loss of C_2H_4 from metastable ions $II^{\bullet+}$ involves a 1,5-H shift to generate the distonic isomer $\mathbf{1c}^{\bullet+}$ can also be discarded : the minimum energy requirement for this reaction is calculated to be 46 kcal/mol (using ΔH_f $\mathbf{1c}^{\bullet+}$ = 62 kcal/mol [Table 3.1a]), i.e. some 11 kcal/mol higher than that calculated for the $C_2H_3^\bullet$ loss.

In contrast, the mechanism proposed in Scheme 3.1 for the loss of C_2H_4 from $II^{\bullet+}$, a β-H transfer (1,3-H shift) to yield "enol" ions $\mathbf{1b}^{\bullet+}$, does account for the observed competition with $C_2H_3^\bullet$ loss. Its minimum energy requirement of 22 kcal/mol (from ΔH_f $\mathbf{1b}^{\bullet+}$ = 37 kcal/mol (Table 3.1b)) is actually lower than that calculated for the loss of $C_2H_3^\bullet$. However, the 1,3-H shift associated with the C_2H_4 loss imposes a barrier, estimated to be 30 - 35 kcal/mol [29], which is expected to be higher than the 1,4-H shift/ H^+ transfer associated with the $C_2H_3^\bullet$ loss. This makes the two reactions

energetically equivalent and accounts for the observation that they are both prominently observed in the MI spectrum of $II^{\bullet+}$.

Thus there is little doubt that *metastable* ions $II^{\bullet+}$ exclusively generate "cold" enol ions $\mathbf{1b}^{\bullet+}$ and this is borne out by its CID spectrum which is shown in Fig. 3.3. The spectrum is similar to that of the source generated ions but the structure diagnostic peaks of the enol ions $\mathbf{1b}^{\bullet+}$ at m/z 91 and m/z 81 are more prominent.

Finally, we have explored yet another route to confirm the CID characteristics of ions $\mathbf{1b}^{\bullet+}$. Protonation of **IV** under conditions of chemical ionization, route (iii) in Scheme 3.1, followed by collision-induced loss of $Cl^{\bullet}$ of the protonated molecule in the 2ffr yields m/z 108 ions whose 3ffr CID spectrum is closely similar to that observed for the "cold" ions $\mathbf{1b}^{\bullet+}$ generated by the dissociative ionization route (ii). The same obtains for ions $\mathbf{1b}^{\bullet+}$ (OD) generated by the deuteronation of **IV** using $CD_3C(=O)CD_3$ as the reactant.

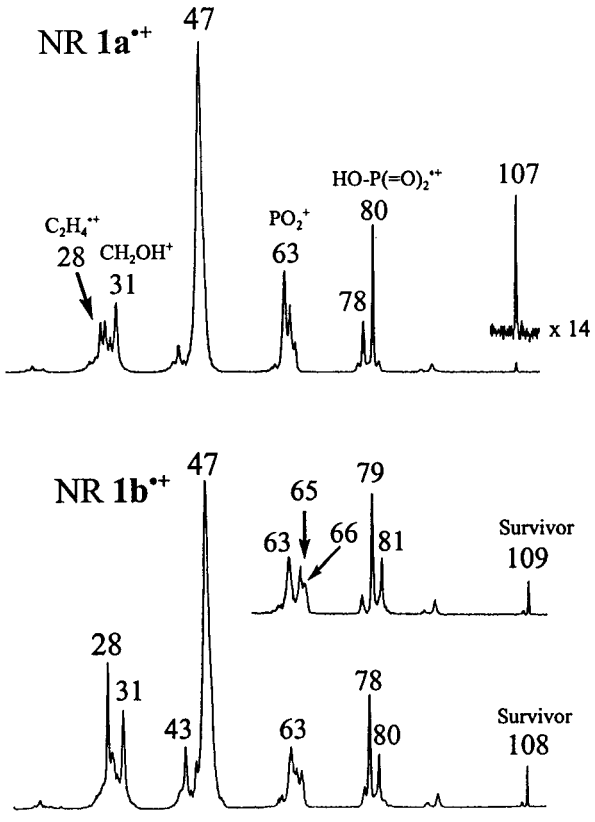

Fig. 3.4. 8 keV Neutralization-Reionization (NR) mass spectra of ions $\mathbf{1a}^{\bullet+}$ and $\mathbf{1b}^{\bullet+}$ The inset shows the partial NR spectrum of $\mathbf{1b}^{\bullet+}$ (OD).

The neutralization-reionization (NR) mass spectra of $\mathbf{1a}^{\bullet+}$ and $\mathbf{1b}^{\bullet+}$ are given in Fig. 3.4. Both spectra are very different from their respective CID spectra: the base peaks in both NR spectra are at m/z 47, $P{=}O^+$. This peak we propose, as well as that at m/z 63 which is not present in the CID spectra, arise from dissociations of the m/z 80 ions, $HOPO_2^{\bullet+}$ (which cleanly shifts to m/z 82 and m/z 79 in the NR spectra of $\mathbf{1a}^{\bullet+}$ (^{18}O) and $\mathbf{1a}^{\bullet+}$ (P-D)) formed by collisional ionization of the $HOPO_2$ molecules formed from the metastable ions: $\mathbf{1a}^{\bullet+}$/ $\mathbf{1b}^{\bullet+} \rightarrow C_2H_4^{\bullet+} + HOPO_2$, $HOPO_2 \rightarrow HOPO_2^{\bullet+} \rightarrow PO_2^{\bullet+} \rightarrow PO^{\bullet+}$. It can also be seen that no survival ion signal is present for the keto ions, whereas such a signal is clearly present for the enol ions. The more extensive dissociation of $\mathbf{1a}^{\bullet+}$ upon NR (as compared to EI or CID) indicates that NR deposits higher average internal energies than EI or CID [30]. It is also of interest to note that m/z 78, $CH_2O\text{-}P\text{-}OH^{\bullet+}$, is more intense in the NR spectrum of $\mathbf{1b}^{\bullet+}$ and that only ions $\mathbf{1b}^{\bullet+}$ can form m/z 78 without rearrangement. Thus the enol ions (at least in part) survive the NR experiment, but the keto ions do not. We take this finding as showing that the enol ions lie in a much deeper well than the keto ions, see Scheme 3.3.

From the above we conclude the following: the ethylene phosphonate and ethylene phosphite ions ($\mathbf{1a}^{\bullet+}$ and $\mathbf{1b}^{\bullet+}$ respectively) can be independently generated and identified in the gas-phase. The non-dissociating ions do not interconvert to a significant extent. However, metastable ions $\mathbf{1a}^{\bullet+}$ and $\mathbf{1b}^{\bullet+}$ do interconvert leading to a common dissociation channel, i.e. that leading to $C_2H_4^{\bullet+} + HOPO_2$ having the same kinetic energy release. Competing fragmentations include the losses of CO and $HCO^{\bullet}$ and ^{18}O-labelling experiments indicate that in these fragmentations all oxygen atoms become positionally equivalent. It is therefore highly likely that such equilibration reactions also occur for the dominant metastable reaction, *viz.* formation of $C_2H_4^{\bullet+} + HOPO_2$. In the following we shall use results from our *ab initio* calculations to rationalize the above experimental observations.

3.3.2. The isomerization and dissociation behaviour of ethylene phosphonate/ phosphite ions

In our analysis of the experimental and theoretical results we will use the energy diagram of Scheme 3.3 as our starting point. This diagram summarizes the CBS-QB3 (298 K) computational results on the various isomerization routes for ions $\mathbf{1a}^{\bullet+}$ and $\mathbf{1b}^{\bullet+}$ and their low energy dissociation by loss of HO-P(=O)$_2$. The geometries of the species encountered are given in Fig. 3.1.

First it can be seen, in agreement with experiment, that ions $\mathbf{1b}^{\bullet+}$ are thermodynamically more stable than $\mathbf{1a}^{\bullet+}$ and that they lie in a deep potential well. This explains the observed survivor signal in the NR mass spectrum of $\mathbf{1b}^{\bullet+}$. Just below the metastable dissociation level, see the dashed line in Scheme 3.3, ions $\mathbf{1a}^{\bullet+}$ can undergo a 1,2-H shift to produce the very stable enol ion $\mathbf{1b}^{\bullet+}$. It is found that these ions can undergo ring-opening below the metastable window to produce ions $\mathbf{1e}^{\bullet+}$. The latter ions, see Fig. 3.1 which depicts two configurations of closely similar energy labelled as $\mathbf{1e}^{\bullet+}$ (α) and $\mathbf{1e}^{\bullet+}$ (β), contain a long O•••C bond and are more accurately described as an ion-dipole complex between $C_2H_4^{\bullet+}$ and $HOPO_2$. This complex is the reacting configuration for formation of $C_2H_4^{\bullet+}$ from both $\mathbf{1a}^{\bullet+}$ and $\mathbf{1b}^{\bullet+}$. The small kinetic energy release associated with this dissociation is attributed to the large density of states of such ion-dipole complexes [31]. It is also found that, again just below the metastable window, ions $\mathbf{1b}^{\bullet+}$ can rearrange by way of a 1,3-H shift to the distonic isomer $\mathbf{1c}^{\bullet+}$. This species is unattainable directly from $\mathbf{1a}^{\bullet+}$ as the calculated barrier for this 1,2-H shift lies very high, see Scheme 3.3. However ions $\mathbf{1a}^{\bullet+}$ can isomerize into the distonic ion via the enol ion $\mathbf{1b}^{\bullet+}$. The distonic ion $\mathbf{1c}^{\bullet+}$ may undergo ring-opening to ion $\mathbf{1d}^{\bullet+}$ and the latter ion may be responsible for some of the other (minor) processes observed for the metastable ions (such as m/z 44, CH_2=CH-$OH^{\bullet+}$) but these matters were not further investigated. However, the transition state for this ring-opening lies slightly above the threshold for dissociation into $C_2H_4^{\bullet+}$ and $HOPO_2$.

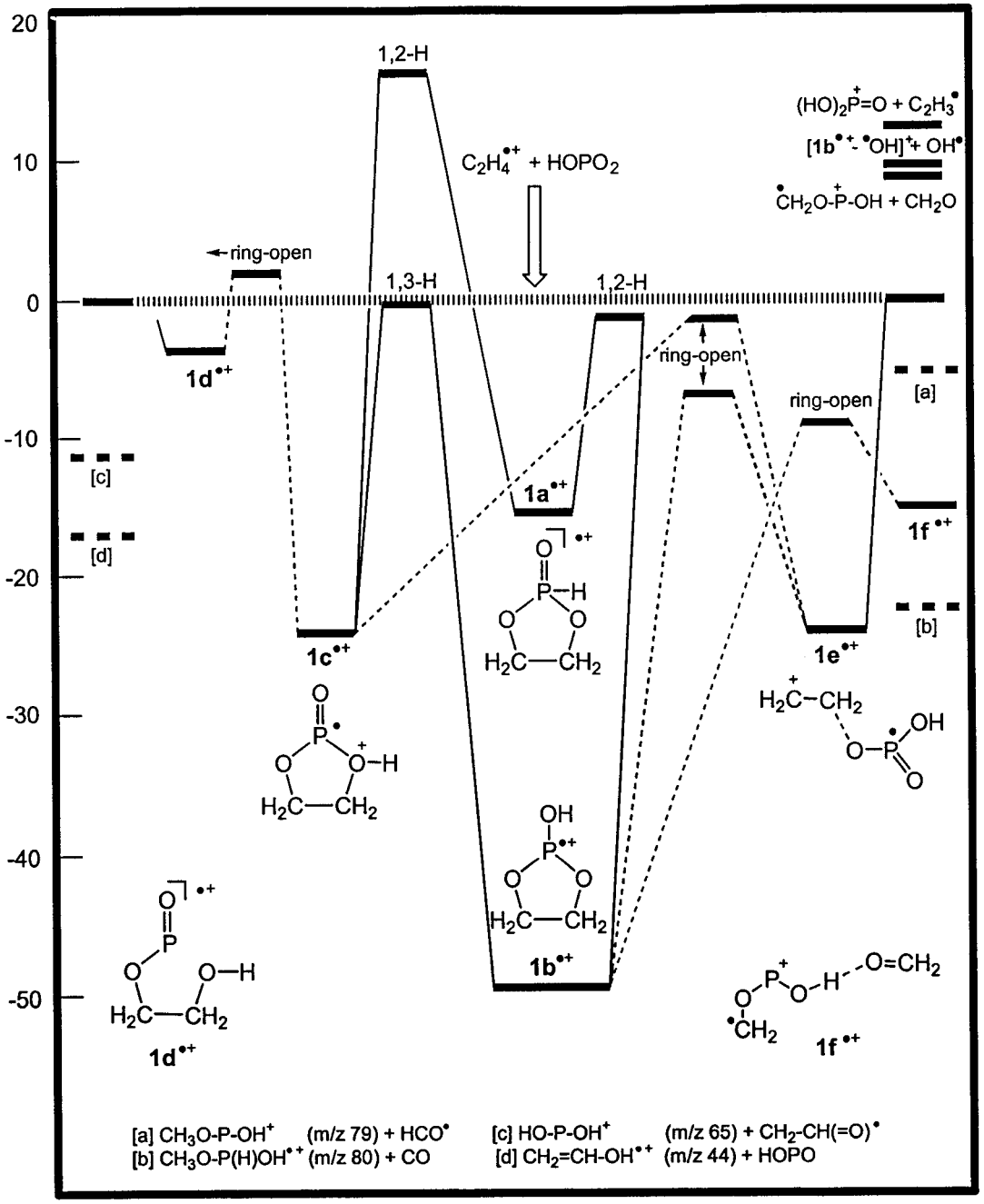

Scheme 3.3

An important reaction upon collisional activation of both ions $\mathbf{1a}^{\bullet+}$ and $\mathbf{1b}^{\bullet+}$ is the formation of $^{\bullet}CH_2\text{-}O\text{-}P^{+}\text{-}OH + CH_2O$, see Fig. 3.3. From NR data we had tentatively concluded that ions $\mathbf{1b}^{\bullet+}$ could lead to these products. Indeed, according to our *ab initio* calculations ions $\mathbf{1b}^{\bullet+}$ can undergo, below the dissociation threshold for loss of HO-

$P(=O)_2$, C-C ring-opening to produce the ion-dipole complex $^{\bullet}CH_2$-O-P^+-OH•••O=CH_2, $\mathbf{1f}^{\bullet+}$ which then dissociates. Ion $\mathbf{1f}^{\bullet+}$ may also be the reacting configuration for the observed (minor) losses of $HCO^{\bullet}$ and CO.

We conclude from our calculations that ions $\mathbf{1a}^{\bullet+}$, $\mathbf{1b}^{\bullet+}$ and $\mathbf{1c}^{\bullet+}$ (and perhaps also $\mathbf{1e}^{\bullet+}$ and $\mathbf{1f}^{\bullet+}$) may more or less freely interconvert prior to dissociation. Nevertheless, this interconversion cannot rationalize the observation that the oxygen atoms become positionally equivalent. However, according to our calculations the distonic ion, $\mathbf{1c}^{\bullet+}$, can undergo an O-C ring-opening to produce the ion-dipole complex $\mathbf{1e}^{\bullet+}$ which can also be formed from the enol ion $\mathbf{1b}^{\bullet+}$. The (inter)conversion $\mathbf{1a}^{\bullet+} \rightarrow \mathbf{1b}^{\bullet+} \rightarrow \mathbf{1e}^{\bullet+} \rightarrow \mathbf{1c}^{\bullet+} \rightarrow \mathbf{1b}^{\bullet+} \rightarrow \mathbf{1a}^{\bullet+}$ rationalizes the observed "scrambling" of the oxygen atoms in ions $\mathbf{1a}^{\bullet+}$ and $\mathbf{1b}^{\bullet+}$.

3.3.3. The benzonitrile-assisted tautomerization of ethylene phosphonate

If we wish to catalyze, by proton-transport catalysis, a 1,2-H shift, then a suitable base should fulfill several criteria [15e], the most important one being the proton affinity (PA) criterion. Following Scheme 3.3, if we wish to successfully isomerize $\mathbf{1a}^{\bullet+}$ to $\mathbf{1b}^{\bullet+}$ then the PA of the base should lie between the PA of the [**1a** - H]$^{\bullet}$ radical at P and O. From the energy of [**1a**-H]$^{\bullet}$ in Table 3.1b and the energies of $\mathbf{1a}^{\bullet+}$ and $\mathbf{1b}^{\bullet+}$ we may evaluate these PA's: PA [**1a** - H]$^{\bullet}$ at P = 159 kcal/mol and PA [**1a** - H]$^{\bullet}$ at O = 194 kcal/mol. Therefore, benzonitrile having a PA of 194 kcal/mol [26] is a suitable candidate to catalyze the above 1,2-H shift.

Benzonitrile was admitted at an indicated pressure of 6 x 10^{-5} to the ion source and a small amount of **1a** was introduced into the ion source. The complex [**1a**•••BN]$^{\bullet+}$ thus formed, see Fig. 3.5 was selectively transmitted into the second ffr. This complex dissociates spontaneously to m/z 108 and BN, together with some other minor fragments, see Fig. 3.5. The ions with m/z 108 were transmitted to the third ffr where they were collisionally probed; the resulting CID mass spectrum is also given in Fig. 3.5. Comparison of this spectrum with those of Fig. 3.3 leaves no doubt that the initial

keto ions $\mathbf{1a}^{\bullet+}$ have completely rearranged to the enol ions $\mathbf{1b}^{\bullet+}$ under the influence of benzonitrile.

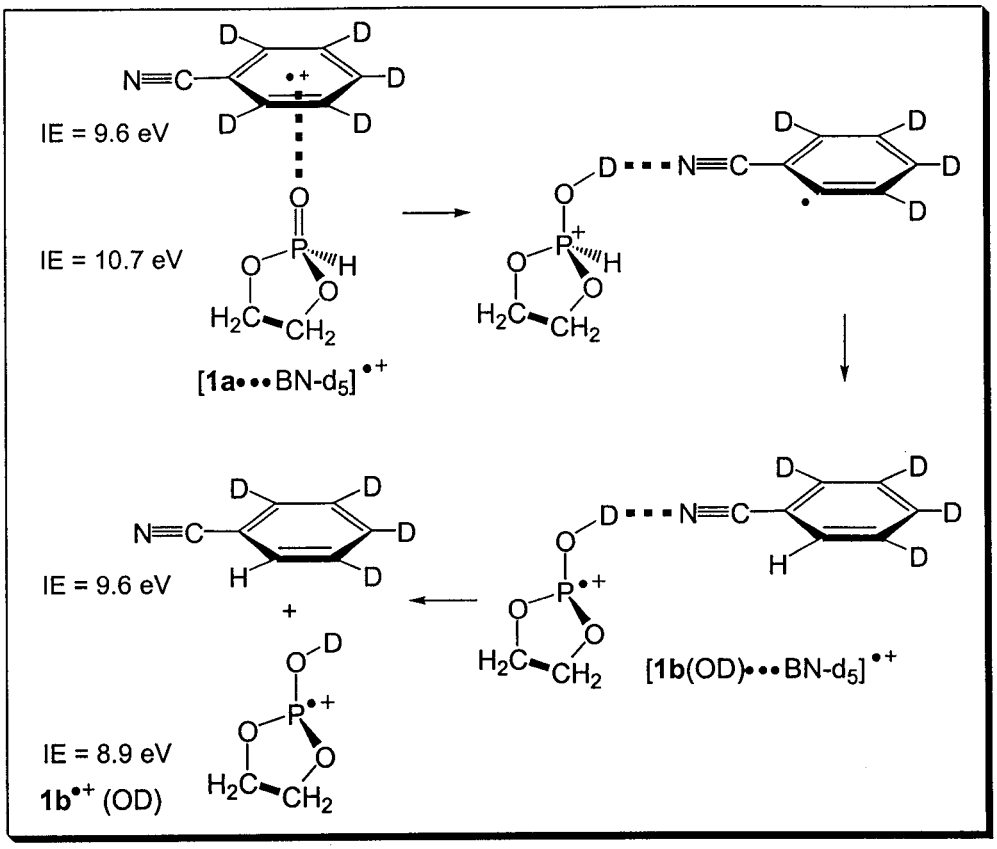

Scheme 3.4

Two different mechanisms may operate for the benzonitrile-assisted tautomerization of $\mathbf{1a}^{\bullet+}$. The first mechanism involves a true proton-transport catalysis in which the P-H proton of *ionized* $\mathbf{1a}^{\bullet+}$ is donated to benzonitrile and the same proton is then donated back to the oxygen atom. In the second mechanism, it is benzonitrile which is ionized and which donates the proton to the P=O oxygen atom of *neutral* **1a**. Next the P-H proton is donated to the benzonitrile radical. This mechanism is termed a "quid-pro-quo" mechanism and is depicted in Scheme 3.4. Labelling can differentiate the two mechanisms: using benzonitrile-d_5 the rearranged enol will appear at m/z 108 if the isomerization is a true proton-transport catalysis; however for a "quid-pro-quo" mechanism the rearranged enol will appear at m/z 109, see Scheme 3.4.

Using benzonitrile-d_5 as the solvent molecule, the reaction in the m/z 216 encounter complex [**1a**•••BN-d_5]$^{\bullet+}$ commences with a D^+ transfer. The next step involves a back-transfer of a $H^\bullet$ radical to the phenyl ring of BN, yielding the hydrogen bridged radical cation (HBRC) [**1b**$^{\bullet+}$(OD)•••BN-d_4] which, either spontaneously or by collisional activation, dissociates into "enol" ions **1b**$^{\bullet+}$ (OD) at m/z 109. If a proton-transport type mechanism were operative, the final complex would be a HBRC of the composition [**1b**$^{\bullet+}$ (OH)•••BN-d_5] which would decompose into "enol" ions **1b**$^{\bullet+}$ (OH) at m/z 108.

Unfortunately, the experimental verification of the above proposal is complicated by the fact that the molecular mass of benzonitrile-d_5 is the same as that of **1a**. From Fig. 3.5 (top spectrum), it follows that in the CI experiment with unlabelled benzonitrile, [BN•••BN]$^{\bullet+}$ dimer ions are formed which are c. 30 times more abundant than the mixed dimer ions [**1a**•••BN]$^{\bullet+}$. Therefore, the m/z 216 peak in the CI experiment of **1a** with BN-d_5 is dominated by isobaric [BN-d_5]$_2^{\bullet+}$ ions, whose MI spectrum is characterized by a single peak at m/z 108, [BN-d_5]$^{\bullet+}$. Moreover, the benzonitrile-d_5 used contained c. 5% of the d_4-isotopologue and since, see Fig. 3.5 (top spectrum) proton-bound dimer ions [BN•••H•••BN]$^+$ are also abundantly generated in the CI experiment, the m/z 216 ions will also contain interfering ions of structure [BN-d_5•••H•••BN-d_4]$^+$. The MI spectrum of [BN•••H•••BN]$^+$ shows a single peak at m/z 104, BNH^+, and by analogy [BN-d_5•••H•••BN-d_4]$^+$ is expected to yield peaks at both m/z 108 [BN-d_4H]$^+$ and m/z 109 [BN-d_5H]$^+$. Finally, the MI spectrum of unlabelled ions [**1a**•••BN]$^{\bullet+}$, see Fig. 3.5 (middle spectrum), also contains a peak at m/z 104, BNH^+, which will shift to m/z 109 in the MI spectrum of [**1a**•••BN-d_5]$^{\bullet+}$.

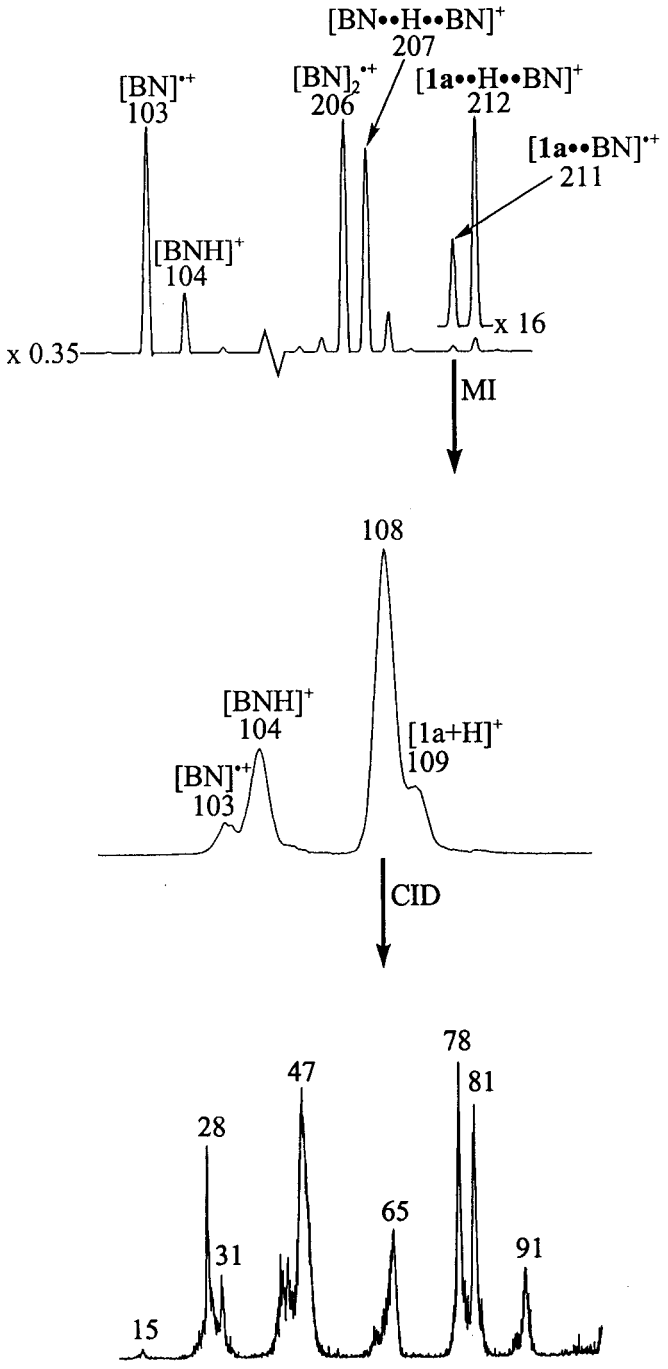

Fig. 3.5. CID mass spectrum of the m/z 108 ions $\mathbf{1b}^{\bullet+}$ generated from metastable ethylene phosphonate/benzonitrile complex ions $[\mathbf{1a}\bullet\bullet\bullet BN]^{\bullet+}$

Thus, the MI spectrum of the m/z 216 ions formed in the CI experiment of **1a** with BN-d_5, which displays prominent peaks at m/z 108 and m/z 109 (in a 3:1 intensity ratio) cannot be used to decide between the proposed "quid-pro-quo" tautomerization mechanism and proton-transport catalysis. However, examination of the CID spectra of the m/z 108 and m/z 109 ions of the m/z 216 MI spectrum does allow differentiation : the CID spectrum of the m/z 108 ions is identical with that of m/z 108 ions independently generated from $[BN\text{-}d_5]_2^{\bullet+}$. The spectrum, even when recorded at a x10 higher amplification, does not show a detectable signal at m/z 47. Since this peak (PO^+) is uniquely characteristic for the presence of phosphorus containing ions, we conclude that m/z 108 ions $\mathbf{1b}^{\bullet+}$ (OH) are **not** formed. This effectively rules out the proton-transport catalysis mechanism.

The CID spectrum of the m/z 109 ions is shown in Fig. 3.6. Although this spectrum is dominated by ions generated from the decomposition of protonated BN-d_5, as evidenced by the base peak at m/z 81 (loss of DCN) and the peaks at m/z 65/66 and 52/54, the spectrum also contains a narrow peak at m/z 28 and the tell-tale peak at m/z 47, indicative of the presence of phosphorus containing ions. Although the $[BN\text{-}d_5H]^+$ interference does not allow us to firmly conclude that "enol" ions $\mathbf{1b}^{\bullet+}$ (OD) are generated in the experiment with benzonitrile-d_5, there is little doubt that a H/D exchange in the encounter complex as dictated by the "quid-pro-quo" mechanism is indeed operative.

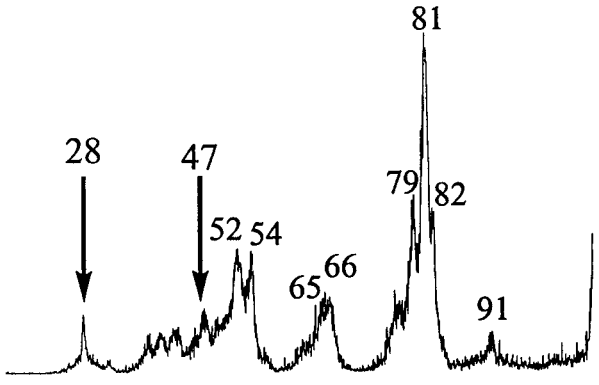

Fig. 3.6. CID mass spectrum (3ffr) of the m/z 109 ions in the MI spectrum (2ffr) of the m/z 216 ions generated from ethylene phosphonate and benzonitrile-d_5 under chemical ionization conditions.

From a theoretical point of view the proton-transport catalysis mechanism is also unlikely since IE (BN) (9.6 eV, Ref. 26) is so much lower than IE (**1a**) (10.7 eV). As a consequence the charge in the [**1a**•••BN]$^{\bullet+}$ complex will be located on the BN moiety, thus prohibiting the first step in the proton-transport catalysis mechanism, i.e. the proton abstraction from **1a**$^{\bullet+}$. However, the same IE difference favours the "quid-pro-quo" mechanism in the following way. An estimate of the relative energies along this pathway may be obtained by combining empirical data with the results given in Table 3.1b, together with computational results obtained previously for the acetamide/BN system [17].

The reaction sequence is given by : [**1a**$^{\bullet+}$ + BN] → [**1a** + BN$^{\bullet+}$] → [**1a**•••BN$^{\bullet+}$] → TS1 → [**1a**H$^+$•••(BN-H)$^\bullet$] → TS2 → [**1b**$^{\bullet+}$•••BN] → [**1b**$^{\bullet+}$ + BN].

With [**1a**$^{\bullet+}$ + BN] as the reference level, and stabilization energies (SE) [32] for the complexes derived from the empirical relationship SE = 30 - 0.25|ΔPA|, we find E_{rel} values of -24, -51 and -64 kcal/mol for [**1a** + BN$^{\bullet+}$], [**1a**H$^+$•••(BN - H)$^\bullet$] and [**1b**$^{\bullet+}$•••BN], respectively (using ΔH_f (BN$^{\bullet+}$) = 274 kcal/mol, ΔH_f([BN - H]$^\bullet$) = 111 kcal/mol [17], PA([**1a/1b** - H]$^\bullet$) at O = 194 kcal/mol, PA(**1a**) = 200 kcal/mol (Table 3.1b), PA([BN - H]$^\bullet$) = 204 kcal/mol [17]). For the complex [**1a**•••BN$^{\bullet+}$], E_{rel} is estimated as -36 kcal/mol, using the SE (12 kcal/mol) calculated for the [acetamide•••BN$^{\bullet+}$] complex [17]. If we further assume that the heights of the isomerization barriers represented by TS1 and TS2 are comparable in magnitude to those calculated for the acetamide/BN system [17], these TSs will lie at about the same energy level as that for [**1a** + BN$^{\bullet+}$]. In our experiments, internal energies up to the [**1a**$^{\bullet+}$ + BN] level of energy may well be available to the reactants, thereby providing sufficient energy for the isomerization reaction [**1a**•••BN]$^{\bullet+}$ → [**1b**•••BN]$^{\bullet+}$ to proceed. The observation, see Fig. 3.5, that the resulting [**1b**•••BN]$^{\bullet+}$ complex also dissociates into BNH$^+$ (m/z 104) + [**1b** - H]$^\bullet$ supports the computational finding that the PA of [**1a/1b** - H]$^\bullet$ at O is closely similar to that of BN (194 kcal/mol, see above).

3.4. Conclusions

In summary, theory and experiment yield a consistent potential energy profile for the cyclic phosphonate/phosphite system showing that non-dissociating ions $\mathbf{1a}^{\bullet+}$ retain their structure identity in the μs time-frame. However, the interaction of **1a** with a benzonitrile (BN) molecule in a chemical ionization type experiment readily yields the more stable "enol" type ion $\mathbf{1b}^{\bullet+}$. Experiments with benzonitrile-d_5 support the proposal that this interaction does not involve the lowering of the 1,2-H shift barrier between the tautomers via a proton-transport catalysis type mechanism. Rather, a "quid-pro-quo" mechanism is operative, analogous to that proposed for the benzonitrile-assisted enolization of acetamide [17]. In this mechanism, the ionized benzonitrile component of the encounter complex $[\mathbf{1a}\bullet\bullet\bullet BN]^{\bullet+}$ donates a proton to the O-atom of the phosphonate's O=P(H) functionality. This is followed by a back-transfer of the P-H hydrogen atom to benzonitrile's phenyl ring, yielding a H-bridged radical cation of the type $C_6H_5C{\equiv}N\bullet\bullet\bullet H\text{-}O\text{-}P[\text{-}OCH_2CH_2O\text{-}]^{\bullet+}$. This ion serves as the immediate precursor in the formation of the ethylene phosphite ion, $\mathbf{1b}^{\bullet+}$, and benzonitrile.

References:

[1] D. E. C. Corbridge, *Phosphorus: an outline of its chemistry, biochemistry, and uses*, 5th ed., Elsevier, New York, 1995.

[2] J. Emsley and D. Hall, *The Chemistry of Phosphorus*, Harper and Row Ltd., London, 1976.

[3] M. Eto, Organophosphorus Pesticides: Organic and Biological Chemistry, CRC Press, Cleveland, Ohio (1974).

[4] Selected reviews: (a) R. A. J. O'Hair, in: *The Chemistry of Organophosphorus Compounds, Vol. 4*, ed. F. R. Hartley, John Wiley and Sons Ltd., 1996, Chapter 8; (b) R. G. Gillis and J. L. Occolowitz, in: *Mass Spectrometry of Phosphorus Compounds* in *Analytical Chemistry of Phosphorus Compounds*, ed. M. Halmann, Wiley-Interscience, New York, 1972, Chapter 8; (c) J. R. Chapman, *Organophosphorus Chem.* 14 (1983) 278; (d) J. Granoth, *Top. Phosphorus Chem.* 8 (1976) 41.

[5] (a) S.Gevrey, A. Luna, M-H.Taphanel, J. Tortajada and J-P.Morizur, *Int. J. Mass Spectrom.* 195/196 (2000) 545; (b) J-F. Gal, M. Herreros, P. C. Maria, L. Operti, C. Pettigiani, R. Rabezanna and G. A. Vaglio, *J. Mass Spectrom.* 34 (1999) 1296; (c) B. L. M. van Baar, A. G. Hulst and E. R. J. Wils, *J. Mass Spectrom.* 32 (1998) 1104.

[6] (a) J. L. Occolowitz and G. L. White, *Anal. Chem.* 35 (1963)1179; (b) J. G. Pritchard, *Org. Mass Spectrom.* 3 (1970) 163; (c) E. Santoro, *Org. Mass Spectrom.* 7 (1973) 589; (d) D. A. Bafus, E. J. Gallegos and R. W. Kiser, *J. Phys. Chem.* 70 (1966) 2614; (e) J. Fischler and M. Halman, *J. Chem. Soc.* 1964, 31.

[7] (a) *Tandem Mass Spectrometry*, ed. F. W. McLafferty, Wiley, New York, 1983; (b) K. Levsen and H. Schwarz, *Mass Spectrom. Rev.* 2 (1983) 77.

[8] K. L. Busch, G. L. Glish and S. A. McLuckey, *Mass Spectrometry/Mass Spectrometry*, VCH, New York, 1988.

[9] J. L. Holmes, *Org. Mass Spectrom.* 20 (1985) 169.

[10] (a) H. I. Kenttämaa and R. G. Cooks, *J. Am. Chem. Soc.* 107 (1985) 1881; (b) J. S. Brodbelt, H. I. Kenttämaa and R. G. Cooks, *Org. Mass Spectrom.* 23 (1988) 6; (c) L. Zeller, J. Farrell Jr., P. Vainiotalo and H. I. Kenttämaa, *J. Am. Chem. Soc.* 114 (1992) 1205; (d) K. M. Stirk, P. Lin, T. D. Ranatunga, L. C. Zeller, J. T. Farrell Jr. and H. I. Kenttämaa, *Int. J. Mass Spectrom. Ion Proc.* 130 (1994) 187.

[11] (a) J. R. Holtzclaw, J. R. Wyatt and J. E. Campana, *Org. Mass Spectrom.* 20 (1985) 90; (b) J.R. Holtzclaw and J. R.Wyatt, *Org. Mass Spectrom.* 23 (1988) 261.

[12] F. Tureček, M. Gu and C. E. C. A. Hop, *J. Phys. Chem.* 99 (1995) 2278.

[13] L.N. Heydorn, Y. Ling, G. de Oliveira, J. M. L. Martin, Ch. Lifshitz and J. K. Terlouw, *Zeitschrift für Physikalische Chemie* 215 (2001) 141.

[14] *The Chemistry of Enols*, ed. Z. Rappoport, Wiley, New York, 1990.

[15] For selected references see: (a) D. K. Böhme, *Int. J. Mass Spectrom. Ion Proc.* 115 (1992) 95. (b) J. W. Gauld, H-E. Audier, J. Fossey and L. Radom, *J. Am. Chem. Soc.* 118 (1996) 6299. (c) J. W. Gauld and L. Radom, *J. Am. Chem. Soc.* 119 (1997) 9831. (d) A. J. Chalk and L. Radom, *J. Am. Chem. Soc.* 119 (1997) 7573. (e) A. J. Chalk and L. Radom, *J. Am. Chem. Soc.* 121 (1999) 1574. (f) J. Chamot-Rooke, G. van der Rest, P. Mourgues, and H-E. Audier, *Int. J. Mass Spectrom.* 195/196 (2000) 385. (g) M. A. Trikoupis, D. J. Lavarato, J. K. Terlouw, P. J. A. Ruttink and P. C. Burgers, *European Mass Spectrom.* 5 (1999) 431.

[16] (a) M.A. Trikoupis, J. K. Terlouw and P. C. Burgers, *J. Am. Chem. Soc.* 120 (1998) 12131; (b) P. Mourgues, J. Chamot-Rooke, G. van der Rest, H. Nedev, H.E. Audier and T.B. McMahon, *Int. J. Mass Spectrom.* 210/211 (2001) 429.

[17] M.A. Trikoupis, P.C. Burgers, P.J.A. Ruttink and J.K. Terlouw, *Int. J. Mass Spectrom.* 210/211 (2001) 489.

[18] (a) A. Oswald, *Can. J. Chem.* 37 (1959) 1498 and references cited therein;
(b) J. Cason, W.N. Baxter and W. DeAcetis, *J. Org. Chem.* 24 (1959) 247;
(c) K. Dimroth and R. Ploch, *Chem. Ber.* 90 (1957) 801.

[19] S.D. Taylor and R. Klugger, *J. Am. Chem. Soc.* 114 (1992) 3067 and references cited therein.

[20] H. F. van Garderen, P. J. A. Ruttink, P. C. Burgers, G. A. McGibbon and J. K. Terlouw, *Int. J. Mass Spectrom. Ion Proc.* 121 (1992) 159.

[21] For a recent review see: G. Schalley, G. Hornung, D. Schröder and H. Schwarz, *Chem. Soc. Rev.* 27 (1998) 91.

[22] M. J. Frisch, G. W. Trucks, H. B. Schlegel, G. E. Scuseria, M. A. Robb, J. R. Cheeseman, V. G. Zakrzewski, J. A. Montgomery, R. E. Stratmann, J. C. Burant, S. Dapprich, J. M. Millam, A. D. Daniels, K. N. Kudin, M. C. Strain, O. Farkas, J. Tomasi, V. Barone, M. Cossi, R. Cammi, B. Mennucci, C. Pomelli, C. Adamo, S. Clifford, J. Ochterski, G. A. Petersson, P. Y. Ayala, Q. Cui, K. Morokuma, D. K. Malick, A. D. Rabuck, K. Raghavachari, J. B. Foresman, J. Cioslowski, J. V. Ortiz, B. B. Stefanov, G. Liu, A. Liashenko, P. Piskorz, I. Komaromi, R. L. Martin, D. J. Fox, T. Keith, M. A. Al-Laham, C. Y. Peng, A. Nanayakkara, R. Gomperts, C. Gonzalez, M. Challacombe, P. M. W. Gill, B. G. Johnson, W. Chen, M. W. Wong, J. L. Andres, M. Head-Gordon, E. S. Replogle, and J. A. Pople, Gaussian 98, Revision A.9, Gaussian, Inc., Pittsburgh, PA, 1998;

[23] (a) M. Dupuis, D. Spangler, J. Wendolowski, NRCC Software Catalogue 1 Program No. QG01, GAMESS (1980); (b) M. Guest, J. Kendrick, GAMESS User Manual, An Introductory Guide, CCP/86/1, Daresbury Laboratories (1986).

[24] (a) J. A. Montgomery Jr, M. J. Frisch, J. W. Ochterski, and G. A. Petersson, *J. Chem. Phys.* 110 (1999) 2822; (b) ibid. 112 (2000) 6532.

[25] L.N. Heydorn, C.Y. Wong, R. Srinivas and J.K. Terlouw, *Int. J. Mass Spectrom.* 225 (2203) 11.

[26] S. G. Lias, J. E. Bartmess, J. F. Liebman, J. L. Holmes, R. D. Levin, W. G. Mallard, *J. Phys. Chem. Ref. Data* 17 (1988) Suppl. 1; see also NIST Chemistry WebBook, http://webbook.nist.gov/chemistry/

[27] J.L. Holmes and J.K. Terlouw, *Org. Mass Spectrom.* 15 (1980) 383.

[28] M.N. Glukhovtsev and R.D. Bach, *Chem. Phys. Lett.* 286 (1998) 51.

[29] The thermochemical energy requirement for the reaction CH_2=CH-$OC_2H_5^{\bullet+}$ → CH_2=CH-$OH^{\bullet+}$ + C_2H_4 is 25 kcal/mol [25], 8 kcal/mol lower than the experimentally observed value of 33 kcal/mol (J.L. Holmes, J.K. Terlouw and F.P. Lossing, *J. Phys. Chem.* 80 (1976) 2860.). The latter value is most readily attributed to the barrier for 1,3-H shift in this dissociation.

[30] S. Beranová and C. Wesdemiotis, *J. Am. Chem. Soc. Mass Spectrom.* 5 (1994) 1093.

[31] P.J.A. Ruttink, *J. Phys. Chem.* 91 (1987) 703.

[31] M. Meot-Ner (Mautner), *J. Am. Chem. Soc.* 106 (1984) 1257.

Chapter 4

The low energy decarbonylation of the $CH_3O\text{-}P{=}O^{\bullet+}$ family of ions : an experimental and CBS-QB3 computational study

The dissociation chemistry of the title ions was investigated using tandem mass spectrometry based experiments in conjunction with isotopic labelling and computational quantum chemistry.

Upon collisional activation, ions $CH_3O\text{-}P{=}O^{\bullet+}$, **1a**, and $CH_2O\text{-}P\text{-}OH^{\bullet+}$, **1b**, readily lose $CH_2{=}O$. This reaction is completely suppressed in the low energy (metastable) ions, which instead abundantly lose CO. The product ion generated in this decarbonylation reaction is the ylide ion $H\text{-}P\text{-}OH_2^{\bullet+}$, rather than its more stable isomer $H_2P\text{-}OH^{\bullet+}$. Remarkably, the oxygen atoms become equivalent in this reaction : ions $CH_3{}^{18}O\text{-}P{=}O^{\bullet+}$ and $CH_2O\text{-}P\text{-}{}^{18}OH^{\bullet+}$ lose $C^{18}O$ and $C^{16}O$ in a 1:1 ratio. The experiments further show that the dissociating ions have a fairly large internal energy content : up to 40 kcal/mol for the distonic ion **1b**, which, along with the "enol" ion $CH_2{=}P(OH){=}O^{\bullet+}$, represents the global minimum of the $CH_3O_2P^{\bullet+}$ potential energy-surface.

The mechanism of this intriguing decarbonylation was studied, using the CBS-QB3 model chemistry to probe the structure and energetics of potential intermediates and their interconversion barriers. It appears that metastable ions **1a** and **1b** have sufficient internal energy to communicate with a great many isomers. Of these, the cyclic ion $P[\text{-}OCH_2O(H)\text{-}]^{\bullet+}$ and ion $[CH_2O\text{-}H{\bullet\bullet\bullet}O{=}P]^{\bullet+}$, a hydrogen-bridged radical cation (HBRC), play a key role in the oxygen equilibration. The HBRC's $[HO\text{-}P{\bullet\bullet\bullet}H\text{-}C(H){=}O]^{\bullet+}$ and $[H\text{-}P\text{-}O(H)\text{-}H{\bullet\bullet\bullet}C{\equiv}O]^{\bullet+}$ are key intermediates in the actual mechanism for the decarbonylation. The latter ion may lose CO to produce $H\text{-}P\text{-}OH_2^{\bullet+}$ or else isomerize into the ion-dipole complex $[H_2O{\bullet\bullet\bullet}P(H){=}C{=}O]^{\bullet+}$, whose dissociation into H_2O + $H\text{-}P{=}C{=}O^{\bullet+}$ accounts for the observed minor loss of water.

* The work described here has been accepted for publication in an article under the same title: L.N. Heydorn, P.C. Burgers, P.J.A. Ruttink and J.K. Terlouw, Int. J. Mass Spectrom. (2003)

4.1. Introduction

In the context of our studies of molecule-assisted tautomerization reactions of radical cations in ion-molecule encounter complexes [1], we recently studied the intriguing gas-phase ion chemistry of the dimethyl phosphonate radical cation, $(CH_3O)_2P(H)=O^{\bullet+}$, using a variety of mass spectrometry based techniques [2]. The interpretation of the experimental results relied heavily on energetic information which, given the dearth of reliable experimental enthalpy values for PO-containing ions and neutrals, was obtained from computational chemistry. From a brief validation study [2], it appears that the CBS-QB3 model chemistry [3] accurately reproduces heats of formation of species comprised of a second row element (P or S) bonded to a highly electronegative element (O). For the $(CH_3O)_2P(H)=O^{\bullet+}$ system of ions, it was further argued that a a conservative estimate for the uncertainty in computed transition states/reaction barrier heights is ± 4 kcal/mol [2].

This combination of theory and experiment was also used [4] to probe the tautomerization of the ethylene phosphonate ion, **I**, into its phosphite and distonic counterparts **II** and **III**, which are lower in energy by 34 and 10 kcal/mol respectively :

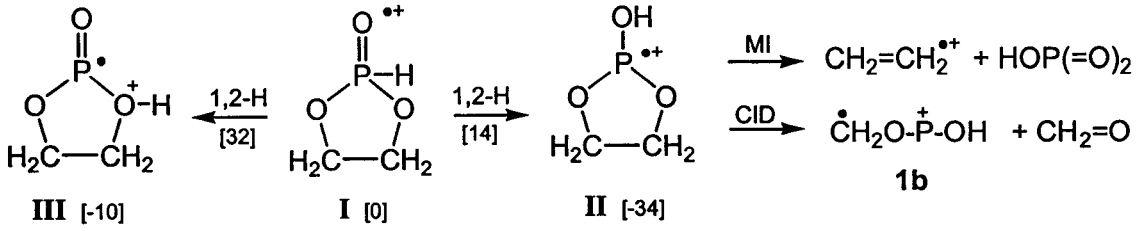

Scheme 4.1

In brief, theory and experiment agree that low energy phosphonate ions **I** readily tautomerize via a 1,2-H shift into phosphite ions **II**, prior to dissociation into $CH_2=CH_2^{\bullet+}$ + $HOP(=O)_2$. This reaction dominates the metastable ion (MI) spectrum of both ions **I** and independently generated ions **II**. The tautomerization **I** → **III** has a much higher barrier, 32 kcal/mol, and the resulting energy-rich distonic ions readily undergo ring opening into the acyclic isomer $HO\text{-}CH_2\text{-}CH_2\text{-}O\text{-}P=O^{\bullet+}$.

Upon collisional activation, ions **I** and **II** show a pronounced loss of CH_2=O, as witnessed by an intense m/z 78 peak in their collision induced dissociation (CID) mass spectra. Prominent m/z 78 ions are also observed in the electron impact (EI) mass spectra of **I** and ethyl ethylene phosphite, the precursor of **II**. Analysis of their CID spectra provides evidence that these m/z 78 ions are distonic ions CH_2O-P-$OH^{\bullet+}$, **1b** [5]. The spectra are characteristically different from those of the experimentally accessible isomers CH_3O-P=$O^{\bullet+}$, **1a**, [5] and CH_2=P(OH)=$O^{\bullet+}$, **1i**, the very stable enol tautomer of the elusive CH_3-$P(=O)_2^{\bullet+}$ ion **1h** [6].

The analysis of the CID spectra of the three $CH_3O_2P^{\bullet+}$ isomers is straightforward [5, 6], but that of their MI spectra is not : the major dissociation of low energy ions **1a** and **1b** appears to be a decarbonylation reaction, which requires a triple H-transfer for ions CH_3O-P=$O^{\bullet+}$. Metastable ions CH_2=P(OH)=$O^{\bullet+}$, **1i**, also undergo decarbonylation but here loss of PO is more pronounced. A multiple collision experiment indicated that the resulting m/z 50 product ion is the as yet unknown ylide ion H-P-$OH_2^{\bullet+}$, rather than its more stable conventional isomer H_2P-$OH^{\bullet+}$. Further, an ^{18}O-labelling experiment revealed that the positional identity of the oxygen atoms in CH_3O-P=$O^{\bullet+}$ and CH_2O-P-$OH^{\bullet+}$ is lost in the decarbonylation. These observations prompted us to study the mechanism of this intriguing reaction, using the CBS-QB3 model chemistry to probe the structure and energetics of potential intermediates and their interconversion barriers. The metastable ions appear to have a substantial internal energy content : ca 40 kcal/mol for ions **1b** and **1i** which represents the global minimum of the $CH_3O_2P^{\bullet+}$ potential energy surface. This broad energy domain comprises some twenty stable $CH_3O_2P^{\bullet+}$ isomers, including various ion-dipole complexes and hydrogen bridged radical cations (HBRCs). Several of these, it will be shown, may account for the communication between metastable ions **1a**, **1b** and **1i** and the oxygen equilibration, whereas the HBRCs [O=CH(H)•••P-OH]$^{\bullet+}$ and [O=C•••H-O(H)-P-H]$^{\bullet+}$ appear to be key intermediates in the actual mechanism for the decarbonylation.

4.2. Experimental and theoretical methods

Sample preparation procedures

Methyl dichlorophosphate, CH_3O-P(=O)Cl_2, was obtained from Aldrich. The labelled isotopologues, CH_3O^{18}-P(=O)Cl_2 and CH_2DO-P(=O)Cl_2 were synthesized on a small scale by controlled methanolysis of O=PCl_3 [7]. In a typical experiment, 110 μL of O=PCl_3 (Aldrich) in 100 μL dry ether was kept frozen in a small glass bulb using liquid N_2. Next, 25 μL of the labelled methanol in an equal volume of ether was transferred into the bulb with a syringe and frozen on top of the solid O=PCl_3/ ether layer. The bulb was then quickly evacuated and, while pumping continuously with a rotary pump, the two layers were allowed to gradually come to room temperature over a period of ca 1 h, using dry ice as the cooling agent. The resulting clear viscous liquid containing the desired isotopologue was sufficiently pure for our mass spectrometric experiments.

Ethylene phosphonate (1,3,2-dioxaphospholane, 2-oxide) and ethyl ethylene phosphite were obtained as described in reference 4. Methyl hypophoshite, CH_3O-$P(H)_2$=O, was synthesized as described in Ref. 8 from a dehydrated 50% hypophosphorous acid / water solution (Aldrich) on the milligram scale. Methyl phosphonic acid, CH_3-$P(OH)_2$=O, was of research grade and obtained from Aldrich. The deuterium isotopologue, CH_3-$P(OD)_2$=O, was obtained by repeated exchange with D_2O.

Tandem mass spectrometry

The tandem mass spectrometry based experiments were performed with the McMaster University ZAB-R mass spectrometer, a three-sector BE_1E_2 (B = magnetic sector, E = electric sector) type instrument [9].

The compounds were introduced into the ion source (kept at 100°C) via a wide-bore all-quartz direct insertion probe connected via an o-ring with a small glass bulb that contains the sample. Ions generated in the source by electron ionization (EI) were accelerated to 8 or 10 keV prior to recording their spontaneous or collision induced dissociations in the second (2ffr) or the third field free (3ffr) regions as MI (metastable ion) or CID (collision induced dissociation) spectra respectively. The structure of a

given product ion in a 2ffr MI or CID spectrum was probed by selectively transmitting the ion by E_1 to a collision chamber in the 3ffr pressurized with O_2 and mass-analyzing its ionic dissociation products by scanning E_2. All of the (high energy) collision experiments were performed at a main beam transmittance (~70%) such that the probability for multiple collisions is negligible. The quoted kinetic energy releases refer to $T_{0.5}$ values derived from the width at half-height of the appropriate metastable peak, by means of the standard one-line equation, with no correction for the width of the main beam [10]. All spectra were recorded using a small PC-based data system developed by Mommers Technologies Inc. (Ottawa).

Computational procedures

The calculations were performed using Gaussian 98 revision A.9 [11]. The standard CBS-QB3 model chemistry [3] was used to probe structures and energies of the key isomeric ions, connecting transition states and dissociation products associated with the $CH_3O_2P^{\bullet+}$ potential energy surface. The energetic results are presented in Table 1a/b (equilibrium and transition state energies), Table 1c (dissociation products) and Schemes 4.2a-c. In the Schemes, the energy levels for the minima and transition states are represented by solid and dashed lines respectively. Detailed geometries of selected species are displayed in Fig. 4.2 (the complete set of geometries is available upon request). Frequency calculations gave the correct number of negative eigenvalues for all minima and transition states and the spin contamination was within the acceptable range. The connections of the transition states have been checked by geometry optimizations and frequency calculations.

Several of the isomeric ions studied were found to have stable conformers, like ion **1b** whose four conformers are shown in Fig. 4.2. The various conformers are listed in Table 4.1 and Fig. 4.2 using a syn (s) /anti (a) notation where we start viewing the C–O bond and move towards the O–H bond in the assignment. For example, in conformer **1b**(s/a) the C atom is on the same side of the CH_2O–P bond as the hydroxylic O atom, designated as "syn", whereas the CO oxygen is on the opposite side of the P–OH bond to the H atom, designated as "anti". Among the conformers of **1b**, the (s/a) conformer is

the most stable, by ca 5 kcal/mol. Since the interconversion barriers are relatively low, ca 5 kcal/mol (Table 1a), the conformers are collectively referred to as **1b** in the text and the energy diagrams.

Table 4.1a. Enthalpies of formation and relative energies, E_{rel}, (kcal/mol) of the $CH_3O\text{-}P{=}O^{\bullet+}$ ion **1a**, and its principal isomers derived from CBS-QB3 calculations.

Ion structure		E_{total} [0 K]*	ZPVE	$\Delta H°_f$[0 K]	$\Delta H°_f$[298 K]	Erel**
$CH_3O\text{-}P{=}O^{\bullet+}$ (anti)	**1a** (a)	-530.68346	27.89	137.9	135.4	14
	1a (s)	-530.68133	27.98	139.2	136.7	15
$CH_2O\text{-}P\text{-}OH^{\bullet+}$ (s/a)	**1b** (s/a)	-530.70506	26.91	124.4	121.5	0
	1b (s/s)	-530.69865	26.04	128.4	125.9	4.5
	1b (a/s)	-530.69905	26.30	128.1	125.5	4
	1b (a/a)	-530.69779	26.47	128.9	126.3	5
$[HO\text{-}P^{\bullet+}\bullet\bullet\bullet H\text{-}C(H){=}O]$ (s)	HBRC-**1b** (s)	-530.65476	24.76	155.9	153.6	32
	HBRC-**1b** (a)	-530.64952	24.19	159.2	157.1	35.5
$CH_2O(H)\text{-}P{=}O^{\bullet+}$ (syn)	**1c** (s)	-530.66664	25.86	148.5	146.5	25
	1c (a)	-530.66566	25.88	149.1	147.1	25.5
$[HO\text{-}CH_2]^{+}\bullet\bullet\bullet O{=}P^{\bullet}$	ID-**1c**	-530.67735	28.76	141.7	139.1	17.5
$[^{+}CH_2\text{-}O\text{-}H\bullet\bullet\bullet O{=}P^{\bullet}]$	HBRC-**1c**	-530.69034	26.77	133.6	131.1	9.5
$CH_2O\text{-}P(H){=}O^{\bullet+}$	**1d**	-530.67567	25.83	142.8	140.1	18.5
$[\text{-}OCH_2O\text{-}]P\text{-}H^{\bullet+}$	**1e**	-530.67022	27.41	146.2	142.6	21
$[\text{-}OCH_2O(H)\text{-}]P^{\bullet+}$	**1f**	-530.67067	29.40	145.9	142.7	21
$H\text{-}C(=O)P(H)\text{-}OH^{\bullet+}$	**1g**	-530.67604	25.39	138.5	135.9	15
$[HO\text{-}PH]^{+}\bullet\bullet\bullet O{=}CH^{\bullet}$	ID-**1g**	-530.65420	24.75	156.3	154.0	32.5
$CH_3\text{-}P(=O)_2^{\bullet+}$	**1h**	-530.65978	26.13	152.8	150.2	28
$CH_2{=}P(OH){=}O^{\bullet+}$	**1i**	-530.70819	26.92	122.4	119.5	-2
$[\text{-}CH_2O\text{-}]P\text{-}OH^{\bullet+}$	**1j**	-530.68488	26.61	137.0	134.3	13
$HOCH_2\text{-}P{=}O^{\bullet+}$	**1k**	-530.67819	27.90	141.2	138.8	17.5
$HOCH{=}P(H){=}O^{\bullet+}$	**1l**	-530.67264	26.99	144.7	141.7	20
$[HO\text{-}P(H)\text{-}H^{\bullet+}\bullet\bullet\bullet C{\equiv}O]$	HBRC-**2a**	-530.69015	23.23	133.7	132.0	10.5
$[H\text{-}P\text{-}O(H)\text{-}H^{\bullet+}\bullet\bullet\bullet C{\equiv}O]$	HBRC-**2b**	-530.68751	24.20	135.4	133.8	12.5
$[O{=}C{=}PH]^{\bullet+}\bullet\bullet\bullet OH_2$	ID-**3b**	-530.69299	24.54	131.9	130.5	9
$[HO\text{-}PH_2]^{\bullet+}\bullet\bullet\bullet O{\equiv}C$	ID-**2a**	-530.69194	23.39	132.6	130.9	9.5

* E_{total} in Hartrees, all other components, including the ZPVE scaled by 0.99, in kcal/mol.
** Using the $\Delta H°_f$[298 K] value of the syn/anti isomer **1b** (s/a) as the anchor point.

Table 4.1b. Enthalpies of formation and relative energies, E_{rel}, (kcal/mol) of transition states describing the isomerization and decarbonylation of the $CH_3O\text{-}P{=}O^{\bullet+}$ ion **1a**, and its principal isomers derived from CBS-QB3 calculations.

	E_{total} [0 K]*	ZPVE	$\Delta H°_f$ [0 K]	$\Delta H°_f$ [298 K]	Erel**
TS **1a** → **1b** (s/s)	-530.65170	27.98	160.0	156.8	35.5
TS **1a** → **1c**	-530.60896	25.86	184.7	182.1	60.5
TS **1a** → **1d**	-530.62240	24.67	176.2	173.1	51.5
TS **1a** (a) → **1h**	-530.62144	25.78	176.8	174.3	53
TS **1a** (1,3-CH_3)	-530.62178	25.34	176.6	174.1	52.5
TS **1b** (s/s → s/a)	-530.69770	25.87	129.0	126.1	4.5
TS **1b** → HBRC-**1b**	-530.65015	24.93	158.8	156.1	34.5
TS **1b** → HBRC-**1c**	-530.67052	26.25	146.0	143.4	22
TS **1b** → **1d**	-530.62551	23.82	174.3	171.6	50
TS **1b** → **1f**	-530.65792	27.74	153.9	150.6	29
TS **1b** → **1j**	-530.67615	25.47	142.5	139.7	18
TS **1d** → HBRC-**1c**	-530.63675	23.23	167.2	164.9	43.5
TS **1d** → **1e**	-530.63511	25.67	168.2	164.8	43.5
TS **1e** → **1f**	-530.61447	25.72	181.2	177.6	56
TS **1f** → ID-**1c**	-530.66233	28.90	151.2	147.7	26
TS **1h** → **1i**	-530.62154	26.08	176.8	173.0	51.5
TS HBRC-**1b** → **1g**	-530.64621	23.49	161.3	158.8	37.5
TS **1g** → HBRC-**2a**	-530.64681	23.19	160.9	158.9	37.5
TS **1g** → HBRC-**2b**	-530.65828	23.62	153.7	151.1	29.5
TS HBRC-**1b** (s → a)	-530.64900	24.25	159.5	156.9	35.5
TS HBRC-**1b** → HBRC-**1c**	-530.65473	25.04	155.9	153.2	31.5
TS ID-**1c** → HBRC-**1c**	-530.67116	27.60	145.6	143.0	21.5
TS HBRC-**1b** → HBRC-**2b**	-530.65099	23.40	158.3	155.7	34
TS HBRC-**2b** → ID-**3b**	-530.67185	23.67	145.2	143.8	22.5
TS **1i** (1,3-H)	-530.63003	23.77	171.4	168.4	47
TS **1i** → **1j**	-530.63765	25.69	166.7	163.7	42
TS **1i** → **1k**	-530.62433	28.94	175.0	171.5	50
TS **1k** → HBRC-**1c**	-530.66656	27.45	148.5	145.7	24
TS **1k** → **1l**	-530.61857	25.02	178.6	174.9	53.5
TS **1g** → **1l**	-530.65832	24.29	153.7	150.2	28.5

* E_{total} in Hartrees, all other components, including the ZPVE scaled by 0.99, in kcal/mol.
** Using the $\Delta H°_f$ [298 K] value of the syn/anti isomer **1b** (s/a) as the anchor point.

Table 4.1c. Relative energies, E_{rel} (kcal/mol), of dissociation reactions of ion **1b** derived from CBS-QB3 calculations.

Dissociation Products		E_{rel}[298K]*
$CH_2O\text{-}P{=}O^+ + H^\bullet$	m/z 77	51
$[\text{-}OCH_2O\text{-}]P^+ + H^\bullet$	m/z 77	51
$O{=}P\text{-}OH^{\bullet+} + CH_2^{\bullet\bullet}$	m/z 64	125
$P\text{-}OCH_3^{\bullet+} + O$	m/z 62	123
$CH_2{=}P\text{-}OH^{\bullet+} + O$	m/z 62	118
$HPCO^{\bullet+} + H_2O$	m/z 60	25
$[\text{-}OC(H)\text{-}]P^{\bullet+} + H_2O$	m/z 60	52
$HCPO^{\bullet+} + H_2O$	m/z 60	96
$H_2POH^{\bullet+} + CO$	m/z 50	14
$H\text{-}P\text{-}OH_2^{\bullet+} + CO$	m/z 50	24
$P\text{-}OH^{\bullet+} + CH_2{=}O$	m/z 48	43
$H\text{-}P{=}O^{\bullet+} + CH_2{=}O$	m/z 48	67
$PO^+ + CH_2OH^\bullet$	m/z 47	59
$CH_2\text{-}OH^+ + PO^\bullet$	m/z 31	39
$HCO^+ + HPOH^\bullet$	m/z 29	51

* Using the ΔH°_f[298 K] value of the syn/anti isomer **1b** as the anchor point.

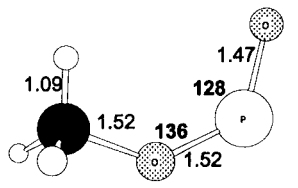

1a (syn)

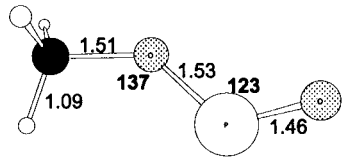

1a (anti)

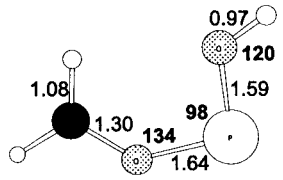

1b (s/a)

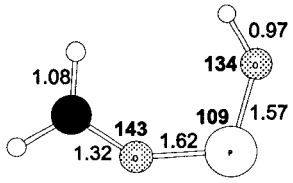

1b (s/s)

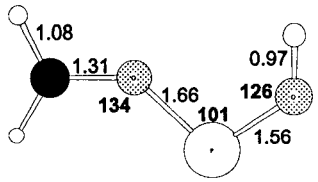

1b (a/s)

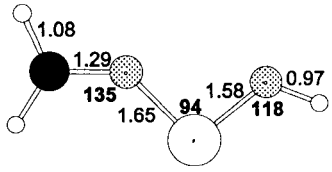

1b (a/a)

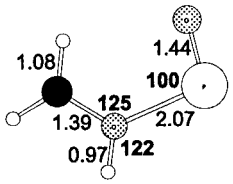

1c (syn)

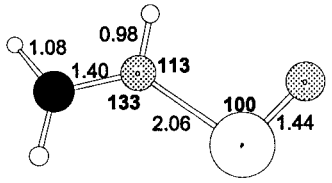

1c (anti)

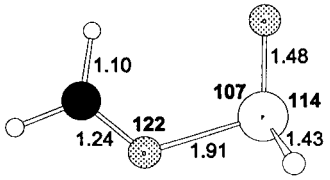

1d

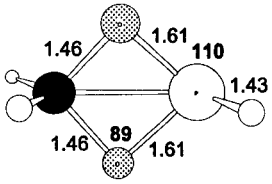

1e

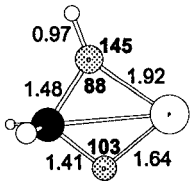

1f

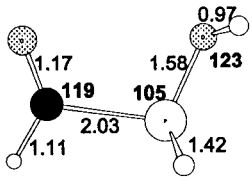

1g (syn)

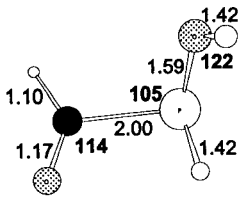

1g (anti)

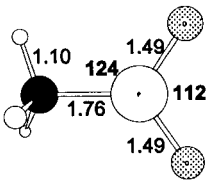

1h

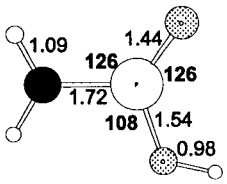

1i

Fig. 4.2a. Optimized geometries of the various isomers of the $CH_3O\text{-}P{=}O^{\bullet+}$ ion (**1a**$^{\bullet+}$). The bond lengths (Å) and angles are presented in normal and bold font, respectively.

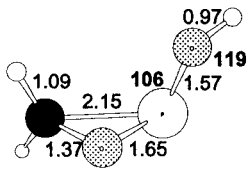

1j

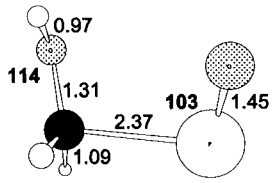

1k

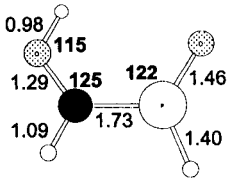

1l

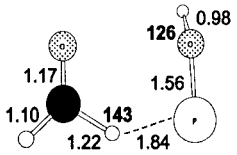

HBRC-1b (syn)

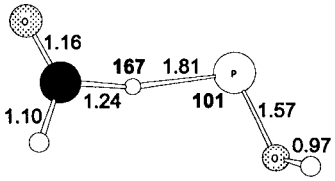

HBRC-1b (anti)

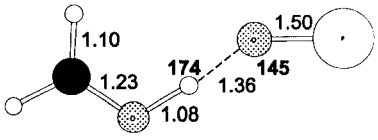

HBRC-1c

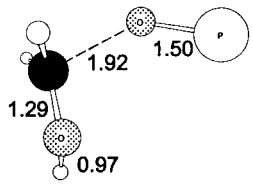

ID-1c

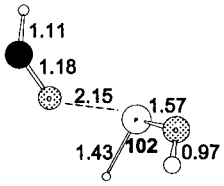

ID-1g

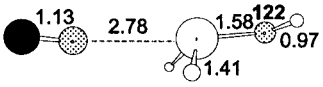

ID-2a

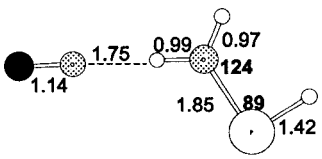

ID-2b

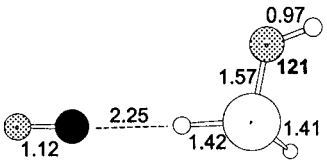

HBRC-2a

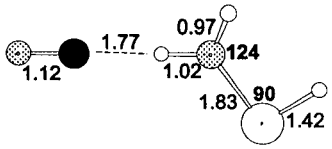

HBRC-2b

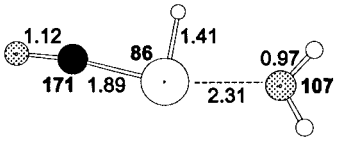

ID-3b

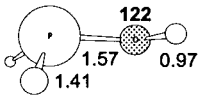

H_2P-$OH^{\bullet+}$

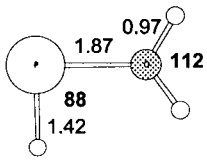

HP-$OH_2^{\bullet+}$

Fig. 4.2a. Optimized geometries of the various isomers of the CH_3O-P=$O^{\bullet+}$ ion (**1a**$^{\bullet+}$). The bond lengths (Å) and angles are presented in normal and bold font, respectively.

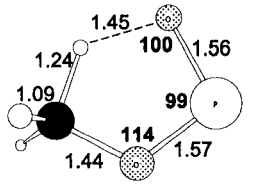

TS 1a - 1b (s/s)

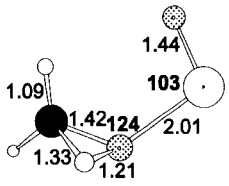

TS 1a - 1c

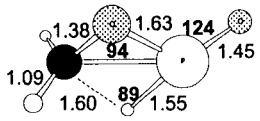

TS 1a - 1d

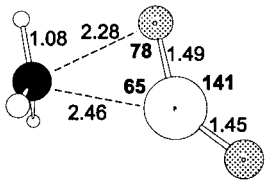

TS 1a (a) **- 1h**

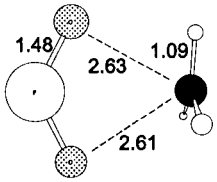

TS 1a - 1a

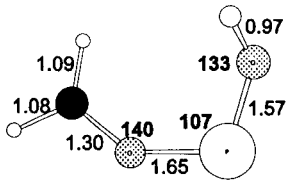

TS 1b - 1b

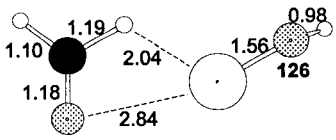

TS 1b - HBRC-1b

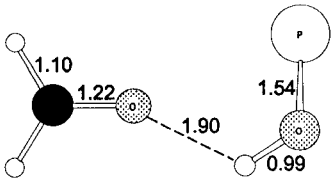

TS 1b - HBRC-1c

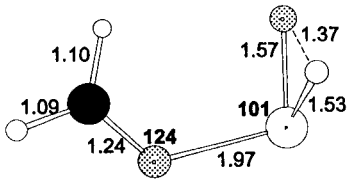

TS 1b - 1d

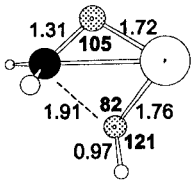

TS 1b - 1f

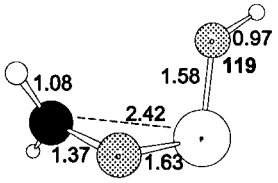

TS 1b - 1j

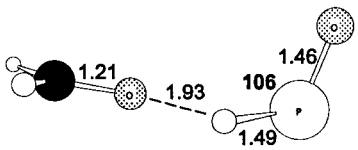

TS 1d - HBRC-1c

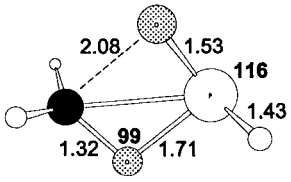

TS 1d - 1e

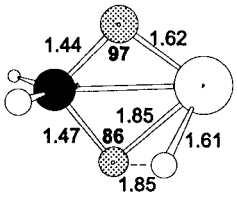

TS 1e - 1f

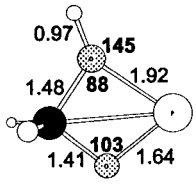

TS 1f - ID-1c

Fig. 4.2b. Optimized geometries of the transition states connecting the various isomers of the CH_3O-$P{=}O^{\bullet+}$ ion (**1a**$^{\bullet+}$). The bond lengths (Å) and angles are presented in normal and bold font, respectively.

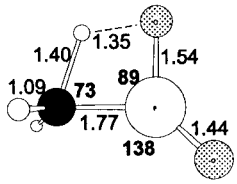

TS 1h - 1i

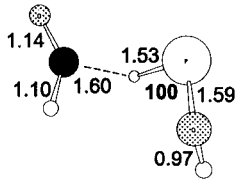

TS HBRC-1b - 1g

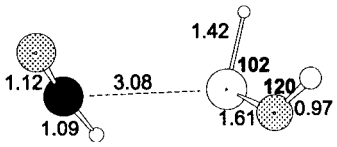

TS 1g - HBRC-2a

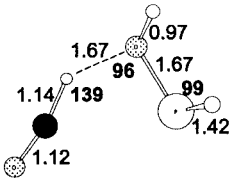

TS 1g - HBRC-2b

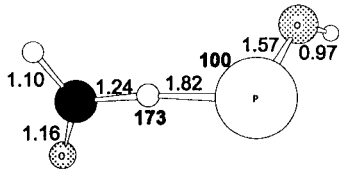

TS HBRC-1b - HBRC-1b

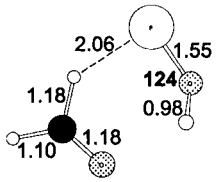

TS HBRC-1b - HBRC-1c

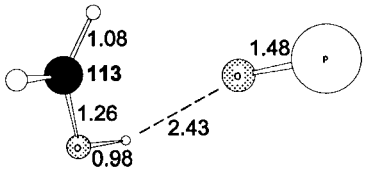

TS ID-1c - HBRC-1c

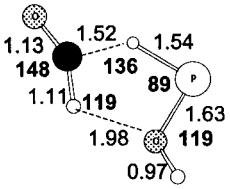

TS HBRC-1b - HBRC-2b

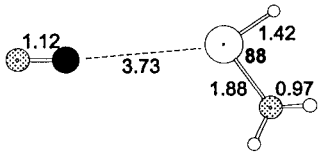

TS HBRC-2b - ID-3b

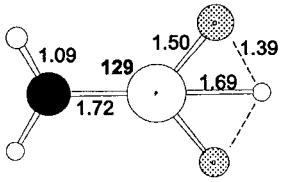

TS 1i - 1i

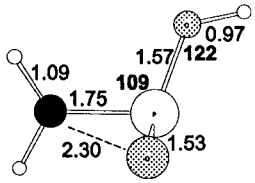

TS 1i - 1j

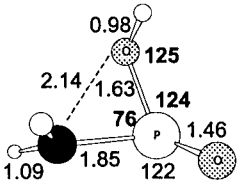

TS 1i - 1k

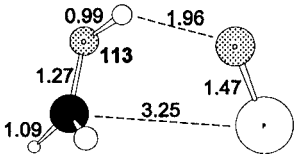

TS 1k - HBRC-1c

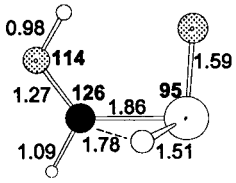

TS 1k - 1l

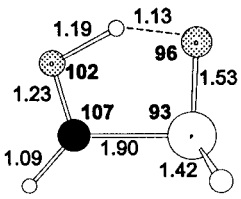

TS 1g - 1l

Fig. 4.2b. Optimized geometries of the transition states connecting the various isomers of the CH_3O-$P{=}O^{\bullet+}$ ion ($\mathbf{1a}^{\bullet+}$). The bond lengths (Å) and angles are presented in normal and bold font, respectively.

4.3. Results and discussion

4.3.1. The dissociation characteristics of ions 1a, 1b and 1i

We will begin our analysis of the results with a brief survey of the spontaneous and collision induced dissociation characteristics of the experimentally accessible $CH_3O_2P^{\bullet+}$ isomers $CH_3O\text{-}P{=}O^{\bullet+}$, **1a**, $CH_2O\text{-}P\text{-}OH^{\bullet+}$, **1b** and $CH_2{=}P(OH){=}O^{\bullet+}$, **1i**, using the energetic information presented in Tables 4.1a-c and the simplified energy diagram of Scheme 4.2a as a guide. The CID and MI spectra of the three isomeric ions and selected isotopologues are presented in Fig. 4.1.

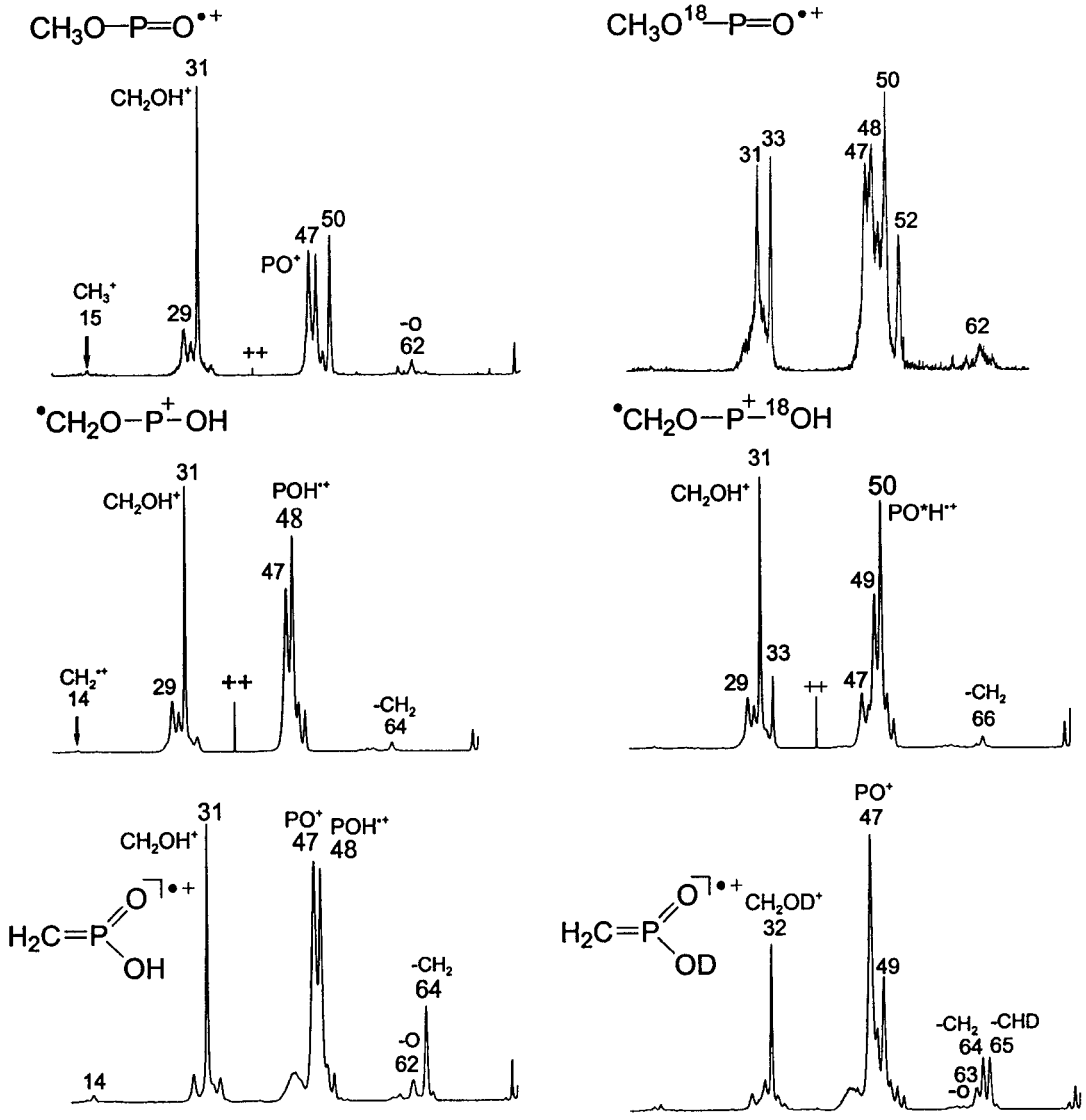

Fig. 4.1a. CID spectra of m/z 78 ions (left) **1a** (top), **1b** (middle) and **1i** (bottom) and their ^{18}O- and D- labelled isotopologues (right).

Ion **1a** was generated from $CH_3O\text{-}P(=O)Cl_2^{\bullet+}$, by the consecutive loss of two $Cl^{\bullet}$ radicals, as discussed in ref. 5, while ion **1b** was obtained from the cyclic precursor ions of Scheme 4.1, see Introduction. As seen in Scheme 4.2a, the distonic ion **1b** is more stable than its H-shift isomer of conventional structure **1a**. The two ions can communicate via a 1,4-H shift at internal energies below that required for dissociation into m/z 31 (CH_2OH^+), m/z 48 ($POH^{\bullet+}$) and m/z 47 (PO^+). These reactions dominate the CID spectra, see Fig. 4.1a, and it is therefore not surprising that these spectra are similar (the sizable peak at m/z 50 in the CID spectrum of **1a** is largely of metastable origin). Nevertheless, the CID spectra do contain tell-tale peaks, at m/z 62 and m/z 64, which attests to the structure identity of the two isomers. Analysis of the CIDI (Collision-Induced Dissociative Ionization [12]) spectrum of neutral $CH_3O\text{-}P{=}O$ [5] confirms that the high energy dissociation $CH_3O\text{-}P{=}O^{\bullet+} \rightarrow CH_3OP^{\bullet+}$ (m/z 62) + O is a characteristic feature of the CID spectrum of ion **1a**. Its H-shift isomer **1b** is characterized by another high energy process *viz.* $CH_2O\text{-}P\text{-}OH^{\bullet+} \rightarrow O{=}P\text{-}OH^{\bullet+}$ (m/z 64) + $CH_2^{\bullet\bullet}$ and also a prominent charge stripping peak at m/z 39. The MI spectra of the two isomers, see Fig. 4.1b, are dominated by loss of CO. The kinetic energy release associated with this reaction, $T_{0.5}$ = 40 meV, is the same for both isomers. This suggests that the energy requirement for the decarbonylation is higher than that for the interconversion of **1a** and **1b**. Loss of H_2O is a minor process but, especially for **1b**, dissociation into CH_2OH^+ (m/z 31) + $PO^{\bullet}$ is more pronounced. The associated small $T_{0.5}$ value (18 meV) suggests that the dissociation $CH_2O\text{-}P\text{-}OH^{\bullet+} \rightarrow CH_2OH^+ + PO^{\bullet}$ takes place at or close to the thermochemical threshold.

As shown in ref. 6, ionized methyl phosphonic acid, $CH_3\text{-}P(OH)_2{=}O^{\bullet+}$, readily loses H_2O to cleanly generate the "enol" ion $CH_2{=}P(OH){=}O^{\bullet+}$, **1i**, rather than its "keto" tautomer $CH_3\text{-}P(=O)_2^{\bullet+}$, **1h**. This is because the enol ion is much lower in energy: ion **1h** is the highest energy isomer on the $CH_3O_2P^{\bullet+}$ PES, whereas its enol counterpart represents the global minimum, see Table 4.1a and Scheme 4.2a. Ion **1h** has been identified as a stable species in a CIDI experiment of its neutral counterpart [6]. However, considering the high isomerization barriers, see Scheme 4.2a, this ion clearly plays no role in the dissociation chemistry of metastable ions **1i** and **1a/b**.

Scheme 4.2a. Potential energy diagram derived from CBS-QB3 (298 K, Table 1) calculations describing the isomerization reactions of the CH_3O_2P ions $CH_3O\text{-}P{=}O^{\bullet+}$ (**1a**), $CH_2O\text{-}P\text{-}OH^{\bullet+}$ (**1b**) and $CH_2{=}P(OH){=}O^{\bullet+}$ (**1i**). All energies, in kcal/mol, are relative to **1b.**

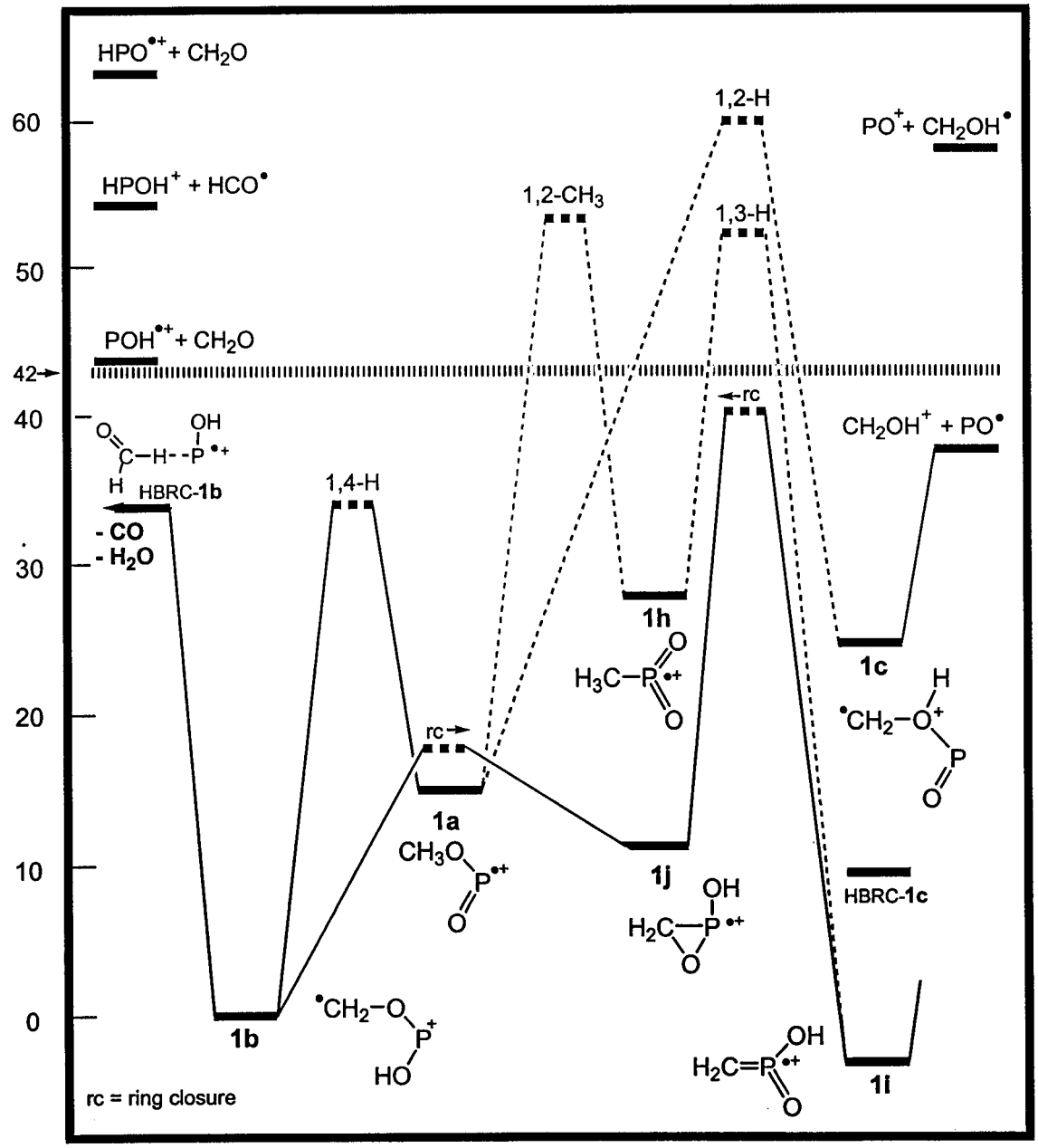

The CID spectrum of **1i**, $CH_2{=}P(OH){=}O^{\bullet+}$ displays structure characteristic peaks for the high energy losses of $CH_2^{\bullet\bullet}$ (m/z 64) and O (m/z 62). Collision experiments involving neutralization-reionization mass spectrometry [13] indicate that non-dissociating ions **1i** retain their structure identity. This too, is in agreement with the

energy diagram of Scheme 4.2a, which shows that the ions lie in a deep potential well with high barriers towards isomerization. However, upon collisional activation some isomerization does occur. It can be seen from the CID mass spectrum of **1i**-OD, see Fig. 4.1a, that the high energy loss of $CH_2^{\bullet\bullet}$ is split into losses of $CH_2^{\bullet\bullet}$ and $CHD^{\bullet\bullet}$. Thus amongst the higher energy ions communication of **1i** with **1a** is possible, see Scheme 4.2a. Fig. 4.1b shows that metastable ions **1i** are less prone to decarbonylate than **1a/b**, while loss of H_2O hardly takes place at all. The kinetic energy release for loss of CO ($T_{0.5}$ = 40 meV) is the same as that for ions **1a/b**, while that for loss of $PO^{\bullet}$ into CH_2OH^+ is smaller, $T_{0.5}$ = 10 meV. These observations indicate that, see Scheme 4.2a, that the small fraction of metastable ions **1i** that undergo decarbonylation does so by entering the potential energy surface populated by ions **1a/b**, via the energy demanding ring-closure that leads to ion **1j**. The majority of the ions generate CH_2OH^+, possibly by an extrusion reaction, at or close to the thermochemical threshold. The energy required for the degenerate 1,3-H shift of the hydroxylic hydrogen atom is high (TS **1i-1i** in Table 4.1b) which indicates that ion **1i** plays no role in the oxygen equilibration of ^{18}O labelled ions **1a/b** discussed below.

Dissociation into $CH_2OH^+ + PO^{\bullet}$ accounts for the common base peak at m/z 31 in the CID spectra of the three isomers. Metastable ions **1a**, **1b** and **1i** also undergo this rearrangement reaction, albeit to a different extent. Its calculated minimum energy requirement is only slightly lower (by 4 kcal/mol, see Table 4.1c) than that for dissociation into $POH^{\bullet+}$ (m/z 48) + CH_2=O. The latter reaction involves a simple bond cleavage in ion **1b**, requiring 43 kcal/mol of internal energy. Yet, although featuring prominently in the CID spectra, loss of CH_2=O is barely detectable in the MI spectra of all three isomers, see Fig. 4.1b. This implies that the internal energy of metastable ions **1b**, and probably also that of **1a** and **1i**, does not exceed the value represented by the hatched line that bisects the energy diagram of Scheme 4.2a at ca 42 kcal/mol. Consequently, computationally derived proposals for the isomerization and dissociation pathways of metastable ions **1a**, **1b** and **1i** must not have steps whose transition state energies lie above the hatched line in the energy diagrams of Schemes 4.2a-c. By the same token, metastable ions **1a** and **1b** cannot dissociate into $CH_2OH^+ + PO^{\bullet}$ via the

pathway **1b** → **1a** → **1c** → products, because the 1,2-H shift connecting **1a** and **1c** is prohibitively high, see Scheme 4.2a. However, ion **1c** has a low lying isomer, the hydrogen-bridged radical cation HBRC-**1c**, [$^{+}CH_2O$-H•••O=P$^{\bullet}$], whose generation from **1b** involves only a modest barrier (Table 4.1b) and which may serve as the direct precursor for the formation of CH_2OH^{+}. As we shall see in Section 4.3.3, HBRC-**1c** plays a key role in our proposed mechanism of the decarbonylation reaction.

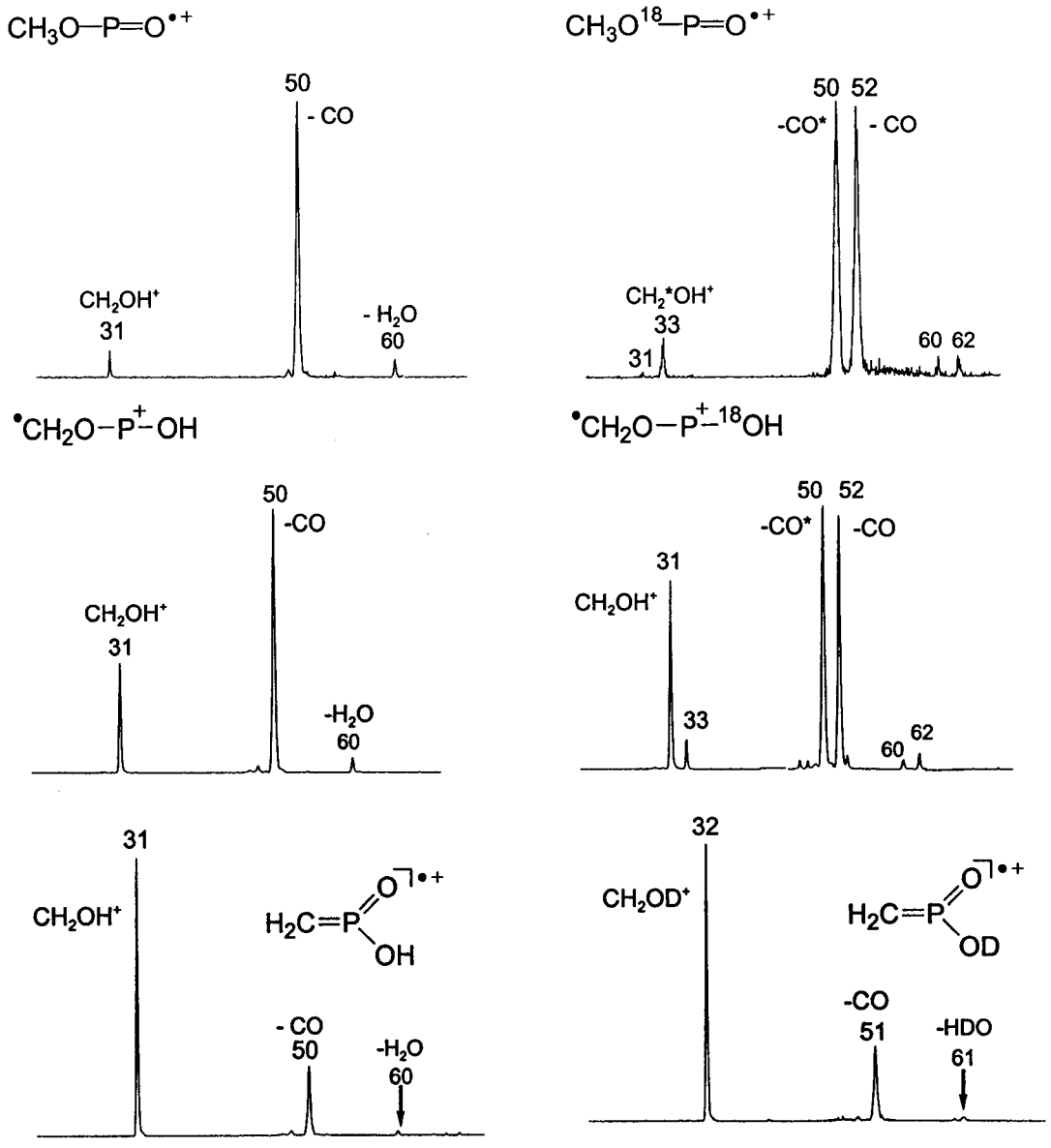

Fig. 4.1b. MI spectra of m/z 78 ions (left) **1a** (top), **1b** (middle) and **1i** (bottom) and their ^{18}O- and D- labelled isotopologues (right).

Two more points deserve to be mentioned with regard to ion **1b** :

(i) The internal energy available to metastable ions **1b** is only marginally lower than that required for formation of $POH^{\bullet+}$ by cleavage of the CH_2O—POH bond. Therefore, lengthening of this bond may well be feasible, allowing metastable ions **1b** to form ion-dipole complexes of the type $[POH^{\bullet+}\bullet\bullet\bullet O{=}CH_2]$. Internal rotations will allow these ions to adopt configurations which are best described as hydrogen-bridged radical cations. One such species, which has been calculated to lie in a shallow well, is HBRC-**1b** in Scheme 4.2a. It has an ideal configuration for H-abstraction from its CH_2=O component that could eventually lead to decarbonylation. As will be discussed in Section 4.3.3, HBRC-**1b** is indeed a key player in the decarbonylation of the metastable ions.

(ii) As stated in the Introduction, ionized ethylene phosphonate, **I**, cleanly generates ions **1b**, via the route **I** → **II** → **1b** (m/z 78) + CH_2O, as depicted in Scheme 4.1. A direct loss of CH_2O from **I** would yield ions of structure $CH_2OP(H){=}O^{\bullet+}$, **1d**, which are 19 kcal/mol higher in energy than **1b**. There is no evidence that this ion is (co)generated from **I** as the CID spectra of the source- and metastably-generated m/z 78 ions from **I** and **II** are virtually identical. However, ion **1d** could still play a role in the decarbonylation mechanism if its isomerization barriers are sufficiently low. Scheme 4.3 summarizes four potential isomerization routes for ion **1d**, and it is seen that their energies (numbers between brackets) are too high for effective communication with metastable ions **1a/b**.

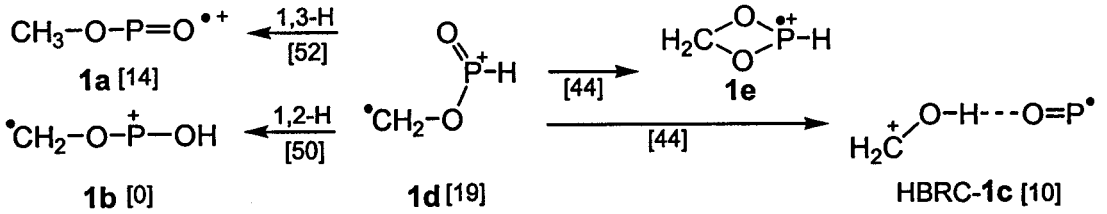

Scheme 4.3

As mentioned before, and shown in Fig. 4.1b, the ^{18}O-labelled isotopologues CH_3O^{18}-P=$O^{\bullet+}$ and CH_2O-P-$^{18}OH^{\bullet+}$ lose CO and CO^{18} in a 1:1 ratio. The positional identity of the oxygen atoms is also lost in the minor loss of H_2O, but not in the loss of $PO^{\bullet}$.

Neither of the two simple transformations depicted in Scheme 4.4 can account for the loss of positional identity of the oxygen atoms in the decarbonylation of metastable ions **1a/b**. The pathway **1a** ⇌ **1b** ⇌ **1f** is energetically feasible but the ensuing 1,2-H shift connecting the cyclic ions **1f** and **1e** is clearly too high in energy. This is also true for the degenerate 1,3-CH_3 shift in ion **1a**, although this process could account for the closely similar intensities of the m/z 31 ($CH_2{}^{16}OH^+$) and m/z 33 ($CH_2{}^{18}OH^+$) peaks in the CID spectrum of CH_3O^{18}-P=O$^{\bullet+}$.

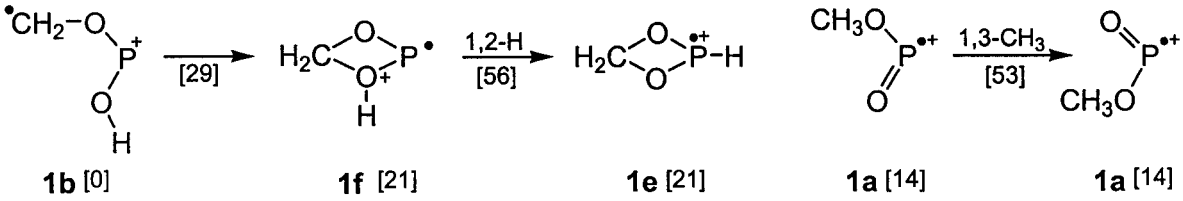

Scheme 4.4

Nevertheless, the remarkably stable cyclic ion **1f** plays a key role in a pathway that does account for the loss of the positional identity of the oxygen atoms in the decarbonylation of ions **1a/b**. This is depicted in Scheme 4.5 where the asterisk is used to indicate the position of the ^{18}O-labelled atom.

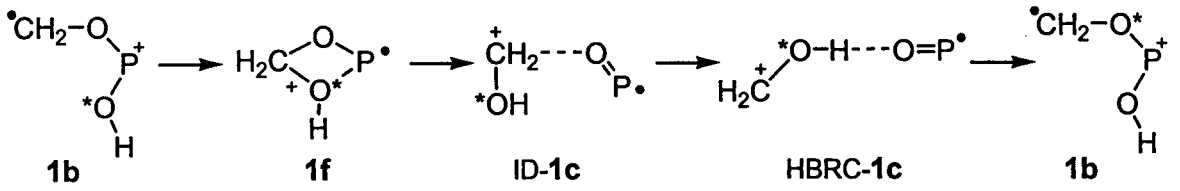

Scheme 4.5

A cursory inspection of the energy diagram of Scheme 4.2c shows that that this sequence of reactions is energetically feasible. A more detailed analysis will be presented in Section 4.3.3. In the next section we will first examine the evidence for the structure of the product ion generated in the decarbonylation reaction and also the accompanying minor loss of water.

4.3.2. The identification of the product ions of the decarbonylation and the H_2O loss

The decarbonylation process generates m/z 50 ions of putative structure H_2P-$OH^{\bullet+}$ or H-P-$OH_2^{\bullet+}$. The calculated energy levels depicted in Scheme 4.2c indicate that both product ions could in principle be generated. The ylide ion H-P-$OH_2^{\bullet+}$ is 10 kcal/mol less stable than its conventional isomer H_2P-$OH^{\bullet+}$ but the two ions cannot easily interconvert : the calculated barrier for the appropriate 1,2-H shift is high, 51 kcal/mol.

The CID spectra of the m/z 50 ions generated from metastable ions **1a**, **1b** and **1i** are virtually identical, and a representative spectrum is presented in Fig. 4.3a. This spectrum displays a prominent peak at m/z 32 for loss of H_2O, but there is no peak at m/z 33 for loss of $OH^{\bullet}$. This suggests that we are dealing with the ylide ion H-P-$OH_2^{\bullet+}$ rather than H_2P-$OH^{\bullet+}$. The latter isomer could be generated independently from ionized methyl phosphinate, **IV**, by the route depicted in Scheme 4.6 :

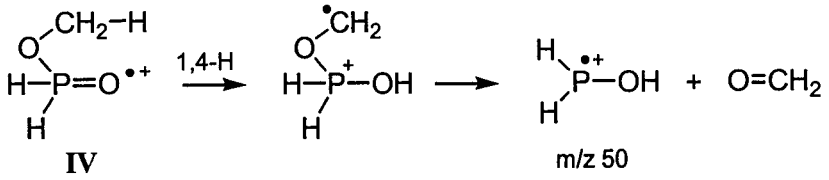

Scheme 4.6

The CID spectrum of the so generated m/z 50 ions, see Fig. 4.3b, shows a prominent tell-tale peak at m/z 33 (loss of $OH^{\bullet}$) and even a weak m/z 17 (OH^{+}) ion, indicative of the H_2P-$OH^{\bullet+}$ structure. This supports our proposal that the decarbonylation of the three isomers results in the formation of the ylide ion H-P-$OH_2^{\bullet+}$. It can also be seen that the conventional isomer shows an intense and characteristically narrow peak for the formation of the doubly charged species H_2P-OH^{++}, while that for the ylide ion H-P-OH_2^{++} is relatively weak, the opposite of what is usually encountered [14].

The minor H_2O loss from the metastable ions yields m/z 60 ions of structure H-P=C=$O^{\bullet+}$. The calculations predict that among the family of stable [C/H/P/O] ions, only H-P=C=$O^{\bullet+}$ is sufficiently low in energy to be generated from the metastable ions, see Scheme 4.2c and Table 4.1c. Confirmation of the proposed ion structure comes from the

CID spectrum of the m/z 60 ions generated from the metastable m/z 78 ions. The spectrum (not shown) displays fairly intense structure characteristic peaks at m/z 28 and m/z 32 corresponding to $CO^{\bullet+}$ and $HP^{\bullet+}$, agreeing with the proposed $HPCO^{\bullet+}$ ion structure.

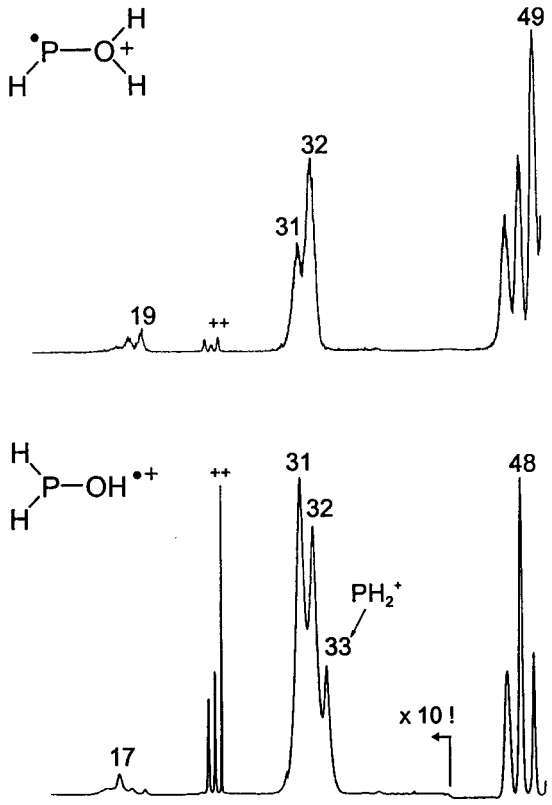

Fig. 4.3. CID spectra of m/z 50 ions generated from : metastable ions **1b** (top) and ionized methyl phosphonic acid (bottom).

4.3.3. Mechanistic proposals for the decarbonylation of the CH_3O-P=$O^{\bullet+}$ and CH_2O-P-$OH^{\bullet+}$ ions and mechanism for the oxygen exchange reaction

Mechanism for decarbonylation

As indicated in Scheme 4.2b, HBRC-**1b** is accessible from ions **1b** having ≥ 35 kcal/mol of internal energy. At this energy, HBRC-**1b** can communicate with HBRC-**2b**, which may dissociate into H-P-$OH_2^{\bullet+}$ and CO by direct bond cleavage. Alternatively, ions HBRC-**1b** with a slightly lower internal energy, 32 kcal/mol, can be formed from

HBRC-**1c** via a proton transfer. Such ions can access HBRC-**2b** with 34 kcal/mol of internal energy relative to **1b**. Thus, the calculated minimum energy requirement for the observed decarbonylation into the ylide ion $HPOH_2^{\bullet+}$ is 34 kcal/mol.

Scheme 4.2b. Potential energy diagram derived from CBS-QB3 (298 K, Table 1) calculations describing the decarbonylation and water loss from metastable ions $CH_2O\text{-}P\text{-}OH^{\bullet+}$, **1b**, and related isomers.

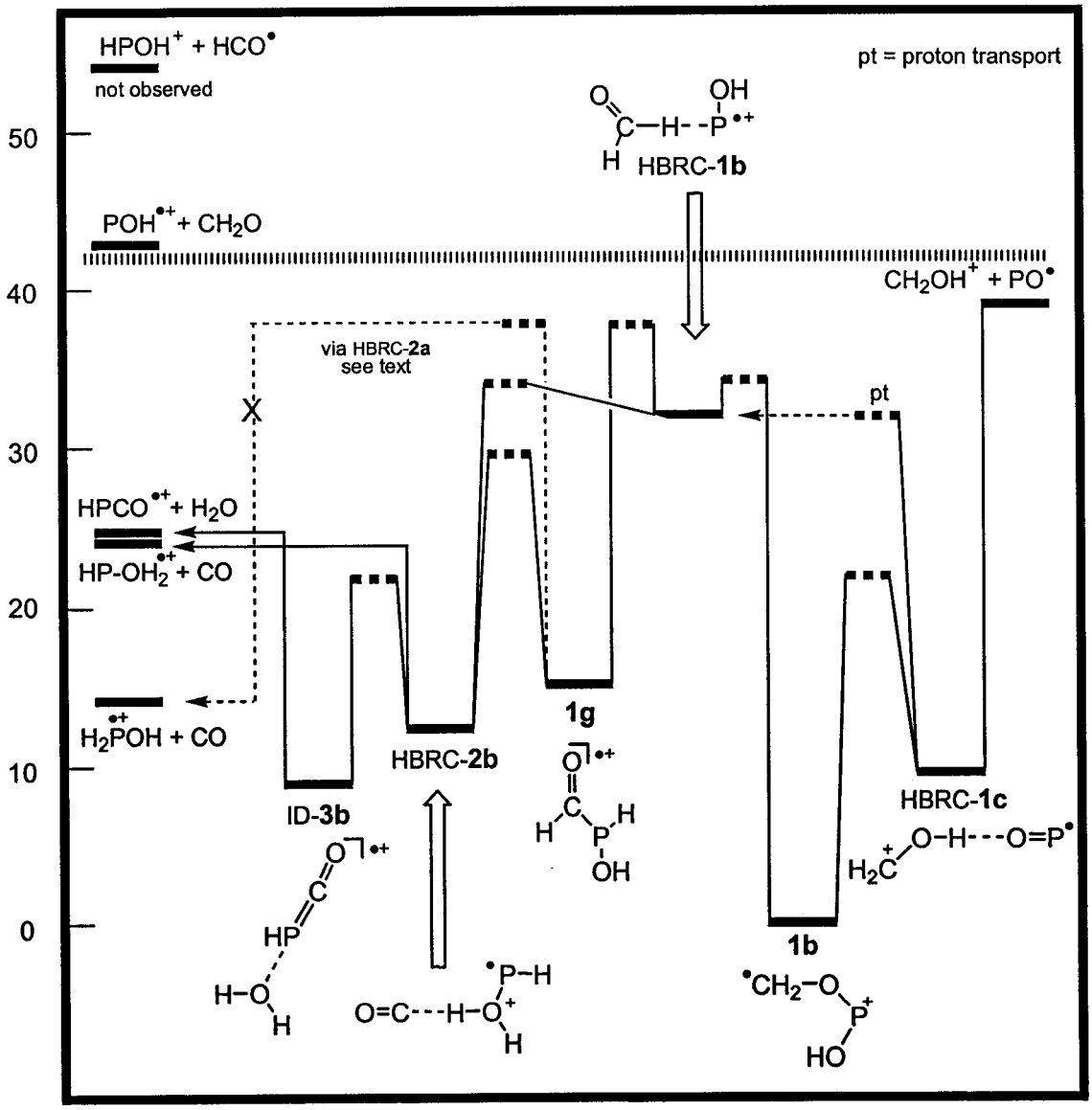

Our experiments show that the lower energy isomer $H_2P\text{-}OH^{\bullet+}$ is not formed as a result of decarbonylation. Theory indicates that this is so because the formation of the

immediate precursor to $H_2P\text{-}OH^{\bullet+}$, *viz.* HBRC-**2a**, HO-P(H)-$H^{\bullet+}$•••C=O, which is 2 kcal/mol lower in energy than HBRC-**2b**, is energetically unfavourable. HBRC-**1b** cannot directly communicate with HBRC-**2a** : it must first isomerize into the relatively stable ion **1g**, H-C(=O)P(H)-$OH^{\bullet+}$, which involves a barrier of 5 kcal/mol, or 38 kcal/mol relative to **1b**. (There is also an ion-dipole complex of **1g**, [HO-PH^+]•••O=$CH^\bullet$, which, see Table 4.1a, lies 17.5 kcal/mol above **1g**.) This barrier is of the same height as that for the subsequent isomerization of **1g** into HBRC-**2a**. However, metastable ions **1b** having more than 38 kcal/mol of internal energy can also dissociate via the route **1b** → HBRC-**1c** → $CH_2OH^+ + PO^\bullet$. This clearly is a fast rearrangement reaction – it effectively competes with direct bond cleavage into $POH^{\bullet+}$ in collisionally energized ions **1b** – which discriminates against the slow multi-step decarbonylation route.

The HBRC-**2b** ion is the direct precursor for loss of CO and a key intermediate for the H_2O loss. Cleavage of the weak C•••H bond in HBRC-**2b** results in the formation of $HP\text{-}OH_2^{\bullet+}$ + CO. Just below the threshold for decarbonylation, see Scheme 4.2b, HBRC-**2b** can also rearrange into ID-**3b**, O=C=$PH^{\bullet+}$•••OH_2, which can dissociate into $HP{=}C{=}O^{\bullet+}$ + H_2O by simple cleavage. The minimum energy requirement for this reaction is very close to that of the decarbonylation reaction. However, loss of H_2O requires formation of two new covalent bonds in the loosely bound ion-dipole complex HBRC-**2b** to form the ion-dipole complex ID-**3b** and so "hot" HBRC-**2b** ions, having about 14 kcal/mol excess energy will preferentially undergo a simple cleavage reaction, i.e. loss of CO. Furthermore, as the dipole moment of CO is very small, it is not surprising that the complex prefers dissociation over rearrangement. These matters explain that compared to loss of CO, the loss of H_2O is a minor process in the dissociation of metastable ions.

One important point should be considered regarding HBRC-**2b**, H-P-O(H)-$H^{\bullet+}$•••CO. This ion can be considered as an encounter complex between a $HP\text{-}OH_2^{\bullet+}$ ion and a CO molecule. In such an encounter complex the neutral molecule may promote the tautomerization of the ionic component by lowering the barrier for the associated H-transfer. This phenomenon, termed proton-transport catalysis by Böhme [15], has been demonstrated in several ionic systems [1]. For example, the isomerization of $HCN^{\bullet+}$ into

its more stable $HNC^{\bullet+}$ tautomer does not occur spontaneously because the barrier for the associated 1,2-H shift is too high, 27 kcal/mol. However, in the presence of CO, the tautomerization readily takes place in the encounter complex, via : $CO + HCN^{\bullet+} \rightarrow OC{\bullet\bullet}H^{+}{\bullet\bullet}[C{\equiv}N]^{\bullet} \rightarrow [C{\equiv}N]^{\bullet}{\bullet\bullet}H^{+}{\bullet\bullet}CO \rightarrow HNC^{\bullet+} + CO$, and the barrier becomes vanishingly small. This system satisfies the criterion proposed by Radom and co-workers [1a] for effective proton-transport catalysis. It stipulates that the proton affinity (PA) of the neutral molecule in the encounter complex (PA CO at C) must lie in between those of the two protonation sites in the deprotonated ion (PA $CN^{\bullet}$ at C and N respectively).

By analogy, the CO molecule in HBRC-**2b** could promote the tautomerization of $HP\text{-}OH_2^{\bullet+}$ into $H_2P\text{-}OH^{\bullet+}$, via $[HP\text{-}OH]^{\bullet}{\bullet\bullet}H^{+}{\bullet\bullet}CO$ (HBRC-**2b**) $\rightarrow OC{\bullet\bullet}H^{+}{\bullet\bullet}[HP\text{-}OH]^{\bullet}$ (HBRC-**2a**) $\rightarrow H_2P\text{-}OH^{\bullet+} + CO$, if the criterion for proton-transport catalysis is satisfied. This implies that PA CO at C, 142 kcal/mol [16a], be in between PA $HP\text{-}OH^{\bullet}$ at O and PA $HP\text{-}OH^{\bullet}$ at P. From the enthalpies of formation of $HP\text{-}OH^{\bullet}$, $H_2P\text{-}OH^{\bullet+}$ and $HP\text{-}OH_2^{\bullet+}$ (-24.7, 162.7 and 172.5 kcal/mol respectively [16b]), we derive PA $HP\text{-}OH^{\bullet}$ at O = 168 kcal/mol and PA $HP\text{-}OH^{\bullet}$ at P = 178 kcal/mol. These PA values are much higher than that of CO and thus a CO assisted tautomerization of $HP\text{-}OH_2^{\bullet+}$ is not expected to occur, in agreement with the experimental observations, which indicate that the ylide ion is exclusively generated.

Finally, we mention that the observed collision characteristics of the various isomeric ions are in complete agreement with the energy diagram presented in Scheme 4.2b. If we compare the MI and CID mass spectra (Fig. 4.1b and Fig. 4.1a) of for example **1a**, we see that loss of CO is insensitive towards collision. For a metastable fragmentation to be collision insensitive, the precursor ion must rearrange to a stable isomer via a transition state whose energy is higher than the dissociation threshold of the new isomer [17], exactly as is the case in Scheme 4.2b.

Oxygen equilibration reactions

The above decarbonylation process becomes even more remarkable when the ^{18}O-labelling results are considered. The MI spectrum of **1a**($^{18}OCH_3$) in Fig. 4.1b displays a 1:1 ratio for the loss of $C^{18}O$: $C^{16}O$ resulting in H-P-$^{16}OH_2^{\bullet+}$ and H-P-$^{18}OH_2^{\bullet+}$ of equal abundance. The same isotopic ratio is observed in the water loss products at m/z 60 and 62. On the other hand, there is a distinct, almost isotopically pure, loss of $P^{16}O^{\bullet}$ to form $CH_2{}^{18}OH^+$ at m/z 33. This indicates that the water loss and decarbonylation result from the same reacting ion, whereas the $PO^{\bullet}$ loss must occur from a different intermediate prior to oxygen equilibration. These results are supported by the ^{18}O-labelling experiments with **1b**($P^{18}OH$). This ion also loses $C^{16}O$: $C^{18}O$ in a 1:1 ratio. The mirror effect for the $PO^{\bullet}$ loss is observed, in that now $P^{18}O^{\bullet}$ is predominantly lost, again indicating that this fragmentation occurs from a different reacting ion configuration. Interestingly, the oxygen equilibration is only observed in the low-energy metastable ions **1b**($P^{18}OH$), see Fig. 4.1b, as opposed to the collisionally energized ions which do not show oxygen equilibration. *This indicates that the oxygen equilibration is a slow process with a fairly high energy requirement.*

Oxygen equilibration must involve a cyclic intermediate, which could be generated directly from either **1b** or **1d**, since these two ions have a methylene group available for bonding to an oxygen atom. Cyclization of **1d** would result in the symmetric ion **1e**, see Scheme 4.3, thus making the equilibration a simple ring closure - ring opening procedure. Ring opening of the original C-O bond results in ion **1d** with the oxygen atoms in reversed positions. However, as mentioned in Section 4.3.1, ion **1d** does not communicate with metastable ions **1a/b**. Furthermore, ion **1a**, which also displays the oxygen equilibration, communicates with **1b** and not **1d**. This signifies that ion **1d** is not involved in the oxygen equilibration. Thus, it must be the cyclization of ion **1b** into ion **1f** which results in the oxygen atom equilibration. This is the rate-limiting step as the barrier to ring closure of ion **1b** lies 30 kcal/mol above ion **1b**. At this energy the ions (now in the **1f** configuration) can communicate easily with ID-**1c**, which in turn can easily isomerize into HBRC-**1c** below the threshold for dissociation into CH_2OH^+ and $PO^{\bullet}$, see Scheme 4.2c. Thus, the equilibration can be described as

depicted in Scheme 4.5, *viz.* **1b**(^{18}OH) → **1f**(^{18}OH) → ID-**1c**(^{18}OH)→ HBRC-**1c**($^{18}OCH_2$) → **1b**($^{18}OCH_2$). This enables the oxygen atom equilibration to occur in the lower energy ions below the threshold for loss of PO$^{\bullet}$. No significant equilibration occurs for those ions that do lose PO$^{\bullet}$ as these higher energy metastable ions (ions **1b** with ca. 40 kcal/mol of internal energy) can communicate with HBRC-**1c** directly and will simply undergo the fast dissociation as opposed to passing through the slow equilibration process. Only the lower internal energy ions access the decarbonylation process with an internal energy content of 30 to 40 kcal/mol above **1b**.

Scheme 4.2c. Potential energy diagram derived from CBS-QB3 (298 K, Table 1) calculations describing the isomerization reactions of metastable ions $[CH_2O\text{-}P\text{-}OH]^{\bullet+}$ which may lead to the oxygen equilibration prior to decarbonylation and loss of water.

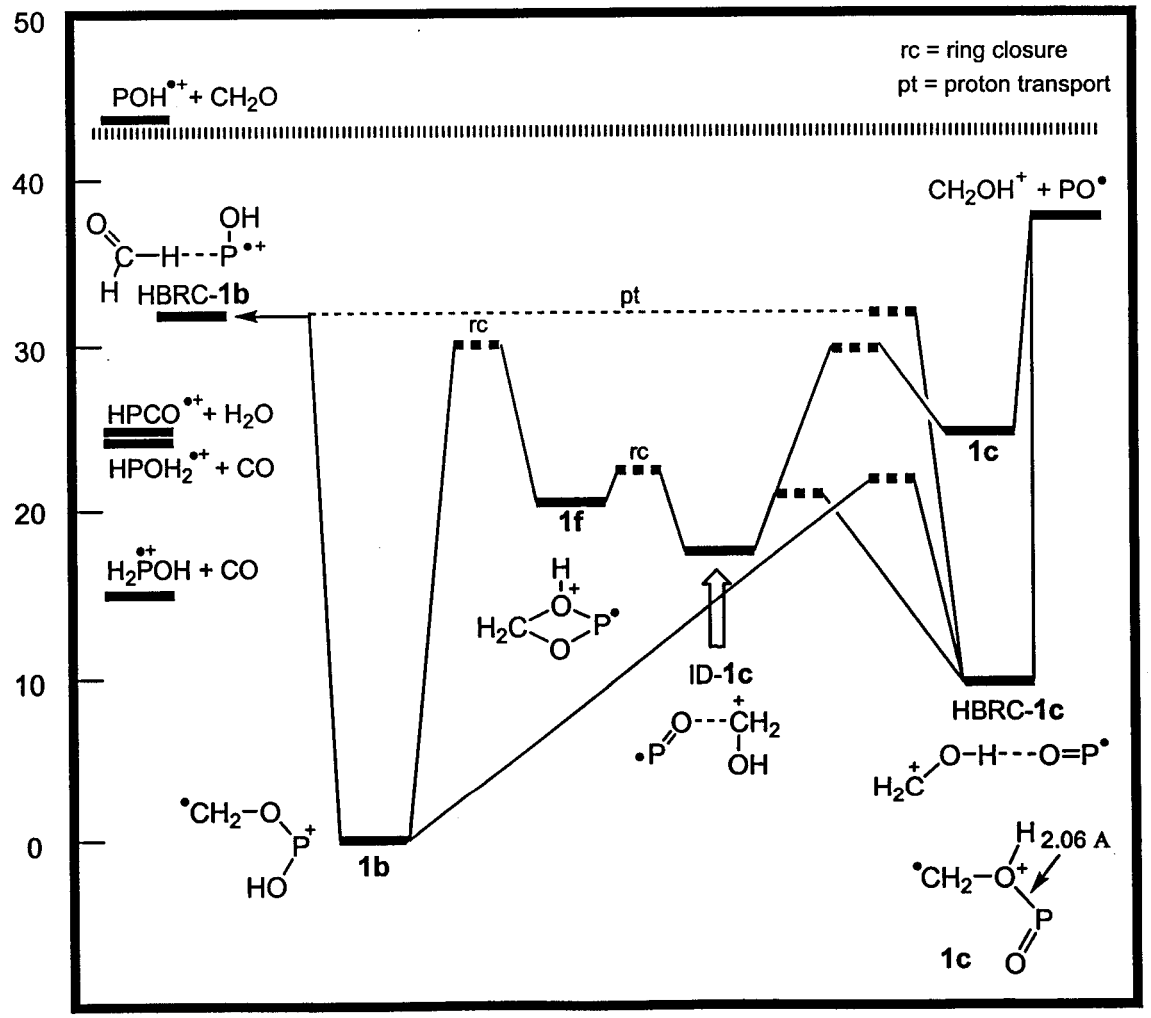

Scheme 4.7 summarizes our results for the decarbonylation reactions starting from **1a**. Oxygen equilibration reactions are denoted as ↔, whereas the reactions that lead to decarbonylation follow the arrows →.

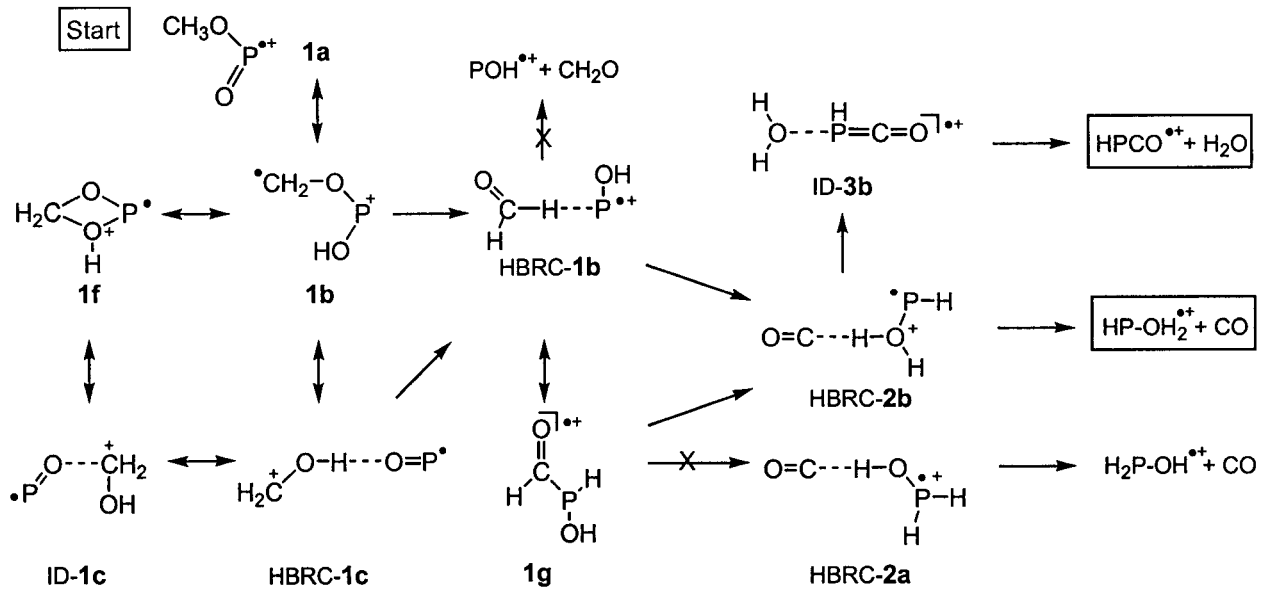

Scheme 4.7. Mechanism for decarbonylation (→) and for oxygen equilibration (↔) starting from **1a**.

4.4. Conclusions

This study truly benefited from the synergy of theory and experiment. One without the other would not have permitted to draw any solid mechanistic conclusion. That the oxygen atoms in metastable ions $CH_3O\text{-}P{=}O^{\bullet+}$ and $CH_2O\text{-}P\text{-}OH^{\bullet+}$ become equivalent in the decarbonylation and the accompanying H_2O loss was revealed by experiments on specifically labelled ions. Theory was used to differentiate between a priori plausible mechanisms for this equilibration. The CBS-QB3 calculations further revealed that metastable ions $CH_3O\text{-}P{=}O^{\bullet+}$ and $CH_2O\text{-}P\text{-}OH^{\bullet+}$ have a high propensity for rearrangement and that they can communicate with a great many stable isomers. The tandem mass spectrometry based experiments established that the product ion generated in the decarbonylation is the ylide ion $HP\text{-}OH_2^{\bullet+}$, rather than $H_2P\text{-}OH^{\bullet+}$, which theory predicts to be the more stable isomer. The intricate details of the decarbonylation

mechanism were revealed by theory, which indicates that $CH_2O\text{-}P\text{-}OH^{\bullet+}$ ions having a narrow range of internal energies at 36 kcal/mol, undergo a facile isomerization into the hydrogen-bridged ion [HO-$P^{\bullet+}$•••H-C(H)=O], which further rearranges into another hydrogen-bridged radical cation, [HP-O(H)-$H^{\bullet+}$•••C=O], the immediate precursor for decarbonylation into $HP\text{-}OH_2^{\bullet+}$.

References:

[1] For selected recent references see : (a) A.J. Chalk, L. Radom, J. Am. Chem. Soc. 121 (1999) 1574; (b) J. Chamot-Rooke, G. van der Rest, P. Mourgues, H.-E.Audier, Int. J. Mass Spectrom. 195/196 (2000) 385 ; (c) M.A. Trikoupis, P.C. Burgers, P.J.A. Ruttink, J.K. Terlouw, Int. J. Mass Spectrom. 217 (2002) 97; (d) M. Haranczyk, P.C. Burgers, P.J.A. Ruttink, Int. J. Mass Spectrom. 220 (2002) 53

[2] L.N. Heydorn, Y. Ling, G. de Oliveira, J.M.L. Martin, Ch. Lifshitz , J.K. Terlouw, Zeitschrift für Physikalische Chemie 215 (2001) 141.

[3] (a) J.A. Montgomery Jr, M.J. Frisch, J.W. Ochterski, G.A. Petersson, J. Chem. Phys. 110 (1999) 2822; (b) ibid. 112 (2000) 6532.

[4] L.N. Heydorn, P.C. Burgers, P.J.A. Ruttink, J.K. Terlouw, Int. J. Mass Spectrom. (2003) in press.

[5] L.N. Heydorn, C.Y. Wong, R. Srinivas, J.K. Terlouw, Int. J. Mass Spectrom. 225 (2003) 11.

[6] L.N. Heydorn, P.C. Burgers, P.J.A. Ruttink, J.K. Terlouw, Chem. Phys. Lett. 368 (2003) 584.

[7] D.G. Hewitt, Aust. J. Chem. 32 (1979) 463.

[8] S.J. Fitch, J. Am. Chem. Soc. 86 (1964) 61.

[9] H.F. van Garderen, , P.J.A. Ruttink, P.C. Burgers, G.A. McGibbon, J.K. Terlouw, Int. J. Mass Spectrom. Ion Proc. 121 (1992) 159.

[10] J.L. Holmes, J.K. Terlouw, Org. Mass Spectrom. 15 (1980) 383.

[11] M.J. Frisch et al., Gaussian 98, Revision A.9, Gaussian, Inc.: Pittsburgh, PA, 1998.

[12] (a) J.K. Terlouw and H. Schwarz, Angew. Chem. Int. Ed. Engl. 26 (1987) 805; (b) M.A. Trikoupis, J.K. Terlouw, P.C. Burgers, M. Peres and C. Lifshitz, J. Am. Soc. Mass Spectrom. 10 (1999) 869.

[13] For selected recent reviews see: (a) G. Schalley, G. Hornung, D. Schröder and H. Schwarz, Chem. Soc. Rev. 27 (1998) 91; (b) N. Goldberg and H. Schwarz, Acc. Chem. Res. 27 (1994) 34.

[14] J.L. Holmes, F.P. Lossing, J.K. Terlouw, P.C. Burgers, J. Am. Chem. Soc. 104 (1982) 2931

[15] D.K. Böhme, Int. J. Mass Spectrom. Ion Proc. 115 (1992) 95

[16] (a) E.P. Hunter, S.G. Lias, J. Phys. Chem. Ref. Data 27 (1998) 41 ;(b) CBS-QB3 (298 K) values, this work.

[17] Y-P. Tu and J.L. Holmes, J. Am. Chem. Soc. 122 (2000) 3695.

Chapter 5

The isobaric ions $CH_3O\text{-}P{=}O^{\bullet+}$ and $CH_3O\text{-}P\text{-}NH_2^+$ and their neutral counterparts: a tandem mass spectrometry and CBS-QB3 computational study

In contrast to a previous report *(Int. J. Mass Spectrom. 171 (1997) 79),* the dissociative electron ionization of acephate does not generate pure m/z 78 ions $CH_3O\text{-}P{=}O^{\bullet+}$. By combining the results of exact mass measurements, (multiple) high energy collision experiments and CBS-QB3 calculations, it is concluded that the m/z 78 ions consist of $CH_3O\text{-}P{=}O^{\bullet+}$ and $CH_2O\text{-}P\text{-}OH^{\bullet+}$ in admixture with isobaric CH_5PON^+ ions. A computational analysis of the dissociation characteristics of the independently generated stable isomers $CH_3O\text{-}P\text{-}NH_2^+$ and $CH_3P(=O)NH_2^+$ shows that the CH_5PON^+ ions from acephate have the structure $CH_3O\text{-}P\text{-}NH_2^+$. As a consequence, the recovery signal in the reported neutralization-reionization (NR) spectrum of acephate's m/z 78 ions does not prove the stability of the $CH_3O\text{-}P{=}O$ neutral. Definitive evidence for its existence as a stable species in the dilute gas phase comes from a collision induced dissociative ionization (CIDI) experiment on the reaction $C_6H_5\text{-}P(=O)OCH_3^+ \rightarrow C_6H_5^+ + CH_3O\text{-}P{=}O$. The calculations indicate that $CH_3O\text{-}P\text{-}NH_2^{\bullet}$ is also a stable species, but attempts to confirm this by experiment have not yet been successful.

The work described here has been published previously in an article under the same title :
L.N. Heydorn, C.Y. Wong, R. Srinivas and J.K. Terlouw, Int. J. Mass Spectrom. **225** (2003) 11.

5.1. Introduction

Neutralization-reionization mass spectrometry (NRMS) has been established as a powerful tool to probe the structure (atom connectivity) and stability of elusive and often highly reactive molecules or radicals in the rarefied gas phase [1]. However, the technique is not without its pitfalls, particularly when the NR experiment involves a weak secondary or tertiary fragment ion in the electron impact mass spectrum of a precursor molecule containing several heteroatoms. In such a case, it is important to check whether the beam of ions to be neutralized contains isobaric and/or isomeric impurities that may compromise the interpretation of the experimental findings. The NR efficiencies of a given set of isobaric or isomeric ions can differ by several orders of magnitude and thus the mere presence of a recovery signal in a NR spectrum does not necessarily attest to the stability of the neutral counterpart of the major ionic component of the neutralized ion beam. The presence of isobaric impurities may be probed by a high resolution experiment but the isomeric purity of a given beam of ions is more difficult to establish. One approach involves selectively transmitting the beam of "survivor" ions represented by the recovery signal to a collision gas chamber to obtain its collision induced dissociation (CID) spectrum [1b]. Comparison of the resulting CID/NR spectrum (which can only be obtained if the recovery signal is sufficiently intense) with the CID spectrum of the source generated ions provides important information on the purity of the initial ion beam. Such an experiment also addresses the question of whether the incipient neutral has retained its structure identity [2]. For many systems of ions, a conclusive analysis of the NR results requires a detailed knowledge of the energy requirements of the potential isomerization and dissociation reactions of both the ion and its neutral counterpart. The use of state-of-the-art computational chemistry, particularly the Gaussian and CBS model chemistries [3], is indispensable in this context. An elegant example of the important role of computational chemistry is the recent NR study of the bi-coordinated dihydroxyphosphenium ion, $P(OH)_2^+$ [4].

Many other O- and/or S-containing low coordinated phosphorus ions have been studied by the NR technique [4], including the m/z 78 ion $CH_3O\text{-}P{=}O^{\bullet+}$, (methoxy)oxo-phosphane [5]. The m/z 78 ions of this study were obtained by the dissociative

ionization of the insecticide acephate [6], which was proposed to yield pure ions CH_3O-$P{=}O^{\bullet+}$ via the sequential losses of $CH_3S^{\bullet}$ and $CH_3C(=O)NH^{\bullet}$, as depicted in Scheme 5.1.

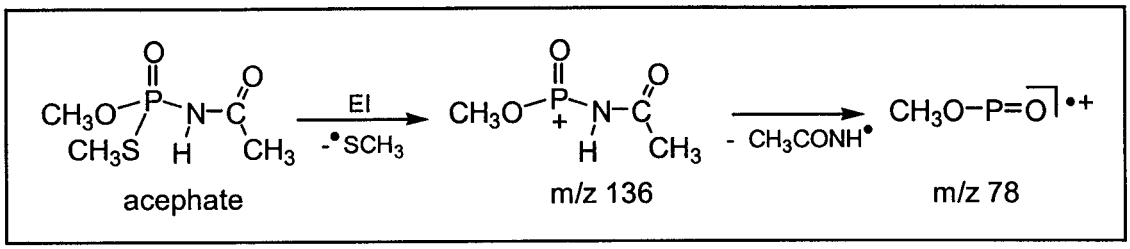

Scheme 5.1

The CID spectrum of these m/z 78 ions displays a prominent peak at m/z 46, which was attributed to a rearrangement reaction involving the unusual loss of an O_2 molecule: CH_3O-$P{=}O^{\bullet+} \rightarrow CH_3P^{\bullet+}$ (m/z 46) + O_2. This interpretation seemed to be at odds with findings from our study of the intriguing decarbonylation reaction of some ten key isomers of the family of $CH_3PO_2^{\bullet+}$ ions, including the CH_3O-$P{=}O^{\bullet+}$ ion [7]. Experiment and theory [7] (CBS-QB3 calculations, see Experimental) agree that CH_3O-$P{=}O^{\bullet+}$ can readily communicate with its more stable distonic isomer CH_2O-P-$OH^{\bullet+}$. The latter ion can readily be obtained by the dissociative ionization of ethylene phosphonate or ethylene phosphite [8]. Its CID spectrum is closely similar but not identical to that of the m/z 78 ions of putative structure CH_3O-$P{=}O^{\bullet+}$, which we had generated by the dissociative ionization of CH_3O-$P(=O)Br_2$ and CH_3O-$P(=O)Cl_2$. The spectra of the two isomers are dominated by peaks at m/z 31 (CH_2OH^+), 47 (PO^+), and 48 ($POH^{\bullet+}$) but a signal at m/z 46 was conspicuously absent. This prompted us to reexamine the structure and origin of the m/z 78 ions generated from acephate. The m/z 78 ions generated from its analogue methamidophos, $CH_3S(CH_3O)P(=O)NH_2$, (a hydrolysis product of acephate [6]) were also examined.

Results from exact mass measurements, (multiple) collision experiments, and CBS-QB3 calculations will be presented to show that the m/z 78 ions generated by acephate consist of the $CH_3PO_2^{\bullet+}$ isomers CH_3O-$P{=}O^{\bullet+}$ and CH_2O-P-$OH^{\bullet+}$, in admixture with the CH_5PON^+ isomer CH_3O-P-NH_2^+. For methamidophos, the latter ion is the principal component. Its NR spectrum displays an intense recovery signal. As a

consequence, the recovery signal in the reported NR spectrum of acephate cannot be used to prove the stability of the CH_3O-P=O neutral. Definitive evidence for its existence as a stable species in the gas phase comes from a collision induced dissociative ionization CIDI [9] experiment on methyl phenylphosphinate, C_6H_5-P(=O)(H)OCH_3.

5.2. Experimental and theoretical methods

5.2.1. Sample preparation procedures

Acephate ($CH_3S(CH_3O)P(=O)N(H)C(=O)CH_3$, O,S-dimethyl acetylphosphoramidothioate) and methamidophos ($CH_3S(CH_3O)P(=O)NH_2$, O,S-dimethylphosphoramidothiolate), were of research grade and obtained from Sigma-Aldrich. The deuterium isotopologue $CH_3S(CH_3O)P(=O)ND_2$ was obtained by exchange of the acidic hydrogens with D_2O.

Methyl dichlorophosphate (CH_3O-P(=O)Cl_2) was obtained from Aldrich. A small sample of its thermally labile dibromo analogue was prepared as described in reference 10a. The labelled isotopologues, $CH_3^{\bullet}O$-P(=O)Cl_2 and CD_3O-P(=O)Cl_2 were synthesized by methanolysis of trichlorophosphate [10b]. Ethylene phosphonate (1,3,2-dioxaphospholane, 2-oxide) and ethyl ethylene phosphite were obtained as described in reference 8. Methyl phenylphosphinate (C_6H_5-P(=O)(H)OCH_3) was obtained by the reaction of phenylphosphinic acid (Aldrich) with methylchloroformate [10b].

Methylphosphonamidic chloride ($CH_3P(=O)NH_2Cl$) was obtained from the reaction of two equivalents of gaseous ammonia with methylphosphonic dichloride (Aldrich) in diethylether, following the general procedure described in reference 10c/d.

5.2.2. Mass spectrometry

The Micromass GC-T time-of-flight mass spectrometer was used to obtain 70 eV EI mass spectra at its standard mass resolution of 4000-6000 (50% valley definition) at m/z 69 of the reference compound 2,4,6-tris(trifluoromethyl)-1,3,5-triazine. The spectra were obtained in the continuous mode which allows an off-line examination of the shape(s) of the signals at each and every nominal mass in the EI spectrum. In the assignment of an elemental composition, all combinations of C/H/N/O/P/S were

considered whose calculated mass deviated by not more than 10 mDa from the measured mass. However, unless stated otherwise, the reported elemental compositions deviated by less than 1 mDa. The acephate and methamidophos samples were introduced via the solids probe in microgram quantities so as to obtain complete evaporation profiles. In these experiments the probe was kept at room temperature and the ion source at c. 100°C.

The tandem mass spectrometry based experiments were performed with the VG Analytical ZAB-R mass spectrometer, a three-sector BE_1E_2 (B = magnetic sector, E = electric sector) type instrument [11].

The compounds were introduced into the ion source (kept at 100°C) via either the solids probe or a wide-bore all-quartz direct insertion probe connected via an o-ring with a small glass bulb that contains the sample. Ions generated in the source by electron ionization (EI) were accelerated to 8 or 10 keV prior to recording their spontaneous or collision induced dissociations in the second or the third field free regions (ffr) as MI (metastable ion) or CID (collision induced dissociation) spectra respectively. The structure of a given product ion in a 2ffr MI or CID spectrum was probed by selectively transmitting the ion by E_1 to a collision chamber in the 3ffr pressurized with O_2 and mass-analyzing its ionic dissociation products by scanning E_2. The resulting MS/MS/MS type spectra are denoted as MI/CID and CID/CID spectra respectively. All the (high energy) collision experiments were performed at a main beam transmittance (~70%) such that the probability for multiple collisions is negligible.

For neutralization–reionization mass spectra [1] (NRMS), 8 keV ions $m^{\bullet+}$ are selectively transmitted by B to the 2ffr where, in the first collision chamber, charge-exchange neutralization occurs with *N,N*-dimethyl aniline (NDMA) : $m^{\bullet+}$ [8 keV] + NDMA $\rightarrow$ m [8 keV] + $NDMA^{\bullet+}$. The unreacted ions are deflected away and the remaining fast neutrals are reionized with O_2 in the second collision cell. Scanning E_1 yields the spectrum of the reionized neutrals $m^{\bullet+}$, the "survivor" ions, and their (structure characteristic) charged dissociation products. For CIDI (collision-induced dissociative ionization) experiments [9], 10 keV ions are selectively transmitted by B to

the 2ffr where the metastable ions spontaneously dissociate. The ions are deflected away and the remaining low energy neutrals, which have a fraction of the original 10 keV translational energy, are reionized by O_2 in the second collision cell. The ionized neutrals and their dissociation products are mass-analyzed by scanning with E_1. All spectra were recorded using a small PC-based data system developed by Mommers Technologies Inc. (Ottawa).

5.2.3. Computational procedures

Structures and energies of the $CH_3O_2P^{\bullet+}$ and CH_5NOP^+ isobaric ions pertinent to this study, connecting transition states and dissociation products were probed by the standard CBS-QB3 model chemistry [12]. A recent study [13] indicates that this method accurately reproduces the heats of formation of species comprised of a second row element (S or P) bonded to a highly electronegative element. The calculations were performed using Gaussian 98 revision A.9 [14].

The calculated energies are presented in Table 5.1a (equilibrium and transition state energies) and Table 5.1b (dissociation products). Frequency calculations gave the correct number of negative eigenvalues for all minima and transition states and the spin contamination was within the acceptable range. The connections of the transition states have been checked by geometry optimizations and frequency calculations.

Table 5.1a. CBS-QB3 derived heats of formation of selected $CH_3PO_2^{\bullet+}$ and CH_5PNO^+ isomeric ions, dissociation products and neutral counterparts.

		E_{total}*	ZPVE	$\Delta H°_f$ [0 K]	$\Delta H°_f$ [298 K]	E_{rel}[298K]
CH_3O-P=$O^{\bullet+}$ (anti)	**1a**$^{\bullet+}$	-530.68346	27.61	137.9	135.4	14
CH_2O-P-$OH^{\bullet+}$ (syn/anti)	**1b**$^{\bullet+}$	-530.70506	26.64	124.4	121.5	0
CH_2O(H)-P=$O^{\bullet+}$ (syn)	**1c**$^{\bullet+}$	-530.66664	25.60	148.5	146.5	25
$[CH_2$-$OH]^+$•••O=$P^{\bullet}$	**1d**$^{\bullet+}$	-530.69034	26.50	133.6	131.1	10
CH_2O-P(H)=$O^{\bullet+}$	**1e**$^{\bullet+}$	-530.67567	25.57	142.8	140.1	19
CH_3O-P=O (anti)	**1a**	-531.06246	28.14	-99.9	-102.7	
TS **1a**$^{\bullet+}$ → **1b**$^{\bullet+}$ (syn/syn)		-530.65170	27.70	160.0	156.8	35
TS **1b**$^{\bullet+}$ → **1d**$^{\bullet+}$		-530.67052	25.99	146.0	143.4	22
TS **1e**$^{\bullet+}$ → **1b**$^{\bullet+}$		-530.62551	23.58	174.3	171.6	50
TS **1a**$^{\bullet+}$ → **1c**$^{\bullet+}$		-530.60896	25.60	184.7	182.1	61
$CH_2OH^+ + PO^{\bullet}$	m/z 31				160.5	39
$POH^{\bullet+} + CH_2$=O	m/z 48				164.3	43
$PO^+ + CH_3O^{\bullet}$	m/z 47				188.8	67
CH_3O-P-NH_2^+	**2a**$^+$	-511.50023	42.91	116.4	111.4	3
CH_3-P(=O)-NH_2^+	**2b**$^+$	-511.50576	42.19	112.9	108.4	0
CH_3O-P(H)=NH^+	**2c**$^+$	-511.44197	41.01	152.9	148.0	40
CH_3O(H)-P=NH^+	**2d**$^+$	-511.45158	41.63	146.9	143.0	35
CH_2O-P(H)-NH_2^+	**2e**$^+$	-511.45918	41.02	142.1	137.9	30
TS **2a**$^+$ → **2c**$^+$		-511.37659	41.01	193.9	188.4	80
TS **2a**$^+$ → **2d**$^+$		-511.42402	39.56	164.2	159.5	51
TS **2a**$^+$ → **2e**$^+$		-511.41573	41.02	169.4	164.5	56
$HNP^+ + CH_3OH$	m/z 46				168.4	60
$H_2NP^{\bullet+} + CH_3O^{\bullet}$	m/z 47				223.3	115
$PO^+ + CH_3NH_2$	m/z 47				179.7	71
$H_2NPH^+ + CH_2$=O	m/z 48				164.1	56
$NH_2PO^{\bullet+} + CH_3^{\bullet}$	m/z 63				212.8	104
$CH_3OP^{\bullet+} + NH_2^{\bullet}$	m/z 62				230.4	122
CH_3O-P-$NH_2^{\bullet}$	**2a**$^{\bullet}$	-511.72871	40.79	-27.0	-31.6	20
CH_3-P(=O)-$NH_2^{\bullet}$	**2b**$^{\bullet}$	-511.76172	41.22	-47.7	-52.1	0
CH_3O-P(H)=$NH^{\bullet}$	**2c**$^{\bullet}$	-511.70356	39.99	-11.2	-15.6	36

* E_{total} is given in Hartrees, all other components, including the ZPVE scaled by 0.99, are in kcal/mol.

Table 5.1b. Auxiliary energetic information derived from CBS-QB3 calculations.

		E_{total}*	ZPVE	$\Delta H°_f$[0 K]	$\Delta H°_f$[298 K]
NH_2-P(OH)$OCH_3^{\bullet+}$	m/z 95	-587.24443	51.63	65.9	60.5
NH_2-P(H)(=O)$OCH_3^{\bullet+}$	m/z 95	-587.19634	50.42	96.0	90.6
NH_3-P(=O)OCH_2^+	m/z 94	-586.64345	44.56	77.7	73.5
NH_2-P(=O)$OCH_3^{\bullet+}$	m/z 94	-586.66456	45.98	64.5	59.5
NH_2-P(OH)OCH_2^+	m/z 94	-586.65380	43.91	71.2	66.8
H-N=P=S^+	m/z 78	-793.59210	8.95	244.2	242.9
CH_3-P=$S^{\bullet+}$	m/z 78	-778.15710	23.03	216.4	213.8
HO-P=$O^{\bullet+}$	m/z 64	-491.45052	10.15	145.7	144.3
PO_2^+	m/z 63	-415.72469	4.15	176.7	176.0
$PO_2^\bullet$		-491.21376	2.60	-71.0	-71.7
PS^+	m/z 63	-738.34694	1.20	219.0	218.8
NH_2-P=$O^{\bullet+}$	m/z 63	-471.59670	18.03	179.7	177.3
$CH_3OP^{\bullet+}$	m/z 62	-455.52242	25.65	187.7	185.4
H-N=P=O^+	m/z 62	-470.94968	9.72	220.4	219.1
H_2N-PH_3^+	m/z 50	-398.28525	33.43	164.7	160.4
H-P-NH_2^+	m/z 48	-397.07402	22.09	194.2	191.4
H-P=$O^{\bullet+}$	m/z 48	-416.25538	5.15	217.0	216.1
P-$OH^{\bullet+}$	m/z 48	-416.29431	7.62	192.5	191.6
P-$NH_2^{\bullet+}$	m/z 47	-396.44950	15.69	220.9	219.0
H-N=P-$H^{\bullet+}$	m/z 47	-396.40210	12.38	250.6	248.9
PO^+	m/z 47	-416.27365	2.03	184.7	184.5
$PO^\bullet$		-416.03233	1.75	-8.4	-8.6
CH_2=$PH^{\bullet+}$	m/z 46	-380.32624	19.54	259.6	257.7
CH_3-$P^{\bullet+}$	m/z 46	-380.33435	20.46	254.5	252.7
N=P-H^+	m/z 46	-395.73221	5.08	305.7	304.7
H-N=P^+	m/z 46	-395.87172	8.07	218.1	217.3
CH_3OH		-115.53992	31.44	-46.2	-48.9
CH_2OH^+	m/z 31	-114.61170	24.94	171.0	169.1
$CH_3O^\bullet$		-114.87446	22.45	6.1	4.3
CH_3NH_2		-95.66848	39.24	-1.2	-4.8
CH_2=O		-113.94253	16.29	-26.4	-27.3
H_2O		-76.33746	13.11	-57.5	-58.2
O		-74.98763	0.00	59.0	59.4
$NH_2^\bullet$		-55.79118	11.61	45.7	45.0
CH_3^+	m/z 15	-39.38466	19.17	262.2	261.3
$CH_3^\bullet$		-39.74479	18.19	36.6	35.5

* E_{total} is given in Hartrees, all other components, including the ZPVE scaled by 0.99, are in kcal/mol.

5.3. Results and discussion

5.3.1. The elemental composition of the m/z 78 ions from acephate and methamidophos

The 70 eV EI mass spectra of acephate and methamidophos are presented in Fig. 5.1, as items (a) and (b) respectively. These spectra were obtained with the ZAB-R instrument. They are virtually the same as those from the GC-TOF instrument and closely similar to the spectra reported in the literature [16]. It is seen from Fig. 5.1a,b that the m/z 78 ions are of only minor abundance and, considering the structure of the precursor molecules, they are obviously not primary fragment ions. From our analysis of the MI and CID spectra (Section 5.3), it follows that the m/z 78 ions from acephate have four precursor ions, *viz.* m/z 136, m/z 96, m/z 95 and m/z 94. For methamidophos m/z 78 ions appear in the CID spectra of m/z 95 and m/z 94.

Fig. 5.1c shows a narrow mass scan of the m/z 78 ions from the two precursor molecules obtained with a GC-TOF instrument at a mass resolution of c. 5000. Both acephate and methamidophos yield a mixture of four isobaric ions whose common components are denoted as w, x, y and z. The relative intensity of the x, y and w components remains constant during the evaporation of the sample, but that of the z component decreases steadily. This z component of centroid mass 78.0458 most likely stems from a minor benzene impurity of the samples : it is not present when the sample was analyzed in the GC/MS mode.

The ions derived from acephate consist of two major components, x and y. Their centroid masses, 77.9870 and 78.0104, agree with the elemental compositions CH_3O_2P and CH_5NOP, whose calculated masses differ from the measured masses by 0.0 and 0.4 mDa. For methamidophos, the CH_5NOP component (y) clearly dominates. The minor w component could refer to the PS containing ions HNPS and/or CH_3PS.

The m/z 94 precursor ions are isobarically pure $CH_5NO_2P^+$ ions; the m/z 95 $CH_6NO_2P^{\bullet+}$ ions from methamidophos are also isobarically pure, but those from acephate consist of a 5:1 mixture of $CH_6NO_2P^{\bullet+}$ and $CH_4O_3P^+$. The m/z 136 $C_3H_7NO_3^+$ and m/z 96 $CH_5O_3P^{\bullet+}$ ions from acephate both have a single elemental composition.

Thus, unlike the proposal of ref. 5, the m/z 78 ions of acephate are not isobarically pure ions $CH_3O\text{-}P{=}O^{\bullet+}$. The minor PS containing component may have little impact on the CID spectrum, but the major CH_5NOP^+ component will certainly contribute. The analysis of the NR spectrum becomes even more problematic. To facilitate the analysis of the CID and NR spectra in Section 5.4, we will first discuss the characterization of isobarically pure $CH_3O\text{-}P{=}O^{\bullet+}$ ions and their neutral counterpart.

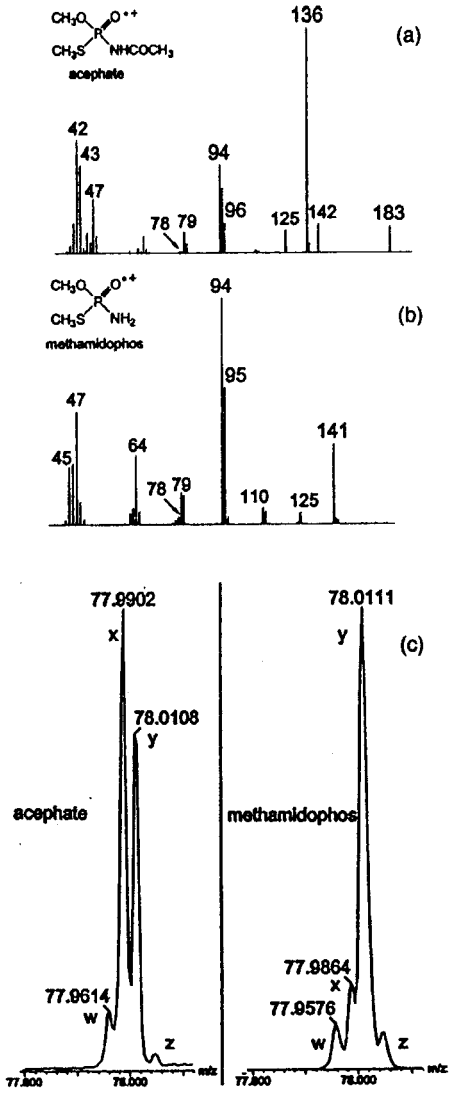

Fig. 5.1. 70 eV EI mass spectra of acephate **(a)** and methamidophos **(b)**; item **(c)** displays the m/z 78 peak profiles for the two compounds obtained at medium mass resolution, see text for further details.

5.3.2. *The dissociation characteristics of CH_3O-P=O$^{\bullet+}$ and its H-shift isomer CH_2O-P-OH$^{\bullet+}$*

As mentioned above, we have studied the $CH_3O_2P^{\bullet+}$ system of isomers in considerable detail [7]. In the context of the present study we will focus on the collision induced dissociation characteristics of CH_3O-P=O$^{\bullet+}$, **1a**$^{\bullet+}$, and its H-shift isomer CH_2O-P-OH$^{\bullet+}$, **1b**$^{\bullet+}$. The ions are generated as depicted in Scheme 5.2 and their CID spectra are presented in Fig. 5.2.

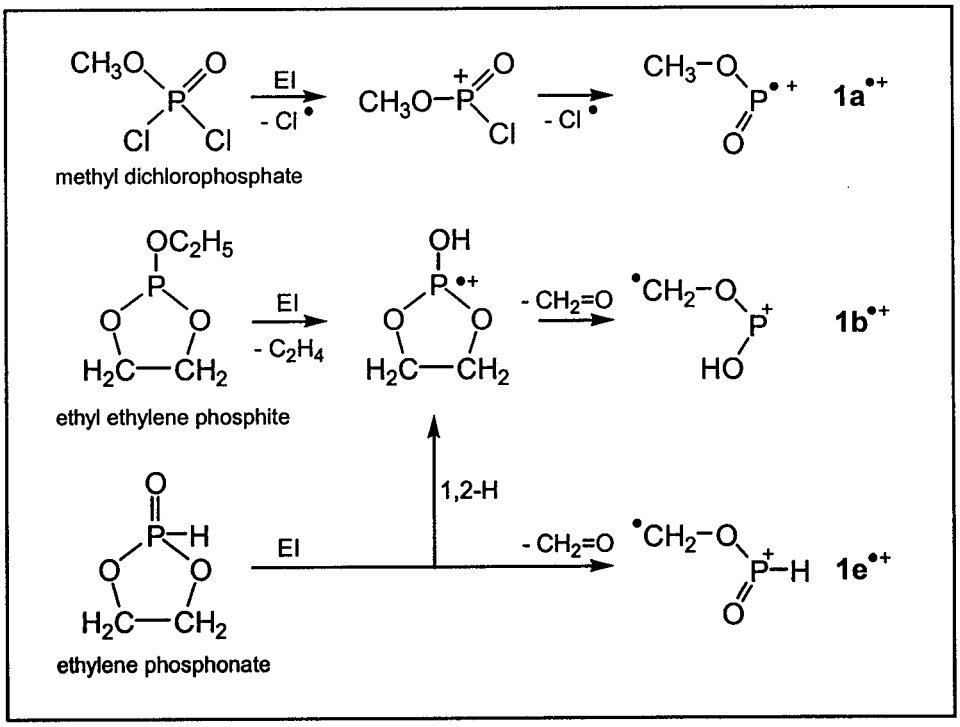

Scheme 5.2

Comparison of the spectra indicates that the major collision induced dissociations of the two isomers lead to the same product ions, *viz.* CH_2OH^+ (m/z 31), PO^+ (m/z 47) and $POH^{\bullet+}$ (m/z 48). From the results presented in Table 5.1, it follows that the minimum energy requirement for dissociation into $CH_2OH^+ + PO^\bullet$ is lower than that for the formation of $PO^+ + CH_3O^\bullet$ and $POH^{\bullet+} + CH_2$=O, by 28 and 4 kcal/mol respectively. The dissociation $CH_2OH^+ + PO^\bullet$ is also observed for metastable ions **1a**$^{\bullet+}$ and **1b**$^{\bullet+}$ – along with a prominent decarbonlylation into m/z 50 $HPOH_2^{\bullet+}$ ions [7] – but

peaks at m/z 48 and m/z 47 are absent in the MI spectra (not shown). The m/z 48 $POH^{\bullet+}$ ion can be generated from $CH_2O\text{-}P\text{-}OH^{\bullet+}$, $\mathbf{1b}^{\bullet+}$, by direct bond cleavage and the same holds true for the formation of PO^+ (m/z 47) from $CH_3O\text{-}P{=}O^{\bullet+}$, $\mathbf{1a}^{\bullet+}$. However, the formation of CH_2OH^+ from either of the isomers requires a H-shift. Our computational results, see Table 5.1, show that the 1,4-H shift associated with the interconversion of $\mathbf{1a}^{\bullet+}$ and $\mathbf{1b}^{\bullet+}$ is less energy demanding than the major CID dissociations. Moreover, ions $\mathbf{1b}^{\bullet+}$ can rearrange via a low barrier into the hydrogen-bridged radical cation $^+CH_2\text{-}O\text{-}H\bullet\bullet\bullet O{=}P^{\bullet}$, $\mathbf{1d}^{\bullet+}$, which may serve as a precursor for the formation of CH_2OH^+. At more elevated energies, CH_2OH^+ ions may also be generated via the sequence $\mathbf{1a}^{\bullet+}$ –1,2-H→ $CH_2O(H)\text{-}P{=}O^{\bullet+}$, $\mathbf{1c}^{\bullet+} \rightarrow CH_2OH^+ + P{=}O^{\bullet}$, see Table 5.1. Thus, it is not surprising that the CID spectrum of $\mathbf{1a}^{\bullet+}$ is similar to that of its more stable distonic isomer $\mathbf{1b}^{\bullet+}$. This is also true for the CID spectrum of another high energy H-shift isomer of $\mathbf{1b}^{\bullet+}$, $CH_2OP(H){=}O^{\bullet+}$, $\mathbf{1e}^{\bullet+}$, which may be generated with $\mathbf{1b}^{\bullet+}$ upon the loss of CH_2O from ionized ethylene phosphonate, see Scheme 5.2 [7].

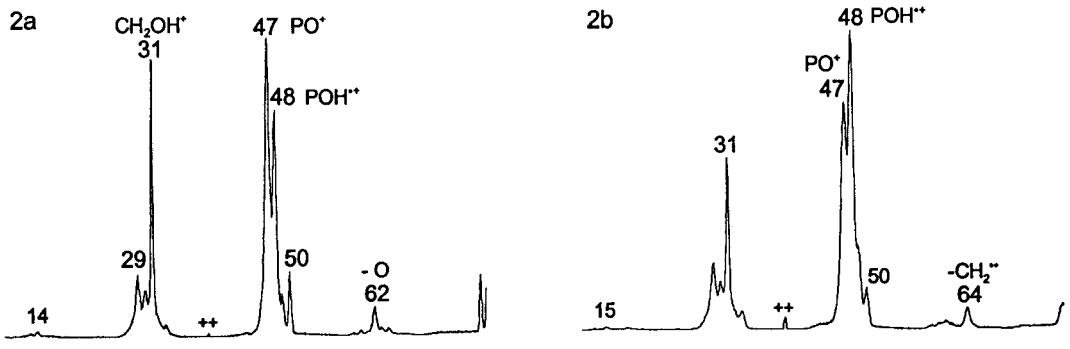

Fig. 5.2. 8 keV CID mass spectra (3ffr) of the m/z 78 CH_3PO_2 isomers $CH_3O\text{-}P{=}O^{\bullet+}$, spectrum 2a, and $CH_2O\text{-}P\text{-}OH^{\bullet+}$, spectrum 2b.

Nevertheless, isomers $\mathbf{1a}^{\bullet+}$ and $\mathbf{1b}^{\bullet+}$ can be differentiated on the basis of the weak but structure diagnostic CID peaks at m/z 62 and 64. These peaks represent high energy dissociations, *viz.* $CH_3O\text{-}P{=}O^{\bullet+} \rightarrow CH_3OP^{\bullet+}$ (m/z 64) + O and $CH_2O\text{-}P\text{-}OH^{\bullet+} \rightarrow HO\text{-}P{=}O^{\bullet+} + CH_2^{\bullet\bullet}$. The loss of O from $\mathbf{1a}^{\bullet+}$ is less pronounced when helium is used as a collision gas rather than O_2, in line with the "oxygen effect" described in ref. 17.

Finally, in line with the expected stability of dications $\mathbf{1b}^{++}$ vs $\mathbf{1a}^{++}$, the distonic ion $\mathbf{1b}^{\bullet+}$ displays a more pronounced m/z 39 charge stripping peak in its CID spectrum.

One further point deserves comment: in the CID spectrum of the m/z 78 ions of putative structure $\mathbf{1a}^{\bullet+}$ derived from acephate [5], a prominent peak is present at m/z 63, see also Section 5.4. This peak has been assigned to the dissociation $CH_3O\text{-}P{=}O^{\bullet+} \rightarrow PO_2^+$ (m/z 63) + $CH_3^\bullet$. Since $\Sigma\Delta H_f\ PO_2^\bullet + CH_3^+$ is lower than $\Sigma\Delta H_f\ PO_2^+ + CH_3^\bullet$, by 22 kcal/mol, the charge is expected to be retained at the methyl moiety upon cleavage of the C-O bond in $\mathbf{1a}^{\bullet+}$. However, the intensity of the m/z 15 CH_3^+ peak in the reported spectrum [5] is negligible indicating that a prominent peak at m/z 63 does not characterize the CID spectrum of $\mathbf{1a}^{\bullet+}$. On the other hand, in our spectrum of $\mathbf{1a}^{\bullet+}$ presented in Fig. 5.2a, both m/z 15 and m/z 63 are minor peaks. This is readily understood considering the ease of isomerization of $CH_3O\text{-}P{=}O^{\bullet+}$ upon collisional activation.

5.3.3. Evidence for the stability of the CH_3O-P=O molecule in the rarefied gas-phase

As discussed above, $CH_3O\text{-}P{=}O^{\bullet+}$ ions yield a structure characteristic CID spectrum, albeit that the ion undergoes a facile interconversion with other H-shift isomers and is generated in a low yield. This makes it less attractive to probe the stability of the neutral by a NR experiment. We have therefore utilized a CIDI experiment, where the neutral of interest is generated by the dissociation of a selected metastable precursor ion and analyzed by its collisional ionization spectrum.

Loss of $H^\bullet$ dominates the 70 eV EI mass spectrum of methyl phenylphosphinate. The resulting even electron ion, $C_6H_5\text{-}P(=O)OCH_3^+$, yields the MI spectrum displayed in Fig. 5.3a. The spectrum shows that low energy ions $C_6H_5\text{-}P(=O)OCH_3^+$ undergo four dissociations. The peaks at m/z 125, 108 and 91 represent rearrangement reactions in which neutral species of 30, 47 and 64 Da are lost, most likely $CH_2{=}O$, $PO^\bullet$ and HPO_2 respectively. The MI spectrum also features the process of interest, the putative direct bond cleavage reaction $155^+ \rightarrow 77^+$ ($C_6H_5^+$) + 78 ($CH_3O\text{-}P{=}O$). The alternative *rearrangement* reaction $155^+ \rightarrow 77^+$ ($CH_2O\text{-}P{=}O^+$) + 78 (C_6H_6) has a lower calculated

minimum energy requirement, by 26 kcal/mol, (from the enthalpy values in Table 5.1 and reference 15). However, this rearrangement reaction must have a significant reverse activation energy since a collision experiment showed that most of the m/z 77 ions are $C_6H_5^+$. In the same vein, the prominent m/z 77 peak in the CID spectrum of C_6H_5-$P(=O)OCH_3^+$ also refers to $C_6H_5^+$ ions.

In the CIDI experiment the beam of mass selected m/z 155 ions, which also contains its ionic dissociation products, is deflected away by an electrode in front of the collision gas chamber. Thus, ideally the only species that enter this chamber are the four neutral species generated from the above reactions. These neutrals are subsequently ionized by collision (albeit with considerably different efficiencies which depend on the translational energy and other factors [18]) and the resulting ions and their ionic dissociation products give rise to the CIDI spectrum of Fig. 5.3b. The spectrum shows a sizable peak at m/z 78, expected to correspond to collisional ionization of CH_3O-P=O. That this is indeed the case follows from Fig. 5.3c which presents the CID spectrum of the m/z 78 ions of Fig 3b. Although the weak spectrum suffers from a fairly high noise level, there is little doubt that we are dealing with ions of structure $\mathbf{1a}^{\bullet+}$.

Thus, we conclude that CH_3O-P=O is a stable molecule in the gas phase, in agreement with our CBS-QB3 calculations from which we derive ΔH_f^{298} [**1a**] = -102.7 kcal/mol and IE_a [**1a**] = 10.3 eV, see Table 5.1.

Two points deserve further comment: (i) The NR spectrum (not shown) of the m/z 155 C_6H_5-$P(=O)OCH_3^+$ ions displays a prominent m/z 77 ($C_6H_5^+$) peak with only minor peaks at higher masses. In a CIDI experiment with O_2 for collisional ionization, the gas pressure in the region immediately in front of the deflector electrode is often sufficiently high to cause some neutralization of the beam of incoming ions [9b]. This phenomenon, we propose, accounts for the presence of the peak at m/z 77 in the CIDI spectrum of Fig. 5.3b; (ii) As mentioned above, decarbonlylation into m/z 50 ions is the major reaction of metastable CH_3O-$P=O^{\bullet+}$ ions. In line with the general observation that ions generated by collisional ionization contain a higher fraction of metastable ions than those generated by electron impact in the ion source [19], the relative intensity of the m/z 50 peak in Fig. 5.3c is higher than that of Fig. 5.2a.

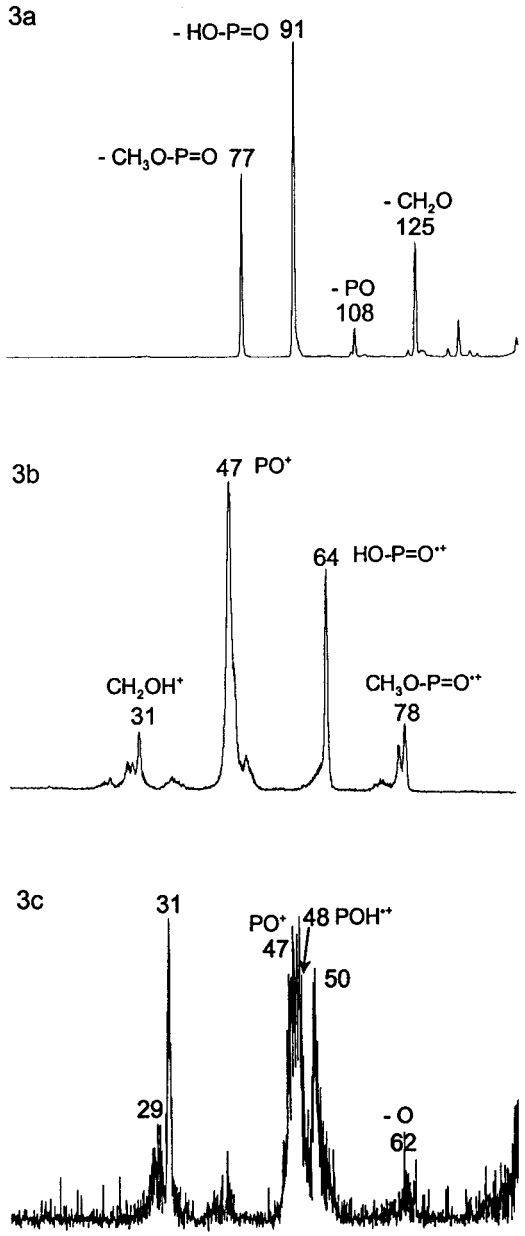

Fig. 5.3. 10 keV MI and CIDI spectra of m/z 155 ions C_6H_5-P(=O)OCH_3^+, spectra 3a and 3b respectively; spectrum 3c is the 3ffr CID spectrum of the m/z 78 peak of spectrum 3b.

5.3.4. The collision induced dissociation characteristics of m/z 78 ions from acephate and methamidophos: evidence for the generation of the CH_3O-P-NH_2^+ ion

Fig. 5.4a displays the CID spectrum of the source generated m/z 78 ions derived from acephate which, see Section 5.1, consist of roughly a 1:1 mixture of $CH_3PO_2^{\bullet+}$ and CH_5NOP^+ ions with a small contribution from $HNPS^+$ and/or $CH_3PS^{\bullet+}$. Comparison of the spectrum with that of CH_3O-P=$O^{\bullet+}$, Fig. 5.2a, shows that the prominent m/z 46 peak does not originate from the $CH_3PO_2^{\bullet+}$ component but rather from the isobaric CH_5NOP^+ ions. This is supported by the enhanced intensity of the m/z 46 peak in the CID spectrum of Fig. 5.4d, which samples the source generated m/z 78 ions from methamidophos which largely consist of CH_5NOP^+ ions. Consequently, the proposal of ref. 5 that the m/z 46 ions originate from the dissociation CH_3O-P=$O^{\bullet+} \rightarrow CH_3P^{\bullet+}$ (m/z 46) + O_2 is clearly not tenable. In fact, the relative high heat of formation of $CH_3P^{\bullet+}$ (Table 5.1b) makes it highly unlikely that this ion is generated to a significant extent from any $CH_3PO_2^{\bullet+}$ isomer.

To probe the structure(s) of the $CH_3PO_2^{\bullet+}$ and CH_5NOP^+ ions from acephate and methamidophos, we analyzed the CID spectra of all potential precursor ions.

For methamidophos, we found two routes: (i) $M^{\bullet+} \rightarrow$ m/z 94 ($CH_5NO_2P^+$) + $CH_3S^{\bullet}$ and (ii) $M^{\bullet+} \rightarrow$ m/z 95 ($CH_6NO_2P^{\bullet+}$) + CH_2=S. The intense m/z 94 ions, see Fig. 5.1, are most likely ions of structure CH_3O-P(=O)NH_2^+, generated by a direct bond cleavage reaction. This ion is lower in energy than its isomers CH_2O-P(=O)NH_3^+ and CH_2O-P(OH)NH_2^+ (Table 5.1b) which could conceivably be generated from rearranged molecular ions. The prominent m/z 95 ions are most likely CH_3O-P(OH)$NH_2^{\bullet+}$ generated by loss of CH_2=S from molecular ions that have rearranged via a facile 1,4-H shift [13] into distonic ions CH_3O-P^+(OH)(NH_2)$SCH_2^{\bullet}$.

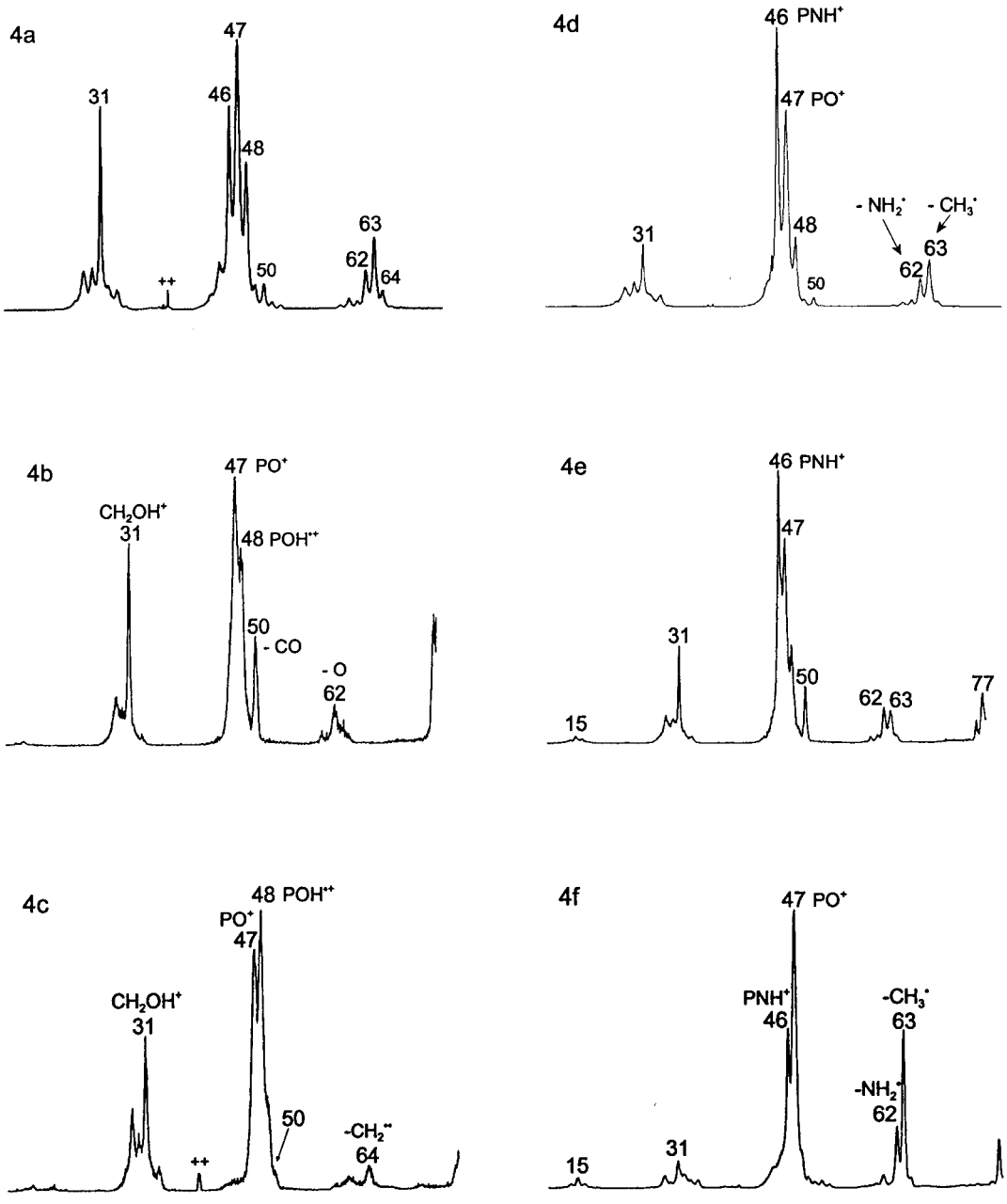

Fig. 5.4. 8 keV CID mass spectra (3ffr) of m/z 78 ions : spectra 4a and 4d represent the source generated ions from acephate and methamidophos respectively; spectra 4b and 4c are derived from the CID processes $136^{+} \rightarrow 78^{\bullet+}$ and $96^{\bullet+} \rightarrow 78^{\bullet+}$ in acephate; spectrum 4e is derived from the CID process $94^{+} \rightarrow 78^{\bullet+}$ in acephate/methamidophos; spectrum 4f refers to source generated ions of structure $CH_3P(=O)(Cl)NH_2^{\bullet+}$.

Ions at m/z 94 and 95 are also present in the EI mass spectrum of acephate. The ions have the same elemental composition as those derived from methamidophos (apart from a minor $CH_4O_3P^+$ component in m/z 95). Their CID spectra were obtained and found to be closely similar to those of the methamidophos derived m/z 94 and m/z 95 ions, signifying that we are dealing with ions of the same structure, i.e. $CH_3O\text{-}P(=O)NH_2^+$ and $CH_3O\text{-}P(OH)NH_2^{\bullet+}$ respectively. For acephate, the immediate precursor for both ions is the m/z 136 ion, but its CID spectrum indicates that a third route to m/z 78 may involve the direct bond cleavage reaction depicted in Scheme 5.1. The m/z 96 ion $CH_5O_3P^{\bullet+}$ in acephate's EI mass spectrum provides the fourth precursor to m/z 78. This ion is generated via the sequence $M^{\bullet+} \rightarrow$ m/z 142 + $C_2H_3N \rightarrow$ m/z 96 + $CH_2{=}S$, which represents a remarkable skeletal rearrangement. The MI spectrum of the m/z 96 ion shows intense peaks at m/z 78 (loss of H_2O) and m/z 66 (loss of CH_2O). These peaks are also prominent in its CID spectrum, along with peaks at m/z 81 (loss of $CH_3^{\bullet}$) and m/z 65 (loss of $CH_3O^{\bullet}$), which support the proposal that the m/z 96 ions have the structure $CH_3O\text{-}P(OH)_2^{\bullet+}$.

For acephate, the CID spectra of the m/z 78 ions generated upon CID of the m/z 136 (route 3) and m/z 96 (route 4) ions are shown in Fig. 5.4b and 5.4c respectively. The MS/MS/MS spectrum of Fig. 5.4b is very close to that of Fig. 5.2a, supporting the mechanistic proposal of Scheme 5.1, which leads to the formation of $CH_3PO_2^{\bullet+}$ ions of structure $CH_3O\text{-}P{=}O^{\bullet+}$. On the other hand, the spectrum of Fig. 5.4c is clearly not that of $CH_3O\text{-}P{=}O^{\bullet+}$ but rather that of $CH_2O\text{-}P\text{-}OH^{\bullet+}$, compare Fig. 5.2b. This is not unexpected : if the m/z 96 ion has the proposed structure $CH_3O\text{-}P(OH)_2^{\bullet+}$, a 1,4-H shift leading to the energetically more favourable distonic ion $CH_2O\text{-}P\text{-}OH^{\bullet+}$ is expected to be favoured over a 1,3-H shift leading to $CH_3O\text{-}P{=}O^{\bullet+}$. From this analysis, it follows that the acephate molecular ion generates m/z 78 $CH_3PO_2^{\bullet+}$ ions which are a mixture of the isomers $CH_3O\text{-}P{=}O^{\bullet+}$ and $CH_2O\text{-}P\text{-}OH^{\bullet+}$.

We now turn to the structure and dissociation characteristics of the CH_5NOP^+ component, which dominates the CID spectrum of the source generated m/z 78 ions from methamidophos, Fig. 5.4d. From a comparison with the $CH_3PO_2^{\bullet+}$ reference spectra of Fig. 5.2, it becomes clear that the peaks at m/z 63 and particularly m/z 46 are tell-tale

peaks of the CH_5NOP^+ ion. Assuming that the m/z 50 peak uniquely characterizes the isobaric $CH_3PO_2^{\bullet+}$ ions $\mathbf{1a}^{\bullet+}$ and $\mathbf{1b}^{\bullet+}$, see Fig. 5.2, it further follows that most of the m/z 62 and a considerable fraction of the m/z 47 ions also originate from CH_5NOP^+. The MI spectrum (not shown) of the m/z 78 ions from methamidophos displays peaks at m/z 46, 48 and 50, with an intensity ratio of 100 : 35 : 25. The m/z 46 and m/z 48 peaks characterize the low energy dissociations of the CH_5NOP^+ component since the $CH_3PO_2^{\bullet+}$ isomers do not display peaks at these m/z values in their MI spectra [7].

The CH_5NOP^+ ions from methamidophos may well have the structure CH_3O-P-NH_2^+, $\mathbf{2a}^+$, considering that there immediate precursor ions, m/z 94 and m/z 95, can generate ions $\mathbf{2a}^+$ via direct bond cleavage reactions : CH_3O-P(=O)NH_2^+ (m/z 94) $\rightarrow$ CH_3O-P-NH_2^+ + O and CH_3O-P(OH)$NH_2^{\bullet+}$ (m/z 95) $\rightarrow$ CH_3O-P-NH_2^+ + $OH^\bullet$. In support of this, our calculations (Table 5.1a) indicate that ion $\mathbf{2a}^+$ is a minimum on the CH_5NOP^+ potential energy surface. Its energy is comparable to that of its methyl-shift isomer CH_3-P(=O)-NH_2^+, $\mathbf{2b}^+$, but considerably lower than that of its H-shift isomers CH_3O-P(H)=NH^+, $\mathbf{2c}^+$, CH_3O(H)-P=NH^+, $\mathbf{2d}^+$, and CH_2O-P(H)-NH_2^+, $\mathbf{2e}^+$. The methyl-shift isomer $\mathbf{2b}^+$ can conveniently be generated by loss of $Cl^\bullet$ from ionized CH_3-(Cl)P(=O)-NH_2 and its CID spectrum, see Fig. 5.4f, is clearly different from that of its isomer $\mathbf{2a}^+$, Fig. 5.4d. We note that precursor molecules of the type CH_3O-P(X)-NH_2 (X = Cl, Br, CH_3O) [10d] which could abundantly yield isobarically pure ions $\mathbf{2a}^+$ upon ionization, are not known to exist.

The next step of our analysis is the CID spectrum of the m/z 78 ions generated by the collision induced dissociation of the m/z 94 ions CH_3O-P(=O)NH_2^+, which is presented in Fig. 5.4e. The spectrum supports our proposal that CH_5NOP^+ ions of structure $\mathbf{2a}^+$ are generated. However, the peak at m/z 50 suggests that isobaric ions $\mathbf{1a}^{\bullet+}$, generated by the collision induced dissociation CH_3O-P(=O)NH_2^+ (m/z 94) $\rightarrow$ CH_3O-P=$O^{\bullet+}$ + $NH_2^\bullet$, are also present. The co-generation of CH_3O-P=$O^{\bullet+}$ also involves a direct bond cleavage reaction, but its minimum energy requirement is higher than that for dissociation into $\mathbf{2a}^+$ + O, by 9 kcal/mol (Table 5.1b). These dissociations are high energy processes and the intensity of the m/z 78 peak in the CID spectrum of m/z 94 is therefore only c. 10 % of the base peak at m/z 47 (PO^+). The m/z 78 peak in the CID

spectrum of m/z 95 is even weaker and in addition it is poorly resolved from the base peak at m/z 79 (CH_3O-P-OH^+) which compromises a straightforward analysis. Nevertheless, the CID spectrum of the m/z 78 ions (not shown) resembles that of Fig. 5.4e and it is in basic agreement with the structure proposal.

Next, we analyzed the CID spectrum of the m/z 96 ion CH_3O-P(=O)ND_2^+, a D-labelled isotopologue of the m/z 94 ion CH_3O-P(=O)NH_2^+, obtained from methamidophos-ND_2. The spectrum shows peaks at m/z 80 and m/z 78, in a 4 : 1 ratio, supporting the proposal that the spectrum of Fig. 5.4e is a mixture of ions $\mathbf{2a}^+$ and $\mathbf{1a}^{\bullet+}$. The CID spectrum of the m/z 80 ions, which should be that of isobarically pure ions CH_3O-P-ND_2^+, has only three peaks in the m/z 45 region, *viz.* m/z 47 (100%, base peak), m/z 49 (25%) and m/z 50 (10%). In the m/z 60 region only two peaks are observed : at m/z 65 and m/z 62, with an intensity ratio of 2 : 1. These observations allow us to identify the processes that give rise to the tell-tale peaks at m/z 46 and m/z 63 in the CID spectrum of Fig. 5.4d as $\mathbf{2a}^+ \rightarrow HNP^+ + CH_3OH$ and $\mathbf{2a}^+ \rightarrow NH_2P{=}O^{\bullet+} + CH_3^{\bullet}$. The peak at m/z 62 may be assigned to the reaction $\mathbf{2a}^+ \rightarrow CH_3OP^{\bullet+} + NH_2^{\bullet}$, whereas the majority of the m/z 47 ions do not originate from the direct bond cleavage reaction $\mathbf{2a}^+ \rightarrow NH_2P^{\bullet+} + CH_3O^{\bullet}$ but rather result from the (formal) extrusion process : $\mathbf{2a}^+ \rightarrow PO^+ + CH_3NH_2$. We further note that the m/z 50 ions in the labelled isotopomer are most likely m/z 48 ions that contain two deuterium atoms, indicating that they are ions $HPNH_2^+$ generated by the rearrangement $\mathbf{2a}^+ \rightarrow HPNH_2^+ + CH_2O$.

Our computational results, see Table 5.1a, agree with this analysis. Ion CH_3O-P-NH_2^+ can undergo a 1,3-H shift (TS $\mathbf{2a}^+ \rightarrow \mathbf{2d}^+$) to yield ion $CH_3O(H)$-P=NH^+, $\mathbf{2d}^+$, which, by direct bond cleavage, yields $HNP^+ + CH_3OH$. Another 1,3-H shift (TS $\mathbf{2a}^+ \rightarrow \mathbf{2e}^+$) converts $\mathbf{2a}^+$ into CH_2O-P(H)-NH_2^+, $\mathbf{2e}^+$, which can lose CH_2O by direct bond cleavage to yield the m/z 48 ion H_2NPH^+. The two processes have comparable energy requirements, 60 and 56 kcal/mol respectively, and are much lower in energy than all other processes observed. This is in line with the observation that m/z 46 and m/z 48 characterize the MI spectrum of $\mathbf{2a}^+$. The activation energy of the direct bond cleavage $\mathbf{2a}^+ \rightarrow NH_2P^{\bullet+}$ (m/z 47) + $CH_3O^{\bullet}$ is very high (116 kcal/mol, Table 5.1a). It even exceeds

that for $\mathbf{2a}^+ \rightarrow NH_2\text{-}P{=}O^{\bullet+}$ (m/z 63) + $CH_3^\bullet$, yet the m/z 47 CID peak is considerably more intense than m/z 63. Formation of isomeric m/z 47 ions $H\text{-}N{=}P\text{-}H^{\bullet+}$, via a 1,2-H shift into $CH_3O\text{-}P(H){=}NH^+$, $\mathbf{2d}^+$, followed by direct bond cleavage, requires even more energy : 146 kcal/mol. In contrast, the calculated minimum energy requirement is only 71 kcal/mol if, as proposed above, the m/z 47 ions are ions PO^+ generated from the reaction $\mathbf{2a}^+ \rightarrow PO^+ + CH_3NH_2$. In the same vein, the m/z 47 ions in the CID spectrum of the methyl-shift isomer $\mathbf{2b}^+$ may also be PO^+. Their generation can be envisaged as a simple extrusion reaction : $CH_3\text{-}P(=O)\text{-}NH_2^+ \rightarrow PO^+ + CH_3NH_2$, but the actual mechanism of this intriguing reaction may be more complex.

5.4. Conclusions

Thus, we conclude that the CH_5NOP^+ ions from methamidophos and acephate have the structure $CH_3O\text{-}P\text{-}NH_2^+$, $\mathbf{2a}^+$. Its neutral counterpart, $CH_3O\text{-}P\text{-}NH_2^\bullet$, **2a**, is calculated to be a stable species, see Table 5.1a, but confirmation of this prediction by a NR experiment on the m/z 78 ions from methamidophos appears to be problematic. The CID spectrum of the fairly abundant survivor ion of the NR process contains major peaks at m/z 63, 47, 46, 45 and 44, whose intensity distribution (100 : 70 : 90 : 85 : 35) is certainly not compatible with that of (pure) ions $\mathbf{2a}^+$. One speculative possibility is that the survivor ions are largely ions $CH_3PS^{\bullet+}/CH_3SP^{\bullet+}$, which could originate from the minor low mass m/z 78 component of methamidophos and acephate. Loss of $CH_3^\bullet$ is calculated to be an energetically favoured dissociation for these ions, which could also account for the prominent peaks at m/z 45 (HCS^+) and m/z 44 ($CS^{\bullet+}$). In any case, these observations reinforce our conclusion that the NR spectrum of the m/z 78 ions from acephate reported in ref. 5 cannot be used to verify by experiment that $CH_3O\text{-}P{=}O$ is a stable species in the gas-phase.

References

[1] For selected recent reviews see: (a) G. Schalley, G. Hornung, D. Schröder and H. Schwarz, Chem. Soc. Rev. 27 (1998) 91; (b) N. Goldberg and H. Schwarz, Acc. Chem. Res. 27 (1994) 34.

[2] For a recent example see: M.A. Trikoupis, P. Gerbaux, D.J. Lavorato, R. Flammang and J.K. Terlouw, Int. J. Mass Spectrom. 217 (2002) 1.

[3] D. Young, Computational Chemistry : A practical Guide for Applying Techniques to Real World Problems, Wiley Interscience, New York, 2001.

[4] R. Srikanth, R. Srinivas, K Bhanuprakash, S. Vivekananda, E.A. Syrstad and F. Tureček, J. Am. Chem. Soc. Mass Spectrom. 13 (2002) 250 and references cited therein.

[5] S. Vivekananda and R. Srinivas, Int. J. Mass Spectrom. Ion Proc. 171 (1997) 79.

[6] A.C. Chukwudebe, M.A. Hussain and P.C. Oloffs, J. Environ. Sci. Health B19(6) (1984) 523.

[7] L.N. Heydorn, P.C. Burgers, P.J.A. Ruttink and J.K. Terlouw, Int. J. Mass Spectrom. (2003) in press.

[8] L.N. Heydorn, P.C. Burgers, P.J.A. Ruttink and J.K. Terlouw, Int. J. Mass Spectrom. (2003) in press.

[9] (a) J.K. Terlouw and H. Schwarz, Angew. Chem. Int. Ed. Engl. 26 (1987) 805; (b) M.A. Trikoupis, J.K. Terlouw, P.C. Burgers, M. Peres and C. Lifshitz, J. Am. Soc. Mass Spectrom. 10 (1999) 869.

[10] (a) C. Furlani and M.V. Andreocci, J. Chem. Soc. (Dalton) (1972) 248; (b) D.G. Hewitt, Aust. J. Chem. 32 (1979) 463; (c) P.C. Crofts and I.S. Fox, J. Chem. Soc. (1958) 2995; Houben-Weyl, Methoden der Organischen Chemie, Vol. XII/2. Georg Thieme Verlag, Stuttgart, 1964.

[11] H.F. van Garderen, P.J.A. Ruttink, P.C. Burgers, G.A. McGibbon and J.K. Terlouw, Int. J. Mass Spectrom. Ion Proc. 121 (1992) 159.

[12] (a) J.A. Montgomery Jr, M.J. Frisch, J.W. Ochterski, and G.A. Petersson, J. Chem. Phys. 110 (1999) 2822; (b) ibid. 112 (2000) 6532.

[13] L.N. Heydorn, Y. Ling, G. de Oliveira, J.M.L. Martin, Ch. Lifshitz and J.K. Terlouw, Zeitschrift für Physikalische Chemie 215 (2001) 141.

[14] M.J. Frisch, et al. Gaussian 98, Revision A.9, GAUSSIAN Inc., Pittsburgh, PA, 1998

[15] S.G. Lias, J.E. Bartmess, J.F. Liebman, J.L. Holmes, R.D. Levin, W.G. Mallard, J. Phys. Chem. Ref. Data 17 (1988) Suppl. 1; see also NIST Chemistry WebBook, http://webbook.nist.gov/chemistry/

[16] NIST Chemistry WebBook, http://webbook.nist.gov/chemistry/

[17] R. Flammang, V. Henrotte, P. Gerbaux and M.T. Nguyen, Eur. Mass Spectrom. 6 (2000) 3.

[18] (a) C.E.C.A. Hop, PhD Thesis, University of Utrecht (1988); (b) C.E.C.A. Hop and J.L. Holmes, Org. Mass Spectrom., 26 (1991) 476.

[19] S. Beranová and C. Wesdemiotis, J. Am. Chem. Soc. Mass Spectrom., 5 (1994) 1093.

Chapter 6

Generation of the elusive methyl dioxophosphorane molecule, $CH_3P(=O)_2$, by delayed dissociation of selected precursors

A recent flame-sampling laser-ionization study [Chem. Phys. Lett. 275 (1997) 278] reported that combustion of dimethyl methyl phosphonate generates the elusive $CH_3P(=O)_2$ molecule and that it has an ionization energy (IE) of 9.24 ± 0.01 eV. Ab initio calculations (CBS-QB3 level of theory) indicate that this IE is that of the "enol" tautomer $CH_2=P(=O)OH$, while that of $CH_3P(=O)_2$ is much higher, 11.66 eV. We propose that in the above experiments a trace amount of the "enol" is co-generated with the "keto" isomer $CH_3P(=O)_2$. Mass spectrometric experiments involving Neutralization-Reionization (NR) and Collision Induced Dissociative Ionization (CIDI) show that $CH_2=P(=O)OH$ and $CH_3P(=O)_2$ are both stable neutral species in the dilute gas-phase.

The work described here has been published previously in an article under the same title : L.N. Heydorn, P.C. Burgers, P.J.A. Ruttink and J.K. Terlouw, Chem. Phys. Lett. **368** (2003) 584 – 588.

6.1. Introduction

Nitromethane, CH_3NO_2, is the smallest member of a well known family of compounds known as nitroparaffins [1]. It is used as a fuel additive in the racing industry and its physico-chemical properties are well documented. By contrast, virtually nothing is known about its phosphorus analogue, CH_3PO_2, methyl dioxophosphorane. However, this elusive molecule has been proposed [2,3,4] as a key intermediate in combustion studies of the nerve agent simulant dimethyl methylphosphonate (DMMP), $CH_3P(=O)(OCH_3)_2$. In one of these studies [2], Werner and Cool used a sophisticated flame-sampling photoionization technique to study the combustion chemistry of DMMP vapour fed into a H_2/O_2/Ar flame. In these experiments prominent signals were observed at m/z 78 and m/z 94. These were taken to correspond to ionized CH_3PO_2 and CH_3OPO_2 on account of their favourable thermodynamic stabilities compared to alternative structures. Using a tunable laser, these elegant experiments also allowed the measurement of the ionization energies (IE) of these elusive molecules. By such experiments, the IE for CH_3PO_2 was reported to be 9.24 ± 0.01 eV.

However, in the context of our mass spectrometric studies of organophosphorus compounds [5-7] we noted that such compounds have IE's similar to (if not larger than) those of their nitrogen analogues [8]. The IE of CH_3NO_2 is accurately known, and is quite large, 11.02 eV [8], and so we surmised that the IE of CH_3PO_2 would be at least 11 eV. That CH_3NO_2 (and presumably also CH_3PO_2) has such a high IE reflects the electron withdrawing nature of the NO_2 substituent resulting in only a limited charge dispersal of the corresponding cation. As a consequence, the measured value of 9.24 eV would appear to be incompatible with the structure CH_3PO_2. In this paper we address this apparent discrepancy and provide definitive evidence from mass spectrometry based experiments that CH_3PO_2 is indeed a stable species as was concluded by Werner and Cool [2].

6.2. Experimental

The experimental set-up consists of a triple sector mass spectrometer of the type $Bc_1Dc_2E_1c_3E_2$ [5] where B is a magnetic sector (a momentum selector), E are electric sectors (kinetic energy selectors), c are collision chambers and D is a deflector electrode which, when charged, purifies the beam from ions. B is situated upstream, while E_2 is positioned downstream. The Collision-Induced Dissociation (CID) mass spectra were obtained as described in Ref. 5. Neutralization-Reionization (NR) [9] mass spectra are obtained as follows. The desired ion, having 10 keV translational energy, is selected by B and enters a drift region between B and E_1. The mass selected ions are neutralized by charge transfer in chamber c_1 using an organic vapour (N,N-dimethylaniline) as reducing agent. All unreacted ions as well as ionic by-products from the redox step are deflected by D and so only fast moving neutrals enter collision chamber c_2. Here, they are reionized by collision with O_2 and the reionized species may subsequently dissociate. Any surviving ions as well as their ionic dissociation products are selected by E_1 and detected resulting in the NR mass spectrum. The survivor ion can also be selectively transmitted through E_1 and then be subjected to collision-induced dissociation in c_3 followed by the analysis of the ionic dissociation products by E_2. This technique was used to obtain the spectrum of Fig. 6.1c.

Collision Induced Dissociative Ionization (CIDI) mass spectra [10] were obtained with the same instrument, but now c_1 is at residual pressure. The mass selected ion is allowed to dissociate spontaneously between B and D. The precursor and product ions are deflected by D and so only the neutral product from the above dissociation enters c_2 where (dissociative) ionization by collision with O_2 occurs. The CIDI mass spectrum is obtained by scanning E_1.

The diphenyl- and dibenzyl- methyl phosphonates used in the CIDI experiments, $CH_3P(=O)(OC_6H_5)_2$, $CH_3P(=O)(OCH_2C_6H_5)_2$ and $CH_3P(=O)(OCH_2C_6D_5)_2$, were obtained by esterification of commercially available $CH_3P(=O)Cl_2$ with the appropriate alcohol. The methyl phosphonic acid, $CH_3P(=O)(OH)_2$, used in the NR experiment was obtained from Aldrich.

6.3. Theoretical methods

The calculations were performed using Gaussian 98 revision A.9 [11]. The standard CBS-QB3 [12, 13] and G2 [14] model chemistries were used to probe the structures and energies of isomeric molecules and radical cations. Spin contaminations were within acceptable range. A brief validation of the CBS-QB3 method for calculations on PO containing ions and neutrals is found in ref. 5.

6.4. Results and Discussion

There is no reason to question that the bulk of the M = 78 neutrals formed in the above combustion experiments are $CH_3P(=O)_2$ but we doubt that the value of 9.24 eV corresponds to the IE of this neutral. We propose that the measured IE corresponds to a trace amount of an isomer having a low IE and which is co-generated in the flame-sampling experiments. We have considered two isomers, *viz.* CH_3O-P=O [6] and CH_2=P(O)OH; the latter can be considered as the "enol" tautomer of $CH_3P(=O)_2$. In Table 6.1 are given the calculated heats of formation (ΔH_f) of these neutral isomers and their radical cations (also shown is the calculated structure of CH_3PO_2). The difference yields the adiabatic IE of the species. It can be seen that the calculated IE for $CH_3P(=O)_2$ is even higher than we had anticipated, it being a staggering 2.4 eV higher than the measured value, 9.24 eV. Such a large discrepancy precludes any experimental or theoretical inaccuracies or imprecisions.

Table 6.1. Heats of formation (kcal/mol) and ionization energies (eV) of $CH_3P(=O)_2$ and isomers derived from CBS-QB3 calculations.

	CBS-QB3 (0K) Hartree	ΔHf (298K)	IEadiabatic (298K)
$CH_3P(=O)_2$	-531.08646	-117.9	11.63 [a]
CH_3O-P=O	-531.06841	-106.6	10.56
CH_2=P(O)OH	-531.04785	- 93.7	9.25 [b]
$CH_3P(=O)_2^{\cdot+}$	-530.65978	150.2	
CH_3O-P=$O^{\cdot+}$	-530.68130	136.7	
CH_2=P(O)$OH^{\cdot+}$	-530.70820	119.5	

[a] G2 (298 K) value = 11.68 eV ; IEvertical (0 K) = 12.10 eV,
[b] G2 (298 K) value = 9.23 eV.

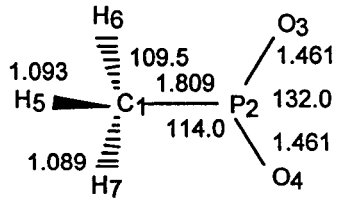

< 5 1 2 = 107.8
< 1 2 3 4 = 179.2
< 5 1 2 3 = - 89.1
< 6 1 2 3 = 29.3
< 7 1 2 3 = 152.4

Optimized geometry of CH_3PO_2

From the results of Table 6.1, it follows that the IE for the CH_3O-P=O isomer does not match the experiment either, but the calculated values for CH_2=P(O)OH are in perfect agreement with the measured value. We therefore propose that in the flame-sampling experiments of Werner and Cool [2], a small amount of CH_2=P(O)OH is co-generated and that it is this species which has been observed at threshold. That the calculated IE for $CH_3P(=O)_2$ (11.66 eV) is larger than that for CH_3O-P=O (10.56 eV) is in line with the experimental IEs for the nitrogen analogues $CH_3N(=O)_2$ (11.02 eV) and CH_3O-N=O (10.38 eV) [8], in keeping with the electron withdrawing nature of the PO_2 and NO_2 groups.

We now wish to generate $CH_3P(=O)_2$ by an alternative method to independently prove that this molecule is indeed a stable species in the gas-phase. This we do by mass spectrometry based experiments using a multisector instrument. There are two approaches.

In the first, a precursor molecule (M) is chosen which conceivably produces the $CH_3PO_2^{\bullet+}$ radical cation by dissociative ionization, i.e. $M^{\bullet+} \rightarrow CH_3P(=O)_2^{\bullet+} + F$ (Eq. 1), where F is the neutral fragment. This $CH_3PO_2^{\bullet+}$ species may then be mass selected and its NR mass spectrum may be obtained as described in the Experimental section. However, the data in Table 6.1 indicate that for $CH_3P(=O)_2^{\bullet+}$ such an experiment will most likely fail, as indeed it did. This is because the $CH_3P(=O)_2^{\bullet+}$ radical cation is much less stable than the other isomers [7], notably when compared with its tautomer CH_2=P(O)$OH^{\bullet+}$, see Table 6.1. (The reverse is true for their neutral counterparts : such a reversal of stability upon one-electron oxidation is more the rule than the exception [15].) Notwithstanding any necessary rearrangements, the most stable tautomer is usually generated in such experiments. Indeed, the prominent loss of H_2O from ionized methyl phosphonic acid, $CH_3P(=O)(OH)_2^{\bullet+}$, does not yield $CH_3P(=O)_2^{\bullet+}$ but rather CH_2=P(O)$OH^{\bullet+}$. This follows from the CID spectrum of Fig. 6.1a, which displays structure characteristic peaks [7] for the high energy losses of CH_2, at m/z 64, and O, at m/z 62. Moreover, CH_2=P(O)$OH^{\bullet+}$ can readily form CH_2OH^+ (m/z 31), by $PO^{\bullet}$ extrusion. Fig. 6.1b shows the NR spectrum of these ions. The spectrum displays an intense "survivor" ion peak at m/z 78, indicating that CH_2=P(O)OH is a stable neutral. To verify this, we obtained the CID spectrum of the "survivor" ions, see Fig. 6.1c, and compared it with that of the source generated ions, Fig. 6.1a. The spectra are closely

similar, which confirms our proposal that CH_2=P(O)$OH^{\bullet+}$ retains its structure upon neutralization.

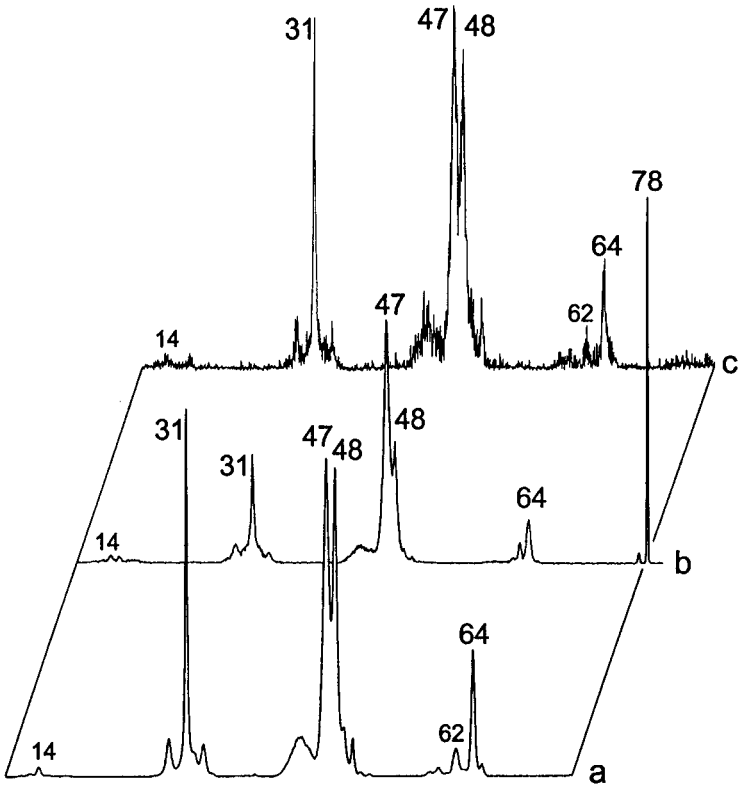

Fig. 6.1. Collision-Induced Dissociation (CID) spectrum (**a**), and Neutralization-Reionization (NR) spectrum of the m/z 78 ions CH_2=P(O)$OH^{\bullet+}$ (**b**). Item (**c**) represents the CID spectrum of the m/z 78 survivor ions in (**b**).

Thus, it is unlikely that the stability of neutral $CH_3P(=O)_2$ can be probed with the NR approach, but fortunately there is an alternative. This is provided by the (charge) reverse process of Eq. 1, i.e. $M^+ \rightarrow CH_3PO_2 + F^+$ (Eq. 2), where the partner fragment now carries the charge. In this case the neutral formed most likely will be CH_3PO_2 because this is the tautomer of lowest ΔH_f, see Table 6.1. Such keV neutrals can be generated and identified by the technique of Collision Induced Dissociative Ionization (CIDI) mass spectrometry [9, 10], which is briefly explained in the Experimental section. We selected the following two reactions for Eq. 2 :

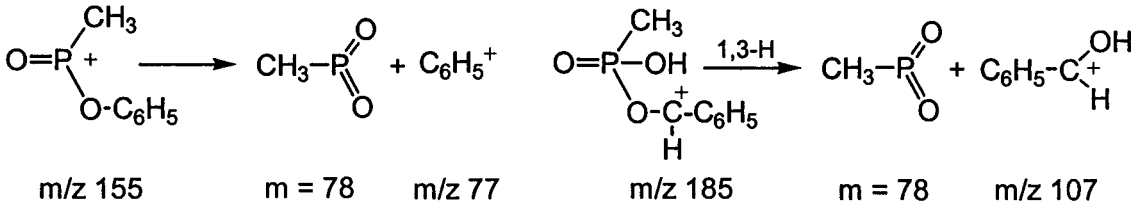

The m/z 155 and m/z 185 precursor ions were generated by dissociative electron ionization of diphenyl- and dibenzyl methyl phosphonate respectively (see Experimental), via unexceptional dissociation routes.

The m/z 155 or m/z 185 precursor ions are selectively transmitted by the magnet and enter a field free region where they are allowed to dissociate according to the above. Next, all ions are deflected away from the beam and only the putative neutrals CH_3PO_2 enter the collision cell situated downstream. Here they are ionized and fragmented by collision with O_2 and the CIDI mass spectrum is obtained by measuring the kinetic energies of the fragments. The two precursor ions yielded essentially the same CIDI spectra and a representative spectrum is shown as item (a) in Fig. 6.2. Item (b) shows the CID spectrum of the $CH_3O\text{-}P{=}O^{\bullet+}$ isomer, which has been characterized in a previous study [6].

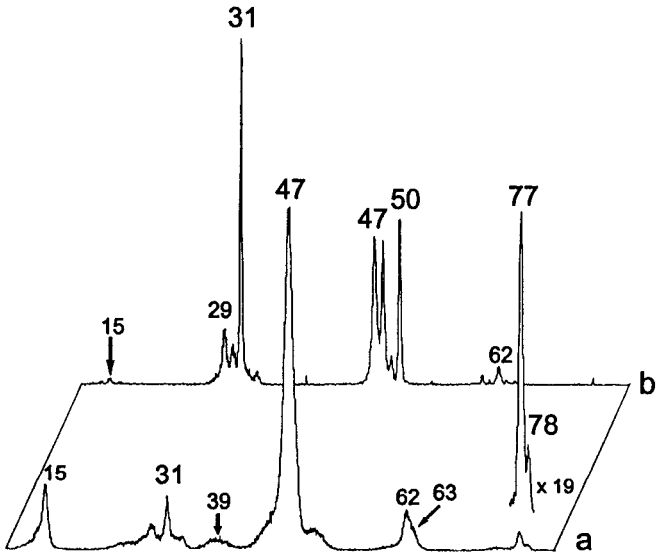

Fig. 6.2. **(a)** CIDI spectrum of $CH_3P(=O)_2$ neutrals generated from the dissociation of metastable ions $CH_3\text{-}P(=O)(OH)OCHC_6H_5^+$, **(b)** CID spectrum of $CH_3O\text{-}P{=}O^{\bullet+}$ ions [9].

The CIDI spectrum shows a distinct peak at m/z 78 but it is dominated by peaks from dissociation products. This is not unexpected for m/z 78 ions of putative structure $CH_3P(=O)_2^{\bullet+}$, considering their high heat of formation. Comparison of the CIDI spectrum of $CH_3P(=O)_2$ with the CID spectra of $CH_2=P(O)OH^{\bullet+}$ (Fig. 6.1a) and $CH_3O\text{-}P=O^{\bullet+}$ (Fig. 6.2b) shows that the spectra are substantially different. Ions $CH_3P(=O)_2^{\bullet+}$ characteristically dissociate into CH_3^+ (m/z 15) + $PO_2^\bullet$ (formation of PO_2^+ (m/z 63) requires more energy) and $CH_3P=O^+$ (m/z 62) + O. The consecutive loss of O and $CH_3^\bullet$ and the direct loss of $CH_3O^\bullet$ contribute to the base peak at m/z 47 (PO^+). These processes are less important in the $CH_3O\text{-}P=O^{\bullet+}$ isomer, which instead readily loses $PO^\bullet$ to yield m/z 31, while it also decarbonylates into m/z 50 [6, 7]. As mentioned above, the enol tautomer $CH_2=P(O)OH^{\bullet+}$ characteristically loses CH_2, its spectrum also contains a (weak) peak at m/z 14 ($CH_2^{\bullet+}$), but clearly not at m/z 15 (CH_3^+).

These observations indicate that neutral CH_3PO_2 is a stable species in the gas-phase. To confirm this proposal, we verified that the m/z 78 peak in the CIDI spectrum represents ionized CH_3PO_2 neutrals and not isobaric neutrals C_6H_6 : these could conceivably be formed from the precursor ions by a process competing with formation of CH_3PO_2. Thus, we examined a deuterium isotopologue of m/z 185, i.e. $CH_3P(O)(OH)OCHC_6D_5^+$. In the molecular ion region of its CIDI spectrum (not shown), peaks are present at m/z 78 ($CH_3PO_2^{\bullet+}$), m/z 77 ($[CH_3PO_2^{\bullet+} - H^\bullet]$) and m/z 82 ($C_6D_5^+$), but not at m/z 83 ($C_6D_5H^{\bullet+}$). Thus, part of the peak[1] at m/z 77 in the CIDI spectrum of Fig. 6.2a is due to $C_6H_5^+$, but **all** of m/z 78 is $CH_3PO_2^{\bullet+}$. This constitutes definitive evidence that CH_3PO_2 is a stable species in the gas-phase and that it has an IE of 11.66 eV. The IE measured by Werner and Cool [2], we conclude is that of the "enol' species $CH_2=P(O)$ OH.

[1] ca 30% of the peak intensity; the $C_6H_5^+$ ions probably originate from $C_6H_5^\bullet$ radicals generated by neutralization of the precursor ion by residual gas in front of the deflector electrode [6, 16]. Their collision induced dissociation accounts for the weak peaks centered around m/z 39 ($C_3H_3^+$) in the spectrum of Fig. 6.2a.

References

[1] J.A. Riddick, in : G. L. Clark, G.G. Hawley (Eds.), The Encyclopedia of Chemistry, Reinhold, New York, 1966, pp. 695-696.

[2] J.H.Werner, T.A. Cool, Chem. Phys. Lett. 275 (1997) 278.

[3] E.J.P. Zegers, E.M. Fisher, Combust. Flame 115 (1998) 230.

[4] J.H. Werner, T.A. Cool, Combust. Flame 117 (1999) 78.

[5] L.N. Heydorn, Y. Ling, G. de Oliveira, J. M. L. Martin, C. Lifshitz, J.K. Terlouw, Z. Phys. Chemie 215 (2001) 141.

[6] L.N. Heydorn, C.Y. Wong, R. Srinivas, J.K. Terlouw, Int. J. Mass Spectrom. 225 (2003) 11.

[7] L.N. Heydorn, P.C. Burgers, P.J.A. Ruttink and J.K. Terlouw, Int. J. Mass Spectrom. in press.

[8] S.G. Lias, J.E. Bartmess, J.F. Liebman, J.L. Holmes, R.D. Levin, W.G. Mallard, J. Phys. Chem. Ref. Data 17 (1988) Suppl. 1.

[9] For a selected review see : N. Goldberg, H. Schwarz, Acc. Chem. Res. 27 (1994) 34.

[10] J.K. Terlouw, H. Schwarz, Angew. Chem. Int. Ed. Engl. 26 (1987) 805.

[11] M.J. Frish et al. Gaussian 98, Revision A.9, Gaussian, Inc.: Pittsburgh, PA, 1998.

[12] J.A. Montgomery Jr, M.J. Frish, J.W. Ochterski, G.A. Petersson, J. Chem. Phys. 110 (1999) 2882.

[13] J.A. Montgomery Jr, M.J. Frish, J.W. Ochterski, G.A. Petersson, J. Chem. Phys. 112 (2000) 6532.

[14] L.A. Curtis, K. Raghavachari, P.C. Redfern, J.A. Pople, J. Chem. Phys. 106 (1997) 1073.

[15] See for example P.C. Burgers , J.K. Terlouw in : J.C. Lindon, G.E. Tranter, J.L. Holmes (Eds.), Encyclopedia of Spectroscopy and Spectrometry, Academic Press, London, 2000, pp. 990 – 1000.

[16] M.A. Trikoupis, J.K. Terlouw, P.C. Burgers, M. Peres, C. Lifshitz, J. Am. Chem. Soc. Mass Spectrom. 10 (1999) 869.

Chapter 7

Reactions of the ionized enol tautomer of acetanilide: elimination of HNCO via a novel rearrangement

The enol of the acetanilide ion $C_6H_5NH(OH)=CH_2^{\bullet+}$ eliminates HNCO at low internal energy via a skeletal rearrangement to give ionized methylene cyclohexadiene; proton transport catalyzed tautomerization of ionized acetanilide does not occur because the ionized enol is less stable than the keto isomer.

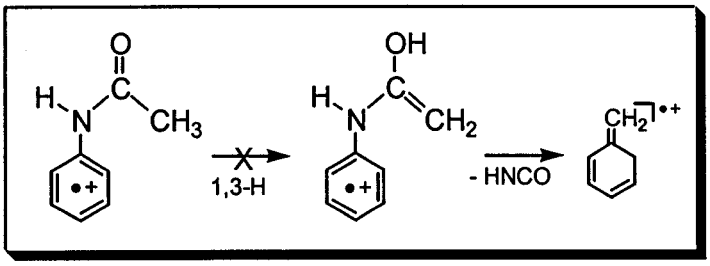

The work described in this Chapter was performed in a collaborative project with Dr R.D. Bowen and L.M. Carter who synthesized the various deuterium labelled compounds.

7.1. Introduction

Hydrogen transfers are of enormous significance in chemistry and biology. An accurate delineation of mechanisms of H-transfers is essential if these reactions are to be understood and controlled. Thus, keto-enol tautomerism, which is a crucial facet of the chemistry of many neutral and ionic species containing a carbonyl group [1], may be formulated as an intramolecular 1,3-H shift, but such processes entail very large energy barriers [2]. These barriers are circumvented for the neutral molecule in solution by acid (or base) catalysis in which a proton is added (or removed) and then lost (or replaced) elsewhere via a mechanism that involves two steps, Eqn 1.

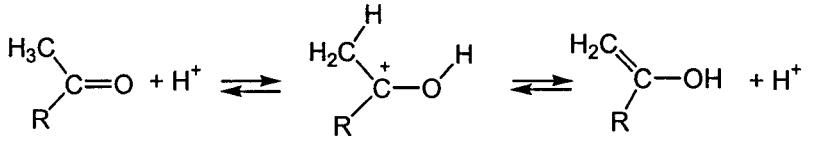

Eqn. 1

Similarly, in the presence of a suitable base (B), keto-enol tautomerism of ionized molecules in the gas-phase is subject to proton-transport catalysis [3, 4], in which a proton is removed from one site by the base and then replaced in a different position, thus circumventing the barriers that are normally associated with 1,3-H shifts [5], Eqn 2. Computational studies [4, 5] indicate that the ionic and neutral components which interact in proton transport catalysis are hydrogen-bridged radical cations [6] and ion-neutral complexes (INCs) [7]. Furthermore, for simple ionic systems the enol ion is invariably more stable than its keto counterpart.

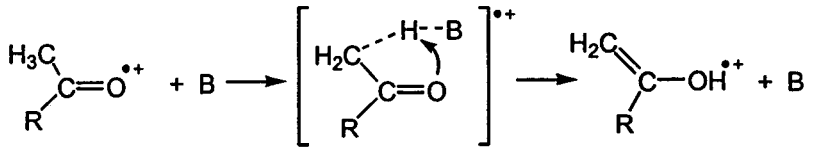

Eqn. 2

Early work on the acetanilide ion $C_6H_5NHC(=O)CH_3^{\bullet+}$, **1**, established that $CH_2=C=O$ (ketene) is abundantly lost from low energy (metastable) ions, yielding ionized aniline as the product ion [8]. The reaction has been described [8] as a four-

centre process but it is perhaps more likely that an INC is involved as part of a route in which C-N cleavage and H-transfer are not synchronously concerted.

At about the same time, it was postulated that low energy ions $C_6H_5NHC(OH)=CH_2^{\bullet+}$, **2**, the enol isomer of **1**, also generate ionized aniline, via a four-centre H-transfer in which ethynol, HC≡COH, rather than ketene is lost [9]. This remarkable claim deserves further scrutiny, partly because unusual neutral species such as ethynol can now be characterized by tandem mass spectrometry [10], but also because the tautomerism of the keto ion **1** into its enol may be subject to proton transport catalysis.

7.2. Experimental

The experimental set-up consists of a VG Analytical ZAB-R mass spectrometer [11]. This is a three-sector mass spectrometer of the type $Bc_1Dc_2E_1c_3E_2$ where B is a magnetic sector, E are electric sectors, c are collision chambers and D is a deflector electrode which, when charged, purifies the beam from ions in CIDI (collision induced dissociative ionization) [10] experiments.

The compounds [12] were introduced into the ion source (kept at 100°C) via either the solids probe or a wide-bore all-quartz direct insertion probe connected via an o-ring with a small glass bulb that contains the sample. Ions generated in the source by electron ionization (EI) or chemical ionization (CI) were accelerated to 8 keV prior to recording their spontaneous or collision induced dissociations in the second or the third field free region (ffr) as MI (metastable ion) or CID (collision induced dissociation) spectra respectively. The kinetic energy releases of Table 7.1 (p. 182) were estimated from the width at half-height of the appropriate metastable peak ($T_{0.5}$) by means of the standard one line equation after applying the usual correction for the width at half-height for the main beam [13]. The structure of a given product ion in a 2ffr MI spectrum was probed by selectively transmitting the ion by E_1 to the 3ffr collision chamber c_3 (pressurized with O_2) and mass-analyzing its ionic dissociation products by scanning E_2. The resulting MS/MS/MS type spectra are denoted as MI/CID spectra. All

the (high energy) collision experiments were performed at a main beam transmittance (~70%) such that the probability for multiple collisions is negligible.

The CIDI-survivor CID spectrum of Fig. 7.3 was obtained as follows. Enol ions **2** (m/z 135) having 10 keV translational energy were selectively transmitted by B to the 2ffr. In the region between B and D, a fraction of the metastable m/z 135 ions spontaneously dissociates into m/z 92 ions and m = 43 neutrals. Upon arrival at the charged deflector electrode all ions are deflected away so that the only species entering collision chamber c_2 are fast moving neutrals. The m = 43 neutral species having 3.2 keV translational energy (43/135 x 10 keV) are ionized by collision with O_2 in c_2 which was held at + 3.8 kV. Upon collisional ionization, part of the incipient m/z 43 ions dissociate but those that do not, the m/z 43 "survivor" ions, enter E_1 with 7 keV of translational energy. These ions are selectively transmitted through E_1 and subjected to collision induced dissociation in c_3. The resulting CID spectrum, Fig. 7.3, is obtained by scanning E_2. All spectra were recorded using a small PC-based data system developed by Mommers Technologies Inc. (Ottawa).

7.3. Computational procedures

Calculations were performed at the B3LYP/CBSB7 level of theory, the first component of the CBS-QB3 model chemistry [14], using Gaussian 98, Revision A.9 [15]. Geometries were fully optimized at the B3LYP/CBSB7 level of theory. Stationary points and transition states were characterized using analytical frequency calculations (i.e. $N_{imag} = 0$ and 1 respectively). The calculated energies are presented in Table 7.2 on p. 182 (including equilibrium and transition state energies) while the complete set of detailed geometries is presented in the Appendix. Frequency calculations gave the correct number of negative eigenvalues for all minima and transition states and the spin contamination was within the acceptable range. The connections of the transition states have been checked by geometry optimizations and frequency calculations.

The E_{rel} (kcal/mol) values in square brackets of Scheme 7.1 for **1** and isomers also refer to the above calculations. Those of dissociation levels are experimental values from ref. 16a relative to ΔH_f **1** = 161 kcal/mol, the anchor point. Since ΔH_f **9H**

(carbonyl protonated oxindole) is not experimentally available, it was calculated by the CBS-QB3 model chemistry : ΔH_f (298K) = 142 kcal/mol. The same method yields ΔH_f (298K) HNCO = -29 kcal/mol, some 4 kcal/mol lower than the experimental value of ref. 16 (-25 ± 3 kcal/mol), but very close to the value obtained from the G2 model chemistry [17]. HNCO is the most stable [H,N,C,O] isomer [18]. At the CBS-QB3 level of theory its isomers HOCN, HCNO and CNOH are higher in energy by 25, 68 and 84 kcal/mol respectively.

The CBS-QB3 model chemistry was also used to calculate ΔH_f (298K) values for the acetanilide ion $C_6H_5NHC(=O)CH_3^{\bullet+}$, **1**, its enol $C_6H_5NHC(OH)=CH_2^{\bullet+}$, **2**, and its deprotonated counterpart $C_6H_5NHC(=O)CH_2^{\bullet}$: 165 [19], 174 and 21 kcal/mol respectively. Using $\Delta H_f\ H^+$ = 366 kcal/mol [16a], one then derives proton affinity (PA) values for protonation of $C_6H_5NHC(=\mathbf{O})CH_2^{\bullet}$ at **O** and **C** of 212 and 222 kcal/mol respectively. PA values for acetanilide, $C_6H_5NHC(=O)CH_3$, NH-deprotonated **2**, $C_6H_5N^{\bullet}C(OH)=CH_2$, and [pyrazole-H(N)]$^{\bullet}$, 205, 226 and 209 kcal/mol respectively, were obtained from CBS-QB3 (298K) enthalpy values for $C_6H_5NHC^{+}(OH)CH_3$ (129 kcal/mol), $C_6H_5N^{\bullet}C(OH)=CH_2$ (35 kcal/mol) and [pyrazole-H(N)]$^{\bullet}$ (101 kcal/mol) in combination with the standard enthalpy values of Ref. 16a.

7.4. Results and Discussion

Table 7.1 summarizes the reactions of metastable ions **1** and (selectively labelled labelled) analogues of its enol, **2**. The keto ion was generated by ionization of acetanilide. The enol ions **2** were generated from the appropriate isocaproanilides by ionization followed by loss of 2-methyl propene via a McLafferty rearrangement.

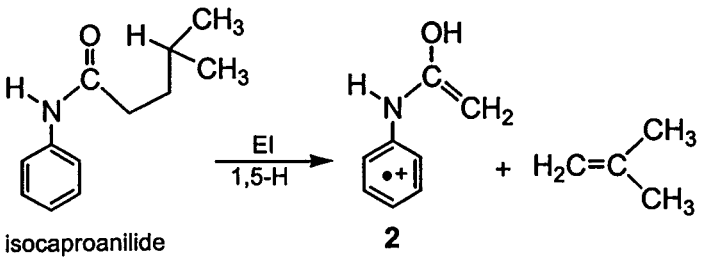

isocaproanilide **2**

Three conclusions follow from these and related data. First, the reactions of **1** and **2** at low internal energy are distinct. Furthermore, the collision-induced dissociation (CID) spectra of **1** and **2**, see Fig. 7.1a/b, also are quite different: **1** shows strong signals at m/z 93 ($C_6H_5NH_2^{\bullet+}$) and 43 ($CH_3C{=}O^+$) via loss of ketene and an anilinium radical, but the spectrum of **2** is dominated by peaks at m/z 134 (loss of $H^\bullet$) and 92, with weak signals at m/z 93 and 43. These data establish that **1** and **2** dissociate independently, rather than tautomerizing to each other. These experimental findings are supported by our calculations which confirm that a high barrier of 56 kcal/mol exists towards interconversion of **1** and **2**, whereas earlier experimental work [21] has established that loss of ketene from **1** only requires 28 kcal/mol.

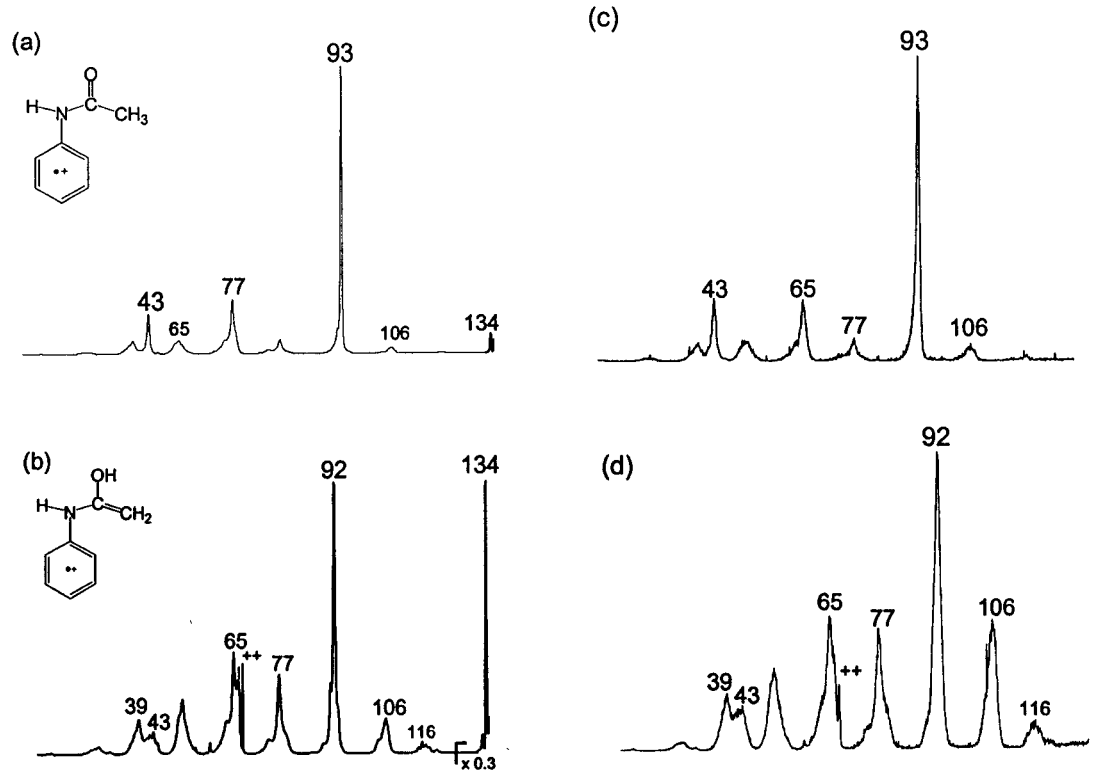

Fig. 7.1. CID spectra of the m/z 135 ions **1**, ionized acetanilide, and **2**, its enol : items (a) and (b) respectively; items (c) and (d) are the CID spectra of m/z 135 ions generated from metastable acetanilide dimer radical cations and the ion-neutral complex between **2** and pyrazole respectively. In spectrum (d) the intense $H^\bullet$ loss is poorly resolved from the main beam and is not shown.

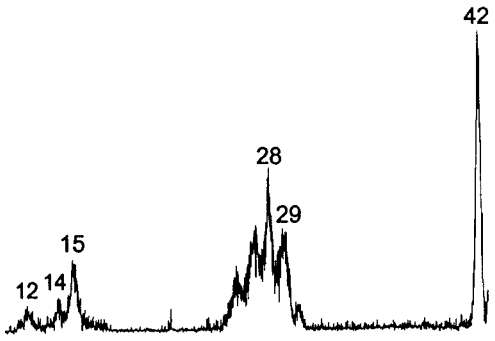

Fig. 7.2. CID spectrum of collisionally ionized HNCO neutrals generated from the dissociation of metastable ions **2** into $C_7H_8^{\bullet+}$ + HNCO.

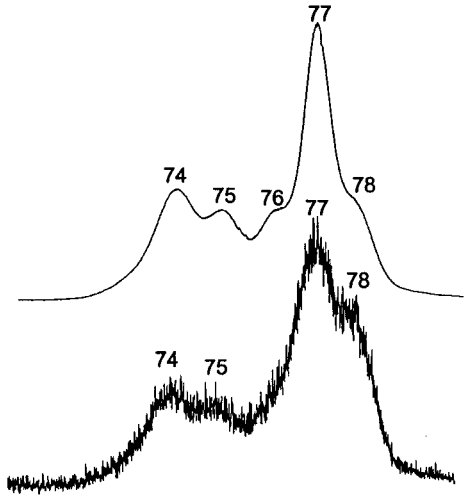

Fig. 7.3. Partial CID spectrum of $C_7H_8^{\bullet+}$ ions from toluene (top) and the methylene cyclohexadiene ions generated from metastable ions $\mathbf{2}^{\bullet+}$ (bottom).

Second, contrary to earlier deductions [9], **2** does not eliminate an m = 42 molecule C_2H_2O, either in the form of ketene (as occurs from **1**) or its high energy isomer ethynol. Instead, an m = 43 neutral, HNCO, is expelled to give the m/z 92 ion $C_7H_8^{\bullet+}$. That the m = 43 neutral is HNCO follows from a comparison of the CID spectrum of Fig. 7.2 with the CID spectra of various isomers of the $[H, C, N, O]^{\bullet+}$ system reported in Ref. 18.

One mechanistic description of this novel skeletal rearrangement, see Scheme 7.1, involves attachment of the methylene group of **2** to the ipso position of the phenyl ring. The resulting four-membered spirocyclic ion is not a minimum on the potential energy surface, but a transition state connecting **2** with **3**, the iminol tautomer of phenyl acetamide, **4**. Ion **3** could also be envisaged to be generated via the cyclic ion **2a** but the ensuing 1,2-H shift yielding **3a** is clearly too high in energy. A final 1,5-H transfer in **3** with an associated C-C cleavage yields the ion-neutral complex INC-**8a**, from which HNCO can be lost with formation of ionized methylenecyclohexadiene **8a.** That ion **8a** is generated rather than its more stable isomer ionized toluene, **8b**, is demonstrated by the partial CID spectra of Fig. 7.3 : as discussed in Ref. 22, the m/z 77 (loss of $CH_3^{\bullet}$)/

m/z 78 (loss of methylene) peak intensity ratio in the CID spectra of **8a** and **8b** are characteristically different.

Scheme 7. 1 (All energies relative to ion **1** in kcal/mol)

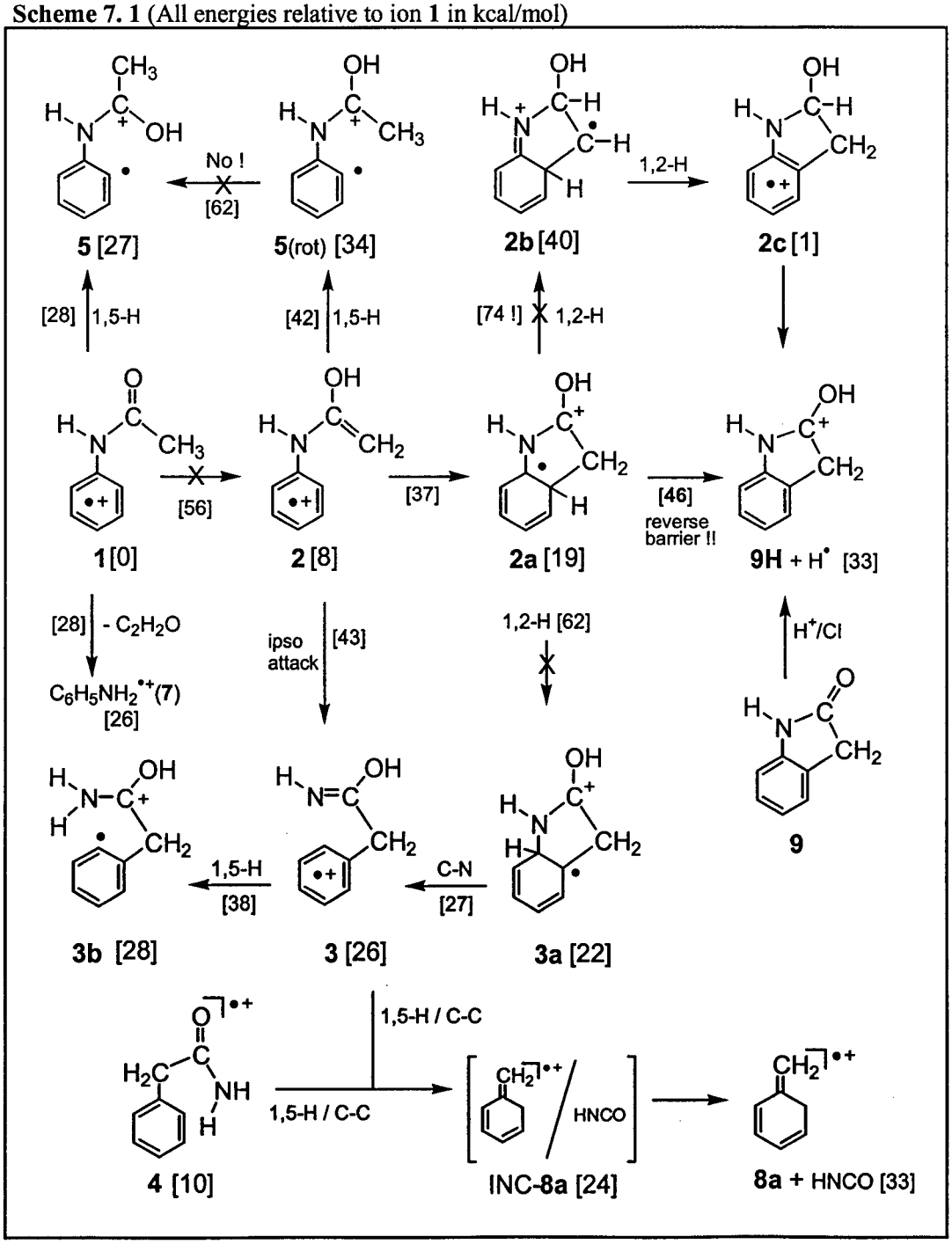

The labelling results, see Table 7.1 (p. 182), are consistent with this mechanism: the eliminated hydrogen isocyanate generally retains the hydrogen atom originally attached to nitrogen, though there is some selection of hydrogen atoms from other sites : the equilibration **3** ⇌ **3b** may account for this. Moreover, ionized phenylacetamide, $C_6H_5CH_2CONH_2^{\bullet+}$, **4**, shows an almost exclusive HNCO loss in its MI spectrum (yielding product ions of structure **8a**), as might be expected given that it may rearrange to the same INC which is accessible to **2**. In this case, the hydrogen transfer has a high selectivity: $C_6H_5CH_2COND_2^{\bullet+}$, loses DNCO, see Table 7.1.

The pathway of Scheme 7.2, which starts from a higher energy rotamer of **2**, could provide an alternative route to INC-**8a**. Its first step is associated with a barrier which is sufficiently low to allow exchange of the hydroxylic H atom with the ortho H atoms. Attempts to characterize the TS for the final step **6**(rot) → INC-**8a**, which we expect to be much higher in energy, were unsuccessful.

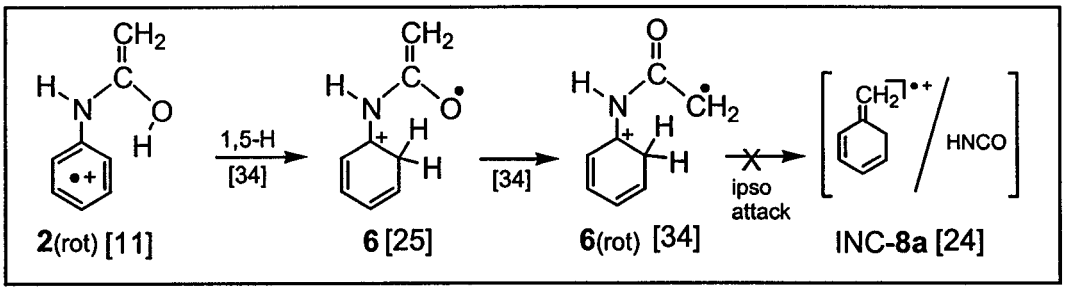

Scheme 7.2

Further support for the proposed mechanism is found in the other reaction of metastable ions **2**, hydrogen atom loss, which may be interpreted in terms of cyclization by formation of a new bond between the methylene group and an ortho carbon atom resulting in the formation of **2a**, Scheme 7.1. The CID spectrum of ion **9H** generated by loss of $H^{\bullet}$ from **2**, is closely similar to that of **9H** formed by protonating oxindole, **9**, under chemical ionization conditions. This would indicate that the $H^{\bullet}$ loss occurs from the bridging carbon in **2a**. Not unexpectedly, this reaction involves a reverse activation energy : TS **2a** → **9H** + H^+ is considerably higher in energy than the dissociation products, see Scheme 7.1, and in line with this, the reaction is associated with a substantial kinetic energy release, $T_{0.5}$ = 185 meV. We further note that the overall

energy requirement for the competing losses of $H^{\bullet}$ and HNCO from metastable ions **2** is about the same (~ 45 kcal/mol) but lower than that required for the keto-enol tautomerization (~ 55 kcal/mol).

Prima facie the observation that the isotopologue $C_6D_5NHC(OH)=CH_2^{\bullet+}$ loses mainly $H^{\bullet}$ does not seem to be consistent with Scheme 7.1. However, the remaining isotopomers of **2** all eliminate $H^{\bullet}$ to a much larger extent than $D^{\bullet}$. One explanation for this surprising selectivity, which is consistent with the experimental results, is that removal of one of the ortho hydrogen atoms of the aromatic ring by the methylene group or to a lesser extent the hydroxyl group followed by back exchange precedes dissociation and that a significant isotope effect is involved. The calculations indicate that the back exchange **2** ⇌ **5**(rot) is energetically feasible. However, the subsequent transformation **5**(rot) ⇌ **5** which would lead to ketonization does not occur. In this context we have also considered the route **2a** → **2b** → **2c** → **9H** + H^+ : this pathway clearly cannot compete, because the barrier for the first isomerization step lies far too high in energy.

Third, attempts to form the enol ion **2** from the keto ion **1** by proton transport catalyzed tautomerism in encounter complexes with various bases, including benzonitrile (BN), pyrazole (PZ), and acetanilide (**1N**) itself, were not successful. The dimer radical cations [**1**/BN], [**1**/PZ] and [**1**/**1N**] can readily be generated in a chemical ionization experiment of **1** in the presence of a 10-fold excess of the base [5b]. However, when these complexes dissociate, either spontaneously or upon collisional activation, they all yield ion **1**, not **2**, as illustrated in Fig. 7.2 (c) for the complex [**1**/**1N**]. This result reflects the unexpected finding from the calculations that **1** is more stable than its enol counterpart, **2**, by 9 kcal/mol. Simple carbonyl compounds are invariably more stable than their enol tautomers [1] but the opposite order of stability normally pertains for their ionized counterparts [23].

Given these results, we have performed some preliminary experiments to see if the ketonization of **2** can be achieved in the presence of a base. For these experiments we have selected pyrazole as the base. Pyrazole has a PA (214 kcal/mol [16b]) that satisfies the criterion proposed by Radom et al. for successful proton-transport catalysis

[4], i.e. its PA lies in between the PA values for protonation of $C_6H_5NHC(=O)CH_2^{\bullet}$ at **O** and **C**, 212 and 222 kcal/mol respectively (Section 7.3). Moreover, its IE (9.25 eV [16a]) lies below that of the enol (estimated as ≤ 7.5 eV). In a chemical ionization type experiment of caproanilide (CA) in the presence of an excess of pyrazole (PZ), the principal ions in the mass spectrum are observed at m/z 68 ($PZ^{\bullet+}$) (100%), m/z 69 (PZH^+) (55%), m/z 93 (40%), m/z 135 (enol **2**) (25%), m/z 191 ($CA^{\bullet+}$) (30%) and m/z 192 (CAH^+) (25%). Also present is a small peak (~ 1%) at m/z 203, the m/z value of the ion-molecule encounter complex between pyrazole and 2, [PZ/2] in the Scheme below.

The MI spectrum of the m/z 203 ion displays peaks at m/z 69 (PZH^+) (35%) and m/z 135 (100 %) respectively. These two processes also dominate the CID spectrum of the stable m/z 203 ions. If the initially generated ion-molecule encounter complex ions have the structure [PZ/**2**](a) in the Scheme below and direct proton-transport catalysis takes place, or else the base accepts a proton and donates another proton as indicated in the Scheme, complex [PZ/**1**] would be formed.

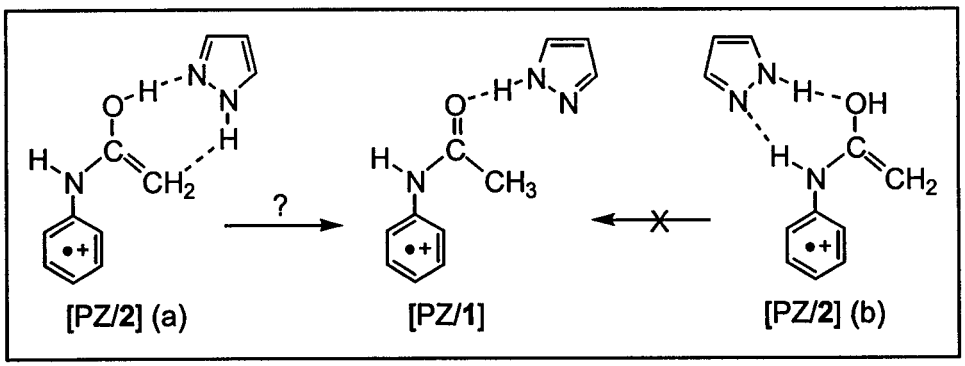

Scheme 7.3

To probe this possibility, we obtained the CID spectrum of the m/z 135 ions from the metastable m/z 203 complex ions. The spectrum is shown in Fig. 1, item (d). This spectrum clearly is that of **2**, not of **1**, indicating that the tautomerization **2** → **1** has not occurred in the complex. This does not necessarily mean that the transformation [PZ/**2**](a) → [PZ/**1**] is not feasible. An alternative explanation would be that we are dealing with complex ions of structure [PZ/**2**](b) rather than [PZ/**2**](a), see Scheme 7.3. In the complex [PZ/**2**](b) the pyrazole molecule interacts with the NH- and OH- groups of

2, that is, it is at the 'wrong' side of the ion to assist its ketonization. Further insight into this intriguing question could be obtained from calculations on the relative stability of the complexes and experiments with other bases. This point will be addressed in a future study.

Table 7.1. Reactions of metastable ions **1**, **2** and **4** and labelled isotopologues

Precursor ion	Loss →	$H^{\bullet}$	$D^{\bullet}$	HNCO	DNCO	C_2H_2O
$C_6H_5NHC(=O)CH_3^{\bullet+}$	**1**	-		-		100
$C_6H_5NHC(OH)=CH_2^{\bullet+}$	**2**	100		30		
$C_6H_5NDC(OH)=CH_2^{\bullet+}$		100	0.5	11	20	
$C_6H_5NHC(OD)=CH_2^{\bullet+}$		100	7	45	5	
$C_6H_5NHC(OH)=CD_2^{\bullet+}$		100	9	32	4	
$C_6D_5NHC(OH)=CH_2^{\bullet+}$		100	37	45	19	
$C_6H_5CH_2C(=O)NH_2^{\bullet+}$	**4**			100		
$C_6H_5CH_2C(=O)NHD^{\bullet+}$				44	100	
$C_6H_5CH_2C(=O)ND_2^{\bullet+}$					100	

Relative abundances were measured by metastable peak heights normalized to a value of 100 units for the most intense signal. The kinetic energy releases for the loss of $H^{\bullet}$ and HNCO from **2** are 35 and 185 meV.

Table 7.2. Relative energies, E_{rel}, of the acetanilide ion, **1**, its principal isomers and connecting transition states derived from B3LYP/CBSB7 calculations. The structures of the ions are presented in Schemes 7.1 and 7.2.

Ion	E_{total} [0 K]*	ZPVE	Erel	Transition State	E_{total} [0 K]*	ZPVE	Erel
1	-440.09382	95.73	0	TS **1** → **2**	-439.99937	92.55	56.1
1(rot)***	-440.09297	95.67	0.4	TS **1** → **5**	-440.04349	92.06	27.9
2	-440.08222	96.12	8.3**	TS **5** → **5**(rot)	-439.99346	94.55	61.8
2(rot)	-440.07592	95.92	11.4	TS **2** → **5**(rot)	-440.02200	92.70	42.1
2a	-440.06572	96.77	18.6	TS **2** → **3**	-440.02243	94.45	43.5**
2b	-440.02988	95.86	40.2	TS **2** → **2a**	-440.03460	95.39	36.9
2c	-440.09522	97.39	0.8	TS **2a** → **9H** + $H^{\bullet}$	-440.01410	92.31	46.1
3	-440.05287	95.93	25.9	TS **2a** → **2b**	-439.97138	93.03	74.1
3(rot)	-440.04552	94.96	29.5	TS **2a** → **3a**	-439.99165	93.14	61.5
3a	-440.06114	96.72	21.5	TS **3** → **3a**	-440.05149	96.03	26.9
3b	-440.05031	96.65	28.2	TS $\mathbf{3}^{\bullet+}$ → **3b**	-440.02851	92.40	37.7
4	-440.07744	95.78	10.3	TS **2** → **6**	-440.03482	92.47	33.7
5	-440.05092	95.64	26.8	TS **6** → **6**(rot)	-440.03648	94.22	34.5
5(rot)	-440.03954	95.92	34.3				
6	-440.05192	94.64	25.2				
6(rot)	-440.03828	94.66	33.8				
INC-**8a**	-440.05059	92.28	23.7				

* E_{total} in Hartrees, all other components, including the ZPVE scaled by 0.99, in kcal/mol.

** Relative energies derived from CBS-QB3 calculations using **1** as the anchor point for **2** and TS **2** → **3** are 9.5 and 43.3 kcal/mol respectively.

*** The notation "rot" refers to a rotational isomer of higher energy.

Notes and references

[1] B. Capon, B.-Z. Guo, F.C. Kwok, A. K. Siddhanta, Z. Zucco, Acc. Chem. Res. 21 (1988) 135.

[2] R.B. Woodward, R Hoffmann Angew Chem. Int. Ed. Eng. 8 (1969) 797.

[3] For an early review see: D.K. Bohme, Int. J. Mass Spectrom. Ion Processes 115 (1992) 95.

[4] A.J. Chalk, L. Radom, J. Am. Chem. Soc. 119 (1997) 7573.

[5] (a) P. Mourgues, J. Chamot-Rooke, G. van der Rest, H. Nedev, H.E. Audier, T.B. McMahon, Int. J. Mass Spectrom. 210/211 (2001) 429; (b) M.A. Trikoupis, P.C. Burgers, P.J.A. Ruttink, J.K. Terlouw, Int. J. Mass Spectrom. 210/211 (2001) 489; (c) M.A.Trikoupis, P.C. Burgers, P.J.A. Ruttink, J.K. Terlouw, Int. J. Mass Spectrom. 217 (2002) 97 and references cited therein.

[6] P.C. Burgers, J.K. Terlouw, Mass Spectrometry: Ion Structures in Mass Spectrometry, Encyclopedia of Spectroscopy and Spectrometry, J.C. Lindon, G.E. Tranter, J.L. Holmes Editors, Academic Press, London, 2000, 990-1000.

[7] For selected reviews see: D.J. McAdoo, T.H. Morton, Acc. Chem. Res. 26 (1993) 295; P. Longevialle, Mass Spectrom. Rev. 11 (1992) 157; R.D. Bowen, Acc. Chem Res. 24 (1991) 364.

[8] A.V. Robertson, C. Djerassi, J. Am. Chem Soc. 90 (1968) 6992; S. Hammerum, K.B. Tomer, C. Djerassi, Tetrahedron Lett. (1973) 915.

[9] K.B. Tomer, C. Djerassi, Tetrahedron 30 (1974) 17.

[10] J.K. Terlouw, H. Schwarz, Angew. Chem. Int. Ed. Engl. 26 (1987) 805.

[11] H.F. van Garderen, P.J.A. Ruttink, P.C. Burgers, G.A. McGibbon, J.K. Terlouw, Int. J. Mass Spectrom. Ion Processes 121 (1992) 159.

[12] The deuterated compounds were prepared by classical methods.

[13] J.L. Holmes, J.K. Terlouw, Org. Mass Spectrom. 15 (1980) 383.

[14] J.A. Montgomery Jr, M.J. Frisch, J.W. Ochterski, G.A. Petersson, J. Chem. Phys. 110 (1999) 2822; ibid. 112 (2000) 6532.

[15] M.J. Frisch, et al., GAUSSIAN Inc., Pittsburgh, PA, 1998

[16] (a) S.G. Lias, J.E. Bartmess, J.F. Liebman, J.L. Holmes, R.D. Levin, W.G. Mallard, J. Phys. Chem. Ref. Data 17 (1988) Suppl. 1; (b) E.P. Hunter, S.G. Lias, J. Phys. Chem. Ref. Data 27 (1998) 41.

[17] L.A. Curtiss, K. Raghavachari, G.W. Trucks, J.A. Pople , J. Chem. Phys. 94 (1991) 7221.

[18] C.E.C.A. Hop, K-J van den Berg, J.L. Holmes, J.K. Terlouw, J. Am. Chem. Soc. 111 (1989) 72.

[19] Ref. 16a proposes ΔH_f **1** = 161 kcal/mol, using ΔH_f $C_6H_5NH(C{=}O)CH_3$ (**1N**) = -31 ± 0.2 kcal/mol and IE **1N** = 8.30 eV. From the CBS-QB3 value of ΔH_f **1** and the experimental value of ΔH_f **1N** we derive IE **1N** = 8.50 eV. The UV photoelectron spectroscopy study of Ref. 20 proposes a vertical IE **1N** of 8.46 eV.

[20] R. Nakagaki, T. Kobayashi, S. Nagakura, Bull. Chem. Soc. Jpn. 53 (1980) 901.

[21] G. Bouchoux. Int. J. Mass Spectrom. Ion Phys. 26 (1978) 379.

[22] P.C. Burgers, J.K. Terlouw, K. Levsen, Org. Mass Spectrom. 17 (1982) 295.

[23] N. Heinrich, F. Louage, Ch. Lifshitz, H. Schwarz, J. Am. Chem. Soc. 110 (1988) 8183; The Chemistry of Enols; Z. Rappoport., Ed.; Wiley: New York (1990).

Chapter 8

Methyl radical loss from ionized sorbic acid $CH_3CH=CHCH=CHCOOH^{\bullet+}$: a hidden hydrogen rearrangement or a displacement process?

The electron impact mass spectrum of sorbic acid, $CH_3CH=CHCH=CHCOOH$, displays a prominent loss of $CH_3^{\bullet}$ which gives rise to the base peak at m/z 97. Metastable sorbic acid ions also readily lose $CH_3^{\bullet}$ along with $COOH^{\bullet}$. Tandem mass spectrometry based experiments in conjunction with computations at the CBS-QB3 level of theory were used to probe the mechanism for this reaction. The loss of $CH_3^{\bullet}$ is not a simple bond cleavage reaction nor a hidden hydrogen rearrangement (1,5-H shift) yielding ions of structure $HC\equiv C\text{-}CH=CH\text{-}C(OH)_2^{+}$. Instead, the molecular ion rearranges into a 6-membered ring from which $CH_3^{\bullet}$ is lost by direct bond cleavage to yield protonated 2*H*-pyran-2-one as the product ion. This displacement reaction has a slightly lower energy requirement than the competing loss of $COOH^{\bullet}$ yielding the $C_5H_7^{+}$ cyclopentenium ion.

The prominent losses of $CH_3^{\bullet}$ from $CH_3CH=CHCH=CHCOOC_2H_5^{\bullet+}$ (ethyl sorbate) and $COOH^{\bullet}$ from $HOOCCH=CH\text{-}CH=CHCOOH^{\bullet+}$ (muconic acid) occur via the same type of displacement reaction.

8.1. Introduction

In the interpretation of the electron impact (EI) mass spectra of organic compounds, it is often assumed that the loss of a radical from the molecular ion results from a direct bond cleavage reaction. However, this is not always the case : a hidden hydrogen (H) rearrangement or a displacement reaction can also lead to the loss of a radical, particularly if the product ion generated has a much higher thermodynamic stability.

A well documented example of a hidden H rearrangement [1-4] is the prominent loss of $CH_3^\bullet$ from ionized 2-methylbutyric acid, $CH_3CH_2CH(CH_3)COOH^{\bullet+}$. Schwarz *et al.* [1] established that the product ion generated by this loss is $H_2C{=}C(CH_3)C(OH)_2^+$, protonated methacrylic acid. The mechanism of this reaction involves two hidden H rearrangements. The molecular ion rearranges via an irreversible 1,4-H shift to the β-distonic ion $\mathbf{CH_3}C^\bullet HCH(CH_3)C^+(OH)_2$, which does not lose a methyl radical. The next step is a 1,2-H shift to form the enol ion $\mathbf{CH_3}CH_2C(CH_3){=}C(OH)_2^{\bullet+}$, which subsequently loses the γ-methyl radical ($\mathbf{CH_3}^\bullet$) to produce $H_2C{=}C(CH_3)C(OH)_2^+$.

A textbook example of a displacement process is the abundant loss of $CH_3^\bullet$ from the 1-chloro-pentane molecular ion, $CH_3CH_2CH_2CH_2CH_2Cl^{\bullet+}$ [5], whereby the chlorine atom becomes a divalent chloronium cation upon formation of a five-membered ring :

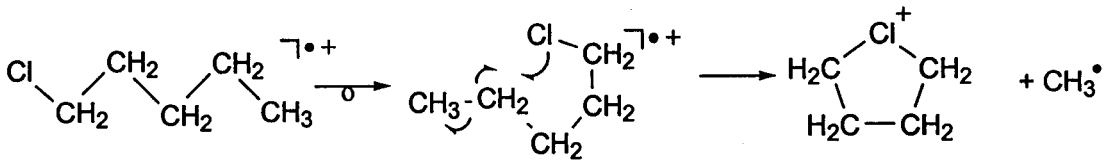

In view of the above, we report here on the mechanism of the prominent loss of $CH_3^\bullet$ from the sorbic acid molecular ion, $CH_3CH{=}CHCH{=}CHCOOH^{\bullet+}$. Sorbic acid is a common food preservative, whose synthesis was described more than a hundred years ago [6]. Its EI mass spectrum is in the NIST (National Institute of Standards and Technology) database but an analysis of the spectrum has not been reported. The spectrum in the database is of moderate quality as witnessed by the sizable peak at m/z 44 ($CO_2^{\bullet+}$) which is indicative of thermal decarboxylation of the sample during its

introduction into the ion source of the mass spectrometer. It is well known that the NIST database contains erroneous spectra, although the quality of the data has improved greatly over the past ten years [7]. The spectrum of Fig. 8.1 does not suffer from this problem, as it was obtained by introducing the sample at room temperature. The only discernible "impurity" in this spectrum is the peak at m/z 18, which stems from a trace of moisture in the sample.

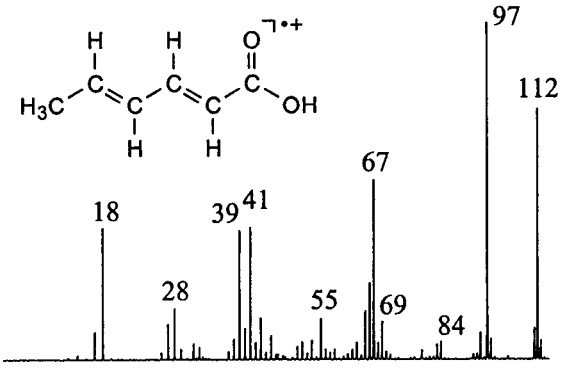

Fig. 8.1. 70 eV EI mass spectrum of sorbic acid.

The database spectrum and that of Fig. 8.1 both have m/z 97 as the base peak, signifying that the loss of $CH_3^\bullet$ from the sorbic acid molecular ion is the most important primary fragmentation reaction. A competing process is the loss of a $COOH^\bullet$ radical which gives rise to the prominent peak at m/z 67, $C_5H_7^+$. A naïve interpretation of these reactions is that they both represent a direct bond cleavage as depicted in Scheme 8.1.

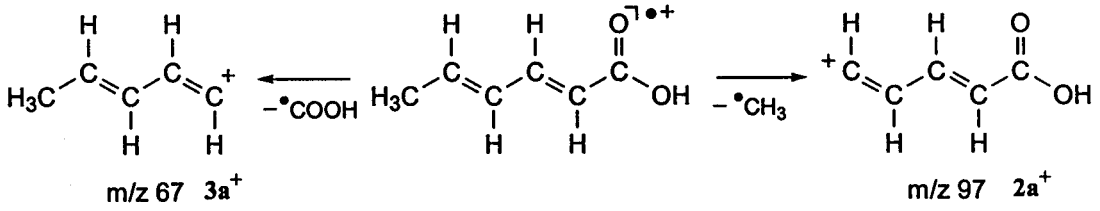

Scheme 8.1

However, the resulting product ions are substituted vinyl cations and such primary carbocations are known to have a very high heat of formation relative to other isomers.

A more plausible alternative for the $CH_3^\bullet$ loss involves a hidden H rearrangement as depicted in Scheme 8.2. The molecular ion rearranges into a distonic

ion via an energetically favourable 1,5-H shift, a McLafferty rearrangement, from which $CH_3^\bullet$ is lost by a direct bond cleavage to yield ion $\mathbf{2b}^+$. The positively charged carbon atom in this ion enjoys a considerable stabilization by the two hydroxyl groups.

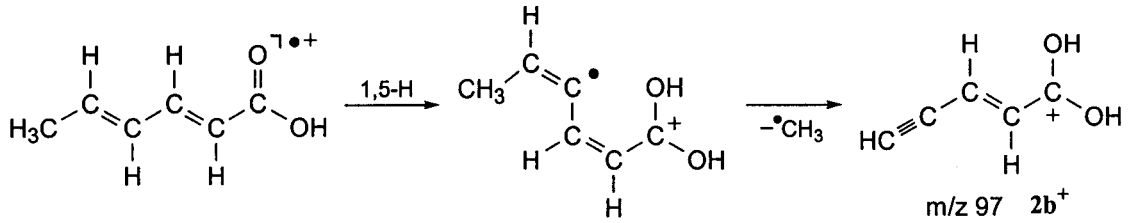

Scheme 8.2

However, the $CH_3^\bullet$ loss could also occur via a displacement process akin to the loss of $CH_3^\bullet$ from ionized 1-chloro-pentane discussed above, as depicted in Scheme 8.3.

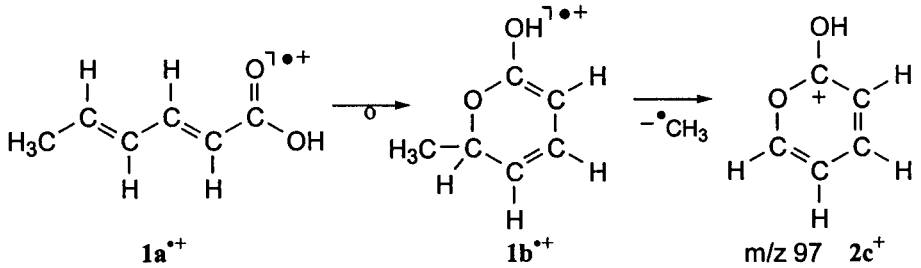

Scheme 8.3

The cyclic product ion generated in this reaction, carbonyl protonated *2H*-pyran-2-one ($\mathbf{2c}^+$), is also expected to be quite stable. The positively charged carbon atom enjoys the same stabilization as that in ion $\mathbf{2b}^+$ and moreover, the ion has several energetically attractive resonance structures.

To probe these mechanistic proposals for the $CH_3^\bullet$ loss from the sorbic acid molecular ion, a variety of tandem mass spectrometry experiments [8] were performed in conjunction with computations using the CBS-QB3 model chemistry.

8.2. Experimental

The samples used in this study were obtained from Aldrich and used without further purification. The experiments were performed on a VG Analytical ZAB-R mass spectrometer of BEE geometry (B = magnet, E = electric sector). Ions were generated by electron ionization (EI) or chemical ionization (CI) and accelerated by 6, 8 or 10 keV. Most of the samples were introduced into the ion source (kept at 100 °C) via a wide-bore all-quartz direct insertion probe connected via an o-ring with a small glass bulb that contains the sample. The sample reservoir was kept at ambient temperature for the analysis of sorbic acid and 2*H*-pyran-2-one and cooled for the introduction of ethyl sorbate. The *trans,trans*-muconic acid was introduced via a direct solid insertion probe. The solid probe tube (glass, 15 mm, f = 1 mm) was filled with tightly packed sample (c 15 mg) and was introduced into the ion source such that the tip of the capillary just protruded into the source, which was kept at 170 °C.

Metastable ion (MI) mass spectra were recorded in the second field-free region (2ffr). Collision induced dissociation (CID) mass spectra were recorded in the 2ffr and third field-free region (3ffr), using oxygen as the collision gas. The quoted kinetic energy releases refer to $T_{0.5}$ values derived from the width at half-height of the appropriate metastable peaks, by means of the standard one-line equation, with no correction for the width of the main beam [9]. All spectra were recorded using a small PC-based data system developed by Mommers Technologies Inc. (Ottawa).

The calculations were performed using Gaussian 98 revision A.9 [10]. The standard CBS-QB3 model chemistry [11] was used to probe structures and energies of the key ions, connecting transition states and associated dissociation products. The energetic results are presented in Table 8.1 and in the energy diagram of Scheme 8.5. Frequency calculations gave the correct number of negative eigenvalues for all minima and transition states and the spin contamination was within the acceptable range. The connections of the transition states have been checked by geometry optimizations and frequency calculations.

8.3. Results and Discussion

As mentioned in the introduction, the EI mass spectrum of sorbic acid is characterized by the primary fragment ions at m/z 97 (loss of $CH_3^\bullet$) and m/z 67 (loss of $COOH^\bullet$). The metastable ion (MI) spectrum of the molecular ion, which reflects the dissociations of low energy ions, also features peaks at m/z 97 (base peak) and m/z 67 (40% of the base peak). This strongly indicates that these fragment ions result from rearrangement reactions. Moreover, the fairly large kinetic energy release associated with the $CH_3^\bullet$ loss, $T_{0.5}$ = 110 meV, is not compatible with a simple bond cleavage reaction.

Table 8.1. Enthalpies of formation (kcal/mol) of the sorbic acid molecular ion, $\mathbf{1a}^{\bullet+}$, its dissociation products and selected transition states derived from CBS-QB3 calculations.

Ion / neutral		m/z	E_{total}*[0 K] Hartree	ZPVE	$\Delta H°_f$ [0 K]	$\Delta H°_f$ [298 K]	$\Delta H°_f$ [expt]	Ref
trans,trans-2,4-hexadienoic acid$^{\bullet+}$	$\mathbf{1a}^{\bullet+}$(t,t)	112	-382.93823	78.91	138	132		
trans,cis-2,4-hexadienoic acid$^{\bullet+}$	$\mathbf{1a}^{\bullet+}$(t,c)	112	-382.93521	79.08	140	134		
cis,trans-2,4-hexadienoic acid$^{\bullet+}$	$\mathbf{1a}^{\bullet+}$(c,t)	112	-382.93735	78.93	138	133		
cyclic sorbic acid$^{\bullet+}$	$\mathbf{1b}^{\bullet+}$	112	-382.96871	81.31	120	113		
trans,trans-2,4-hexadienoic acid	**1a**(t,t)		-383.26374		-66	-72	-70	[a]
CH_2=C-CH=CH-COOH$^+$	$\mathbf{2a_1}^+$	97	-343.08227	53.65	171	168		
HC≡C-CH=CH-C(OH)$_2^+$	$\mathbf{2b}^+$	97	-343.10595	55.38	156	153		
protonated *2H*-pyran-2-one	$\mathbf{2c}^+$	97	-343.17027	57.93	116	112		
$CH_3^\bullet$			-39.74479	18.37	37	36		
2H-pyran-2-one			-342.84459	49.70	-45	-48	-46	[a]
CH=CH-CH=CH-CH_3^+	$\mathbf{3a_1}^+$	67	-193.97857	61.62	237	233		
cyclopentenium cation	$\mathbf{3b}^+$	67	-194.02338	64.40	209	204	201	[b]
$COOH^\bullet$			-188.86832	13.05	-44	-45	-46	[c]

[a] Calculated using Benson additivity terms (N. Cohen and S.W. Benson, Chem. Rev. 93 (1993) 2419.

[b] Using $\Delta H°_f$ (cyclopentadiene) = 31 kcal/mol [12a] and PA (cyclopentadiene) = 196.4 [12b], the value based on appearance energy measurements is 199 kcal/mol [12a].

[c] Experimental value derived from appearance energy measurements : J.L. Holmes, F.P. Lossing and P.M. Mayer, J. Am. Chem. Soc. 113 (1991) 9723.

In line with this, the associated product ion, $\mathbf{2a}^+$, is calculated to have a much higher heat of formation than the rearrangement product ions $\mathbf{2b}^+$ and $\mathbf{2c}^+$, see Table 8.1. In fact, ion $\mathbf{2a}^+$ is not even a minimum on the potential energy surface : in the geometry optimization it collapses by a 1,2-H shift into CH_2=C-CH=CH-$COOH^+$, $\mathbf{2a_1}^+$ (similarly the primary vinyl cation $\mathbf{3a}^+$ yields $\mathbf{3a_1}^+$ upon geometry optimization).

However, the rearrangement product ions $\mathbf{2b}^+$ and $\mathbf{2c}^+$ are also considerably different in energy : ion $\mathbf{2c}^+$ is more stable than its isomer $\mathbf{2b}^+$, by 40 kcal/mol. From the computational results of Table 8.1, it follows that the competing dissociation $\mathbf{1a}^{\bullet+} \rightarrow C_5H_7^+ + COOH^\bullet$ has a minimum energy requirement of 159 kcal/mol, assuming that the product ion is the most stable $C_5H_7^+$ isomer, the cyclopentenium ion, $\mathbf{3b}^+$. This reaction may well take place at the thermochemical threshold because the associated kinetic energy release is small, $T_{0.5}$ = 20 meV. If this is indeed the case, the hidden H rearrangement $\mathbf{1a}^{\bullet+} \rightarrow \mathbf{2b}^+ + CH_3^\bullet$ cannot effectively compete with the $COOH^\bullet$ loss because its minimum energy requirement, 189 kcal/mol, is far too high. On the other hand, the minimum energy requirement for the displacement reaction $\mathbf{1a}^{\bullet+} \rightarrow \mathbf{2c}^+ + CH_3^\bullet$, 148 kcal/mol, is lower than that for loss of $COOH^\bullet$ and thus this pathway is the only plausible option.

In this context, we note that the minimum energy requirement for the two competing reactions is in principle experimentally accessible via the measurement of the appearance energies (AEs) of the metastable peaks [13]. Unfortunately, such an experiment cannot be performed with our instrumentation. Furthermore, although isomeric product ions can often be differentiated on the basis of their CID spectra, this does not hold true for the $C_5H_7^+$ system of ions [14].

To probe the structure of the m/z 97 ion generated from the sorbic acid molecular ion, we obtained its CID spectrum, see Fig. 8.2 (a). We also obtained the CID spectrum of ion $\mathbf{2c}^+$ generated from protonated 2*H*-pyran-2-one under chemical ionization (CI) conditions, see Fig. 8.2 (b). Protonation of 2*H*-pyran-2-one is expected to occur at the site with the highest proton affinity, the carbonyl oxygen atom, yielding ions of structure $\mathbf{2c}^+$. A comparison of the CID spectra shows that they are virtually the same, indicating that we are dealing with ions of the same structure.

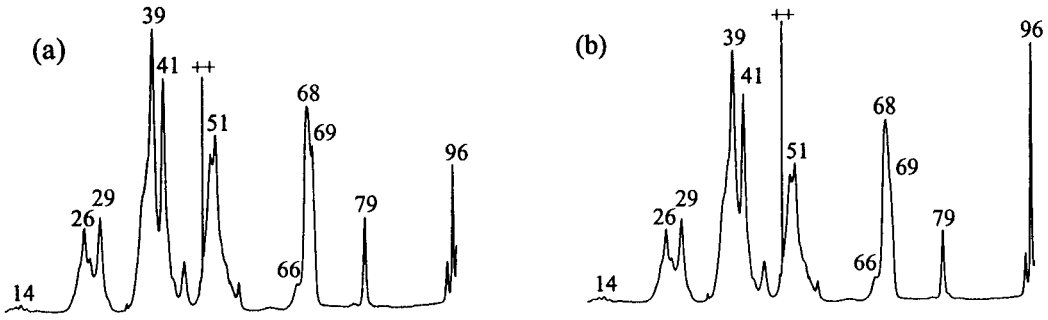

Fig. 8.2. (a) CID mass spectrum from *m/z* 97 of sorbic acid. **(b)** CID mass spectrum of protonated 2*H*-pyran-2-one.

We note that the CID spectra contain peaks at m/z 79 (loss of H_2O), m/z 69 (loss of CO) and m/z 68 (loss of CHO), in support of the proposal that the ions do have the structure of $\mathbf{2c}^+$. The remaining fragment ions may result from secondary fragmentations. These findings lead us to propose that the losses of $CH_3^\bullet$ and $COOH^\bullet$ from the sorbic acid molecular ions occur via the mechanisms presented in Scheme 8.4.

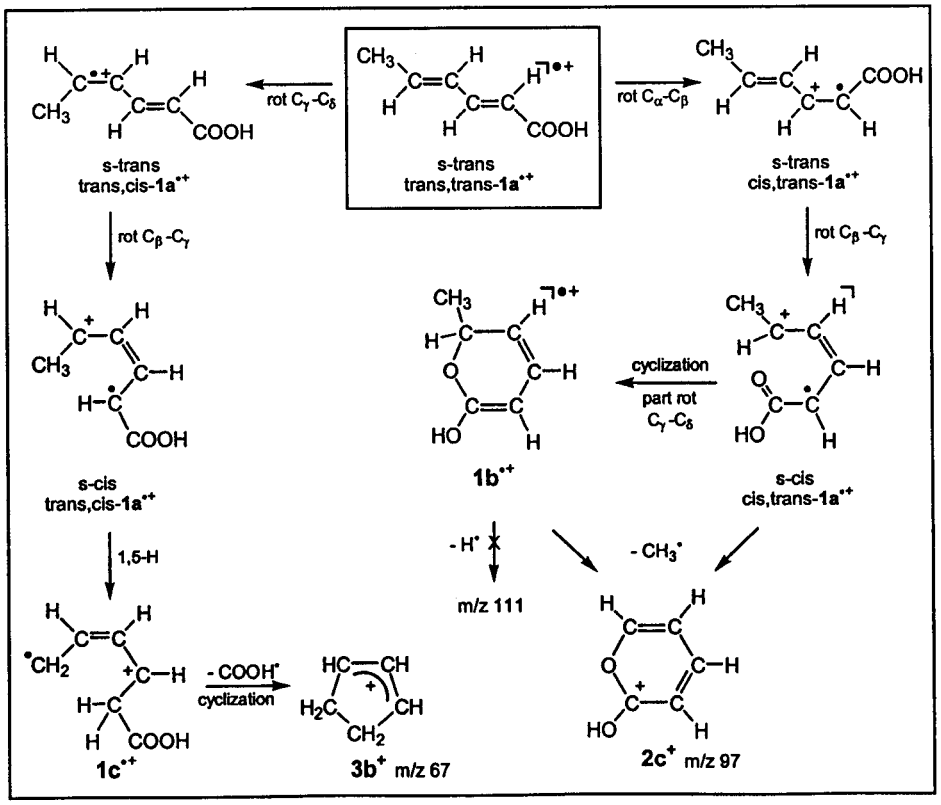

Scheme 8.4

Sorbic acid has a calculated ionization energy (IE) of 8.8 eV, see Table 8.1. This relatively low value is compatible with the removal of an electron from the π_{cc} system rather than carboxyl group [12a]. The first step of this mechanism involves rotation of either the C_α-C_β or the C_γ-C_δ bond in sorbic acid molecular ions **1a**$^{\bullet+}$ having the trans,trans-configuration. This yields the isomers cis,trans-**1a**$^{\bullet+}$ or trans,cis-**1a**$^{\bullet+}$, which likely have energies comparable to the trans,trans-**1a**$^{\bullet+}$ isomer. However, these rotations may well be associated with high barriers. For example, the 60 kcal/mol energy barrier associated with the rotation of the CH_2 group in CH_2=CH-CH=CH_2 is reduced when an electron is removed from the π_{cc} bond to form the radical cation, but only to ~ 30 kcal/mol [15]. In the next step, the s-trans conformers rearrange into their s-cis counterparts, via rotation of the C_β-C_γ single bond. This conversion is expected to have a fairly low energy barrier : in neutral butadiene it only requires 5 kcal/mol, in its radical cation the value is expected to be slightly higher, because the C_β-C_γ bond may now have some double bond character.

Loss of $CH_3^\bullet$ from the s-cis conformer of the cis,trans-**1a**$^{\bullet+}$ ion may then occur upon attack of the carbonyl oxygen atom at the C_δ atom yielding the cyclic product ion **2c**$^+$. Alternatively, the attack may lead to formation of the cyclic intermediate **1b**$^{\bullet+}$ from which $CH_3^\bullet$ is lost by a single bond cleavage.

The competing loss of COOH$^\bullet$ may occur from s-cis conformer of the trans,cis-**1a**$^{\bullet+}$ ion, which could generate ion **1c**$^{\bullet+}$ via a facile 1,5-H shift. Cyclization of **1c**$^{\bullet+}$ with the concomitant displacement of COOH would then lead to loss of COOH$^\bullet$ and formation of the $C_5H_7^+$ cyclopentenium ion.

To support this mechanistic proposal, we have probed the energetics of the key components using the CBS-QB3 model chemistry, see Table 8.1 and the energy diagram in Scheme 8.5. In this Scheme the dotted energy levels represent an estimate of the energy of the activation energy for the two reactions based upon the metastable ion characteristics of **1a**$^{\bullet+}$. So far the calculation of the various transition states has not been successful.

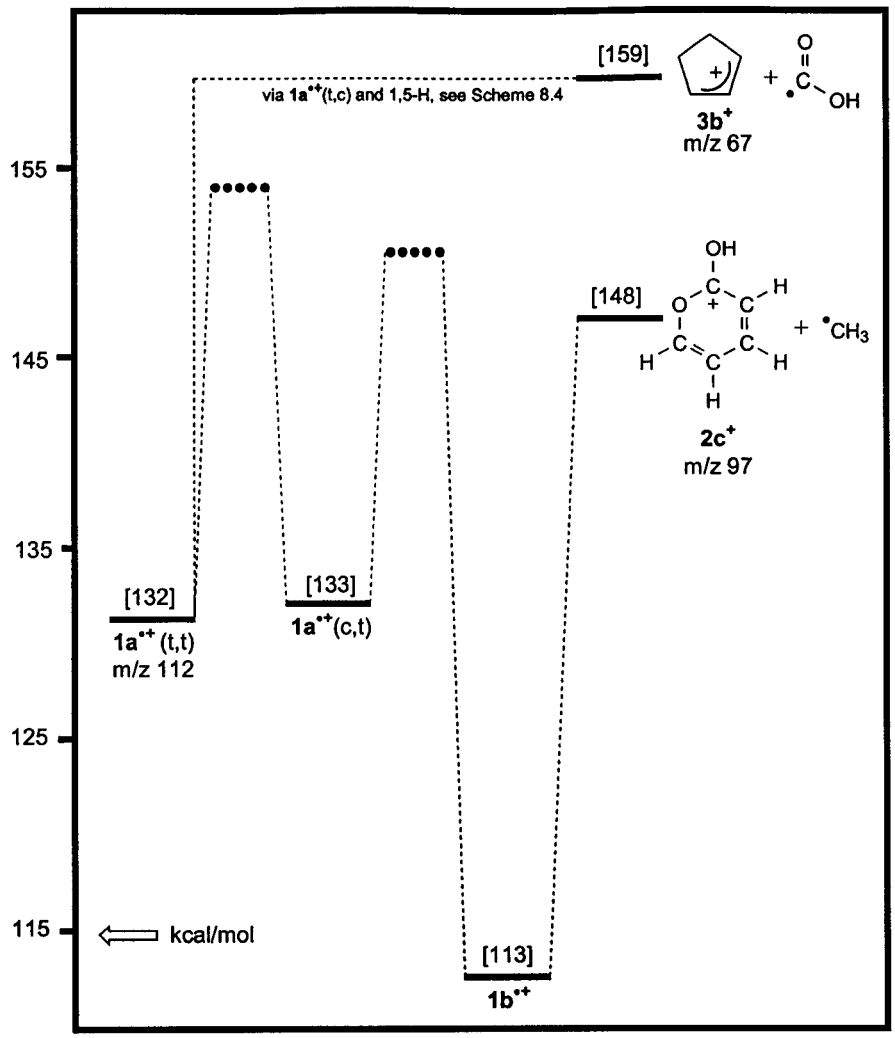

Scheme 8.5

The above observations raise the intriguing question whether the cyclization mechanism of Scheme 8.3 also holds true for the prominent radical losses from the molecular ions of related compounds. Two prime candidates are trans,trans-muconic acid and ethyl sorbate which show a prominent peak for the loss of $COOH^{\bullet}$ and $CH_3^{\bullet}$ respectively in their EI mass spectra. As depicted in Scheme 8.6, loss of $COOH^{\bullet}$ from ionized muconic acid, $\mathbf{4}^{\bullet+}$, could yield m/z 97 product ions of structure $\mathbf{2c}^{+}$, whereas loss of $CH_3^{\bullet}$ from ionized ethyl sorbate, $\mathbf{5}^{\bullet+}$, would yield m/z 125 ions having the structure of the ethylated $\mathbf{2c}^{+}$ ion.

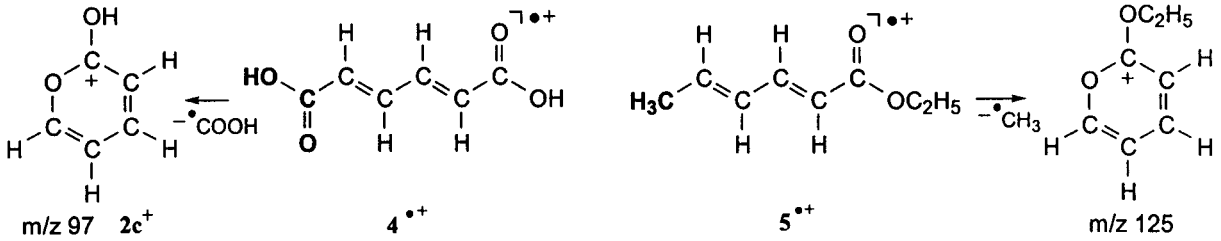

Scheme 8.6

The MI spectrum of the muconic acid molecular ion, $\mathbf{4}^{\bullet+}$, has m/z 97 as the base peak, confirming that loss of COOH$^{\bullet}$ is also an important dissociation of the low energy ions. This again indicates that we are dealing with a rearrangement reaction. The CID spectra (not shown) of the m/z 97 ions generated from low- and high-energy ions $\mathbf{4}^{\bullet+}$ are both closely similar to the spectrum of protonated *2H*-pyran-2-one, $\mathbf{2c}^{+}$, shown in Fig. 8.2. This provides compelling evidence that the loss of COOH$^{\bullet}$ from ionized muconic acid occurs via a displacement mechanism akin to that proposed for sorbic acid in Scheme 8.3.

In the same vein, the MI spectrum of the ethyl sorbate molecular ion, $\mathbf{5}^{\bullet+}$, has m/z 125 as the base peak, confirming that loss of $CH_3^{\bullet}$ is also an important dissociation of the low energy ions. The CID spectrum (not shown) of the m/z 125 ions has m/z 97 as the base peak. These m/z 97 ions are clearly ions $\mathbf{2c}^{+}$ because their CID spectrum appears to be indistinguishable from that of protonated *2H*-pyran-2-one. This strongly indicates that the m/z 125 ions are ethylated ions $\mathbf{2c}^{+}$, which lose C_2H_4 (via a β H-transfer) upon collisional activation, see Scheme 8.7 :

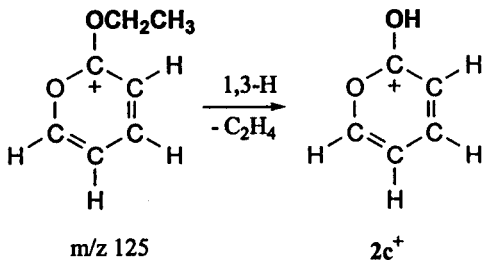

Scheme 8.7

Thus, it is likely that the prominent loss of $CH_3^{\bullet}$ from ethyl sorbate ions also takes place via a displacement process akin to that proposed for sorbic acid in Scheme 8.3.

References

[1] T. Weiske and H. Schwarz, Tetrahedron **42** (1986) 6245.
[2] P. C. Burgers and J. K. Terlouw, Mass Spectrometry **10** (1989) 35.
[3] D. Suh, P. C. Burgers and J. K. Terlouw, Int. J. Mass Spectrom. Ion Proc. **144** (1995) L1.
[4] R. Thissen, C. Alcaraz, O. Dutuit, P. Mourgues, J. Chamot-Rooke and H. E. Audier, J. Phys. Chem. A. **103** (1999) 5049.
[5] F.W. McLafferty and F. Tureček, Interpretation of Mass Spectra, University Science Books, California, (1993) pages. 78, 165, 213-218.
[6] E. Luck, Deutsche Lebensmittel-Rundschau **81** (1985) 287.
[7] P. Ausloos, C. L. Clifton, S.G. Lias, A.I. Mikaya, S.E. Stein, D.V. Tchekhovskoi, O.D. Sparkman, V. Zaikin and D. Zhu, J. Amer. Soc. Mass Spectrom. **10** (1999) 287.
[8] H. F. van Garderen, P. J. A. Ruttink, P. C. Burgers, G. A. McGibbon and J. K. Terlouw, Int. J. Mass Spectrom. Ion Processes **121** (1992) 159.
[9] J.L. Holmes and J.K. Terlouw, Org. Mass Spectrom. 15 (1980) 383.
[10] M.J. Frisch et al., Gaussian 98, Revision A.9, Gaussian, Inc.: Pittsburgh, PA, 1998.
[11] (a) J.A. Montgomery Jr, M.J. Frisch, J.W. Ochterski, G.A. Petersson, J. Chem. Phys. **110** (1999) 2822; (b) ibid. **112** (2000) 6532.
[12] S. G. Lias, J. E. Bartmess, J. F. Liebman, J. L. Holmes, R. D. Levin and W. G. Mallard, *Gas Phase Ion and Neutral Thermochemistry*, American Chemical Society & The American Institute of Physics for the National Bureau of Standards, New York (1988).
[13] P.C. Burgers and J.L. Holmes, Org. Mass Spectrom.**17** (1982) 123.
[14] (a) P. Wolkoff and J. L. Holmes, Adv. Mass Spectrom. **8A** (1980) 743; (b) P. Wolkoff and J. L. Holmes, Can. J. Chem. **57** (1978) 348; (c) P. Wolkoff, J. L. Holmes, F. P. Lossing, Can. J. Chem. **58** (1980) 251.
[15] H. Beyer, W. Walter, Lehrbuch der Organischen Chemie, S. Hirzel Verlag, Stuttgart, Ch. 2, p. 107.

Chapter 9

The chemistry of some low energy $C_5H_9O^+$ oxonium ions

The reactions of the low energy oxonium ions $CH_3CH{=}CH\text{-}C^+(H)OCH_3$, $\mathbf{b_1}^+$, $CH_2{=}CH\text{-}C^+(CH_3)OCH_3$, $\mathbf{b_2}^+$, and $CH_2{=}C(CH_3)\text{-}C^+(H)OCH_3$, $\mathbf{b_3}^+$, are reported and compared with those of their 1,3-H shift isomers $CH_3CH{=}CHCH_2OCH_2^+$, $\mathbf{b_4}^+$, $CH_2{=}CHCH(CH_3)OCH_2^+$, $\mathbf{b_5}^+$, and $CH_2{=}C(CH_3)CH_2OCH_2^+$, $\mathbf{b_6}^+$. The metastable ion (MI) spectrum of the $C_4H_6OCH_3^+$ ions $\mathbf{b_1}^+$ - $\mathbf{b_3}^+$ is dominated by loss of CH_2O. Elimination of C_3H_6, which is associated with a composite metastable peak, is also significant from $\mathbf{b_2}^+$ and $\mathbf{b_3}^+$.

From (multiple) collision experiments and analysis of D- and ^{13}C-labelled isotopologues, it follows that $\mathbf{b_1}^+$ - $\mathbf{b_3}^+$ do not readily interconvert. Loss of CH_2O is proposed to involve a 1,5-H shift followed by a (dipole-assisted) 1,3-H shift into an energy-rich ion-neutral complex (INC) $[C_4H_7^+/CH_2{=}O]$. Loss of CH_2O from $\mathbf{b_4}^+$ - $\mathbf{b_6}^+$ may also occur via an INC. This reaction is associated with a very small kinetic energy release, indicating that it generates the most stable $C_4H_7^+$ ion, $CH_2{=}CHC^+(H)CH_3$, at the thermochemical threshold. However, this process is only prominent for ions $\mathbf{b_5}^+$, which also undergo a facile loss of H_2O, via rearrangement in the INC $[C_4H_7^+/ CH_2{=}O]$, to yield $C_5H_7^+$ (most probably the cyclopentenyl cation). Loss of C_3H_6 and CO dominates the MI spectra of $\mathbf{b_4}^+$ and $\mathbf{b_6}^+$ and these reactions, which also occur from $\mathbf{b_5}^+$, are proposed to take place from 1,2-H shift isomers of the cyclic counterparts of $\mathbf{b_4}^+$ - $\mathbf{b_6}^+$.

The behaviour of $\mathbf{b_1}^+$ - $\mathbf{b_3}^+$ and $\mathbf{b_4}^+$ - $\mathbf{b_6}^+$ differs considerably from their $C_4H_7O^+$ homologues, $CH_2{=}CH\text{-}C^+(H)OCH_3$, $\mathbf{a_1}^+$, and $CH_2{=}CHCH_2OCH_2^+$, $\mathbf{a_2}^+$. Differences in the dissociation characteristics of the $C_nH_{2n-2}OCH_3^+$ species (n = 3 - 5) are discussed in terms of the energetics of the products that may be formed. ΔH_f (298 K) values for the key ions in this study were obtained from CBS-QB3 calculations and thermochemical estimates.

The work described here has been published previously in an article under the same title: R. D. Bowen, L.N. Heydorn and Johan K. Terlouw, Int. J. Mass Spectrom. **209** (2001) 153-169.

9.1. Introduction

The chemistry of $C_nH_{2n+1}O^+$ oxonium ions has been intensively studied, particularly for n = 1-5 [1]. In contrast, $C_nH_{2n-1}O^+$ oxonium ions have been given relatively little attention [2-7]. In the dissociation of the $C_4H_7O^+$ metastable ions CH_2=CH-C^+(H)OCH_3, $\mathbf{a_1}^+$, and CH_2=$CHCH_2OCH_2^+$, $\mathbf{a_2}^+$, double or triple H-transfer reactions feature prominently [7]. Both these ions lose CO in high abundance, but this reaction is rarely, if ever, observed from $C_nH_{2n+1}O^+$ oxonium ions. The associated composite metastable peak indicates the presence of competing reaction channels, one of which is characterized by a large kinetic energy release (KER) [8].

Whereas metastable ions $\mathbf{a_2}^+$ expel essentially only CO, ions $\mathbf{a_1}^+$ eliminate CO and CH_2O at similar rates. Moreover, the ratio of CH_2O to CO loss from $\mathbf{a_1}^+$ decreases as the average internal energy of the dissociating ions increases. In addition, H_2O loss also occurs, though much less readily than CO expulsion.

From D- and ^{13}C-labelling experiments, it follows that the C atom of the CH_3O group is included in the CH_2O lost from $\mathbf{a_1}^+$, but there is some exchange of the H atoms of this substituent prior to dissociation. On the other hand, the C atom of the OCH_3 group is not always retained in the eliminated CO : both CO and ^{13}CO are lost from metastable $\mathbf{a_1}^+$ [$O^{13}CH_3$] ; furthermore, the metastable peaks for CO and ^{13}CO loss are both composite. Consequently, CO loss from $\mathbf{a_1}^+$ proceeds via more than one mechanism. The minor route involves expulsion of CO derived from the OCH_3 group by a formal triple H-transfer ; but the major channel entails a skeletal rearrangement and cleavage of the OCH_3 bond.

In view of this intriguing reactivity of $\mathbf{a_1}^+$ and $\mathbf{a_2}^+$, a study of the chemistry of the next higher homologues of these $C_4H_7O^+$ ions seemed worthwhile. This paper reports the reactions of six $C_5H_9O^+$ ions : $\mathbf{b_1}^+$ - $\mathbf{b_3}^+$, homologues of $\mathbf{a_1}^+$, as well as $\mathbf{b_4}^+$ - $\mathbf{b_6}^+$, homologues of $\mathbf{a_2}^+$, see Scheme 9.1, and compares their chemistry with that of other $C_nH_{2n-1}O^+$ oxonium ions. The numbers in square parentheses in Scheme 9.1 refer to 298 K enthalpy values in kcal/mol. They were obtained from computational chemistry (numbers in bold) and/or by estimation, as discussed in the Section 8.2.

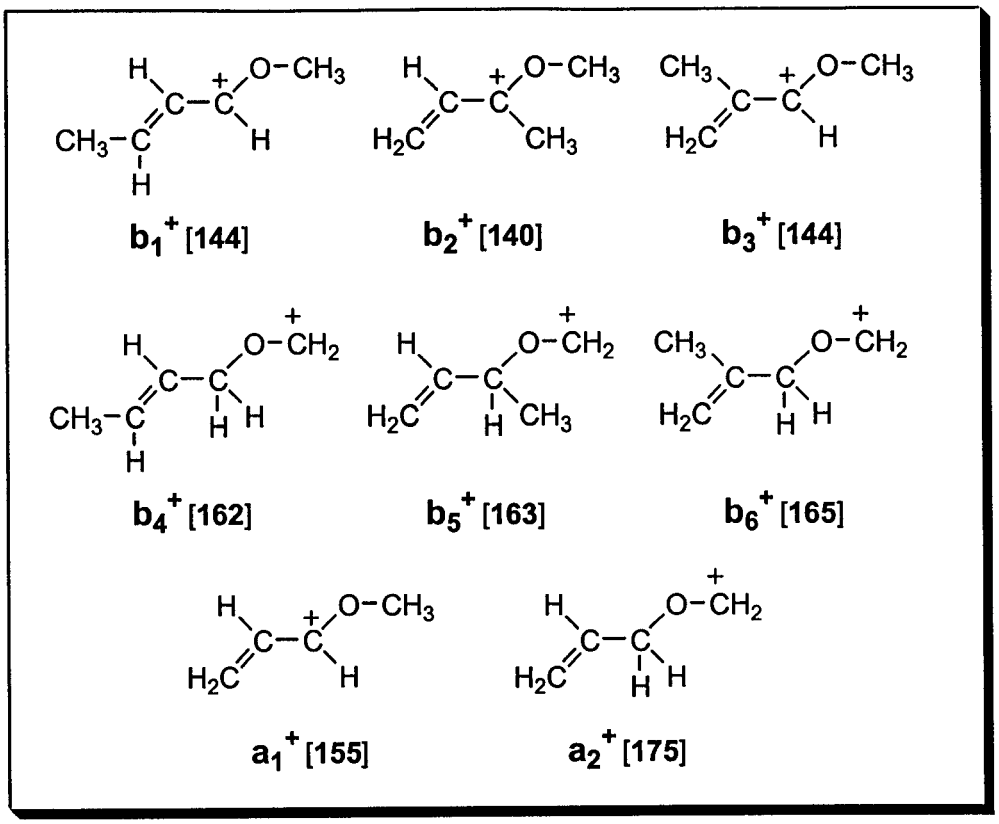

Scheme 9.1

9.2. Experimental and Theoretical

All mass spectrometric experiments were performed on the VG Analytical ZAB-R mass spectrometer. Details of the geometry of this three-sector (BEE) instrument have been reported elsewhere [23]. Data on the dissociation of metastable ions in the second field-free region (ffr) were obtained from MI spectra [8]. The quoted spectra are integrated data, compiled from 2-5 individual scans. Typical operating conditions were 70 eV ionising electron energy and 8 or 10 kV accelerating voltage. The KERs were estimated from the width at half-height of the appropriate metastable peak, by means of the standard one-line equation after applying the usual correction for the width at half-height of the main beam [8].

The CID spectra of the $C_5H_9O^+$ ions of Fig. 9.1 were obtained in the 2ffr with oxygen as the collision gas. The CID spectra of the $C_2H_3O^+$ ions generated from dissociation of metastable ions $\mathbf{a_2}^+$, $\mathbf{b_2}^+$ and $\mathbf{b_3}^+$ in the 2ffr were obtained in the 3ffr

using O_2 as the collision gas and mass selected ions of 10 keV translational energy. The neutralisation-reionisation mass spectra were obtained in the 2ffr, using N,N-dimethylaniline as the reducing agent and oxygen gas for reionisation. All spectra were recorded using a small PC-based data system developed by Mommers Technologies Inc. (Ottawa).

The oxonium ions studied in this work were generated by dissociative ionisation of the appropriate alkenyl methyl ethers. Illustrative examples of the synthesis of these ethers have been described in detail [24].

The (298K) enthalpy values for ions $\mathbf{a_1}^+$, $\mathbf{a_2}^+$, $\mathbf{b_1}^+$ - $\mathbf{b_6}^+$, see Scheme 9.1, and $\mathbf{b_7}^+$ - $\mathbf{b_9}^+$, see Scheme 9.2a, were obtained from computations involving standard CBS-QB3 model chemistry [25] with the Gaussian 98 suite of programs [26]. The detailed geometries of the various species are available upon request. Frequency calculations gave the correct number of negative eigenvalues for all minima.

ΔH_f values for the cyclic isomers c-$\mathbf{b_4}^+$ and c-$\mathbf{b_6}^+$ were estimated from the enthalpies of the 2-and 1-methyl-cyclopentyl cations, 179 and 170 kcal/mol respectively [12, 22], and the effect of O substitution at a non-charge-bearing group, - 25 kcal/mol, as given by $\Delta(\Delta H_f)$ cyclopentane and tetrahydrofuran. ΔH_f [c-$\mathbf{b_5}^+$] is expected to be close to that of the c-$\mathbf{b_4}^+$ isomer.

For c-$\mathbf{b_{5a}}^+$ and c-$\mathbf{b_{6a}}^+$, enthalpy values were derived from the PA of 5- and 4-methyl-2,3-dihydrofuran, 207.6 and 217.6 kcal/mol respectively [22], and the closely similar ΔH_f values of the corresponding neutral molecules, - 30 kcal/mol, as obtained from the Benson additivity method [27]. ΔH_f [c-$\mathbf{b_{4a}}^+$] can reasonably be expected to be close to that of the c-$\mathbf{b_{6a}}^+$ isomer.

9.3. Results and Discussion

The reactions of the metastable ions $\mathbf{b_1}^+$ - $\mathbf{b_6}^+$, are summarised in Table 9.1. Generation of $\mathbf{b_2}^+$ is readily achieved by ionization and alkyl radical loss from the tertiary alkenyl methyl ethers CH_2=CHCR(CH_3)OCH_3 (R = CH_3, C_2H_5). The production of $\mathbf{b_1}^+$ and $\mathbf{b_3}^+$ is not so straightforward, because isomerization of ionised primary and

secondary alkenyl methyl ethers sometimes precedes $CH_3^\bullet$ expulsion. However, $\mathbf{b_1}^+$ and $\mathbf{b_3}^+$ may be obtained by $C_2H_5^\bullet$ loss from ionised $CH_3CH{=}CHCH(C_2H_5)OCH_3$ and $CH_2{=}C(CH_3)CH(C_2H_5)OCH_3$ [9].

Earlier research [9a,b] has shown that $\mathbf{b_1}^+$ is produced by $CH_3^\bullet$ elimination from $(CH_3)_2C{=}CHCH_2OCH_3^{\bullet+}$ or $CH_2{=}C(CH_3)CH_2CH_2OCH_3^{\bullet+}$; $\mathbf{b_3}^+$ is similarly formed from $C_2H_5CH{=}CH(CH_3)OCH_3^{\bullet+}$ or $CH_3CH{=}CH(CH_3)CH_2OCH_3^{\bullet+}$. Moreover, $CH_3^\bullet$ loss from $CH_2{=}CHCH(C_2H_5)OCH_3^{\bullet+}$ and $CH_2{=}C(C_2H_5)CH_2OCH_3^{\bullet+}$ also affords $\mathbf{b_3}^+$. These specific fragmentations allow $\mathbf{b_1}^+$ and $\mathbf{b_3}^+$ to be generated from several precursors, see Table 9.1.

Table 9.1. Relative abundances [a] and kinetic energy releases [b] for the main dissociations of metastable $C_5H_9O^+$ ions

Precursor molecule		Loss→ Ion	CH_2O		C_3H_6		H_2O		CO	
$CH_3CH{=}CHCH(C_2H_5)OCH_3$	**1a**	$\mathbf{b_1}^+$	100	[33]	2	[20/380]*	2	[47]	1	[c]
$(CH_3)_2C{=}CHCH_2OCH_3$	**1b**	$\mathbf{b_1}^+$	100	[32]	3	(3:1)	1		2	
$CH_2{=}C(CH_3)CH_2CH_2OCH_3$	**1c**	$\mathbf{b_1}^+$	100	[33]	5		2		3	
$CH_2{=}CHC(CH_3)_2OCH_3$	**2a**	$\mathbf{b_2}^+$	100	[19]	25	[20/380]*	1	[41]	1	[c]
$CH_2{=}CHC(CH_3)(C_2H_5)OCH_3$	**2b**	$\mathbf{b_2}^+$	100	[19]	30	(1:1)	1	[34]	1	
$CH_2{=}C(CH_3)CH(C_2H_5)OCH_3$	**3a**	$\mathbf{b_3}^+$	100	[25]	20	[20/380]*	3	[37]	10	[c]
$CH_3CH_2CH{=}CHCH_2OCH_3$	**3b**	$\mathbf{b_3}^+$	100	[29]	10	(1:1)	1		6	
$CH_3CH{=}C(CH_3)CH_2OCH_3$	**3c**	$\mathbf{b_3}^+$	100	[27]	10		1		5	
$CH_3CH{=}CHCH_2OCH_2CH(CH_3)_2$	**4**	$\mathbf{b_4}^+$	8	[1]	45	[17]	10	[27]	100	[17]
$CH_2{=}CHCH(CH_3)OCH_2C_2H_5$	**5**	$\mathbf{b_5}^+$	80	[1]	25	[22]	100	[24]	10	[30]
$CH_2{=}C(CH_3)CH_2OCH_2CH(CH_3)_2$	**6**	$\mathbf{b_6}^+$	2	[2]	100	[21]	25	[36]	45	[18]

[a] Relative abundance measured by peak height and normalized to a total of 100 units for the base peak in the metastable ion spectrum of ions dissociating in the second field-free region. The MI spectra of $\mathbf{b_1}^+$ and $\mathbf{b_3}^+$ also contain weak signals for the loss of CH_3OH, C_3H_4 and CH_3CHO, see text and Fig. 9.2.

[b] Numbers in square brackets represent kinetic energy releases, $T_{0.5}$, in meV as obtained from the width at half height of the peak. An asterisk indicates that the peak is composite ; the approximate $T_{0.5}$ values for the narrow / broad component and their intensity ratio (in round brackets) are quoted.

[c] Composite metastable peaks dominated by a broad component whose $T_{0.5}$ values are estimated as ~370, ~460 and ~310 meV for $\mathbf{b_1}^+$, $\mathbf{b_2}^+$ and $\mathbf{b_3}^+$ respectively.

The isomeric species, $\mathbf{b_4}^+$, $\mathbf{b_5}^+$ and $\mathbf{b_6}^+$, in which the $-CH_2OCH_2^+$ subunit replaces the $-C^+(H)OCH_3$ entity, may be generated by simple bond cleavage of $CH_3CH{=}CHCH_2OCH_2CH(CH_3)_2^{\bullet+}$ and $CH_2{=}C(CH_3)CH_2OCH_2CH(CH_3)_2^{\bullet+}$, which yield $\mathbf{b_4}^+$ and $\mathbf{b_6}^+$, via loss of iso-$C_3H_7^\bullet$, and $CH_2{=}CHCH(CH_3)OCH_2C_2H_5^{\bullet+}$, which yields $\mathbf{b_5}^+$, via loss of $C_2H_5^\bullet$. However, the incipient ions $\mathbf{b_4}^+$ - $\mathbf{b_6}^+$may well cyclise to their more stable counterparts ***c*-b$_4$**$^+$ - ***c*-b$_6$**$^+$. Alternatively, these cyclic ions may be generated directly from their precursor ions, by a displacement type reaction.

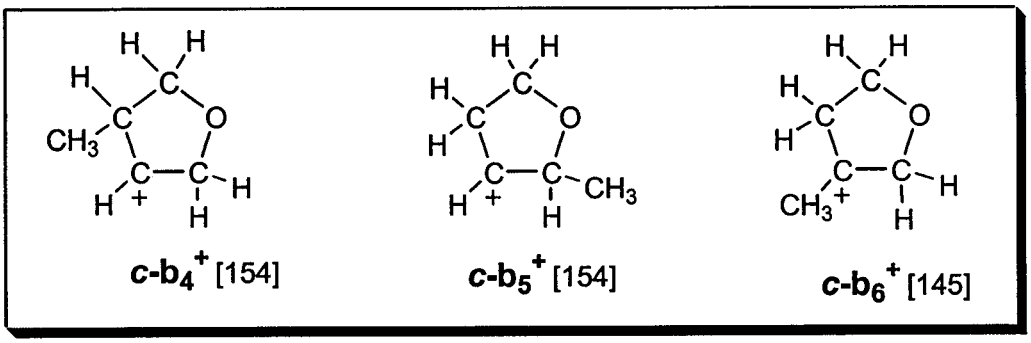

Each of the oxonium ions containing the $-C^+(H)OCH_3$ entity has a distinctive collision-induced dissociation (CID) spectrum [9a,b], thus indicating that $\mathbf{b_1}^+$, $\mathbf{b_2}^+$, and $\mathbf{b_3}^+$ are stable species existing in appreciable potential energy wells. This deduction is supported by the CID, NR (Neutralisation-Reionisation [10]) and survivor CID [11] spectra presented in Fig. 9.1. All three isomeric ions yield NR spectra with an intense survivor signal at m/z 85 (denoted by an asterisk in Fig. 9.1). The CID spectra of these survivor ions (denoted by S-CID in Fig. 9.1) are very close to those of the corresponding ions, i.e. the conventional CID spectra of the (source-generated) ions. This attests to the isomeric purity of $\mathbf{b_1}^+$ - $\mathbf{b_3}^+$ and confirms that the intensity difference in the conventional CID spectra for peaks of structure diagnostic value, *viz.* m/z 69, 45, 43 and 41, reflects distinct ion structures rather than (internal energy dependent) mixtures of the isomeric species. Thus, when a mixture of ions $\mathbf{b_1}^+$ - $\mathbf{b_3}^+$ is generated from a given precursor molecule, see Ref. 9c, its composition can easily and reliably be quantified on the basis of its CID spectrum.

Also presented in Fig. 9.1 are the CID spectra of ions of putative structures $\mathbf{b_4}^+$ - $\mathbf{b_6}^+$. It is seen that these $C_4H_7OCH_2^+$ ions yield distinct spectra. We further note that loss of CH_2O by direct bond cleavage is only prominent for $\mathbf{b_5}^+$. For $\mathbf{b_4}^+$ and $\mathbf{b_6}^+$ the major collision-induced dissociation yields m/z 43 ions, which, as will be shown below, involves loss of C_3H_6 to give CH_3CO^+ ions.

9.3.1. Overview of the reactions of low energy $C_5H_9O^+$ oxonium ions

The behaviour of metastable $\mathbf{b_1}^+$, $\mathbf{b_2}^+$ and $\mathbf{b_3}^+$, each of which expels predominantly CH_2O, differs from that of the lower homologue, $\mathbf{a_1}^+$, which loses CO and CH_2O in comparable amounts. Indeed, CO elimination, which is the most abundant fragmentation of $\mathbf{a_1}^+$, is of only minor significance in the dissociation of $\mathbf{b_1}^+$ - $\mathbf{b_3}^+$. Similarly, expulsion of H_2O is reduced in importance from 6-8% for $\mathbf{a_1}^+$ to 1-3% for $\mathbf{b_1}^+$ - $\mathbf{b_3}^+$. However, C_3H_6 loss, which is barely noticeable in the dissociation of $\mathbf{a_1}^+$, is significant for $\mathbf{b_1}^+$ and $\mathbf{b_3}^+$, and particularly so for $\mathbf{b_2}^+$. For all three ions, this process is associated with a composite metastable peak. This is illustrated in Fig. 9.2, which also shows that ions $\mathbf{b_1}^+$ and $\mathbf{b_3}^+$ display signals at m/z 53, 45 and 41 for the minor losses of CH_3OH, C_3H_4, and CH_3CHO, respectively.

The combined [product ion + neutral] enthalpy for loss of C_3H_4 as either propyne or allene to give $CH_3OCH_2^+$ is 202 kcal/mol, while loss of CH_3CHO to give CH_2=C-CH_2^+ or CH_3-C^+=CH_2 yields values of 186 and 191 kcal/mol, respectively [12]. The corresponding value for loss of CH_2O to yield CH_2=CHC^+(H)CH_3, 176 kcal/mol (Table 9.4), is much lower. This thermochemical analysis indicates that the dissociation of these oxonium ions occurs at an energy level considerably above the thermochemical threshold, at least for metastable ions $\mathbf{b_1}^+$ and $\mathbf{b_3}^+$.

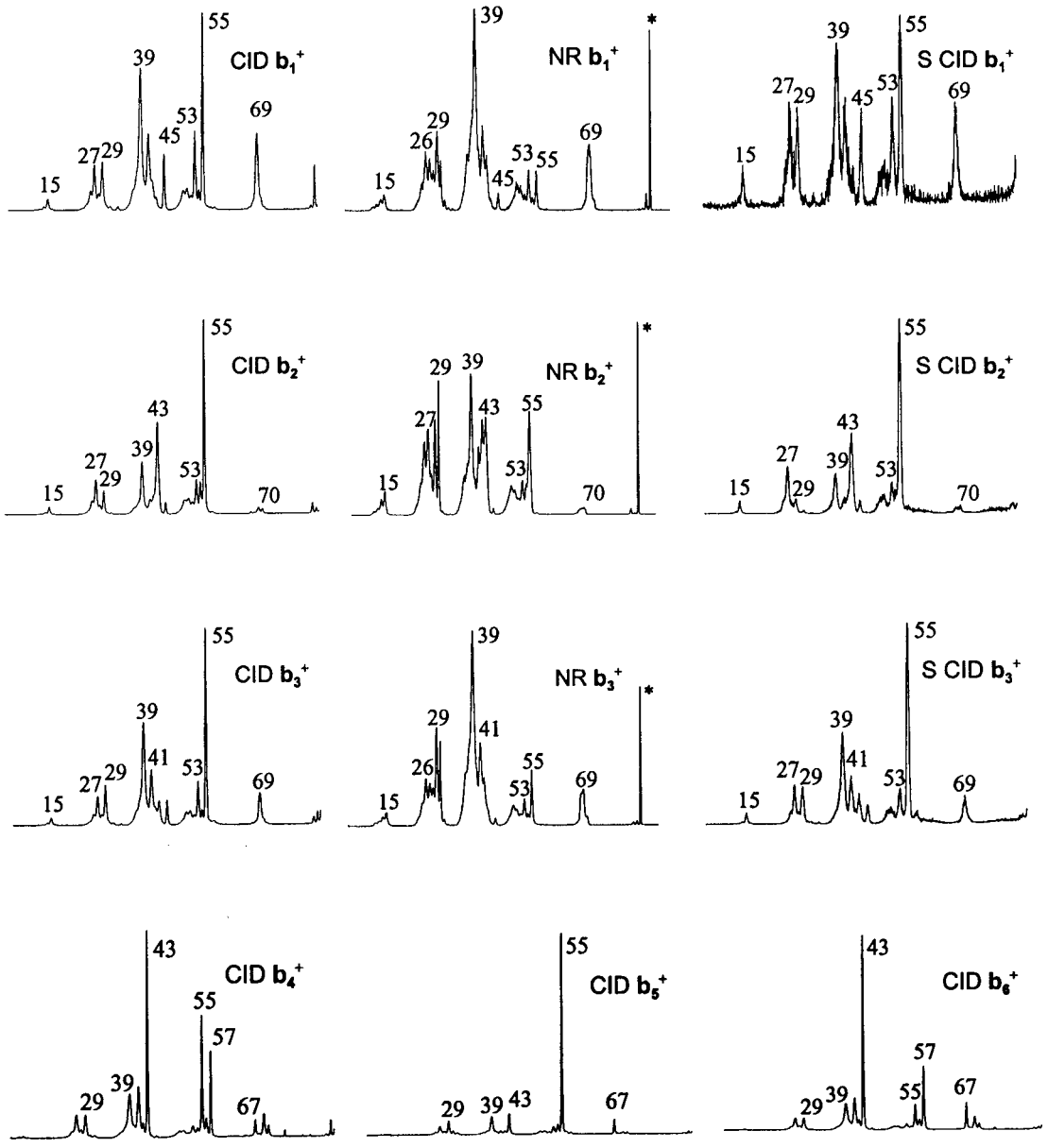

Fig. 9.1. CID, NR and survivor CID (S CID) spectra of the $C_4H_6OCH_3^+$ ions $\mathbf{b_1}^+$ - $\mathbf{b_3}^+$. The survivor signal at m/z 85 in the NR spectra is denoted with an asterisk. CID spectra of the isomeric $C_4H_7OCH_2^+$ ions $\mathbf{b_4}^+$ - $\mathbf{b_6}^+$ are displayed on the fourth row.

Comparison of the behaviour of the isomeric pairs of oxonium ions $\mathbf{b_1}^+/\mathbf{b_4}^+$, $\mathbf{b_2}^+/\mathbf{b_5}^+$ and $\mathbf{b_3}^+/\mathbf{b_6}^+$, in which $-C^+(H)OCH_3$ is replaced by $-CH_2OCH_2^+$, reveals that some trends observed for the archetypal $C_4H_7O^+$ species, $\mathbf{a_1}^+$ and $\mathbf{a_2}^+$, persist for their higher homologues. Thus, see Table 9.1, the proportion of $\mathbf{b_4}^+$ - $\mathbf{b_6}^+$, which lose CO is greater than that for $\mathbf{b_1}^+$ - $\mathbf{b_3}^+$. However, the stark contrast between $\mathbf{a_1}^+$ - which loses CH_2O, CO and a little H_2O - and ion $\mathbf{a_2}^+$ - which loses essentially only CO - no longer holds. Similarly, CH_2O is lost less readily, see Table 9.1, from $\mathbf{b_4}^+$ - $\mathbf{b_6}^+$ than from $\mathbf{b_1}^+$ - $\mathbf{b_3}^+$, but this reaction is not entirely superseded by CO loss as is the case for $\mathbf{a_2}^+$. On the other hand, H_2O elimination occurs to a greater extent from metastable $\mathbf{b_4}^+$ - $\mathbf{b_6}^+$ than from $\mathbf{b_1}^+$ - $\mathbf{b_3}^+$. This reversal of the situation found for metastable ions $\mathbf{a_1}^+$ and $\mathbf{a_2}^+$ is especially pronounced for $\mathbf{b_5}^+$, which loses mainly H_2O.

The apparent discrimination against CH_2O elimination from $\mathbf{a_2}^+$ and $\mathbf{b_4}^+$ - $\mathbf{b_6}^+$, each of which contains an intact formaldehyde unit, is at first sight very surprising, especially since $\mathbf{a_1}^+$ and $\mathbf{b_1}^+$ - $\mathbf{b_3}^+$, which do not contain this structural feature, expel CH_2O exclusively or predominantly. A logical explanation is that this reaction is favoured at higher internal energies and that it occurs preferentially after $\mathbf{a_1}^+$ and $\mathbf{b_1}^+$ - $\mathbf{b_3}^+$ have undergone rate-limiting isomerization to form their $\mathbf{a_2}^+$ and $\mathbf{b_4}^+$ - $\mathbf{b_6}^+$ counterparts with internal energies higher than is needed to cause dissociation. Support for this interpretation is found in the $T_{0.5}$ values (the KER estimated from the width at half-height of the associated metastable peaks [8]) for CH_2O loss from $\mathbf{a_1}^+$ and $\mathbf{b_1}^+$ - $\mathbf{b_3}^+$, which are consistently greater than those for the isomeric counterparts $\mathbf{a_2}^+$ and $\mathbf{b_4}^+$ - $\mathbf{b_6}^+$.

This reaction from $\mathbf{b_4}^+$ - $\mathbf{b_6}^+$ occurs with a very small KER : the metastable peaks are barely wider than the main beam of parent ions ($T_{0.5}$ = 1 - 2 meV). These values are consistent with CH_2O loss from $\mathbf{b_4}^+$ - $\mathbf{b_6}^+$ essentially without reverse critical energy. In contrast, CH_2O loss from $\mathbf{b_1}^+$, $\mathbf{b_2}^+$ and $\mathbf{b_3}^+$ produces broader metastable peaks with $T_{0.5}$ values of 33, 19 and 27 meV, respectively. The increased $T_{0.5}$ values reflect the excess energy in the transition state when ions formed as $\mathbf{b_1}^+$, $\mathbf{b_2}^+$ and $\mathbf{b_3}^+$ eventually lose CH_2O.

Parallel trends are found for other common reactions of $\mathbf{b_1}^+$ - $\mathbf{b_3}^+$ and $\mathbf{b_4}^+$ - $\mathbf{b_6}^+$. Thus, CO loss from $\mathbf{b_1}^+$ - $\mathbf{b_3}^+$ yields a very broad metastable peak, with $T_{0.5}$ in the range

310 - 465 meV, see Table 9.1, but the analogous fragmentation of $\mathbf{b_4}^+$, $\mathbf{b_5}^+$ and $\mathbf{b_6}^+$ is characterized by narrow peaks of Gaussian profile with $T_{0.5}$ values of 17, 30 and 18 meV, respectively.

All these data are consistent with the view that the CH_2O elimination from $\mathbf{b_4}^+$ - $\mathbf{b_6}^+$ has a higher critical energy than loss of C_3H_6, CO or H_2O. However, CH_2O expulsion may occur by simple C-O cleavage from $\mathbf{b_4}^+$ - $\mathbf{b_6}^+$, whereas CO or H_2O loss entail H-transfers and, at least in the latter case, skeletal isomerization. At the low internal energies appropriate to the dissociation of metastable ions [8] generated as $\mathbf{b_4}^+$, $\mathbf{b_5}^+$ and $\mathbf{b_6}^+$, the fragmentations with the lower critical energies are favoured; consequently, CH_2O expulsion competes comparatively poorly with loss of C_3H_6, CO and H_2O. On the other hand, at the relatively high internal energies appropriate to the dissociation of ions formed by rate-limiting isomerization of $\mathbf{b_1}^+$- $\mathbf{b_3}^+$ to their counterparts $\mathbf{b_4}^+$ - $\mathbf{b_6}^+$, CH_2O loss is favoured because it may occur by simple bond cleavage, without further rearrangement.

Parallel behaviour was found in a seminal study [13] of CH_3-$C^+(H)OCH_3$, and $CH_3CH_2OCH_2^+$, and in later work [14] on several isomers of $C_4H_9O^+$. Consequently, the tendency of oxonium ions containing the -$C^+(H)OCH_3$ entity to lose CH_2O, even though their isomers with the -$CH_2OCH_2^+$ subunit do not, appears to be general in both the $C_nH_{2n+1}O^+$ and $C_nH_{2n-1}O^+$ series.

Details of the rate-limiting isomerization(s) of $\mathbf{b_1}^+$ - $\mathbf{b_3}^+$ to $\mathbf{b_4}^+$ - $\mathbf{b_6}^+$ cannot be established from the current data. It is possible that $\mathbf{b_1}^+$ isomerises to $\mathbf{b_4}^+$, $\mathbf{b_2}^+$ to $\mathbf{b_5}^+$ and $\mathbf{b_3}^+$ to $\mathbf{b_6}^+$ by a 1,3-hydride shift in each case. Such a shift was initially suggested in experimental studies [13] of $C_3H_7O^+$ and subsequently was supported by high-level ab initio calculations [15, 16]. However, other mechanisms are possible, in particular a 1,5-H shift followed by a (dipole assisted) 1,3-H shift to form an ion-neutral complex (INC) [17], see Section 8.3.2.

The metastable ion characteristics of $\mathbf{b_1}^+$, $\mathbf{b_2}^+$ and $\mathbf{b_3}^+$ are superficially similar, but there are sufficient differences to suggest that these isomeric oxonium ions do not interconvert before fragmenting. Thus, $\mathbf{b_1}^+$ and $\mathbf{b_3}^+$ both lose CH_3OH, C_3H_4, and CH_3CHO, see Fig. 9.2, whereas $\mathbf{b_2}^+$ does not. Moreover, $\mathbf{b_1}^+$ shows a less pronounced

loss of C_3H_6 than either $\mathbf{b_2}^+$ or $\mathbf{b_3}^+$ and the importance of CO loss is greatest from $\mathbf{b_3}^+$. The competition between possible fragmentation routes of metastable ions can be influenced by variations in the internal energy of the dissociating population of ions, as is the KER associated with each reaction [17]. Such an effect has already been noted in the comparative importance of CO and CH_2O loss from $\mathbf{a_1}^+$ [7a]. However, the variations in the ratios of CO, CH_3OH, C_3H_4 and, especially, C_3H_6 elimination from $\mathbf{b_1}^+$, $\mathbf{b_2}^+$ and $\mathbf{b_3}^+$ seem too large to be explained solely in terms of changes in the internal energy of the fragmenting ions. Similarly, the $T_{0.5}$ values for CH_2O expulsion from $\mathbf{b_1}^+$, $\mathbf{b_2}^+$ and $\mathbf{b_3}^+$, 33, 19 and 27 meV, respectively, also vary substantially. Some reactions of $\mathbf{b_1}^+$, $\mathbf{b_2}^+$ and $\mathbf{b_3}^+$, particularly CH_2O loss, may involve closely related intermediates or transition states, but in agreement with the CID data of Fig. 9.1, $\mathbf{b_1}^+$, $\mathbf{b_2}^+$ and $\mathbf{b_3}^+$ do not easily interconvert prior to dissociation.

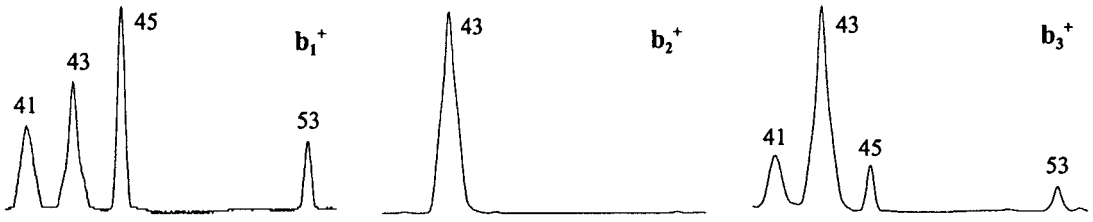

Fig. 9.2. The m/z 40 - 54 region of the MI spectra of the $C_4H_6OCH_3^+$ ions $\mathbf{b_1}^+$ - $\mathbf{b_3}^+$.

Similarly, the disparate behaviour of $\mathbf{b_4}^+$, $\mathbf{b_5}^+$ and $\mathbf{b_6}^+$ suggests that the barriers towards interconversion of these oxonium ions are fairly high and that isomerization to a common structure occurs at a relatively late stage in their dissociation, if it occurs at all.

This deduction is confirmed for $\mathbf{b_1}^+$, $\mathbf{b_2}^+$ and $\mathbf{b_3}^+$ by the behaviour of labelled analogues, see Tables 8.2 and 8.3. Elimination of formaldehyde from $\mathbf{b_1}^+$ occurs only after fairly extensive exchange of the H atoms of the OCH_3 group.

Thus, see Table 9.2, $\mathbf{b_1}^+[OCD_3]$, expels CD_2O and CHDO in approximately equal amounts; a little CH_2O loss is also observed. In contrast, $\mathbf{b_3}^+[OCD_3]$, and particularly $\mathbf{b_2}^+[OCD_3]$, show a much greater preference for losing formaldehyde as CD_2O derived

from the intact OCD_3 group. Differences are also evident in the site-selectivities of propene/cyclopropane loss from $\mathbf{b_1}^+$ - $\mathbf{b_3}^+$: ions $\mathbf{b_2}^+[OCD_3]$ lose $C_3H_4D_2$ and $C_3H_3D_3$ in roughly equal abundance, but C_3H_5D and C_3H_6 expulsion are negligible; $\mathbf{b_3}^+[OCD_3]$ behaves similarly, with a slight tendency to expel C_3H_5D and C_3H_6. The weak and partially overlapping signals for this reaction from $\mathbf{b_1}^+[OCD_3]$ are more equally divided between the $C_3H_{6-n}D_n$ (n = 0-3) species. This trend persists for the ^{13}C-labelled analogues : $\mathbf{b_2}^+[O^{13}CH_3]$ and $\mathbf{b_3}^+[O^{13}CH_3]$ lose $^{13}CC_2H_6$ with high selectivity, but $\mathbf{b_1}^+[O^{13}CH_3]$, shows weak signals for elimination of C_3H_6 and $^{13}CC_2H_6$.

Table 9.2. Relative abundances [a] and kinetic energy releases [b] for the main dissociations of metastable $C_5H_6D_3O^+$ ions

Precursor	Loss→ Ion	CH_2O		CHDO		CD_2O		C_3H_6	C_3H_5D	$C_3H_4D_2$	$C_3H_3D_3$
1a$[OCD_3]$	$\mathbf{b_1}^+[OCD_3]$	9	[31]	100	[31]	88	[30]				
1b$[OCD_3]$	$\mathbf{b_1}^+[OCD_3]$	11	[37]	76	[34]	100	[31]				
1c$[OCD_3]$	$\mathbf{b_1}^+[OCD_3]$	12	[36]	83	[31]	100	[31]				
2a$[OCD_3]$	$\mathbf{b_2}^+[OCD_3]$	-		4	[30]	100	[23]	-	-	7	6
2a$[1\text{-}(CD_3)_2]$	$\mathbf{b_2}^+[1\text{-}CD_3]$	100	[20]	1	[26]	-		14	-	-	10
2c$[1\text{-}CD_3]$	$\mathbf{b_2}^+[1\text{-}CD_3]$	100	[20]	2	[25]	-		10	-	-	6
2d$[1\text{-}CD_3]$	$\mathbf{b_2}^+[1\text{-}CD_3]$	100	[20]	2	[29]	-		8	-	-	6
3a$[OCD_3]$	$\mathbf{b_3}^+[OCD_3]$	-		20	[30]	100	[23]	1	1	9	9
3b$[OCD_3]$	$\mathbf{b_3}^+[OCD_3]$	7		44	[31]	100	[34]	1	1	5	5

[a] Relative abundance measured by peak height normalized to a total of 100 units for the base peak in the MI spectrum for ions dissociating in the second field-free region.

[b] Numbers in square brackets represent kinetic energy releases, $T_{0.5}$, in meV as obtained from the width at half height of the peak.

[c] Compound **2c** is $CH_2{=}C(CH_3)CH(CD_3)OCH_3$; **2d** is $CH_3CH{=}CHCH(CD_3)OCH_3$.

Table 9.3. Relative abundances [a] for the main dissociations of metastable $^{13}CC_4H_9O^+$ ions

Precursor	Ion / Loss→	CH_2O	$^{13}CH_2O$	C_3H_6	$^{13}C_3H_6$	CO	^{13}CO
1c$[O^{13}CH_3]$	$\mathbf{b_1}^+[O^{13}CH_3]$	<0.5	100	~1	~2	2	<0.1
2a$[O^{13}CH_3]$	$\mathbf{b_2}^+[O^{13}CH_3]$	<0.4	100	<0.1	30	3	< 0.1
3a$[O^{13}CH_3]$	$\mathbf{b_3}^+[O^{13}CH_3]$	<0.4	100	1	19	12	< 0.4

[a] Relative abundance measured by peak height normalized to a total of 100 units for the base peak in the MI spectrum of ions dissociating in the second field-free region

9.3.2. Elimination of formaldehyde

This fragmentation typically accounts for 75% of the total metastable ion current. It is characterized by a Gaussian metastable peak; the associated KER increases in the order $\mathbf{b_2}^+ < \mathbf{b_3}^+ < \mathbf{b_1}^+$. All three $[O^{13}CH_3]$ labelled analogues expel $^{13}CH_2O$ with selectivities of at least 99%, thus establishing that the carbon atom of the expelled formaldehyde originates from the OCH_3 group. Similarly, $\mathbf{a_1}^+[O^{13}CH_3]$ does not lose a measurable amount of CH_2O [7]. These data suggest that formaldehyde loss occurs after H-transfer from the OCH_3 group to the C_4H_6 entity in $C_4H_6OCH_3^+$. Such an H-transfer should be more favourable than for the analogous $C_4H_8OCH_3^+$ ions because the C=C double bond permits a 1,5-H shift via a six-membered ring transition state, see Scheme 9.2a.

The D-labelling data of Table 9.2 reveal that the 1,5-H transfer is essentially unidirectional for $\mathbf{b_2}^+$: thus, $\mathbf{b_2}^+[OCD_3]$ loses CD_2O with ~95% selectivity. The KERs for the minor elimination of formaldehyde containing 'exchanged' H atoms are greater than those for loss of the formaldehyde obtained by simple hydrogen abstraction from the initial OCH_3 group of $\mathbf{b_2}^+$. This trend applies regardless of whether an H or D atom is incorporated as 'exchanged' hydrogen. Consequently, it appears that the higher energy ions show an increased propensity for undergoing the steps that result in exchange of H atoms of the OCH_3 group with those of the four-carbon chain.

Rather more exchange is observed for $\mathbf{b_1}^+[OCD_3]$ and $\mathbf{b_3}^+[OCD_3]$, which expel CHDO in high and moderate abundance. Moreover, in the case of $\mathbf{b_3}^+[OCD_3]$, the extent to which this exchange occurs depends on how the ions were formed. When the ion is generated by direct α-cleavage of $CH_2=C(CH_3)CH(C_2H_5)OCD_3^{\bullet+}$, **3a**$[OCD_3]$ in Table 9.2, the preference for CD_2O loss is greater than when it is formed by rearrangement and γ-cleavage of $C_2H_5CH=CHCH_2OCD_3^{\bullet+}$, **3b**$[OCD_3]$. This trend is intelligible if $\mathbf{b_3}^+[OCD_3]$ has more internal energy when generated by rearrangement via the enol ion $(C_2H_5)(CH_3)C=C(H)OCD_3^{\bullet+}$ followed by γ-cleavage than by direct α-cleavage of **3a**$[OCD_3]$, provided that the higher energy ions have an enhanced tendency to undergo the H-transfer steps. This possibility is supported by the significantly greater KER

values for CD_2O/CHDO loss from $\mathbf{b_3}^+[OCD_3]$ formed from **3b**$[OCD_3]$ than from **3a**$[OCD_3]$.

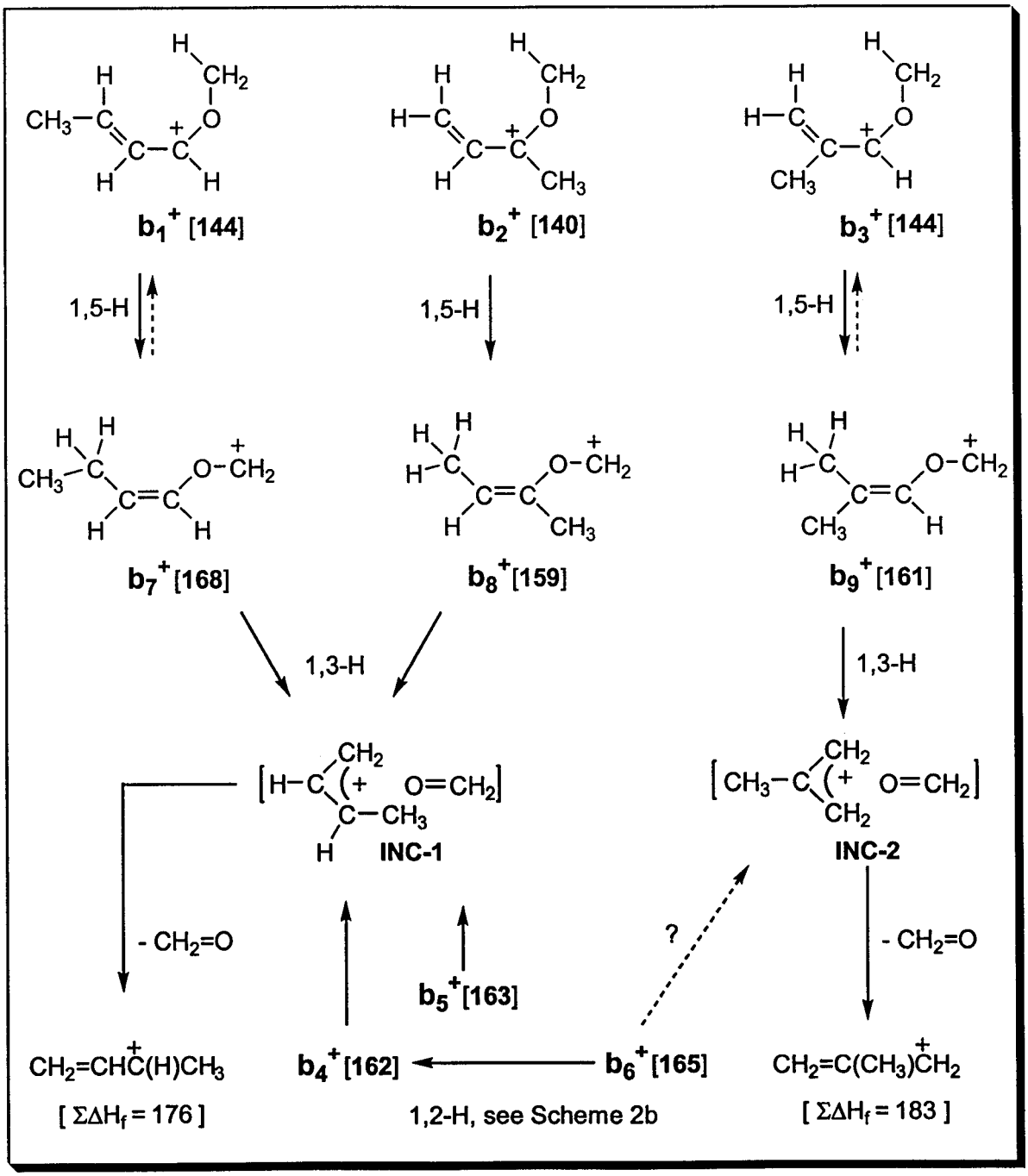

Scheme 9.2a

The order of increasing KERs for formaldehyde expulsion : $\mathbf{b_1}^+[OCD_3]$ > $\mathbf{b_3}^+[OCD_3]$ > $\mathbf{b_2}^+[OCD_3]$ is the same as that for increasing incorporation of 'exchanged' hydrogen in the eliminated formaldehyde. Both these trends are consistent with the view that formaldehyde loss and the exchange of the H atoms of the methoxy group are favoured at higher internal energies. If the 1,5-H/D shift in $\mathbf{b_1}^+$, $\mathbf{b_2}^+$ and $\mathbf{b_3}^+$ were reversible, this step would result in exchange of the H atoms of the methoxy group. According to this interpretation, the tendency of $\mathbf{b_7}^+$, $\mathbf{b_8}^+$ and $\mathbf{b_9}^+$ to revert to their original structures would vary : $\mathbf{b_8}^+$ rarely returns to $\mathbf{b_2}^+$; $\mathbf{b_9}^+$ occasionally reverts to $\mathbf{b_3}^+$; and $\mathbf{b_7}^+$ rearranges back to $\mathbf{b_1}^+$ rather more rapidly than it expels CH_2O, see Scheme 9.2. If $\mathbf{b_1}^+$ reverted to $\mathbf{b_7}^+$ on average once before losing CH_2O, the ratio of CD_2O : CHDO elimination from $\mathbf{b_1}^+[OCD_3]$ would be 2:1 in the absence of isotope effects.

An alternative to the 1,5-H shift proposed to initiate the isomerization of $\mathbf{b_1}^+$, $\mathbf{b_2}^+$ and $\mathbf{b_3}^+$ is a 1,3-H shift, which would lead directly to $\mathbf{b_4}^+$, $\mathbf{b_5}^+$ and $\mathbf{b_6}^+$, respectively. This possibility has several features which make it superficially attractive: there are fewer constraints on the geometry of the transition state, the need to invoke the involvement of $\mathbf{b_7}^+$, $\mathbf{b_8}^+$ and $\mathbf{b_9}^+$ is removed and CH_2O loss may occur by simple C-O cleavage of $\mathbf{b_4}^+$, $\mathbf{b_5}^+$ and $\mathbf{b_6}^+$. Moreover, there is precedence for a 1,3-H shift in the reactions of the analogous oxonium ions which do not contain the C=C bond that is present in $\mathbf{b_1}^+$, $\mathbf{b_2}^+$ and $\mathbf{b_3}^+$. However, mechanisms involving a direct 1,3-H shift in closed-shell systems have serious disadvantages and it is known from both experimental [13,14] and computational [15,16] studies of $C_nH_{2n+1}O^+$ that these processes have very high critical energies and are usually irreversible. Thus, $CH_3C^+(H)OCD_3$ and $CH_3CH_2C^+(H)OCD_3$ lose CD_2O, but not CHDO or CH_2O [13, 14]. In contrast, 1,5-H shifts in oxonium ions are often partially reversible. Consequently, if $\mathbf{b_1}^+$, $\mathbf{b_2}^+$ and $\mathbf{b_3}^+$ rearranged via a 1,3-H shift to $\mathbf{b_4}^+$, $\mathbf{b_5}^+$ and $\mathbf{b_6}^+$, respectively, that step would probably be rate-limiting and CH_2O loss would be expected to occur rapidly by C-O cleavage before H/D-exchange could occur. In actual fact, some H/D-exchange is observed, especially for $\mathbf{b_1}^+[OCD_3]$ and $\mathbf{b_3}^+[OCD_3]$. Furthermore, the amount of exchange increases as the internal energy of the dissociating ions increases. The opposite trend

would be expected if a 1,3-H shift led directly from $\mathbf{b_1}^+[OCD_3]$, $\mathbf{b_2}^+[OCD_3]$ and $\mathbf{b_3}^+[OCD_3]$ to $\mathbf{b_4}^+[OCD_2]$, $\mathbf{b_5}^+[OCD_2]$ and $\mathbf{b_6}^+[OCD_2]$ because the higher energy ions would show an increased tendency to expel CD_2O rather than undergo any processes that resulted in H/D-exchange. In contrast, the possibility of a 1,5-H shift offers a natural route to explain the H/D-exchange that precedes formaldehyde loss from $\mathbf{b_1}^+[OCD_3]$, $\mathbf{b_3}^+[OCD_3]$ and, to a lesser extent, $\mathbf{b_2}^+[OCD_3]$. This possibility is not open to $CH_3C^+(H)OCD_3$ and $CH_3CH_2C^+(H)OCD_3$, thus accounting for the absence of H/D-exchange when formaldehyde is lost from oxonium ions in which there is no C=C bond to facilitate the 1,5-H shift. Nevertheless, the possibility of a 1,3-H shift cannot be entirely excluded on the basis of the current data, particularly for $\mathbf{b_2}^+[OCD_3]$, in which relatively little H/D-exchange is observed.

Further rearrangement after the 1,5-H shift must precede or accompany CH_2O elimination because it is most unlikely that the final product will be a vinyl type cation, like $CH_3CH_2CH=C^+H$, resulting from direct fission of $\mathbf{b_7}^+$. Formation of such energetically unfavourable species would be expected to be pre-empted by isomerization of the developing cation, perhaps via a dipole-assisted 1,3-H transfer within an ion-neutral complex (INC) [17] comprising $C_4H_7^+$ coordinated to CH_2O. This mechanism would permit the production of a more stable conjugated allylic cation, i.e. $CH_2=CHC^+(H)CH_3$ from $\mathbf{b_1}^+$ and $\mathbf{b_2}^+$ or $CH_2=C(CH_3)CH_2^+$ from $\mathbf{b_3}^+$. The likelihood of this further rearrangement is an important difference between $C_5H_9O^+$ ions of the type $C_4H_7OCH_2^+$ and $C_5H_{11}O^+$ ions of the type $C_4H_9OCH_2^+$ formed by isomerization of $C_4H_6OCH_3^+$ and $C_4H_8OCH_3^+$, respectively.

The secondary cation, $CH_2=CHC^+(H)CH_3$, is 9 kcal/mol [12] more stable than the primary isomer $CH_2=C(CH_3)CH_2^+$. However, the energy barriers to interconversion of the 1- and 2-methallyl cations are less than those towards decomposition (~ 60 kcal/mol). Consequently, the reactions of metastable $[C_4H_7]^+$ ions are not significantly dependent on the origin of the ion [18]. In line with this, we found that the CID spectra (not shown) of ions of putative structure $CH_2=CHC^+(H)CH_3$ and $CH_2=C(CH_3)CH_2^+$ (generated by loss of $Cl^\bullet$ from 3-chloro-1-butene and 3-chloro-2-methyl propene,

respectively) are virtually identical. Thus, it is not possible to determine which of the allylic $C_4H_7^+$ isomers is generated in the loss of CH_2O from the oxonium ions studied.

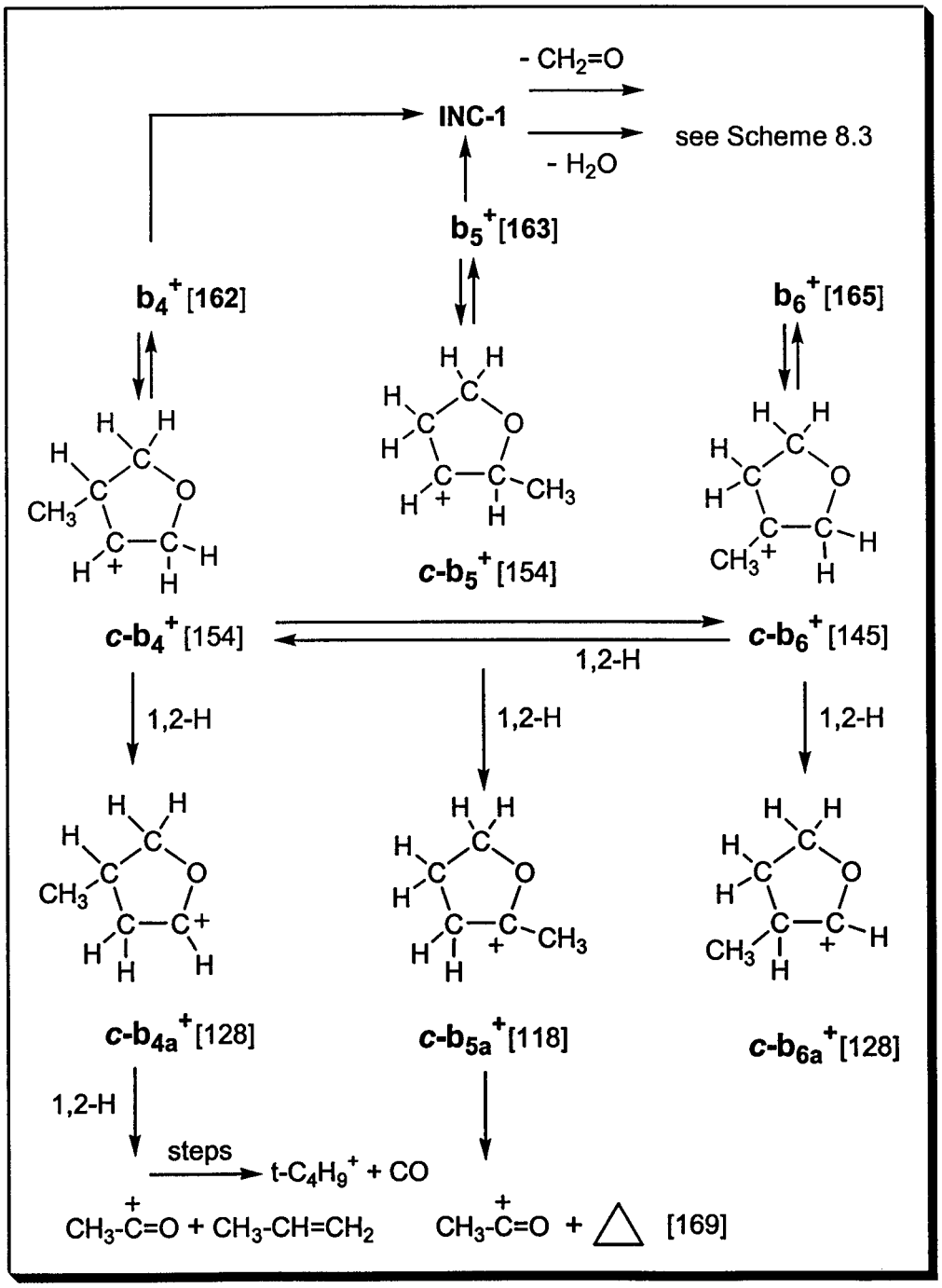

Scheme 9.2b

Considering the very small KERs, it seems probable that $\mathbf{b_4}^+$ - $\mathbf{b_6}^+$ lose CH_2O via an INC and we propose that all three ions dissociate via INC-1 of Scheme 9.2a, to generate the most stable $C_4H_7^+$ isomer, the 1-methallyl cation. For $\mathbf{b_4}^+$ and $\mathbf{b_5}^+$, see Scheme 9.2a, this reaction entails a simple bond cleavage. Direct bond cleavage in $\mathbf{b_6}^+$ would yield the less favourable 2-methallyl cation, via INC-2. However, $\mathbf{b_6}^+$ and $\mathbf{b_4}^+$ may interconvert via a 1,2-H shift in their cyclic counterparts ***c*-b$_6$**$^+$ and ***c*-b$_4$**$^+$ prior to the loss of CH_2O from $\mathbf{b_6}^+$, see Scheme 9.2b.

Finally, we note that the average internal energies of any ions with a common structure generally depends on their origin. This caveat is necessary to explain the divergent site-selectivites and KERs for formaldehyde loss from $\mathbf{b_1}^+[OCD_3]$, $\mathbf{b_2}^+[OCD_3]$ and $\mathbf{b_3}^+[OCD_3]$ and also generic differences in the reactions of $\mathbf{b_1}^+$, $\mathbf{b_2}^+$ and $\mathbf{b_3}^+$ compared to $\mathbf{b_4}^+$, $\mathbf{b_5}^+$ and $\mathbf{b_6}^+$. Any common intermediate in CH_2O loss is likely to lie at a relatively late stage of the route when the reacting species is beginning to resemble $[C_4H_7^+/CH_2{=}O]$.

9.3.3. Elimination of C_3H_6 (propene or cyclopropane)

Loss of C_3H_6 involves either propene or cyclopropane. The latter isomer is 8 kcal/mol less stable but its (co)generation should be feasible since the minimum energy requirement for dissociation to CH_3CO^+ + c-C_3H_6 [$\Sigma\Delta H_f$ (products) = 169 kcal/mol] remains below the calculated threshold for the competing CH_2O loss, 176 kcal/mol, see Scheme 9.2a.

For $\mathbf{a_1}^+$, loss of C_3H_6 is negligible and only a slight increase is found on progressing to $\mathbf{b_1}^+$. However, for $\mathbf{b_2}^+$ and $\mathbf{b_3}^+$, this reaction competes quite well with CH_2O loss, see Table 9.1. Similarly, loss of C_3H_6 plays no role in the dissociation of $\mathbf{a_2}^+$ [7a], but it does occur to an appreciable extent from $\mathbf{b_4}^+$, $\mathbf{b_5}^+$ and $\mathbf{b_6}^+$.

The eliminated neutral of mass 42 units is clearly C_3H_6 and not C_2H_2O (ketene) : inspection of the (3ffr) CID spectra (not shown) of the metastably generated m/z 43 product ions leaves no doubt that CH_3CO^+ [19], rather than $C_3H_7^+$, is produced by the dissociation of metastable ions $\mathbf{b_1}^+$ - $\mathbf{b_3}^+$ and $\mathbf{b_4}^+$ - $\mathbf{b_6}^+$.

For ions $\mathbf{b_1}^+$ - $\mathbf{b_3}^+$, this dissociation is characterized by a composite metastable peak consisting of a (conceivably common) narrow and broad component, see Table 9.1. However, the proportion of the components in $\mathbf{b_2}^+$ and $\mathbf{b_3}^+$ (1 : 1) differs from that for $\mathbf{b_1}^+$ (3 : 1).

The behaviour of $\mathbf{b_2}^+[O^{13}CH_3]$, which loses $^{13}CC_2H_6$ but not C_3H_6, reveals that the carbon atom of the OCH_3 group is always incorporated in the expelled neutral. However, $C_3H_3D_3$ and $C_3H_4D_2$ are eliminated at approximately equal rates from both $\mathbf{b_2}^+[OCD_3]$ and $\mathbf{b_3}^+[OCD_3]$; this finding indicates that up to one H atom from the OCH_3 substituent can become part of the ionic fragment. The third isomer, $\mathbf{b_1}^+[OCD_3]$, may behave similarly, but the low intensities of the partially overlapping signals prevent a meaningful analysis.

The elimination of comparable amounts of $C_3H_3D_3$ and C_3H_6 but no $C_3H_4D_2$ or C_3H_5D from $\mathbf{b_2}^+[1\text{-}CD_3]$ shows that all the atoms of the intact carbon-bound methyl group of $\mathbf{b_2}^+$ are included in either the ionic or neutral product. However, upon collisional activation, $\mathbf{b_2}^+[1\text{-}CD_3]$ yields a prominent peak at m/z 48 (CD_3CO^+) whereas that at m/z 43 (CH_3CO^+) is of only minor importance. This result indicates that the rearrangement reaction of metastable ions $\mathbf{b_2}^+[1\text{-}CD_3]$ that leads to dissociation to $CH_3CO^+ + C_3H_3D_3$ is a slow process, possibly because one of the steps involves a methyl migration. The dissociation to $CD_3CO^+ + C_3H_6$ seems to be more straightforward and one possibility to rationalize this pathway involves the route : $\mathbf{b_2}^+ \rightarrow \mathbf{b_5}^+$, either via $\mathbf{b_8}^+$ or else via a direct 1,3-H shift, followed by the steps : $\mathbf{b_5}^+ \rightarrow \textit{c}\text{-}\mathbf{b_5}^+ \rightarrow \textit{c}\text{-}\mathbf{b_{5a}}^+ \rightarrow CD_3CO^+ + c\text{-}C_3H_6$, as outlined in Scheme 9.2b.

We note that this proposal accounts for the specific loss of $^{13}CC_2H_6$ from $\mathbf{b_2}^+[O^{13}CH_3]$, but want to stress that the complete picture is more complex because both the $C_3H_3D_3$ loss and the C_3H_6 loss from $\mathbf{b_2}^+[1\text{-}CD_3]$ are still associated with composite metastable peaks.

9.3.4. Elimination of Carbon Monoxide

Loss of CO from the isomeric $\mathbf{b}^+$-type oxonium ions yields $C_4H_9^+$ product ions. Of the four isomeric butyl cations that could conceivably be formed, only the tert-$C_4H_9^+$ and the sec-$C_4H_9^+$ isomers are likely candidates. Loss of CO obviously involves extensive rearrangement and for this reaction to compete with CH_2O loss – which for $\mathbf{b_4}^+$ - $\mathbf{b_6}^+$ involves a direct bond cleavage at the thermochemical threshold – its minimum energy requirement must be considerably lower than that for loss of CH_2O. This condition is satisfied for the production of either the tert- or the sec-butyl cation [$\Sigma\Delta H_f$ (products) = 139 and 157 kcal/mol, respectively], but not for the other two isomers. Unfortunately, isomeric $C_4H_9^+$ species cannot be distinguished on the basis of CID experiments.

Loss of CO is the major reaction of $\mathbf{a_1}^+$, but it is of only minor importance for $\mathbf{b_1}^+$ - $\mathbf{b_3}^+$. The eliminated neutral must be mainly or wholly CO, rather than C_2H_4, because no D-labelled analogue of $\mathbf{b_1}^+$, $\mathbf{b_2}^+$ and $\mathbf{b_3}^+$ expels C_2H_3D in measurable abundance. If ethylene loss did occur, either $\mathbf{b_2}^+[OCD_3]$ or $CH_2{=}CHC^+(CD_3)OCH_3$, $\mathbf{b_2}^+[1\text{-}CD_3]$, would eliminate C_2H_3D.

The absence of ^{13}CO elimination from $\mathbf{b_1}^+[O^{13}CH_3]$, $\mathbf{b_2}^+[O^{13}CH_3]$ and $\mathbf{b_3}^+[O^{13}CH_3]$, indicates that these ions do not expel carbon monoxide by double H-transfer between the components of any intermediate INC $[C_4H_7^+/^{13}CH_2{=}O]$ en route to $^{13}CH_2O$ expulsion. Instead, skeletal rearrangement and cleavage of the C-O bond of the OCH_3 group occurs.

The signal for CO loss from $\mathbf{b_3}^+$ is appreciably stronger than that starting from $\mathbf{b_1}^+$ or $\mathbf{b_2}^+$. The metastable peak is very broad and the associated $T_{0.5}$ value (~300 meV) is very large. This value is even greater than that for CO elimination from $\mathbf{a_1}^+$. However, in contrast to $\mathbf{a_1}^+[O^{13}CH_3]$, which loses both CO and ^{13}CO, with the former predominating, the $[O^{13}CH_3]$ isotopologues of the higher homologues $\mathbf{b_1}^+$ - $\mathbf{b_3}^+$ all lose CO with high selectivity, possibly via rearrangement to the stable cyclic intermediates of the $\mathbf{b_4}^+$ - $\mathbf{b_6}^+$ manifold of ions.

All of these ions, particularly $\mathbf{b_4}^+$ and $\mathbf{b_5}^+$, expel an appreciably greater percentage of CO than the corresponding isomer containing a methoxy group. This

trend in the relative abundance of CO loss is parallel to but less pronounced than that found for $\mathbf{a_1}^+$ and $\mathbf{a_2}^+$. However, in contrast to the situation found for $\mathbf{a_2}^+$, which expels CO by two routes one of which has a large KER [7], the metastable peaks for CO loss from $\mathbf{b_4}^+$, $\mathbf{b_5}^+$ and $\mathbf{b_6}^+$ have a non-composite Gaussian shape; moreover, the associated $T_{0.5}$ values (17, 30 and 18 meV, respectively) are small.

This contrast must reflect a profound change in the mechanism for CO loss on progressing from $\mathbf{a_2}^+$ to the $\mathbf{b_4}^+$ - $\mathbf{b_6}^+$ system of ions. In both systems a cyclization reaction may occur but an important difference is that for the $\mathbf{b_4}^+$ - $\mathbf{b_6}^+$ system energetically very favourable tertiary alkyl cations could be formed as the product ion. For example, $\mathbf{b_4}^+$, see Table 9.1, readily loses CO in competition with C_3H_6. This reaction may well take place from the very stable cyclic intermediate $\boldsymbol{c}$-$\mathbf{b_{4a}}^+$ of Scheme 9.2b. A 1,2-H shift in this ion yields a reactive intermediate from which both CH_3-$CH{=}CH_2$ and CO could be lost by direct bond cleavages. However, loss of CO by direct bond cleavage to form iso-$C_4H_9^+$ cannot compete with propene loss : $\Sigma\Delta H_f$ [CH_3CO^+ + $CH_3CH{=}CH_2$], 161 kcal/mol, is much lower than $\Sigma\Delta H_f$ [iso-$C_4H_9^+$ + CO], 173 kcal/mol [12]. On the other hand, en route to the loss of CO from the (INC type) reactive intermediate, rearrangement of the incipient primary carbenium ion $(CH_3)_2CHCH_2^+$ to the tert-butyl cation $(CH_3)_3C^+$ may occur. This would allow CO loss to compete with propene elimination, particularly for long-lived low energy ions. In support of this proposal, we note that the MI spectrum of m/z 85 $\mathbf{b_4}^+$ ions generated from *metastable* precursor ions displays only one signal, at m/z 57. The same peak dominates the CID spectrum of these ions. Thus, for these long-lived low energy ions $\mathbf{b_4}^+$, loss of CO prevails.

9.3.5. Elimination of Water

Ions $\mathbf{b_2}^+[OCD_3]$ lose water as H_2O, whereas significant amounts of H_2O and HOD are lost from $\mathbf{b_3}^+[OCD_3]$ and $\mathbf{b_1}^+[OCD_3]$. Since the reaction is of only minor importance, a detailed analysis is not possible. The metastable peaks are Gaussian in shape and the associated KERs are only moderately large ($T_{0.5}$ = 30 - 50 meV). This behaviour resembles that of $\mathbf{a_1}^+$, which expels H_2O rather more readily.

Elimination of H_2O is much more important starting from $\mathbf{b_4}^+$ - $\mathbf{b_6}^+$ and particularly from $\mathbf{b_5}^+$. This trend is the reverse of that found for $\mathbf{a_1}^+$ and $\mathbf{a_2}^+$. The enhanced competition of H_2O expulsion with CO loss from $\mathbf{b_4}^+$ - $\mathbf{b_6}^+$, compared to $\mathbf{a_2}^+$, may reflect the presence of a four-carbon chain in these $C_5H_9O^+$ isomers.

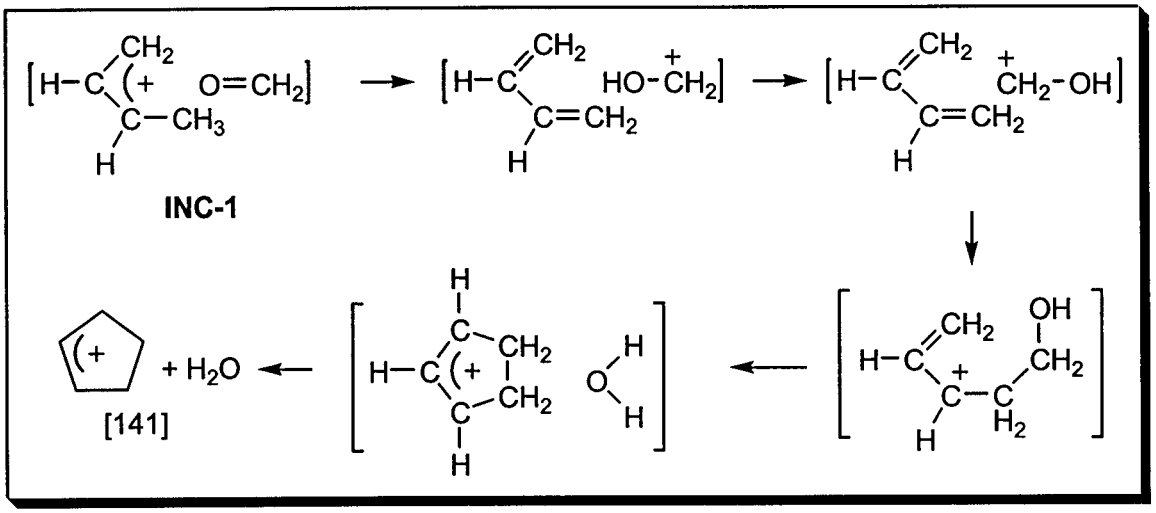

Scheme 9.3

Loss of H_2O is a remarkable process in which two C-O connections must be broken with the formation of two O-H bonds and one new C-C bond. It often occurs for the analogous metastable $C_nH_{2n+1}O^+$ ions with a non-terminal oxygen atom and it has been interpreted in terms of isomerization involving INCs [20, 21]. A similar mechanism, see Scheme 9.3, offers a means of interpreting H_2O loss from $\mathbf{b_4}^+$ - $\mathbf{b_6}^+$ in terms of the previously proposed INC-1 associated with the loss of CH_2O from these ions. In this context, we note that the CID spectrum (not shown) of the $\mathbf{b_5}^+$ type ions generated from *metastable* (low energy) precursor ions differs from that presented in Fig. 9.1 for the high energy (source generated) ions : the former spectrum is dominated by a peak at m/z 43 (CH_3CO^+), while the losses of CH_2O (to give m/z 55) and H_2O (to give m/z 67) are barely present. This strongly suggests that long-lived, low energy ions $\mathbf{b_5}^+$ have adopted cyclic structures, see Fig. 9.2b, from which losses of both CH_2O and H_2O are not favoured. This reinforces our proposal that these two reactions take place from non-cyclic ions, which have sufficient internal energy to adopt the INC-1 configuration.

The crucial steps in this route are probably the initial proton transfer from the $C_4H_7^+$ cation to CH_2O and the subsequent recombination of C_4H_6 with $[CH_2OH]^+$ to form $[C_4H_6CH_2OH]^+$. Although the proton affinity (PA) of butadiene is 17 kcal/mol greater than that of formaldehyde [22], the proton-transfer may be feasible given the ability of butadiene to stabilise CH_2OH^+ by π-donation. Subsequent H-transfer and rearrangement of the developing $C_5H_7^+$ cyclopentenyl cation may then lead to a combination of products that is energetically very favourable, see Table 9.4.

Table 9.4. Product enthalpies, $\Sigma\Delta H_f$ in kcal/mol, for possible dissociation reactions of $C_nH_{2n-1}O^+$ ions [a]

Ion	Products			$\Sigma\Delta H_f$
$C_4H_7O^+$	$(CH_3)_2C^+(H)$	+	CO	165
	$CH_2=CHCH_2^+$	+	$CH_2=O$	200
	$CH_3C=O^+$	+	C_2H_4	169
	$HC=O^+$	+	$CH_3CH=CH_2$	202
	$C_4H_5^+$ [b]	+	H_2O	179
	$C_3H_3^+$ [c]	+	CH_3OH	209
$C_5H_9O^+$	$(CH_3)_2C^+(CH_3)$ [d]	+	CO	139
	$(C_2H_5)C^+(H)CH_3$	+	CO	157
	$CH_2=CHC^+(H)CH_3$	+	$CH_2=O$	176
	$CH_2=C(CH_3)CH_2^+$	+	$CH_2=O$	185
	$CH_3C=O^+$	+	$CH_3CH=CH_2$	161
	$C_5H_7^+$ [e]	+	H_2O	141
	$C_4H_5^+$ [b]	+	CH_3OH	189
$C_6H_{11}O^+$	$(CH_3)_2C^+(C_2H_5)$	+	CO	132
	$(C_3H_7)C^+(H)CH_3$	+	CO	149
	$CH_2=CHC^+(CH_3)_2$	+	$CH_2=O$	157
	$CH_3C=O^+$	+	C_4H_8	152
	$C_6H_9^+$ [f]	+	H_2O	132
	$C_5H_7^+$ [e]	+	CH_3OH	151

[a] values from ref. 22, rounded to the nearest kcal/mol.
[b] most stable isomer, methylcyclopropenium cation.
[c] most stable isomer, cyclopropenium cation.
[d] $\Sigma\Delta H_f$ = 143 kcal/mol if the revised ΔH_f value of tert-$C_4H_9^+$, 169.9 kcal/mol, is used, see Ref. 22, p. 418.
[e] most stable isomer, cyclopentenyl cation.
[f] most stable isomer, 2-methylcyclopentenyl cation.

Several factors may favour H_2O loss on progressing from $\mathbf{a_2}^+$ to $\mathbf{b_4}^+$, $\mathbf{b_5}^+$ and $\mathbf{b_6}^+$. First, the extra CH_2 unit makes possible the formation of a stable cyclic ionic product, namely the cyclopentenyl cation. Secondly, the initial proton-transfer from $C_4H_7^+$ to CH_2O should be easier than the analogous process from $C_3H_5^+$, especially for stable allylic species. Deprotonation of the allyl cation on the central carbon atom leads to an unfavourable geometry of allene in which the p-orbitals from which the developing new C=C bond is formed are orthogonal, Eq. 1.

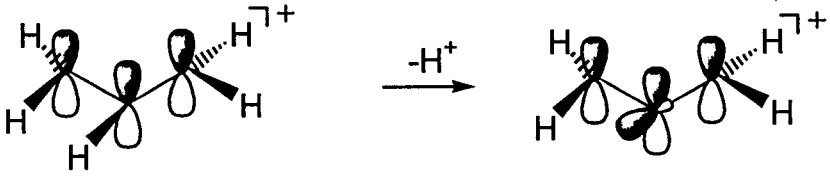

Eq. 1

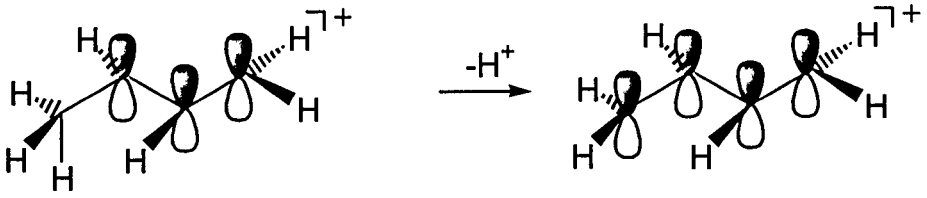

Eq. 2

No such unfavourable factors operate in the deprotonation of the 1-methallyl cation, which may lead smoothly to butadiene, Eq. 2. Thirdly, the stabilisation conferred on the INC $[CH_2OH^+/C_3H_4]$ is likely to be much less than the corresponding stabilisation of $[CH_2OH^+/C_4H_6]$ because the possibility of donating electron density from both π-bonds is geometrically feasible only for a conjugated diene.

9.3.6. Trends in the reactions of $C_nH_{2n-2}OCH_3^+$ ions for n = 3 – 5

Homologation of $\mathbf{a_1}^+$ to $\mathbf{b_1}^+$, $\mathbf{b_2}^+$ or $\mathbf{b_3}^+$ induces strong changes in the reactions of metastable $C_nH_{2n-2}OCH_3^+$ ions. Some of these variations persist for metastable ions $CH_2{=}CHC^+(C_2H_5)OCH_3$, $\mathbf{c_1}^+$, which resemble $\mathbf{b_1}^+$ - $\mathbf{b_3}^+$ in expelling mainly CH_2O (67%) but very little CO (~3%). However, $\mathbf{c_1}^+$ differs from $\mathbf{b_1}^+$ - $\mathbf{b_3}^+$ in losing a substantial amount of CH_3OH (27%).

These trends may be understood in terms of the energies of the possible products, Table 9.4. Despite uncertainties about the structure of several of the ionic

products and the magnitude of reverse critical energies associated with reactions that entail skeletal rearrangements, the following points can be made.

First, CO loss may always give more favourable products than CH_2O elimination, but the difference between the energies of the products decreases on ascending the homologous series of ions if the products of CO loss are assumed to be secondary or tertiary alkyl cations. The product enthalpy differential favouring CO elimination to give a secondary cation is 35, 19 and 8 kcal/mol, respectively for n = 3 - 5. This differential is so great for $\mathbf{a_1}^+$ that CO loss competes effectively with CH_2O expulsion, even though it involves more rearrangement and a sizeable reverse critical energy. In contrast, for $\mathbf{b_1}^+$, $\mathbf{b_2}^+$ and $\mathbf{c_1}^+$, the advantages of the lower energy products given by CO loss are insufficient to offset the disadvantages of more extensive isomerization and the larger reverse critical energy for the final step compared to CH_2O elimination. It may not be coincidental that of the three $C_4H_6OCH_3^+$ ions, only $\mathbf{b_3}^+$, which contains a branched hydrocarbon chain from which a tertiary cation may be formed without skeletal isomerization, expels CO in more than very minor abundance.

Secondly, CH_3OH loss becomes important only for $\mathbf{c_1}^+$. This trend reflects the enthalpies of formation of the unsaturated $C_{n-1}H_{2n-5}^+$ carbocations, which diminish rapidly when $n \geq 6$ because it becomes possible to accommodate an allylic system within a five-membered ring, whereas smaller cycloalkenyl cations are much less stable. Another factor favouring methanol elimination from $\mathbf{c_1}^+$ is the greater facility of the larger oxonium ions for isomerising to suitable intermediates (e.g. protonated dienyl methyl ethers) from which CH_3OH may be expelled. Thus, Scheme 9.4 gives a mechanistic proposal for the CH_3OH loss from $\mathbf{c_1}^+$ in which, via consecutive 1,2- and 1,4-H shifts, an INC is formed consisting of a 1,4-pentadienyl cation and a CH_3OH molecule. This species may further rearrange into an INC comprising cyclopentenyl cation and CH_3OH, which may dissociate to give favourable products. The cyclopentenyl cation is considerably more stable than its acyclic 1,4-pentadienyl counterpart, by 21 kcal/mol [12]. No analogous routes leading to such favourable products exist for the lower homologues.

Parallel trends to those found for CH_3OH expulsion could be considered to operate for H_2O loss. Such considerations would suggest that H_2O elimination should become more important once $n \geq 5$. However, a major difference between these two fragmentations is the need to disrupt the C-O bond of the OCH_3 group in order to permit expulsion of H_2O. If this process entails extensive reorientation in an INC involving the CH_2O molecule or CH_2OH^+ ion, as proposed in Scheme 9.3, a delicate internal energy balance may determine the degree of competition between the loss of CH_2O and H_2O from the metastable ions.

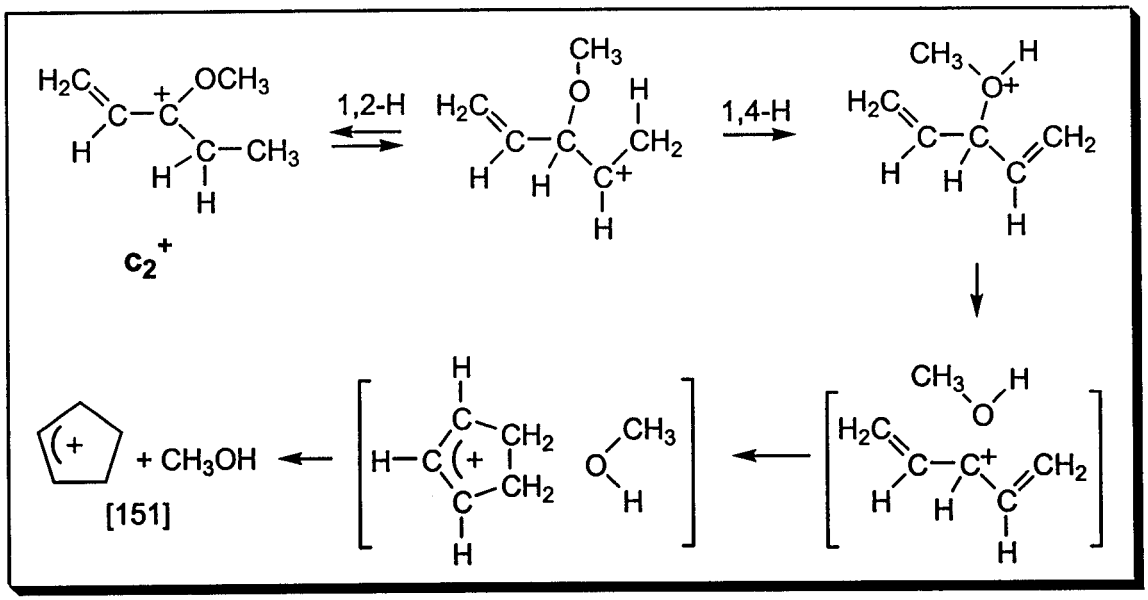

Scheme 9.4

9.4. Conclusions

The reactions of $CH_3CH{=}CHC^+(H)OCH_3$, $\mathbf{b_1}^+$, $CH_2{=}CHC^+(CH_3)OCH_3$, $\mathbf{b_2}^+$, and $CH_2{=}CH(CH_3)\text{-}C^+(H)OCH_3$, $\mathbf{b_3}^+$, show some resemblance to those of the lower homologue $CH_2{=}CH\text{-}C^+(H)OCH_3$, but there are appreciable differences and CO loss ceases to be of much importance for the $C_4H_6OCH_3^+$ ions. Although the chemistries of $\mathbf{b_1}^+$, $\mathbf{b_2}^+$ and $\mathbf{b_3}^+$ are closely related, they are not identical and the distinctions become clearer when labelled analogues are examined. Elimination of CH_2O is by far the most important fragmentation of the $C_4H_6OCH_3^+$ ions. The first step of the reaction is proposed to involve a 1,5-H shift, from the OCH_3 group to the hydrocarbon chain. This H-transfer is usually unidirectional, especially for $\mathbf{b_2}^+$, but it is partly reversible for $\mathbf{b_3}^+$ and particularly $\mathbf{b_1}^+$. The second step may entail a (dipole-assisted) 1,3-H shift to give energy-rich ion-neutral complexes (INCs) of 1- or 2-methallyl cations and neutral CH_2O, which dissociate.

The strong preference of these $C_5H_9O^+$ ions for expelling CH_2O persists for the higher homologue, $CH_2{=}CH\text{-}C^+(C_2H_5)OCH_3$. Consequently, CH_2O loss is the major and characteristic reaction of these unsaturated oxonium ions containing the -$C(H)OCH_3^+$ entity.

Loss of CH_2O from $\mathbf{b_4}^+$ - $\mathbf{b_6}^+$ may also occur via an INC. This reaction is associated with a very small kinetic energy release, suggesting that it generates the most stable $C_4H_7^+$ ion, 1-methallyl cation, at the thermochemical threshold. However, this process is only prominent for ions b_5^+, which also undergo a facile loss of H_2O, via rearrangement in the INC [$C_4H_7^+$/ $CH_2{=}O$] to yield $C_5H_7^+$ (cyclopentenyl cations). Loss of C_3H_6 and CO dominates the MI spectra of $\mathbf{b_4}^+$ and $\mathbf{b_6}^+$ and these reactions, which also occur from $\mathbf{b_5}^+$, are proposed to take place from 1,2-H shift isomers of the cyclic counterparts of $\mathbf{b_4}^+$ - $\mathbf{b_6}^+$.

References

[1] R.D. Bowen, A.W. Colburn and P.J. Derrick, Org. Mass. Spectrom. 25 (1990) 509 and references cited therein.

[2] T.J. Mead and D.H. Williams, J. Chem. Soc. (B) (1971) 1654.

[3] J. Hegedus Vajda and A.G. Harrison, Int. J. Mass Spectrom. Ion. Phys. 38 (1979) 293.

[4] G. Bouchoux, Y. Hoppilliard, R. Flammang, A. Maquestiau and P. Meyrant, Org. Mass Spectrom. 18 (1983) 340.

[5] R.D. Bowen, J. Chem. Soc. Chem. Commun. (1985) 807.

[6] G. Bouchoux, Y. Hoppilliard and P. Jaudon, Org. Mass Spectrom. 22 (1987) 98.

[7] (a) R.D. Bowen, A.W. Colburn and P.J. Derrick, Org. Mass Spectrom. 27 (1992) 625 ; (b) R.D. Bowen, A.D. Wright and P.J. Derrick, J. Chem. Soc. Perkin 2 (1993) 501.

[8] J.L. Holmes and J.K. Terlouw, Org. Mass Spectrom. 15 (1980) 383.

[9] (a) R.D. Bowen and A.D. Wright, J. Chem. Soc. Chem. Commun. (1991) 1055; (1992) 96 (b) A.D. Wright and R.D. Bowen, Can. J. Chem. 71 (1993) 1073 ; (c) R.D. Bowen, M.A. Trikoupis and J.K. Terlouw, Eur. J. Mass Spectrom. 7 (2001) 225.

[10] C.A. Schalley, G. Hornung, D. Schröder and H. Schwarz, Chem. Soc. Rev. 27 (1998) 91.

[11] D.J. Lavorato, J.K. Terlouw, T.K. Dargel, W. Koch, G.A. McGibbon and H. Schwarz, J. Am. Chem. Soc. 118 (1996) 11898.

[12] S.G. Lias, J.E. Bartmess, J.F. Liebman, J.L. Holmes, R.D. Levin and W.G. Mallard, J. Phys. Chem. Ref. Data 17 (1988) Suppl. 1.

[13] G. Hvistendahl and D.H. Williams, J. Am. Chem. Soc. 97 (1975) 3097.

[14] R.D. Bowen and D.H. Williams, J. Am. Chem. Soc. 99 (1977) 6822.

[15] C.E. Hudson and D.J. McAdoo, J. Am. Chem. Soc. Mass Spectrom. 9 (1998) 130.

[16] A.J. Chalk and L. Radom, J. Am. Chem. Soc. 120 (1998) 8430.

[17] (a) R.D. Bowen, Acc. Chem. Res. 24 (1991) 364 ; (b) P. Longevialle, Mass Spectrom. Rev. 11 (1992) 157 ; (c) D.J. McAdoo and T.H. Morton, Acc. Chem. Res. 26 (1993) 295.

[18] (a) M.A. Shaw, R. Westwood and D.H. Williams, J. Am. Chem. Soc. Perkin 2 (1970) 1529 ; (b) B.J. Stapleton, R.D. Bowen and D.H. Williams, Tetrahedron 34 (1978) 259.

[19] P.C. Burgers, J.L. Holmes, J.E. Szulejko, A.A.M. Mommers and J.K. Terlouw, Org. Mass Spectrom. 18 (1983) 254.

[20] S. Hammerum in Fundamentals of Gas-Phase Ion Chemistry, K.R. Jennings (ed.), Kluwer, Dordrecht, (1990) 379.

[21] R.D. Bowen and D.H. Williams, J. Am. Chem. Soc. 100 (1978) 7454.

[22] E. P. Hunter and S. G. Lias, J. Phys. Chem. Ref. Data 27 (1998) 413.

[23] H.F. van Garderen, P.J.A. Ruttink, P.C. Burgers, G.A. McGibbon and J.K. Terlouw, Int. J. Mass Spectrom. Ion Processes 121 (1992) 159.

[24] R.D. Bowen, H.G.M. Edwards, D.W. Farwell, I. Rusike and D.M. Saunders, J. Chem. Res. (S) (1998) 426 ; J. Chem. Res. (M) (1998) 1901.

[25] (a) J. A. Montgomery Jr, M. J. Frisch, J. W. Ochterski, and G. A. Petersson, J. Chem. Phys. 110 (1999) 2822. (b) ibid. 112 (2000) 6532.

[26] M.J. Frisch et al. Gaussian 98, Revision A.3, Gaussian, Inc., Pittsburgh, PA, 1998.

[27] N. Cohen and S.W. Benson, Chem. Rev. 93 (1993) 2419.

Summary

This thesis presents several studies on a unified mass spectrometric and computational chemistry approach to analyze reaction mechanisms in gas-phase ion chemistry. Attention is focused on the mechanisms of intra- and inter-molecular hydrogen transfer reactions in radical cations derived from molecules containing a carbonyl (O=C) or a phosphoryl (O=P) functional group. It is shown that such ions may rearrange into more stable enol- or distonic-type isomers and that ion-dipole complexes and hydrogen-bridged radical cations play a key role in the concomitant hydrogen transfer reactions. This is particularly true when the isomerization involves an intermolecular reaction.

The first Chapter introduces the combined approach by describing tandem mass spectrometry and computational chemistry. Some general mechanistic aspects of hydrogen transfer reactions are also discussed and a brief outline is given of the research methodology, using the enolization of ionized acetophenone as an example.

Chapter 2 discusses the gas phase chemistry of ionized dimethyl phosphonate, $(CH_3O)_2P(H)=O^{\bullet+}$. An intramolecular 1,2-H shift would yield its tautomer $(CH_3O)_2P\text{-}OH^{\bullet+}$, ionized dimethyl phosphite, which is 31 kcal/mol more stable. Theory and experiment clearly show that this reaction does not occur in the solitary ions. Instead, a 1,4-H shift takes place yielding the distonic isomer $CH_2O\text{-}(CH_3O)P(H)OH^{\bullet+}$, which serves as the precursor for the low energy loss of $CH_2=O$.

The dimethyl phosphite ion also abundantly loses $CH_2=O$: via a 1,3-H shift into the above distonic ion and a competing 1,4-H shift leading to the ion-dipole complex $CH_2O\text{-}P(OH)\text{-}O(H)CH_3^{\bullet+}$. Experiment shows that a mixture of isomeric product ions $CH_3O\text{-}P(H)\text{-}OH^{\bullet+}$ and $CH_3O(H)\text{-}P\text{-}OH^{\bullet+}$ is generated. Theory shows that their high

interconversion barrier (44 kcal/mol) is not sufficiently lowered by the CH_2O component in the precursor ions to realize intramolecular proton-transport catalysis.

In the μs timeframe, all dimethyl phosphonate ions have rearranged into their distonic counterpart. These distonic ions do not significantly communicate with their more stable 1,3-H shift isomer dimethyl phosphite. However, this isomerization may be realized by an intermolecular interaction, i.e. in an ion-molecule reaction of dimethyl phosphonate with benzonitrile under conditions of chemical ionization. Under these conditions the distonic ions readily isomerize into ionized dimethyl phosphite by virtue of a benzonitrile-assisted "catalytic" lowering of the 1,3-H shift barrier separating the isomers.

In Chapter 3, theory and experiment are used to obtain a consistent potential energy profile for the system of cyclic phosphonate/phosphite radical cations. It appears that solitary ethylene phosphonate ions $[\text{-}OCH_2CH_2O\text{-}]P(H)=O^{\bullet+}$ (EPA) retain their structure identity in the μs time-frame. However, the interaction with a benzonitrile (BN) molecule in a chemical ionization type experiment readily yields the more stable ethylene phosphite ion $[\text{-}OCH_2CH_2O\text{-}]P\text{-}OH^{\bullet+}$. Experiments with benzonitrile-d_5 support the proposal that this interaction does not involve the lowering of the 1,2-H shift barrier between the tautomers via a proton-transport catalysis type mechanism. Rather, a "quid-pro-quo" mechanism is operative, in which the ionized benzonitrile component of the encounter complex $[EPA\bullet\bullet\bullet BN]^{\bullet+}$ donates a proton to the O-atom of the phosphonate's O=P(H) functionality. This is followed by a back-transfer of the P-H hydrogen atom to benzonitrile's phenyl ring, yielding a H-bridged radical cation of the type $C_6H_5C{\equiv}N\bullet\bullet\bullet H\text{-}O\text{-}P[\text{-}OCH_2CH_2O\text{-}]^{\bullet+}$. This ion serves as the immediate precursor in the formation of the ethylene phosphite ion and benzonitrile.

Chapter 4 deals with the decarbonylation of $CH_3O\text{-}P=O^{\bullet+}$ and its various isomers. This study truly benefited from the synergy of theory and experiment : one without the other would not have permitted us to draw any solid mechanistic conclusion. That the oxygen atoms in low energy ions $CH_3O\text{-}P=O^{\bullet+}$ and $CH_2O\text{-}P\text{-}OH^{\bullet+}$ become equivalent in the decarbonylation and the accompanying H_2O loss was revealed by experiments on isotopically labelled ions. Theory was used to differentiate between a priori plausible

mechanisms for this equilibration. The CBS-QB3 calculations further revealed that low energy ions $CH_3O\text{-}P{=}O^{\bullet+}$ and $CH_2O\text{-}P\text{-}OH^{\bullet+}$ have a high propensity for rearrangement and that they can communicate with a great many stable isomers. The tandem mass spectrometry based experiments established that the product ion generated in the decarbonylation is the ylide ion $HP\text{-}OH_2^{\bullet+}$, rather than $H_2P\text{-}OH^{\bullet+}$, which theory predicts to be the more stable isomer. The intricate details of the decarbonylation mechanism were revealed by theory, which indicates that $CH_2O\text{-}P\text{-}OH^{\bullet+}$ ions having a narrow range of internal energies at 36 kcal/mol, undergo a facile isomerization into the hydrogen-bridged ion $[HO\text{-}P^{\bullet+}\bullet\bullet\bullet H\text{-}C(H){=}O]$, which further rearranges into another hydrogen-bridged radical cation, $[HP\text{-}O(H)\text{-}H^{\bullet+}\bullet\bullet\bullet C{=}O]$, the immediate precursor for decarbonylation into $HP\text{-}OH_2^{\bullet+}$.

Chapter 5 argues that, in contrast to a previous report, the dissociative electron ionization of the insecticide acephate does not generate pure m/z 78 ions $CH_3O\text{-}P{=}O^{\bullet+}$. By combining the results of exact mass measurements, (multiple) high energy collision experiments and CBS-QB3 calculations, it is concluded that the m/z 78 ions consist of $CH_3O\text{-}P{=}O^{\bullet+}$ and $CH_2O\text{-}P\text{-}OH^{\bullet+}$ in admixture with isobaric CH_5PON^+ ions. A computational analysis of the dissociation characteristics of the independently generated stable isomers $CH_3O\text{-}P\text{-}NH_2^+$ and $CH_3P(=O)NH_2^+$ shows that the CH_5PON^+ ions from acephate have the structure $CH_3O\text{-}P\text{-}NH_2^+$. As a consequence, the recovery signal in the reported neutralization-reionization spectrum of acephate's m/z 78 ions does not prove the stability of the $CH_3O\text{-}P{=}O$ neutral. Definitive evidence for its existence as a stable species in the dilute gas phase comes from a collision induced dissociative ionization experiment on the reaction $C_6H_5\text{-}P(=O)OCH_3^+ \rightarrow C_6H_5^+ + CH_3O\text{-}P{=}O$. The calculations indicate that $CH_3O\text{-}P\text{-}NH_2^\bullet$ is also a stable species, but attempts to confirm this by experiment have not yet been successful.

A recent flame-sampling laser-ionization study reported that combustion of dimethyl methyl phosphonate generates the elusive $CH_3P(=O)_2$ molecule and that it has an ionization energy of 9.24 eV. Our *ab initio* calculations (CBS-QB3 level of theory) indicate that this ionization energy is that of the "enol" tautomer $CH_2{=}P(=O)OH$, while that of $CH_3P(=O)_2$ is much higher, 11.66 eV. We propose in Chapter 6 that in the above

experiments a trace amount of the "enol" is co-generated with the "keto" isomer $CH_3P(=O)_2$. Mass spectrometric experiments involving neutralization-reionization and collision-induced dissociative ionization show that $CH_2=P(=O)OH$ and $CH_3P(=O)_2$ are both stable neutral species in the dilute gas-phase.

In Chapter 7, it is shown that the enol counterpart of ionized acetanilide, $C_6H_5NH(OH)=CH_2^{\bullet+}$, eliminates HNCO at low internal energy and not ketene, as has been proposed previously. This reaction occurs via an intriguing skeletal rearrangement, whose mechanism was explored using isotopic labelling and computational chemistry. Surprisingly, the ionized enol appears to be *less* stable than its keto counterpart. This explains why molecule-assisted enolization reactions of ionized acetanilide cannot be realized. The reverse process, i.e. a molecule-assisted ketonization of the enol ion, does not take place either but this may be due to the formation of unreactive encounter complexes.

In Chapter 8, the electron impact mass spectrum of the food preservative sorbic acid, $CH_3CH=CHCH=CHCOOH$, is discussed. The spectrum displays a prominent loss of $CH_3^{\bullet}$ which gives rise to the base peak at m/z 97. Low energy (metastable) sorbic acid ions also readily lose $CH_3^{\bullet}$, along with $COOH^{\bullet}$. Tandem mass spectrometry based experiments in conjunction with computations at the CBS-QB3 level of theory were used to probe the mechanism for this reaction. The loss of $CH_3^{\bullet}$ is not a simple bond cleavage reaction nor a hidden hydrogen rearrangement (1,5-H shift) yielding ions of structure $HC\equiv C\text{-}CH=CH\text{-}C(OH)_2^+$. Instead, the molecular ion rearranges into a six membered ring from which $CH_3^{\bullet}$ is lost by direct bond cleavage to yield protonated 2*H*-pyran-2-one as the product ion. This displacement reaction has a slightly lower energy requirement than the competing loss of $COOH^{\bullet}$ yielding the $C_5H_7^+$ cyclopentenium ion. The prominent losses of $CH_3^{\bullet}$ from $CH_3CH=CHCH=CHCOOC_2H_5^{\bullet+}$ (ionized ethyl sorbate) and $COOH^{\bullet}$ from $HOOCCH=CH\text{-}CH=CHCOOH^{\bullet+}$ (ionized muconic acid) occur via the same type of displacement reaction.

Chapter 9 discusses the reactions of the metastable oxonium ions $CH_3CH=CHC^+(H)OCH_3$, $CH_2=CHC^+(CH_3)OCH_3$, and $CH_2=CH(CH_3)\text{-}C^+(H)OCH_3$. Although the chemistries of these isomeric ions are closely related, they are not identical and the

distinctions become clearer when labelled analogues are examined. Elimination of CH_2O is by far the most important fragmentation. The first step of the reaction is proposed to involve a largely unidirectional 1,5-H shift, from the OCH_3 group to the hydrocarbon chain. The second step may entail a dipole-assisted 1,3-H shift to give energy-rich ion-neutral complexes of 1- or 2-methallyl cations and neutral CH_2O, which dissociate. Such ion-neutral complexes may also play a role in the loss of CH_2O from the isomeric ion CH_2=CH-CH(CH_3)OCH_2^+. For this ion, the reaction is associated with a very small kinetic energy release, suggesting that it generates the most stable $C_4H_7^+$ ion, 1-methallyl cation, at the thermochemical threshold. The enthalpies of formation for the key ions in this study were obtained from CBS-QB3 calculations and thermochemical estimates.

Appendix

Supplementary information to Chapter 7

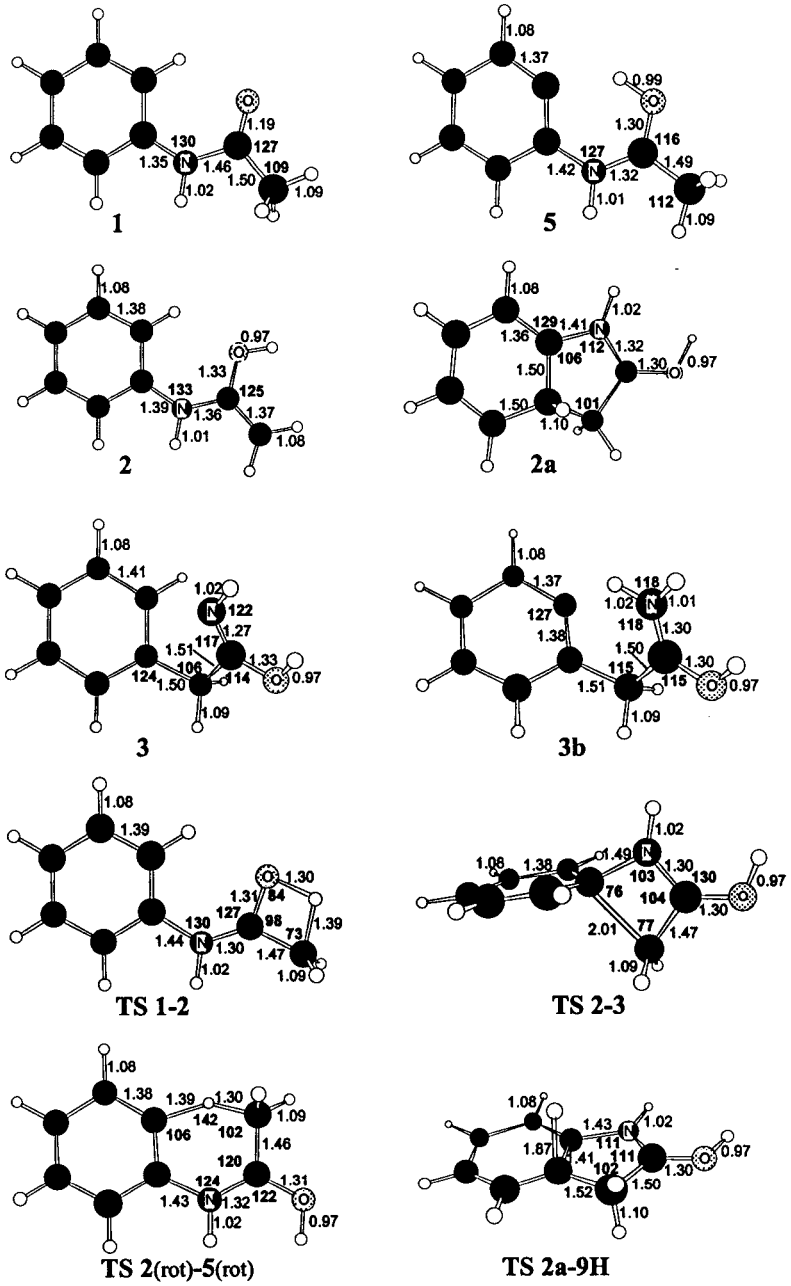

Fig. A.7.1. Optimized geometries of selected ions and transition states of the acetanilide system. The bond lengths (Å) and angles are presented in normal and bold font, respectively.

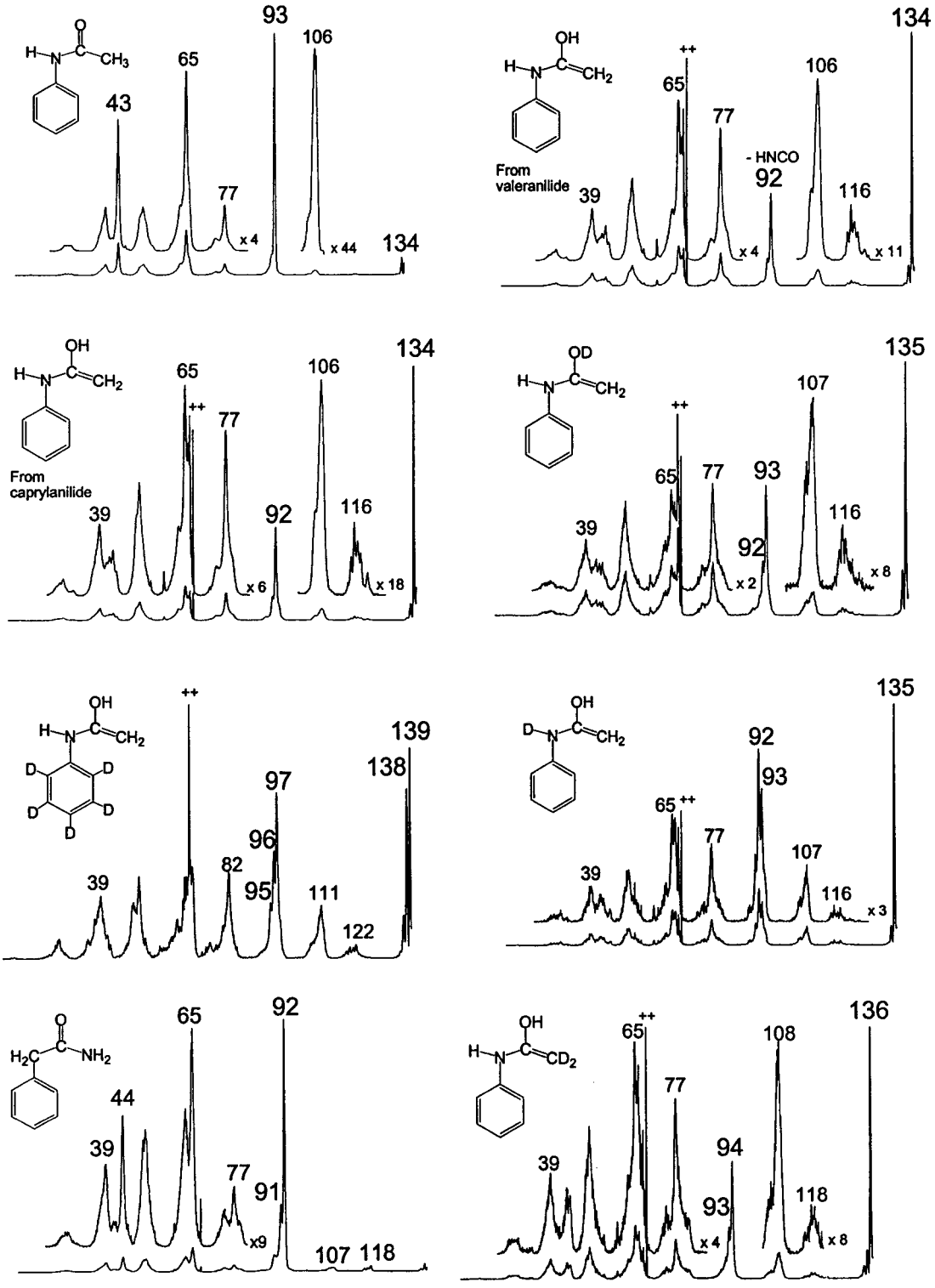

Fig. A.7.2. CID spectra of the m/z 135 ions of acetanilide, its enol and selected d-labelled isotopologues.

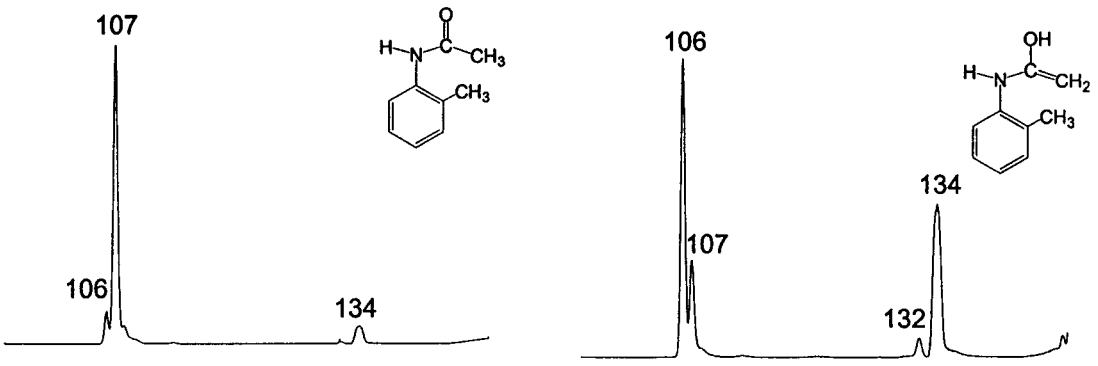

Fig. A.7.3. Metastable ion spectra of the m/z 149 ions generated directly (top) or from the methyl valeranilide precursor.